# The Cenozoic paleoelevation and paleogeographic history of the southwestern US Cordillera: a combined sedimentologic and isotopic approach

by

**Alex R. Lechler**

A dissertation submitted in partial fulfillment
of the requirements for the degree of
Doctor of Philosophy
(Geology)
in The University of Michigan
2011

**Doctoral Committee:**

**Assistant Professor Nathan A. Niemi, Chair**
**Professor Kyger Lohmann**
**Assistant Professor Nathan D. Sheldon**
**Assistant Professor Allison L. Steiner**

To my Mom,
Dawn Lechler (1956 – 2004)

**Acknowledgements**

I must first thank my dissertation advisor, Dr. Nathan Niemi, for not only being a great advisor throughout the PhD process but also for being a great collaborator and mentor. This dissertation research was an evolutionary process, and Nathan's clever mind and geologic know-how always pushed this work into new and exciting research directions that were not yet evident during this project's commencement. I thank my committee members, Kacey Lohmann, Nathan Sheldon, and Allison Steiner, for their thoughtful feedback and advice throughout the dissertation process. I also thank Marin Clark and Mike Hren both of whom consistently offered great insights and expertise that greatly benefitted this work. Mike is thanked, in particular, for the field support and lab instruction that made Chapter 5 of this dissertation possible.

I owe a debt of gratitude to all of my amazing colleagues in the Department of Geological Sciences at the University of Michigan. Most importantly, my SCALE lab mates and SCALE den family of Alison Duvall, Boris Avdeev, Nora Lewandowski, and Lydia Staisch who have kept my life balanced and full of laughter even during the long days and nights 'trapped' on the first floor of CC Little. Hopefully, one day we'll get that couch. I must also acknowledge all of my intramural volleyball teammates, particularly Dan Horton, Mike D'Emic and Boris Avdeev, for sticking through losing season after losing season but keeping the enthusiasm level high enough that we kept coming back.

I also really want to express my gratitude to all of the wonderful students I have had the privilege to teach during my time at UM. Teaching classes that ranged from

Introductory Geology to graduate level computer programming was a definite challenge, but the hard work and enthusiasm of the countless students I have both taught and learned from made every class a joy to be a part of. I am particularly indebted to my GSI colleagues, Mike D'Emic, Kelly Umlauf, and Tim O'Brien, who offered support, comraderie, and insight in so many challenging situations.

Finally, I have to thank my dad, Mike Lechler, for his unending support and constant reminders that I can do and should do whatever I want in life, no matter the pay or prestige, as long as it made me happy. And to my mom, who passed away too soon, I thank her for the motivation she provided when I took my first geology class. I wouldn't be where I am today if it weren't for her shared enthusiasm for the 'coolness' of plate tectonics.

## TABLE OF CONTENTS

## LIST OF FIGURES

**FIGURE**

## LIST OF TABLES

**TABLE**

# CHAPTER I

## Introduction

Topography reflects the interplay among climatic, tectonic, geodynamic and erosion processes. As a result, accurate paleoelevation histories can inform models for orogen development by elucidating the complex interactions of Earth's atmosphere, lithosphere and asthenosphere during the lifespan of an orogenic system. Prior to recent developments of paleoaltimetry methodologies, direct estimates of regional paleoelevations for many of the world's prominent orogens (e.g., Himalaya-Tibetan Plateau, South American Andes, Western US Cordillera) were scarce. Early estimates of paleotopography were generally indirect and qualitative, often derived from documented changes in fluvial incision and sedimentation rates (e.g., Clark, 2007 and references therein) or expected isostatic compensation effects of thickened continental crust that formed as a result of significant crustal shortening (e.g., England and Houseman, 1989). While providing a reasonable first order approximation to regional paleoelevation histories, these indirect measures lack the resolution needed to fully constrain and validate competing models for orogen development, leaving the paleoelevation history for many of the world's dominant orogens poorly constrained.

The topographic evolution of the Western US Cordillera is of particular interest in geologic research as the complex tectonic history of the region, which is characterized by

Mesozoic-early Cenozoic convergence and subduction that transitioned to widespread Tertiary extension, has relevance to our understanding of convergent and extensional orogenic systems worldwide. The Sierra Nevada magmatic arc and the Basin and Range Province are of particular interest as the paleoelevation histories for each region have been subject to copious research (e.g., Axelrod, 1968; Gregory and Chase, 1992; Wolfe et al., 1997; Unruh, 1991; Wakabayashi and Sawyer, 2001; Poage and Chamberlain, 2002; Horton et al., 2004; Horton and Chamberlain, 2006; Kent-Corson et al., 2006; Mulch et al., 2006; Cassel et al., 2009; Hren et al., 2010) yet remain subject to contentious debate. In the case of the Sierra Nevada, debate centers on whether or not the Sierra Nevada is a young or ancient topographic feature (e.g., Unruh, 1991; Wakabayashi and Sawyer, 2001; Mulch et al., 2006; Hren et al., 2010). The answer to this question has far-reaching implications as evidence for young topography provides support for models citing delamination of thickened mantle lithosphere from below the range in late Cenozoic time as the primary driver for young surface uplift (e.g., Jones et al., 2004; Zandt et al., 2004). Similar delamination models have been proposed for the topographic evolution of the South American Andes (e.g., Garzione et al., 2006) and Tibetan Plateau (Molnar et al., 1993). Thus, the validity of delamination models to the topographic evolution of the Sierra Nevada will directly impact our understanding of orogenic systems across the globe.

Understanding the topographic evolution of the Basin and Range Province has equal or even greater relevance and importance to tectonics and geodynamics research as this region is the prototype for continental crustal extension. Despite this importance, however, fundamental questions remain concerning the primary driving forces for

widespread Tertiary extension as well as the physical mechanisms by which this extension occurred. Observations of relatively high regional mean elevations (~ 1.5 km), uniform crustal thicknesses (~ 30 km) and a flat, regional Moho place specific constraints on the plausible mechanisms for Tertiary extension, but unanswered questions of how strain was partitioned throughout the crust and lithospheric mantle and whether or not mass was conserved throughout the extended region leave open the possibility for a wide-range of tectonic and geodynamic models (e.g., Clark, 2007). Regional variability in the timing and magnitude of extension (e.g., McQuarrie and Wernicke, 2005) and magmatism (Armstrong and Ward, 1991) places additional constraints on models for Basin and Range evolution, but the complexity of these trends makes it difficult to synthesize a province-wide model that satisfies all criteria.

Internal buoyancy forces of a high elevation continental plateau, plate boundary forces associated with a change in plate kinematics during the Cenozoic, and basal normal forces resulting from removal of the Farallon slab from below western North America have all been cited as possible drivers for Basin and Range extension (see Sonder and Jones, 1999 for review). Evaluating the respective role of each of these proposed mechanisms requires accurate and quantitative paleoelevation histories as each tectonic and/or geodynamic model is characterized by a unique and predictable topographic history (e.g., Clark, 2007). Accordingly, contrasting models for Basin and Range extension provide testable topographic hypotheses that can be evaluated directly through regional paleoelevation study. For example, internal buoyancy forces acting as a primary driver for Tertiary extension requires that a high elevation (> 3 km) orogenic plateau was located throughout much of the Cordilleran interior prior to extension (e.g.,

Ernst, 2010). If such a plateau existed, we expect to see direct evidence for it in the paleoaltimetry record. In contrast, if regional elevations were low or comparable to modern (~ 1.5 km) in the proto-Basin and Range province, distinct mechanisms of lower crustal flow from surrounding areas of high topography and/or magmatic additions at the base of the lithosphere are more likely to account for the observed modern crustal thicknesses and Moho character (Clark, 2007).

### 1.1. Quantitative paleoaltimetry techniques

The recent development of multiple quantitative paleoaltimetry techniques (Kohn, 2007 and references therein) has greatly enhanced the capability to make accurate and direct estimates of paleoelevations. The earliest quantitative paleoelevation studies utilized paleotemperature estimates derived from leaf types and morphologies (i.e. leaf physiognomy) in fossil flora assemblages in combination with empirical temperature-elevation relationships to make quantitative estimates of regional paleoelevations. This technique has been widely applied to Cenozoic basin systems throughout western North America (e.g., Axelrod, 1968; Gregory and Chase, 1992; Wolfe et al., 1997) as well as to the Tibetan Plateau (Spicer et al., 2003). Recent applications of this paleobotanical approach have been relatively scarce, however, due to the limited availability of dense, diverse and well-preserved fossil floral assemblages in the geologic record. Interpretations of paleobotanical-based paleotemperature and paleoelevation records are further limited due to the complex interaction of both climate and elevation on surface temperatures, thus requiring that climatic influences to fossil records are independently constrained.

More recently developed paleoaltimetry methodologies aim to circumvent complications arising from climatic influences by using proxy-elevation relationships that are climate independent. Basalt vesicularity (e.g., Sahagian and Maus, 1994), plant stomatal frequency (e.g., Kouwenberg et al., 2007), and cosmogenic nuclide paleoaltimetry (e.g., Riihimaki and Libarkin, 2007) techniques utilize the elevation dependence of atmospheric pressure, partial pressure of atmospheric $CO_2$, and cosmogenic nuclide production rates, respectively, to quantify paleoelevations. While each of these techniques has the benefit of investigating proxy-elevation relationships that are independent of climatic influence, each is significantly limited in terms of applicability and/or by high inherent uncertainties. Basalt vesicularity studies require specific geologic proxies (well-preserved basalt flows) that are spatially and temporally restricted in the geologic record. In addition, high inherent uncertainties (~ ± 1.5 km) also significantly limit application of basalt vesicularity techniques to paleoelevation studies. Limited proxy availability similarly restricts application of plant stomatal density techniques. This methodology is also characterized by large uncertainties due to the fact that the modern calibrations that are fundamental to quantifying $pCO_2$ values using the fossil leaf record are unable to account for stomatal trends under the high $pCO_2$ conditions that characterize much of the geologic past. Finally, cosmogenic nuclide techniques, while sound in theory, have yielded very few paleoelevation values to date due to the strict requirement that the complete depositional and burial history of a sample is known (Riihimaki and Libarkin, 2007), a restriction which is difficult to ensure in most settings.

By far, the most widely applied quantitative paleoelevation technique is stable isotope paleoaltimetry, which utilizes the stable isotopic compositions ($\delta^{18}O$ and $\delta D$) of paleo-meteoric water proxies for paleoelevation reconstructions. Fundamental to this approach is the observation that the stable isotopic composition of modern precipitation exhibits a systematic relationship with elevation at the site where the precipitation falls (e.g., Chamberlain and Poage, 2000). Due to the preferential removal of heavy isotopes ($^{18}O$ and D) during condensation events, precipitation falling farther from the moisture source (i.e. at high elevations) is expected to be characterized by lower $\delta^{18}O$ and $\delta D$ values than at sites proximal to the source, with the $\delta$ value measured as:

$$\delta_{sample} = \frac{R_{sample} - R_{standard}}{R_{standard}} * 1000$$

Where R is the measured isotopic ratio ($^{18}O/^{16}O$ or D/H), the reference standard is standard mean ocean water (SMOW), and $\delta$ is measured in units permil (‰). Both empirical (Poage and Chamberlain, 2001) and theoretical models using Rayleigh distillation principles (Rowley et al., 2001; Rowley and Garzione, 2007) show that such a systematic $\delta^{18}O$ (or $\delta D$)-elevation relationship (~ -2.8‰/km) does exist in most orographic settings. In theory, all that is then required for paleoelevation calculations is a proxy for the isotopic composition of paleo-meteoric waters. Meteoric water proxies are common constituents of sedimentary basin systems that commonly form in response to orogen growth and development. As a result, proxy materials that are contemporaneous with orogen development are often readily accessible.

Commonly analyzed stable isotopic proxies include lacustrine, riverine, and pedogenic carbonates, weathered volcanic ashes, and fossil teeth and bone (see Kohn,

2007). With these proxies, paleoelevations can be calculated in several different ways, including: (1) using changes in the isotopic composition of meteoric waters through time at a single site to propose changes in regional paleoelevations (e.g., Horton et al., 2004), (2) comparison of paleo-meteoric water isotopic compositions to those of modern waters to estimate elevation changes relative to the present (e.g., Garzione et al., 2000) and, in rare cases, (3) comparison of modern and paleo-$\delta^{18}O$-elevation gradients to estimate regional paleotopographic distributions (Mulch et al., 2006). In cases 2 and 3, the isotopic composition of the water in which the proxy formed must first be calculated for direct comparison with modern values. Due to the temperature-dependent fractionation between source water and carbonate proxies (e.g., Kim and O'Neil, 1997), calculation of water $\delta^{18}O$ values requires that temperatures of carbonate formation are known or can be assumed. Uncertainty in paleotemperatures, therefore, can lead to significant uncertainties in paleoelevation calculations.

In addition to complications arising from uncertainty in the temperature of carbonate formation, stable isotope paleoaltimetry studies may be prone to significant elevation uncertainties due to factors that directly affect the variability of surface water $\delta^{18}O$ (or $\delta D$) values independent of elevation change. As with paleobotany-based paleoelevation estimates, meteoric water stable isotopic compositions are directly influenced by climate. Changes in local temperature, storm tracks, dominant moisture source, and seasonality of precipitation, as well as natural interannual variability in precipitation $\delta^{18}O$ (or $\delta D$) can all complicate interpretation of the proxy record. Additionally, the type of meteoric water proxy must be considered as the elevation signal derived from each proxy record is unique to the meteoric water system in which the

proxy formed. For example, lacustrine carbonates form in and reflect the isotopic composition of waters sourced from throughout the contributing catchment (e.g., Rowley and Garzione, 2007), whereas pedogenic carbonates form in local soil waters (e.g., Quade et al., 1989) and, accordingly, are more likely to reflect local precipitation isotopic compositions. As a result, the isotopic composition of lacustrine proxies inform about trends in elevation and topographic relief over a much greater spatial scale and are thus often not analogous to paleosol carbonate isotopic records. Accurate interpretation of paleo-meteoric water proxy records also requires that the influence of any process that alters the isotopic composition of surface waters (e.g., evaporation) during the transition from initial meteoric precipitation to preservation in the proxy record is accounted for. Evaluating evaporative influence to proxy records has been shown to be vital to stable isotope paleoaltimetry as evaporation acts in contrast to Rayleigh distillation rainout (i.e. increases $\delta^{18}O$ values) and can thus lead to significant paleoelevation underestimates (e.g., Quade et al., 2007).

In addition to the processes that may influence or alter meteoric water isotopic compositions independent of elevation effects, another major source of uncertainty in stable isotope paleoaltimetry is variability in the quantitative relationship between $\delta^{18}O$ (or $\delta D$) and elevation. As noted above, the global average $\delta^{18}O$-elevation gradient is -2.8 ‰/km, but observed $\delta^{18}O$-elevation gradients are quite variable, ranging from ~ -1 to -5 ‰/km in mid-latitude regions. This variability is particularly evident in continental interior and high elevation orogenic plateau regions where observed isotope-elevation gradients are consistently reduced in magnitude compared to the global average (e.g., Blisniuk and Stern, 2005; Quade et al., 2007). If the global average gradient is incorrectly

applied to proxy records collected from these regions, we can expect that significant errors in paleoelevation calculations will result. The potential error and increased uncertainty associated with $\delta^{18}O$-elevation gradient variability points to the need to better constrain the primary environmental influences on isotope-elevation gradients. Specifically, the degree to which these gradients are systematically related to physiographic and climatic characteristics must be further investigated so that more accurate interpretations of paleo-meteoric water proxy records can be made.

### 1.2 Thesis outline

Part I (Chapters 2 and 3) of this dissertation critically evaluates the stable isotope paleoaltimetry technique and its fundamental assumptions, with a primary focus on identifying systematic trends in isotope-elevation gradients and potential causes for observed gradient variability. Chapter 2 presents multivariate statistical analysis of compiled modern precipitation records from the western US and east Asia. In this analysis, precipitation $\delta^{18}O$ values were modeled as a function of geographic (latitude, longitude, elevation) and climatic (mean annual temperature, mean annual precipitation) variables at the precipitation site in order to determine which environmental variables exert a dominant control on modern $\delta^{18}O$ values as well as to quantify the magnitude of each environmental control. These statistical analyses also investigated the variability in modern isotopic relationships on a regional and subregional scale with particular focus on how isotope-elevation gradients are influenced by physiographic and climatic environment. This work reveals that continental interior rainshadows (e.g., Basin and Range) and high elevation orogenic plateau regions (e.g., Tibetan Plateau) are

characterized by $\delta^{18}O$-elevation gradients (~ 1.5‰/km) that are a factor of two lower in magnitude than those observed in simple orographic settings (Sierra Nevada, Himalaya), where observed $\delta^{18}O$-elevation gradients are similar in magnitude to empirical global average gradients and gradients derived from theoretical Rayleigh distillation models (~ -2.8‰/km; Poage and Chamberlain, 2001; Rowley et al., 2001). The work presented in Chapter 2 is currently in preparation for submission to *Water Resources Research* or a journal with similar focus.

Empirical $\delta^{18}O$-elevation gradients derived from modern stream and spring water sampling in the orographic slope and orographic rainshadow of the southern Sierra Nevada region of the southwestern US (Chapter 3) builds on the statistical analyses presented in Chapter 2. Again, we observe a systematic shift to reduced isotope-elevation gradients in continental interior rainshadow regions, but to empirical magnitudes that are even lower (~ -0.8 ‰/km) than observed in the statistical analyses of modern precipitation (Chapter 2). The reduced isotope-elevation gradients observed for interior spring and stream waters is shown to be plausibly explained by post-depositional isotopic modification resulting from elevation-dependent sublimation processes that are likely to affect winter snowpacks in continental interior, alpine settings. This work has important implications for future stable isotope paleoaltimetry studies, particularly in areas where snowmelt-derived meteoric waters dominate regional hydrology. An additional implication of our modern stream and spring water sampling is that stable isotope-based hydrologic studies must also account for snow sublimation influences, particularly in light of current trends toward earlier onset of spring season snowmelt (e.g., Cayan et al., 2001) and increased proportion of annual precipitation falling as rain instead of snow in

the arid, mountainous western US. This work has undergone peer-review and is currently in revision for *GSA Bulletin*.

Part II of this dissertation (Chapters 4 and 5) shifts focus to applications of paleoaltimetry techniques to better constrain the Cenozoic paleoelevation history of the southwestern US Cordillera. A primary aim of this section is to investigate potential complimentary techniques to pair with standard stable isotope paleoaltimetry in order to circumvent the limitations and uncertainties outlined in this Introduction and in Part I of the dissertation. Chapter 4 presents the results of a combined sedimentologic and isotopic study of Paleocene-Eocene sedimentary basin systems in the southern Sierra Nevada region. U-Pb detrital zircon provenance studies of basin sediments indicates that the southernmost Sierra Nevada was located at or near sea level in early Paleogene time, thus, requiring ~ 1.5–2 km of post-Eocene uplift to account for modern exposure elevations. This work provides new constraints on the Paleogene paleotopographic and paleogeographic evolution of the region and suggests that significant along-strike variations may explain the discrepancy among published Sierran paleoelevation models. The results of this study are published in the April 2011 issue of *Geology*. The format and content of the published manuscript match that presented in this dissertation.

Chapter 5 utilizes the novel carbonate clumped isotope paleothermometry technique to constrain Late Cretaceous-Eocene paleoelevations in the proposed high elevation orogenic plateau region of the western US Cordilleran interior (termed the 'Nevadaplano' by DeCelles, 2004). This work combines clumped isotope paleotemperature data with standard stable isotopic analysis of Tertiary carbonate paleo-meteoric water proxies from the Goler basin of the southern Sierra Nevada region and the

Sheep Pass basin of east-central Nevada. These carbonate clumped isotope temperatures are some of the earliest temperature values produced in the University of Michigan Stable Isotope Lab, and they provide definitive evidence for a high elevation (≥ 2.6 km) continental plateau immediately prior to widespread Basin and Range extension. This work also points to the utility of carbonate clumped isotope paleoaltimetry as calculated water $\delta^{18}O$ values provide direct evidence for significant evaporative influence to continental interior proxy records. This work is in preparation for submission to *Nature Geoscience* or a similar, high-impact journal.

Chapter 6 summarizes the primary conclusions of this dissertation. Appendices provide complete data tables for compiled modern precipitation records (Chapter 2), zircon U-Pb analyses and corresponding sample locations (Chapter 4), and detailed clumped isotope analytical results (Chapter 5).

## 1.3 References cited


Armstrong, R. L., and Ward, P., 1991, Evolving geographic patterns of Cenozoic magmatism in the North American Cordillera - the temporal and spatial association of magmatism and metamorphic core complexes: Journal of Geophysical Research-Solid Earth and Planets, v. 96, no. B8, p. 13201-13224.

Axelrod, D. I., 1968, Tertiary floras and topographic history of Snake River Basin Idaho: Geological Society of America Bulletin, v. 79, no. 6, p. 713-734.

Blisniuk, P. M., and Stern, L. A., 2005, Stable isotope paleoaltimetry: A critical review: American Journal of Science, v. 305, no. 10, p. 1033-1074.

Cassel, E. J., Graham, S. A., and Chamberlain, C. P., 2009, Cenozoic tectonic and topographic evolution of the northern Sierra Nevada, California, through stable isotope paleoaltimetry in volcanic glass: Geology, v. 37, no. 6, p. 547-550.

Cayan, D. R., Kammerdiener, S. A., Dettinger, M. D., Caprio, J. M., and Peterson, D. H., 2001, Changes in the onset of spring in the western United States: Bulletin of the American Meteorological Society, v. 82, no. 3, p. 399-415.

Chamberlain, C. P., and Poage, M. A., 2000, Reconstructing the paleotopography of mountain belts from the isotopic composition of authigenic minerals: Geology, v. 28, no. 2, p. 115-118.

Clark, M. K., 2007, The significance of paleotopography: Paleoaltimetry: Geochemical and Thermodynamic Approaches, v. 66, p. 1-21.

DeCelles, P. G., 2004, Late Jurassic to Eocene evolution of the Cordilleran thrust belt and foreland basin system, western USA: American Journal of Science, v. 304, no. 2, p. 105-168.

England, P., and Houseman, G., 1989, Extension during continental convergence, with application to the Tibetan Plateau: Journal of Geophysical Research-Solid Earth and Planets, v. 94, no. B12, p. 17561-17579.

Ernst, W. G., 2010, Young convergent-margin orogens, climate, and crustal thickness-A Late Cretaceous-Paleogene Nevadaplano in the American Southwest?: Lithosphere, v. 2, no. 2, p. 67-75.

Garzione, C. N., Molnar, P., Libarkin, J. C., and MacFadden, B. J., 2006, Rapid late Miocene rise of the Bolivian Altiplano: Evidence for removal of mantle lithosphere: Earth and Planetary Science Letters, v. 241, no. 3-4, p. 543-556.

Garzione, C. N., Quade, J., DeCelles, P. G., and English, N. B., 2000, Predicting paleoelevation of Tibet and the Himalaya from $\delta^{18}O$ vs. altitude gradients in meteoric water across the Nepal Himalaya: Earth and Planetary Science Letters, v. 183, no. 1-2, p. 215-229.

Gregory, K. M., and Chase, C. G., 1992, Tectonic significance of paleobotanically estimated climate and altitude of the Late Eocene erosion surface, Colorado: Geology, v. 20, no. 7, p. 581-585.

Horton, T. W., and Chamberlain, C. P., 2006, Stable isotopic evidence for Neogene surface downdrop in the central Basin and Range Province: Geological Society of America Bulletin, v. 118, no. 3-4, p. 475-490.

Horton, T. W., Sjostrom, D. J., Abruzzese, M. J., Poage, M. A., Waldbauer, J. R., Hren, M. T., Wooden, J. L., and Chamberlain, C. P., 2004, Spatial and temporal variation of Cenozoic surface elevation in the Great Basin and Sierra Nevada: American Journal of Science, v. 304, no. 10, p. 862-888.

Hren, M. T., Pagani, M., Erwin, D. M., and Brandon, M., 2010, Biomarker reconstruction of the early Eocene paleotopography and paleoclimate of the northern Sierra Nevada: Geology, v. 38, no. 1, p. 7-10.

Jones, C. H., Farmer, G. L., and Unruh, J., 2004, Tectonics of Pliocene removal of lithosphere of the Sierra Nevada, California: Geological Society of America Bulletin, v. 116, no. 11-12, p. 1408-1422.

Kent-Corson, M. L., Sherman, L. S., Mulch, A., and Chamberlain, C. P., 2006, Cenozoic topographic and climatic response to changing tectonic boundary conditions in Western North America: Earth and Planetary Science Letters, v. 252, no. 3-4, p. 453-466.

Kim, S. T., and O'Neil, J. R., 1997, Equilibrium and nonequilibrium oxygen isotope effects in synthetic carbonates: Geochimica Et Cosmochimica Acta, v. 61, no. 16, p. 3461-3475.

Kohn, M. J., 2007, Paleoaltimetry: Geochemical and thermodynamic approaches, Reviews in Mineralogy and Geochemistry, v. 66, 278 p.

Kouwenberg, L. L. R., Kurschner, W. M., and McElwain, J. C., 2007, Stomatal frequency change over altitudinal gradients: Prospects for paleoaltimetry: Paleoaltimetry: Geochemical and Thermodynamic Approaches, v. 66, p. 215-241.

McQuarrie, N., and Wernicke, B. P., 2005, An animated tectonic reconstruction of southwestern North America since 36 Ma: Geosphere, v. 1, no. 3, p. 147-172.

Molnar, P., England, P., and Martinod, J., 1993, Mantle Dynamics, Uplift of the Tibetan Plateau, and the Indian Monsoon: Reviews of Geophysics, v. 31, no. 4, p. 357-396.

Mulch, A., Graham, S. A., and Chamberlain, C. P., 2006, Hydrogen isotopes in Eocene river gravels and paleoelevation of the Sierra Nevada: Science, v. 313, no. 5783, p. 87-89.

Poage, M. A., and Chamberlain, C. P., 2001, Empirical relationships between elevation and the stable isotope composition of precipitation and surface waters: Considerations for studies of paleoelevation change: American Journal of Science, v. 301, no. 1, p. 1-15.

Poage, M. A. and Chamberlain, C.P., 2002, Stable isotopic evidence for a pre-Middle Miocene rain shadow in the western Basin and Range: Implications for the paleotopography of the Sierra Nevada: Tectonics, v. 21, no. 4, p. 16-1 - 16-10.

Quade, J., Cerling, T. E., and Bowman, J. R., 1989, Systematic variations in the carbon and oxygen isotopic composition of pedogenic carbonate along elevation transects

in the southern Great Basin, United-States: Geological Society of America Bulletin, v. 101, no. 4, p. 464-475.

Quade, J., Garzione, C., and Eiler, J., 2007, Paleoelevation reconstruction using pedogenic carbonates: Paleoaltimetry: Geochemical and Thermodynamic Approaches, v. 66, p. 53-87.

Riihimaki, C. A., and Libarkin, J. C., 2007, Terrestrial cosmogenic nuclides as paleoaltimetric proxies: Paleoaltimetry: Geochemical and Thermodynamic Approaches, v. 66, p. 269-278.

Rowley, D. B., and Garzione, C. N., 2007, Stable isotope-based paleoaltimetry: Annual Review of Earth and Planetary Sciences, v. 35, p. 463-508.

Rowley, D. B., Pierrehumbert, R. T., and Currie, B. S., 2001, A new approach to stable isotope-based paleoaltimetry: implications for paleoaltimetry and paleohypsometry of the High Himalaya since the Late Miocene: Earth and Planetary Science Letters, v. 188, no. 1-2, p. 253-268.

Sahagian, D. L., and Maus, J. E., 1994, Basalt vesicularity as a measure of atmospheric pressure and palaeoelevation: Nature, v. 372, no. 6505, p. 449-451.

Sonder, L. J., and Jones, C. H., 1999, Western United States extension: How the West was widened: Annual Review of Earth and Planetary Sciences, v. 27, p. 417-462.

Spicer, R. A., Harris, N. B. W., Widdowson, M., Herman, A. B., Guo, S. X., Valdes, P. J., Wolfe, J. A., and Kelley, S. P., 2003, Constant elevation of southern Tibet over the past 15 million years: Nature, v. 421, no. 6923, p. 622-624.

Unruh, J. R., 1991,The uplift of the Sierra Nevada and implications for Late Cenozoic epeirogeny in the Western Cordillera: Geological Society of America Bulletin, v. 103, no. 11, p. 1395-1404.

Wakabayashi, J., and Sawyer, T. L., 2001, Stream incision, tectonics, uplift, and evolution of topography of the Sierra Nevada, California: Journal of Geology, v. 109, no. 5, p. 539-562.

Wolfe, J. A., Schorn, H. E., Forest, C. E., and Molnar, P., 1997, Paleobotanical evidence for high altitudes in Nevada during the Miocene: Science, v. 276, no. 5319, p. 1672-1675.

Zandt, G., Gilbert, H., Owens, T. J., Ducea, M., Saleeby, J., and Jones, C. H., 2004, Active foundering of a continental arc root beneath the southern Sierra Nevada in California: Nature, v. 431, no. 7004, p. 41-46.

# CHAPTER II

## Spatial variability of modern meteoric $\delta^{18}O$: empirical constraints from the western US and east Asia and implications for stable isotope studies*

### 2.1 Abstract

We conduct a statistical analysis of modern precipitation and meteoric waters from the western US and east Asia to determine the dominant environmental controls (latitude, longitude, elevation, MAT, MAP) on meteoric water isotopic ($\delta^{18}O$ and $\delta D$) compositions as a function of physiographic and climatic environment. Multiple linear regression analysis reveals that latitude and elevation act as dominant controls on meteoric $\delta^{18}O$ in much of the western US and east Asia but independent influences from site longitude, MAT, and MAP can be significant depending on location. Our regression analysis also indicates that the magnitude of environmental controls is region-dependent. Isotope elevation gradients are reduced by approximately a factor of two in continental interior rainshadows (e.g., Basin and Range) and high elevation continental plateaus (e.g., Tibetan Plateau) in comparison to Rayleigh distillation-type isotope-elevation gradients

* **Citation:** Lechler, A.R. and Niemi, N.A., *in prep*, Spatial variability of modern meteoric $\delta^{18}O$: empirical constraints from the western US and east Asia and implications for stable isotope studies.

which characterize orographic settings with a single dominant moisture source and relatively simple storm track trajectories (e.g., Sierra Nevada, Himalaya). This statistical analysis of modern meteoric waters informs stable isotope paleoclimate, hydrologic, and paleoelevation studies by providing quantitative constraints on isotopic relationships with multiple environmental parameters and identifying how isotopic relationships are influenced by physiographic and climatic environment. The results of this study can greatly improve the accuracy of stable isotope-based determinations of climatic change, location of groundwater recharge, and changes in or absolute paleoelevations, particularly for cases where paleogeographic setting of proxy formation site can be constrained.

## 2.2 Introduction

The stable isotopic composition ($\delta^{18}O$ and $\delta D$) of precipitation is a reflection of the integrated effects of all atmospheric and isotopic fractionation processes taking place between the time of initial evaporation from the oceanic source region to the time of deposition. Temperature along the moisture path, distance from the moisture source, precipitation amount, and overall degree of rainout from the initial moisture parcel are all well-documented controls on the isotopic composition of precipitation (e.g., Dansgaard, 1964; Rozanski et al., 1993; Gat, 1996). Having the ability to isolate and quantify the relationship between isotopic composition and each isotopic control, however, is the challenge fundamental to paleoclimate, hydrologic and paleoelevation studies utilizing meteoric water stable isotope proxies (e.g., ice, lacustrine sediments, plant material, fossil teeth and bone). These stable isotope studies are further limited by the inaccessibility to

studying paleo-isotope-environment relationships, thus requiring a robust calibration using modern isotopic relationships. Regional and global precipitation isotopic monitoring networks provide such a calibration by giving researchers the opportunity to study and quantify meteoric water isotopic relationships as a function of various climatic and geographic parameters. Studies of the dense datasets produced by these monitoring networks (e.g., Dansgaard, 1964; Yurtsever and Gat, 1981; Rozanski et al., 1993; Araguás-Araguás et al., 1998, Welker, 2000; Bowen and Wilkinson, 2002) reveal both the systematic trends in isotopic compositions of precipitation in relation to individual environmental parameters (temperature, elevation, mean annual precipitation), as well as indicate the significant variability exhibited in isotopic relationships as a function of temporal and spatial scale (e.g., Rozanski et al., 1993; Vachon et al., 2010).

The International Atomic Energy Agency's (IAEA) global network for isotopes in precipitation (GNIP) has been the basis for seminal works (e.g., Dansgaard, 1964; Rozanski et al., 1993) that enhanced our understanding of water isotopes in the hydrologic cycle, particularly in continental environments. The recognized relationships between temperature, precipitation amount, elevation, and distance from the moisture source and degree of rainout from a moisture parcel, and, ultimately, isotopic composition of precipitation, has since served as the foundation for stable isotope-based paleoclimate, hydrologic, and paleoelevation research. Paleoclimate studies utilize the documented $\delta^{18}O$ (or $\delta D$)-temperature relationship to interpret changes in mean annual temperature through time (Jouzel et al., 1997 and references therein). Hydrologic studies can make use of either the seasonal fluctuations in precipitation isotopic compositions, which are controlled by the interactions of changes in temperature, moisture source,

and/or precipitation type throughout the year, or the elevation dependence of precipitation $\delta^{18}O$ and $\delta D$ to assess both timing and location of groundwater recharge (e.g., Allison, 1988). The observed depletion in precipitation isotopic compositions as a function of increasing elevation has also served as the basis for stable isotope paleoelevation studies in orogenic systems worldwide (e.g., Poage and Chamberlain, 2001; Rowley and Garzione, 2007). Each of the highlighted research directions utilizes the observed isotope-rainout relationships in a unique way, but in all cases a quantitative understanding of the relationship between isotopic composition and the climatic or geographic parameter of interest must be known or assumed.

While the GNIP database acts as a solid foundation for isotopic studies utilizing paleo-meteoric water proxies, its coarse spatial resolution, particularly in the western US and central Asia, requires regional and local precipitation and surface meteoric water (i.e. streams, rivers, lakes) sampling campaigns to attain the spatial resolution needed to produce an accurate modern calibration. These higher resolution sampling campaigns (e.g., Friedman and Smith, 1972; Friedman et al., 1992, 2002b; Garzione et al., 2000; Stern and Blisniuk, 2002; Hren et al., 2009) not only add to global precipitation isotope datasets but also reveal that there is a high degree of regional variability in terms of both: (1) which climatic (i.e. temperature, precipitation amount) and geographic (i.e. latitude, longitude, elevation, distance from the moisture source) factors exert dominant controls on precipitation isotopic compositions and (2) the magnitude of the quantitative relationship between isotopic composition and individual environmental parameters, findings which are also supported by analyses of regional isotopic network datasets (Rozanski and Araguás-Araguás, 1995; Araguás-Araguás et al., 1998; Tian et al., 2001;

Johnson and Ingram, 2004; Vachon et al., 2010). This observed regional variability points to the need to better constrain and quantify meteoric water isotopic relationships to individual environmental parameters on a range of spatial scales and in variable physiographic and climatic environments.

Of particular research interest is the degree of variability in the $\delta^{18}O$-elevation and $\delta^{18}O$-temperature relationship as these gradients serve as the foundation for stable isotope paleoaltimetry and paleoclimate studies, respectively. A global compilation of $\delta^{18}O$-elevation gradients revealed that an average gradient of -2.8‰/km characterizes most orographic settings (Poage and Chamberlain, 2001), but the observed variability in this dataset (~ -1 to -5‰/km) requires attention as application of the global average to regions characterized by significantly lower (or higher) $\delta^{18}O$-elevation gradients will lead to significant under- or overestimates of absolute paleoelevation or changes in paleoelevation through time. Theoretical models assuming Rayleigh distillation rainout processes predict $\delta^{18}O$-elevation gradients similar in magnitude to the empirical global average in relatively simple orographic settings (e.g., Rowley et al., 2001), but these same models fail to capture the observed variability in meteoric water isotopic relationships in continental interior settings and over high elevation plateaus (Araguás-Araguás et al., 1998; Quade et al., 2007; Lechler and Niemi, *in revision*). In order to refine theoretical models so that they more accurately predict isotopic compositions in these continental interior and plateau settings, we must first assess, empirically, the primary controls on isotopic and isotope-elevation gradient variability in order to determine which of the proposed mechanisms [e.g., amount effects (Lee and Fung, 2008), seasonality (Araguás-Araguás et al., 1998; Tian et al., 2001), convective storm activity

(Liu et al., 2008), snow sublimation (Lechler and Niemi, *in revision*)] are likely causes for the observed variability. Similarly, $\delta^{18}O$-temperature gradients have been shown to vary (0.1 – 0.6‰/°C) depending on physiographic setting (e.g., Vachon et al., 2010 and references therein). Identification of the primary controls on and reasons for both $\delta^{18}O$-elevation and $\delta^{18}O$-temperature gradient variability will greatly improve the accuracy of stable isotope-based determinations of paleoelevation and paleotemperature.

For this study, we compiled annual and multi-year precipitation and meteoric water isotope monitoring records collected from the western US and east Asia in order to perform a new statistical analysis of modern annual precipitation $\delta^{18}O$ on a regional (e.g., western US) and subregional (e.g., Basin and Range) scale. The western US and east Asia were selected for this study due to each region: (1) having good spatial coverage of modern meteoric water $\delta^{18}O$ (or $\delta D$) data, (2) consisting of distinct physiographic and climatic regions that are likely to be characterized by unique isotopic relationships and (3) being an area of active stable isotope paleoclimate (e.g., Quade et al., 1989; Koch et al., 1995; Thompson et al., 1997; Tian et al., 2001) and paleoelevation (e.g., Garzione et al., 2000; Horton et al., 2004; Cyr et al., 2005; Kent-Corson et al., 2006; Mulch et al., 2006; Rowley et al., 2006; DeCelles et al., 2007; Saylor et al., 2009) research and debate. In this analysis, we investigate and quantify the degree of influence climatic (mean annual temperature, mean annual precipitation) and geographic (latitude, longitude, elevation) site parameters exert on modern meteoric $\delta^{18}O$ values and how these controls vary in different topographic and climatic settings. The investigated parameters were selected because they have been proposed to be major controls on precipitation isotopic compositions (e.g., Dansgaard, 1964; Rozanski et al., 1993; Gat, 1996) and can be

potentially constrained in the proxy record. The capability to perform both regional and subregional analyses is afforded by the dense spatial coverage of our compiled dataset (Figure 2.1), and this increased spatial coverage allows for the derivation of robust predictive equations for isotopic distributions in each environment.

## 2.3 Isotopic datasets

### *2.3.1 Western United States*

We compiled published precipitation isotopic ($\delta^{18}O$ and $\delta D$) records for 206 sites distributed throughout the western US (Figure 2.1; see Table A2.1 in the Appendix for references for data sources). GNIP sites make up a substantially small proportion (3 out of 206) of the western US compiled dataset as spatial coverage of GNIP stations is sparse in this region. Good spatial coverage with a relatively uniform distribution, however, is obtained through the United States Network for Isotopes in Precipitation (USNIP) dataset (Welker, 2000), which was accessed online as recently as February 2011 (http://www.uaa.alaska.edu/enri/databases/usnip/index.cfm). Compiled datasets varied in terms of spatial and temporal sampling with some studies providing isotopic data for a single station while others provided a regional dataset (e.g., Friedman and Smith, 1972; Friedman et al., 1992, 2002b). Sampling for most datasets was conducted on a seasonal basis but some studies include higher resolution weekly (e.g., USNIP) and monthly sampling. However, in most cases only seasonal or annual precipitation $\delta^{18}O$ (or $\delta D$) values were reported in the literature. Due to seasonal and storm-by-storm variability in precipitation isotopic composition at a single site (Gat, 1996; Friedman et al., 2002b), only stations with records of at least one continuous annual cycle of precipitation

## Figure 2.1

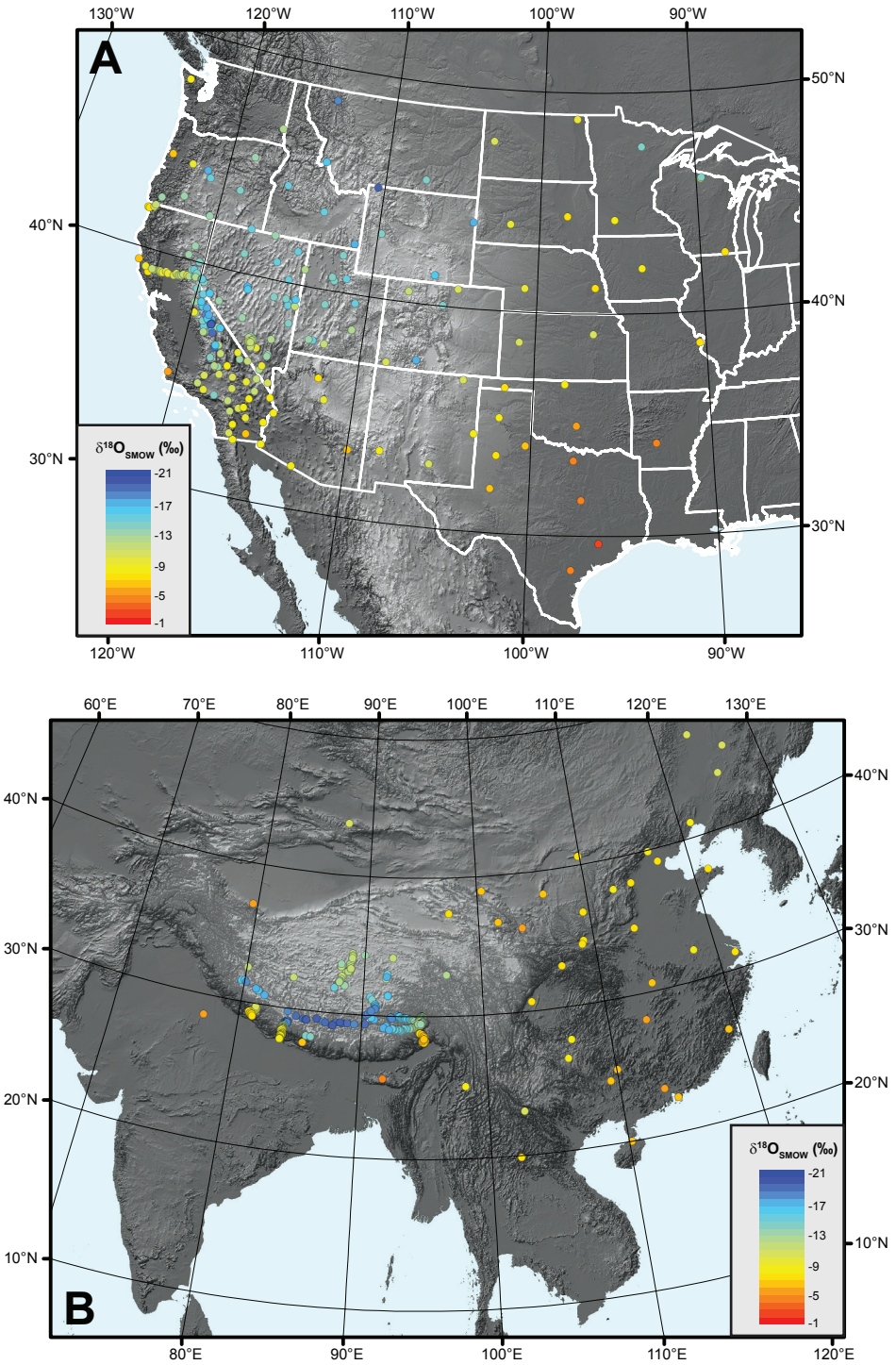


Figure 2.1 – 30 meter digital elevation models (DEM) for the western US (A) and east Asia (B) showing modern distribution of precipitation-weighted mean annual $\delta^{18}O$ values for each region, color-coded by $\delta^{18}O$ value. Sites in (A) are exclusively precipitation stations. Sites in (B) are both precipitation station stations (GNIP) as well as small stream and tributary sampling, primarily focused in the Himalaya and Tibetan Plateau (Garzione et al., 2000; Hren et al., 2009). See Appendix Table A2.1 for reference sources for precipitation and streamwater sampling sites.

collection were included in this analysis. The one exception to this protocol is the inclusion of Sierra Nevada snowcore data (Friedman and Smith, 1972) which includes yearly samples with only one recorded season of precipitation (winter). However, the dominance of winter season precipitation over summer precipitation in the Sierra Nevada region (winter-summer ratio ≥ 4; Pandey et al., 1999) supports inclusion of this dataset as the dominant seasonal isotopic signal in this region (winter) is recorded.

Whenever possible, annual precipitation-weighted mean $\delta^{18}O$ and $\delta D$ values were calculated for each site. In cases where precipitation amounts were not provided (15 out of 206 sites), annual arithmetic mean $\delta^{18}O$ and $\delta D$ values were calculated. Comparison of arithmetic and weighted mean annual isotopic compositions for stations with precipitation amount data reveal that arithmetic averages approximate weighted averages quite well (average |weighted – arithmetic| $\delta^{18}O$ = 0.21‰). As a result, inclusion of arithmetic means should not significantly alter model results. For studies that provided seasonal isotopic values and precipitation amounts (e.g., Friedman et al., 1992; 2002b), we selected records with only paired winter and summer seasons for our weighted mean annual calculations in order to ensure no bias towards a particular season for sites where some seasonal records had been lost or were unavailable. We also calculated precipitation-weighted seasonal averages (winter, summer) for these datasets in order to investigate how isotopic controls varied on a seasonal basis.

*2.3.2 East Asia*

We compiled 298 meteoric water records collected from east Asia (Figure 2.1B; Table A2.2 in Appendix). Unlike the western US compilation, which includes only

precipitation records, the majority of isotopic records in east Asia are derived from small stream and tributary sampling campaigns (Garzione et al., 2000; Hren et al., 2009). We included these surface meteoric waters in order to ensure good regional spatial coverage, particularly within the Himalaya and Tibetan Plateau physiographic subregions. In all cases, the measured meteoric water isotopic compositions are shown to approximate closely precipitation-weighted hypsometric mean elevations for the contributing catchment (see Hren et al., 2009 for calculations). As a result, these values effectively reflect weighted mean annual precipitation 'point' measurements analogous to the GNIP stations that comprise the remainder (50 out of 298) of the east Asia dataset. Duration of sampling at GNIP sites is site-dependent. In cases where multiple publications reported weighted mean annual isotopic compositions for the same station, the record with the longest duration was selected for this analysis. For stations with published records that did not overlap in time (e.g., Johnson and Ingram, 2004 and Liu et al., 2008) an arithmetic average of the reported values was calculated unless precipitation amounts for each record were provided.

*2.3.3 Geographic and climatic parameters*

Geographic (latitude, longitude, elevation) and climatic (mean annual temperature (MAT), mean annual precipitation (MAP)) parameters were also compiled for each isotopic sample site (Table A2.1 in Appendix). In cases where required parameters were not reported in original data sources, information was acquired from independent datasets. Site elevations were extracted from the US Geological Survey STOPO30 digital elevation model (DEM) using reported site latitude and longitude locations. MAT and MAP site values were provided for most GNIP stations in both the western US and east

Asia. At locations with no reported MAT or MAP, values were extracted from global gridded temperature and precipitation datasets compiled and interpolated by Matsuura and Wilmott at the University of Delaware and accessed online (http://climate.geog.udel.edu/~climate, August 2008).

## 2.4 Statistical models of the spatial distribution of $\delta^{18}O$ in precipitation

### *2.4.1 Previous studies*

Investigating how best to interpolate precipitation site $\delta^{18}O$ values to locations lacking a nearby precipitation monitoring station, Bowen and Revenaugh (2003) showed that the interpolation scheme of Bowen and Wilkinson (2002) produced global $\delta^{18}O$ distributions with the highest degree of accuracy. The Bowen and Wilkinson model (hereafter referred to as the BW model) utilized the GNIP dataset to model empirically precipitation-weighted mean annual $\delta^{18}O$ distributions on a global scale. Deconvolving the temperature and rainout effect on $\delta^{18}O$ values into geographic parameters (latitude and elevation) alone, the BW model provides a predictive equation that calculates an expected mean annual precipitation $\delta^{18}O$ value at any geographic location: $\delta^{18}O = -0.0051(LAT^2) + 0.1805|LAT| - 0.0020(ELEV) - 5.247$ (latitude in degrees, elevation in meters). By accounting for the general trend of greater heavy isotope depletion at high latitude and/or high elevation sites, the BW model, to a first degree, predicts global $\delta^{18}O$ distributions reasonably well. While this global model is a powerful predictive tool, particularly in regions with sparse GNIP station coverage (e.g., western United States, central Asia), it does not account for potential regional variability, both in

terms of which environmental parameters are dominant controls on precipitation $\delta^{18}O$ as well as the magnitude of the respective control on $\delta^{18}O$ values.

Following the procedure of Bowen and Wilkinson (2002), Dutton and others (2005) and Liu and others (2008) augmented GNIP datasets with regional precipitation isotope sampling campaigns (see references within each manuscript) to create predictive regional models for $\delta^{18}O$ distributions in the western US [$\delta^{18}O = -0.0057(LAT^2) + 0.1078|LAT| - 0.0029(ELEV) - 1.6544$; Dutton et al., 2005)] and east Asia [$\delta^{18}O = -0.0073(LAT^2) + 0.3261|LAT| - 0.0015(ELEV) - 9.7776$; Liu et al., 2008], respectively. The general trends observed in these regional studies (i.e. depleted isotopic compositions with increasing latitude and elevation) also characterize our compiled datasets from the western US (Figure 2.1A) and east Asia (Figure 2.1B). However, comparison of the derived equations for these regional studies with one another, as well as to the global BW model, reveals significant variability in both $\delta^{18}O$-latitude and $\delta^{18}O$-elevation relationships across different regions. Presumably, this regional variability in isotopic relationships may also reflect variable influences from climatic parameters, such as MAT and MAP, as well. Furthermore, both the western US (Dutton model) and east Asia (Liu model) predictive models are characterized by significant $\delta^{18}O$ residuals (approximately -5‰ to +5‰) when comparing model-predicted values with observed station values. In particular, in both the Dutton and Liu models, continental interior regions (Basin and Range, Rocky Mountain Cordillera in the western US; Tibetan Plateau in east Asia) are characterized by large model residuals. This result is not surprising due to sparse precipitation station coverage in these continental interior regions, but this pattern of model residuals also suggests these continental interior and high elevation continental

plateau regions may be characterized by isotopic relationships distinct from those in simple orographic settings.

*2.4.2 A multivariate approach to modeling $\delta^{18}O$ in modern precipitation*

In this study, we expand on earlier modern precipitation $\delta^{18}O$ modeling efforts by investigating a wider spectrum of possible environmental controls at a range of spatial scales. Our approach aims to identify the dominant climatic (MAT, MAP) and geographic (latitude, longitude, elevation) controls on modern $\delta^{18}O$ distributions on a regional and subregional scale. For each analysis, we model the observed isotopic ($\delta^{18}O$ or $\delta D$) composition of meteoric water at a specific site as a multiple linear regression of the unique set of environmental parameters for a given site:

$$\delta^{18}O = \beta_0 + \beta_1 x_1 + \beta_1 x_1 + \beta_2 x_2 + \beta_3 x_3 + \beta_4 x_4 + \beta_5 x_5 + .... + \beta_n x_n \qquad \textbf{(Eq. 1)}$$

where $x_1, x_{2,...,} x_{n-1,} x_n$ represent independent climatic and geographic parameters (MAT, MAP, latitude, longitude, and elevation) and $\beta_1, \beta_2, \ldots, \beta_{n-1}, \beta_n$ are the linear coefficients for each independent variable. In this multiple regression approach the dependent variable ($\delta^{18}O$ or $\delta D$) can be analyzed as either a linear function of independent variables (as shown in Eq. 1, with all variables raised to a power of 1) or as a polynomial function (e.g., $LAT^2 + LAT$, as in the BW, Dutton and Liu models).

Our approach differs from published predictive models for global (Bowen and Wilkinson, 2002) and regional (Dutton et al., 2005; Liu et al, 2008) isotopic distributions in two ways. First, the BW, Dutton and Liu models investigated only latitude and elevation as dominant controls on precipitation $\delta^{18}O$. This approach neglects to account

for the influence continentality and amount (i.e. MAP) effects might have on $\delta^{18}O$ compositions by assuming that latitudinal and altitudinal effects are the only dominant controls on precipitation isotopic compositions. Second, these models calculate coefficients for latitude and elevation separately. Latitudinal coefficients are solved for by using only the subset of precipitation sampling stations that are at low elevations (< 200 m). Elevation coefficients are then calculated by dividing the $\delta^{18}O$ residual (difference between observed isotopic composition and isotopic composition calculated using the derived latitudinal effect alone) by the station elevation (see Bowen and Wilkinson, 2002 and Dutton et al., 2005 for details).

We investigate the impact of proposed controlling 'effects' on precipitation $\delta^{18}O$ and $\delta D$ values (Dansgaard, 1964; Rozanski et al., 1993; Gat, 1996) by including environmental parameters that directly relate to each of these effects: (1) the temperature effect (MAT), (2) the amount effect (MAP), (3) continentality effect (longitude, latitude) and (4) the altitude effect (elevation). Additionally, our model approach solves for each parameter coefficient simultaneously as part of a single linear model. For example, in this approach the relationship between isotopic composition and elevation is calculated with the quantitative influence of every other parameter taken into account. This approach allows for the component of the isotopic signal attributable to each parameter to be calculated rather than prescribing all isotopic variability to a single parameter, as is commonly done when performing simple one-to-one comparisons of isotopic composition to an individual environmental parameter. These one-to-one comparisons often account for only a modest amount of isotopic variability, as evidenced by low $R^2$ values (generally < 0.5) and are only informative in cases where each independent

parameter (e.g., latitude, elevation) is uncorrelated with the others. In most settings, however, this assumption of independence is difficult to ensure. For example, a precipitation monitoring transect trending N-S from the Indian subcontinent up the southern flank of the Himalaya would exhibit a high degree of correlation between latitude and elevation as elevation steadily increases from south to north along the Himalayan front. As a result, it may be difficult to discern whether latitude or elevation is the dominant control on the observed decrease in isotopic values as a function of northward position. It's important to point out, however, that this issue of covariance can be partially circumvented if the quantitative relationships between individual environmental parameters and $\delta^{18}O$ values differ significantly in terms of magnitude. For example, expected depletion due to latitudinal effects alone (~ 1–2‰) is likely to be an order of magnitude less than depletion from expected altitudinal effects (~20‰) for a mid-latitude region with a topographic gradient comparable to the Himalaya Mountains. As a result, elevation effects should still be discerned from the isotopic record in regions characterized by high relief. In any case, this simple example reveals the potential for complications to arise when interpreting one-to-one comparisons in settings characterized by significant covariance among the environmental parameters influencing isotopic compositions, thus pointing to the need to investigate quantitative relationships within the context of other influential parameters.

*2.4.3 Application of a multivariate approach to the western US and east Asia*

For each regional and subregional analysis we start by modeling precipitation weighted mean annual $\delta^{18}O$ as a multiple regression model that includes all investigated parameters (latitude, longitude, elevation, MAT, MAP) (full linear model). Using

regression diagnostics for the full linear model we test the null hypothesis for each independent parameter by identifying parameters that do not exert a statistically significant influence on the dependent isotopic composition through analysis of the corresponding p-value (probability of obtaining a t-value greater than that observed). High p-values (> 0.05) indicate that the null hypothesis for the corresponding variable is statistically satisfied; in other words, the independent variable does not exert significant control on the dependent variable ($\delta^{18}O$). We then create a regression model that includes only the statistically significant independent variables with the aim of reducing the model to include only the parameters that significantly influence observed isotopic compositions. We repeat this process iteratively to test how p-values for independent variables change with a new subset of parameters. After these iterations, we arrive at a reduced linear model that has the minimum number of independent predictor variables (i.e. out of latitude, longitude, elevation, MAT, MAP) but a maximum coefficient of determination ($R^2$). This reduced linear model is verified statistically using analysis of variance (ANOVA) tests which compare the reduced linear models to the full linear models and test the null hypothesis that the difference in prediction between the two models is not statistically significant, i.e. the reduced model has the same predictive capabilities as the full linear model.

This statistical approach is built on a number of assumptions that must be satisfied in order to ensure reliable results. As discussed above, covariance among independent variables (multicollinearity) complicates multiple regression analysis. As part of each regional and subregional analysis we calculate variance inflation factors (VIF) for all full and reduced linear models to assess the degree of multicollinearity. VIF values increase

with higher degree of multicollinearity and, in practice, the cutoff for acceptable VIF values ranges from 5 (e.g., Marquardt, 1980) to 10 (O'Brien, 2007) depending on the system being studied and accuracy required. In models with VIF values greater than 5 (i.e. high multicollinearity) we eliminate individual parameters that exhibit a high level of covariance with other independent variables (e.g., temperature) in order to reduced model VIF values to acceptable levels.

Another assumption that must be verified in our statistical analysis is normal distribution of independent variables and model residuals in order for relevant t- and p-values to be calculated. Independent environmental variables that are not sufficiently normally distributed require transformation in order to be included in the regression analysis. Biased model residuals indicate that the fitted regression model does not accurately predict isotopic compositions. The requirement that independent environmental parameters are normally distributed can be difficult to ensure in a natural system, particularly with non-uniform geographic distributions of sample sites. Fortunately, in all our analyses both independent variables and model residuals are reasonably well-fit by a normal distribution and do not require subsequent transformations or re-analysis.

### 2.5 Model Results

Statistical analyses for each region and subregion (Figure 2.2) followed the iterative procedures outlined above. Regression models for both a linear and polynomial (e.g., BW model) fit for latitude were analyzed for all regions and subregions to assess

the degree to which a polynomial fit for latitude is required by the data. For the east Asia dataset, in addition to exploring the effects of a polynomial fit for latitude, we also investigated non-linear parameterization of elevation as suggested by Rayleigh distillation modeling studies of precipitation processes at high elevations over the Himalaya-Tibetan Plateau system (Rowley et al., 2001). Table 2.1 summarizes the most reduced multiple regression model that is accepted for each subregion based on the p-value, ANOVA, and VIF criteria outlined in section 2.4.3. For direct comparison of our model results to the BW and regional (Dutton for western US; Liu for east Asia) regression models, model coefficients for the regression model consisting exclusively of latitude (both linear and polynomial fits) and altitude alone are also provided (Table 2.2). In specific subregions (e.g., Basin and Range, North-Central Tibetan Plateau), latitude and elevation alone are statistically verified to sufficiently explain the observed variability in isotopic data. In these cases, the latitude and elevation model is also termed the 'reduced' model.

### *2.5.1 Western US $\delta^{18}O$analysis*

The compiled precipitation isotopic dataset for the western US region was subdivided into four subregions based on physiographic and climatic characteristics (Figure 2.2): (1) Coast, (2) Basin and Range, (3) Rocky Mountain-Colorado Plateau (RMCP) and (4) Great Plains. The Coast and Great Plains subregions are characterized by a proximal dominant seasonal moisture source (Pacific Ocean for the Coast; Gulf of Mexico for the Great Plains), while the Basin and Range and RMCP provinces are subject to complex moisture source interactions (Figure 2.2) and are generally distal from moisture sources. Due to the relatively sparse spatial coverage in the RMCP subregion

## Figure 2.2

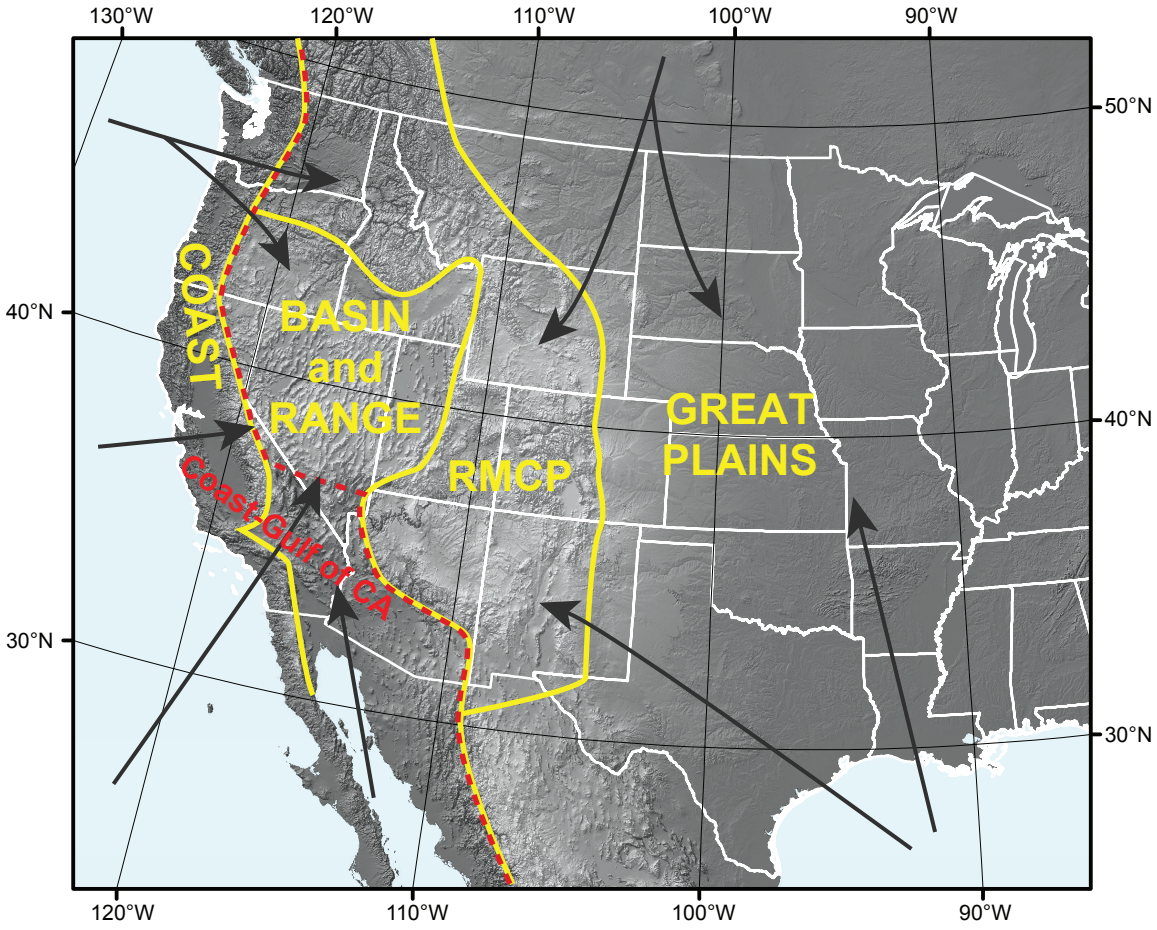


Figure 2.2 – DEM of the western US outlining the physiographic and climatic subregions analyzed as part of this study. Four primary subregions were analyzed in the western US: (1) Coast, (2) Basin and Range, (3) Rocky Mountain-Colorado Plateau (RMCP), and (4) Great Plains. We also analyzed two subregion reorganizations: Coast-Gulf of CA (outlined with red dashed line) and the Continental Interior subregion which combines the Basin and Range and RMCP subregions. Note that the Basin and Range subregion includes all of the Gulf of CA area that is also part of the Coast-Gulf of CA subregion. Arrows indicate the dominant annual moisture sources that deliver moisture to the western US (see Friedman et al., 2000a for discussion). Dominant moisture source varies seasonally depending on location.

and similarity in physiography and moisture source complexity with the Basin and Range subregion, a statistical analysis of a joint Basin and Range-RMCP subregion (Continental Interior) was also performed. A final subregion reorganization was explored based on the influence of the North American monsoon in areas of the southern Basin and Range and Colorado Plateau (Adams and Comrie, 1997). The influence of Gulf of California and Gulf of Mexico-derived moisture to this region during the summer season gives it characteristics more akin to that of the Coast subregion (i.e. close to moisture source, no orographic barrier). The corresponding subregion is termed Coast-Gulf of CA.

Analysis of the full regional dataset (all western US sites) reveals that all independent variables, with the exception of longitude, are required to explain the observed variability in $\delta^{18}O$. The $R^2$ values for both the linear and polynomial models (0.66 and 0.68, respectively) suggest these models sufficiently capture the majority of observed isotopic variability but the magnitude of these $R^2$ values suggest that either isotopic controls and relationships to individual environmental parameters vary on a subregional spatial scale, or that our analysis has not considered important environmental controls (e.g., temperature at moisture source (Vachon et al., 2010); temperature during precipitation event (Kohn and Welker, 2005); individual storm precipitation amount).

Statistical analysis of the Coast subregion of the western US (Fig. 2.2) reveals that latitude, elevation, and mean annual precipitation amount (MAP) are the primary controls on the isotopic composition of regional precipitation and the high $R^2$ value associated with this reduced model (0.86) suggests that $\delta^{18}O$ distributions are well-modeled by these environmental parameters. Both latitude and elevation are negatively correlated with $\delta^{18}O$ (-0.64 ‰/ºN and -3.0 ‰/km, respectively), whereas MAP exhibits a positive

correlation (0.025–0.029 ‰/cm/yr). A regression model of elevation alone reveals that elevation is highly correlated ($R^2$ = 0.76) with precipitation $\delta^{18}O$, with a $\delta^{18}O$-elevation gradient very similar in magnitude to the reduced linear model which also includes the influences of latitude and MAP.

The Great Plains subregion is characterized by a $\delta^{18}O$-elevation gradient (-2.8 to -2.9 ‰/km) similar to that of the Coast subregion, as well as to the global empirical average (-2.8 ‰/km; Poage and Chamberlain, 2001) and the Dutton model (-2.9 ‰/km) gradients. In the Great Plains, latitude and elevation alone act as the primary controls on precipitation $\delta^{18}O$ but model fit ($R^2$ = 0.71) is not as high as in the Coast subregion. In contrast to the Coast subregion, elevation alone accounts for only a minor proportion of subregional $\delta^{18}O$ variability ($R^2$ = 0.2), perhaps due to the limited topographic relief in this geographic region.

The Basin and Range subregion is best-fit by either a reduced model including only latitude and elevation ($R^2$ = 0.78), analogous to the BW and Dutton models, or including mean annual temperature (MAT) alone ($R^2$ = 0.76). The derived $\delta^{18}O$-elevation gradient (~ -1.5‰/km) is significantly reduced in magnitude compared to both the empirical global mean gradient (-2.8‰/km) and the regional gradient of the Dutton model (-2.9‰/km), as well as to those observed in our analysis of the Coast and Great Plains subregions. The similarity in predictive capabilities between the 'MAT-only' and 'latitude + elevation' reduced models is consistent with the high degree of absolute covariance observed among reduced model variables (latitude-MAT= 0.81; elevation-MAT = 0.83).

The Rocky Mountain-Colorado Plateau (RMCP) subregion is unique in that it is the only subregion where elevation is not a required parameter in the reduced linear model; instead latitude and MAT are the only statistically significant controls on precipitation $\delta^{18}O$ ($R^2$ = 0.75). Due to the covariance between elevation and MAT, however, a model of latitude and elevation also fits the data reasonably well ($R^2$=0.66).

The joint Basin and Range-RMCP subregion ("Continental Interior") analysis exhibits similar characteristics to that of the Basin and Range subregion, with a $\delta^{18}O$-elevation gradient lower than the global mean (~ -1.5‰/km), but requiring longitude as a predictor variable for regional $\delta^{18}O$ distribution, with longitude positively correlated with $\delta^{18}O$ (0.13‰/ºE).

The reduced model of the Coast-Gulf of CA subregion has characteristics similar to those of the Coast subregion. Latitude, elevation and MAP are dominant controls on $\delta^{18}O$, and, like the Coast analysis, this subset of environmental parameters produces a linear model with a high $R^2$ value (0.88) and $\delta^{18}O$-elevation gradient (-2.8‰/km) similar to published global and regional averages (Poage and Chamberlain, 2001; Dutton et al., 2005).

As part of our western US analysis we also tested the sensitivity of our approach to single year records. Multi-year precipitation records reveal that significant interannual variability can influence isotopic records, particularly during climatic extremes (e.g., ENSO; Friedman and Smith, 1972; Cole et al., 1999). Over 75% (156 out of 206) of our compiled isotopic records from the western US provide a $\geq$ 2 year record, with many having records of three years of more. The results of regional and subregional analyses

(Table 2.1) for this data subset reveal that longer term records confirm the trends observed in the analyses utilizing annual records. Required environmental parameters and $R^2$ values are consistent for both long-term and single year records, and we again see a reduction in $\delta^{18}O$-elevation gradient for the Basin and Range and Continental Interior subregions (Tables 2.1 and 2.2). The only region that displays any significant variability is the Coast region, with long-term records requiring a greater $\delta^{18}O$-elevation gradient (-3.6 to -4.0‰/km).

### *2.5.2 East Asia $\delta^{18}O$analysis*

The east Asia dataset was subdivided into 3 subregions (Figure 2.3) based on physiographic and climatic characteristics: (1) eastern Asia, (2) Himalaya-Southern Tibet, and (3) North-Central Tibetan Plateau. The eastern Asia subregion is characterized by low to moderate elevations and relative proximity to the dominant annual moisture source, the western Pacific Ocean (Figure 2.3). The Himalayan Mountains are grouped with the southern Tibetan Plateau (south of Lhasa) based on published work indicating that this portion of the Tibetan Plateau receives the vast majority of its moisture from the South Asian monsoon and can thus be considered part of the same precipitation system as the Himalayan front (Tian et al., 2007; Hren et al., 2009). In contrast, interseasonal variability in moisture source, complex moisture source interaction and increased continental moisture recycling characterize much of the North-Central Tibetan Plateau subregion (Tian et al., 2001; Johnson and Ingram, 2004; Liu et al., 2008; Hren et al., 2009). With the exception of the eastern Asia subregion, including a polynomial parameterization for elevation has little to no effect in improving model $R^2$ values (Table 2.2).

## Figure 2.3

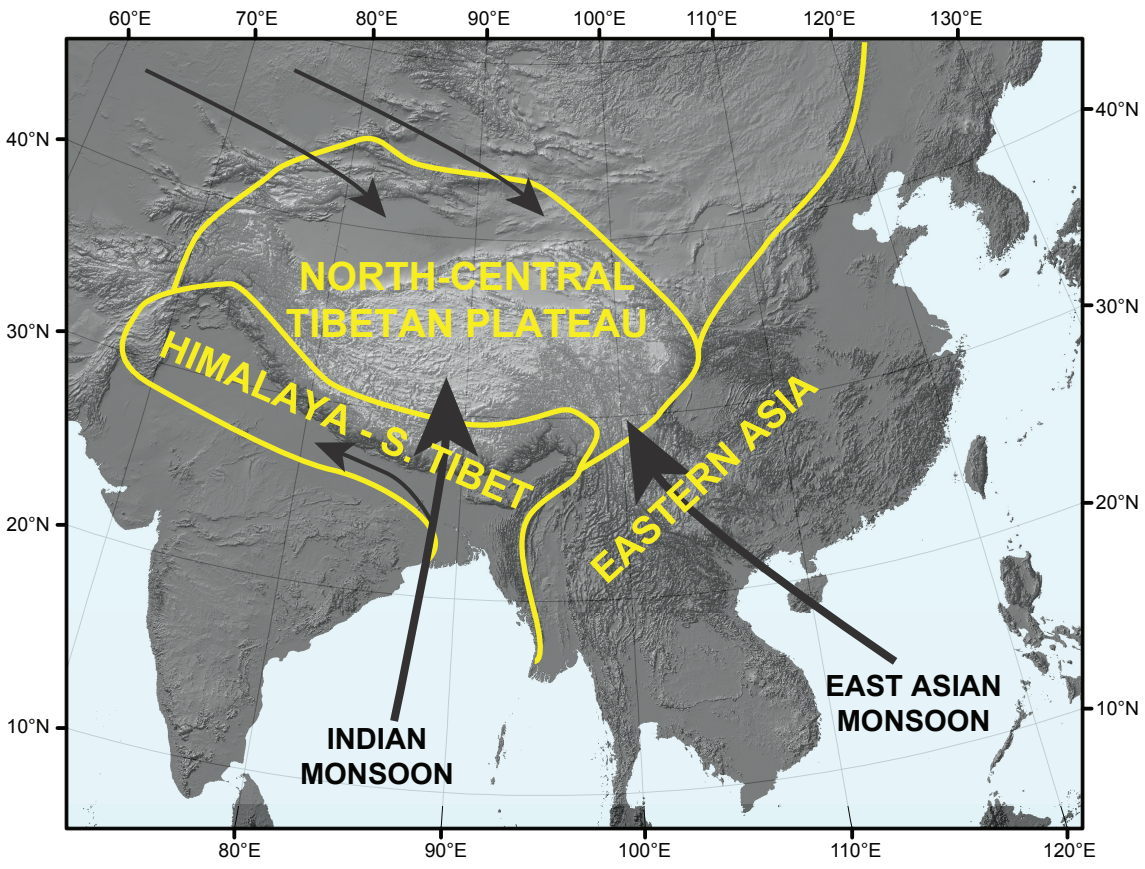


Figure 2.3 – DEM of east Asia region outlining the physiographic and climatic subregions analyzed as part of this study: (1) Eastern Asia, (2) Himalaya-South Tibet and (3) North-Central Tibetan Plateau. Dominant annual moisture sources shown by arrows (modified from Liu et al., 2008 and Hren et al., 2009). The dominant summer moisture sources, highlighted by enlarged arrows (Indian monsoon and East Asian monsoon), contribute the vast majority of annual precipitation to the Himalaya-South Tibet and Eastern Asia subregions, whereas the North-Central Tibetan Plateau is subject to increased influence from moisture sources north and west of the Plateau.

**TABLE 2.1** – Reduced multiple regression models for Western US and East Asia

| Region/Subregion | Regression Model | Coefficients | | | | | | | |
|---|---|---|---|---|---|---|---|---|---|
| | | $LAT^2$ | LAT(°) | LON(°) | ELEV (m) | MAT (°C) | MAP (cm/yr) | Intercept | $R^2$ |
| ***WESTERN US ALL RECORDS*** | | | | | | | | | |
| *All Sites* | Linear | | -0.44 | 0.10 | -0.0025 | | 0.017 | 18.7 | 0.77 |
| *LAT+LON+ELEV+MAP* | Poly(LAT) | 0.0006 | -0.49 | 0.10 | -0.0025 | | 0.017 | 19.6 | 0.77 |
| *Coast* | Linear | | -0.64 | | -0.0030 | | 0.029 | 13.8 | 0.85 |
| *LAT+ELEV+MAP* | Poly(LAT) | 0.0251 | -2.54 | | -0.0030 | | 0.025 | 49.9 | 0.86 |
| *Basin and Range* | Linear* | | -0.57 | | -0.0015 | | | 10.9 | 0.78 |
| *LAT+ELEV* | Poly(LAT)* | 0.0061 | -1.04 | | -0.0014 | | | 19.9 | 0.78 |
| *RMCP* | Linear | | -0.27 | | | 0.49 | | -5.8 | 0.75 |
| *LAT+MAT* | Poly(LAT) | -0.0036 | 0.03 | | | 0.50 | | -11.9 | 0.75 |
| *Continental Interior* | Linear | | -0.52 | 0.13 | -0.0016 | | | 24.8 | 0.72 |
| *LAT+LON+ELEV* | Poly(LAT) | 0.0158 | -1.77 | 0.11 | -0.0014 | | | 46.7 | 0.72 |
| *Great Plains* | Linear* | | -0.41 | | -0.0028 | | | 9.1 | 0.71 |
| *LAT+ELEV* | Poly(LAT)* | -0.0042 | -0.08 | | -0.0029 | | | 2.9 | 0.71 |
| *Coast-Gulf of CA* | Linear | | -0.63 | | -0.0028 | | 0.026 | 13.6 | 0.81 |
| *LAT+ELEV+MAP* | Poly(LAT) | 0.0217 | -2.24 | | -0.0027 | | 0.023 | 43.3 | 0.81 |
| ***WESTERN US ≥ 2 YEAR RECORDS*** | | | | | | | | | |
| *All Sites* | Linear | | -0.42 | 0.08 | -0.0027 | | 0.019 | 15.7 | 0.77 |
| *LAT+LON+ELEV+MAP* | Poly(LAT) | -0.0045 | -0.07 | 0.08 | -0.0027 | | 0.019 | 9.0 | 0.77 |
| *Coast* | Linear | | -0.71 | | -0.0037 | | 0.036 | 17.8 | 0.90 |
| *LAT+ELEV+MAP* | Poly(LAT) | -0.0467 | 2.73 | | -0.0040 | | 0.052 | -45.9 | 0.91 |
| *Basin and Range* | Linear* | | -0.51 | | -0.0018 | | | 9.1 | 0.79 |
| *LAT+ELEV* | Poly(LAT)* | 0.0022 | -0.67 | | -0.0017 | | | 12.2 | 0.79 |
| *Continental Interior* | Linear | | -0.49 | 0.14 | -0.0017 | | | 24.7 | 0.72 |
| *LAT+LON+ELEV* | Poly(LAT) | 0.0112 | -1.39 | 0.12 | -0.0016 | | | 40.3 | 0.72 |
| *Great Plains* | Linear* | | -0.41 | | -0.0028 | | | 9.1 | 0.70 |
| *LAT+ELEV* | Poly(LAT)* | -0.0042 | -0.08 | | -0.0029 | | | 2.8 | 0.70 |
| *Coast-Gulf of CA* | Linear | | -0.66 | | -0.0032 | | 0.036 | 15.0 | 0.87 |
| *LAT+ELEV+MAP* | Poly(LAT) | -0.0421 | 2.42 | | -0.0036 | | 0.050 | -41.2 | 0.88 |
| ***EASTERN ASIA*** | | | | | | | | | |
| *All Sites* | Linear | | 0.29 | | -0.0012 | 0.09 | 0.013 | -18.4 | 0.66 |
| *LAT+ELEV+MAT+MAP* | Poly(LAT) | -0.0264 | 2.03 | | -0.0014 | 0.11 | 0.010 | -45.6 | 0.68 |
| *Eastern Asia* | Linear | | -0.07 | -0.10 | -0.0022 | | | 6.6 | 0.68 |
| *LAT+LON+ELEV* | Poly(LAT) | -0.0077 | 0.42 | -0.06 | -0.0020 | | | -5.1 | 0.79 |
| *Himalaya-S. Tibet* | Linear | | 0.58 | 0.18 | -0.0031 | | | -35.3 | 0.85 |
| *LAT+LON+ELEV* | Poly(LAT) | 0.2048 | -11.19 | 0.18 | -0.0031 | | | 133.7 | 0.86 |
| *North-Central Tibet* | Linear* | | 1.15 | | -0.0007 | | | -47.1 | 0.69 |
| *LAT+ELEV* | Poly(LAT)* | -0.1270 | 9.37 | | -0.0015 | | | -175.8 | 0.71 |
| *Himalaya only* | Linear | | | 0.07 | -0.0033 | | | -8.6 | 0.92 |
| *(LAT or Lon)+ELEV* | Linear B* | | -0.26 | | -0.0033 | | | 4.7 | 0.91 |
| | Poly(LAT)* | 0.0960 | -5.61 | | -0.0033 | | | 79.1 | 0.91 |
| *All Tibet* | Linear | | 1.01 | 0.21 | -0.0012 | | | -59.4 | 0.57 |
| *LAT+LON+ELEV* | Poly(LAT) | -0.1861 | 13.02 | 0.24 | -0.0019 | | | -251.6 | 0.62 |

**Table 2.1 Notes** – Reduced multivariate linear regression models for all regions and subregions of the western US and east Asia with environmental parameter coefficients provided. Poly(LAT) indicates models fit with a polynomial function of latitude in combination with linear parameterization of remaining environmental parameters. *Indicates that the statistically-verified reduced regression model consists of only latitude and elevation.

**TABLE 2.2** – Regression model coefficients for models with latitude and elevation

| Region/ Subregion | Regression Model | Coefficients | | | | | |
|---|---|---|---|---|---|---|---|
| | | $LAT^2$ | LAT(°) | $ELEV^2$ | ELEV(m) | Intercept | $R^2$ |
| | | ***WESTERN US*** | | | | | |
| *All Sites* | LAT+ELEV | | -0.37 | | -0.0028 | 6.1 | 0.69 |
| | $LAT^2$+LAT+ELEV | 0.0165 | -1.67 | | -0.0027 | 31.1 | 0.70 |
| | ELEV only | | | | -0.0027 | -8.3 | 0.55 |
| *Coast* | LAT+ELEV | | -0.24 | | -0.0031 | 1.0 | 0.78 |
| | $LAT^2$+LAT+ELEV | 0.0481 | -3.98 | | -0.0030 | 73.5 | 0.81 |
| | ELEV only | | | | -0.0028 | -8.5 | 0.76 |
| *Basin and Range* | LAT+ELEV | | -0.57 | | -0.0015 | 10.9 | 0.78 |
| | $LAT^2$+LAT+ELEV | 0.0061 | -1.04 | | -0.0014 | 19.9 | 0.78 |
| | ELEV only | | | | -0.0024 | -9.1 | 0.51 |
| *RMCP* | LAT+ELEV | | -0.63 | | -0.0021 | 16.1 | 0.66 |
| | $LAT^2$+LAT+ELEV | -0.0022 | -0.45 | | -0.0021 | 12.7 | 0.66 |
| | ELEV only | | | | -0.0009 | -11.5 | 0.04 |
| *Continental Interior* | LAT+ELEV | | -0.53 | | -0.0015 | 9.6 | 0.69 |
| | $LAT^2$+LAT+ELEV | 0.0252 | -2.52 | | -0.0012 | 48.5 | 0.71 |
| | ELEV only | | | | -0.0020 | -9.6 | 0.34 |
| *Great Plains* | LAT+ELEV | | -0.41 | | -0.0028 | 9.1 | 0.71 |
| | $LAT^2$+LAT+ELEV | -0.0042 | -0.08 | | -0.0029 | 2.9 | 0.71 |
| | ELEV only | | | | -0.0029 | -6.8 | 0.20 |
| *Coast-Gulf of CA* | LAT+ELEV | | -0.23 | | -0.0028 | 0.3 | 0.75 |
| | $LAT^2$+LAT+ELEV | 0.0442 | -3.60 | | -0.0026 | 64.1 | 0.78 |
| | ELEV only | | | | -0.0027 | -8.4 | 0.72 |
| | | ***EAST ASIA*** | | | | | |
| *All Sites* | LAT+ELEV | | 0.10 | | -0.0019 | -9.2 | 0.65 |
| | $LAT^2$+LAT+ELEV | -0.0292 | 2.04 | | -0.0021 | -40.0 | 0.65 |
| | $LAT^2$+LAT+$ELEV^2$+ELEV | -0.0302 | 2.09 | 4.50E-08 | -0.0024 | -40.4 | 0.65 |
| | ELEV only | | | | -0.0019 | -6.1 | 0.62 |
| *Eastern Asia* | LAT+ELEV | | -0.12 | | -0.0014 | -3.4 | 0.60 |
| | $LAT^2$+LAT+ELEV | -0.0090 | 0.47 | | -0.0015 | -12.5 | 0.76 |
| | $LAT^2$+LAT+$ELEV^2$+ELEV | -0.0083 | 0.42 | -7.70E-07 | -0.0003 | -11.8 | 0.78 |
| | ELEV only | | | | -0.0010 | -7.4 | 0.14 |
| *Himalaya-S. Tibet* | LAT+ELEV | | 0.48 | | -0.0029 | -17.0 | 0.79 |
| | $LAT^2$+LAT+ELEV | 0.1942 | -10.69 | | -0.0029 | 143.3 | 0.80 |
| | $LAT^2$+LAT+$ELEV^2$+ELEV | 0.2190 | -12.10 | -2.16E-07 | -0.0016 | 161.8 | 0.81 |
| | ELEV only | | | | -0.0028 | -3.6 | 0.79 |
| *North-Central Tibet* | LAT+ELEV | | 1.15 | | -0.0007 | -47.1 | 0.69 |
| | $LAT^2$+LAT+ELEV | -0.1270 | 9.37 | | -0.0015 | -175.8 | 0.71 |
| | $LAT^2$+LAT+$ELEV^2$+ELEV | -0.1041 | 7.96 | -2.35E-07 | 0.0005 | -158.3 | 0.71 |
| | ELEV only | | | | -0.0019 | -5.2 | 0.22 |
| *Himalaya only* | LAT+ELEV | | -0.26 | | -0.0033 | 4.7 | 0.91 |
| | $LAT^2$+LAT+ELEV | 0.0960 | -5.61 | | -0.0033 | 79.1 | 0.91 |
| | $LAT^2$+LAT+$ELEV^2$+ELEV | 0.0747 | -4.39 | -3.37E-07 | -0.0015 | 59.6 | 0.92 |
| | ELEV only | | | | -0.0034 | -2.8 | 0.91 |
| *All Tibet* | LAT+ELEV | | 0.91 | | -0.0018 | -34.3 | 0.52 |
| | $LAT^2$+LAT+ELEV | -0.1596 | 11.20 | | -0.0025 | -196.2 | 0.56 |
| | $LAT^2$+LAT+$ELEV^2$+ELEV | -0.1477 | 10.71 | -4.68E-07 | 0.0019 | -222.6 | 0.63 |
| | ELEV only | | | | -0.0018 | -6.0 | 0.22 |

**Table 2.2 notes** – Regression model coefficients for models of latitude and elevation alone (i.e. analogous to the BW model). Coefficients and intercepts for elevation only (ELEV only) regression models also provided. In our east Asia statistical analysis, the influence of both elevation and latitude polynomial parameterization were also investigated.

Statistical analysis of all east Asia $\delta^{18}O$ collection sites constrains latitude, elevation, MAT, and MAP to be primary controls on $\delta^{18}O$ variability with an $R^2$ value of 0.68 (Table 2.1). In all subregional analyses, however, MAP and MAT are not significant independent parameters and $\delta^{18}O$ can be modeled as a function of geographic parameters alone. In the eastern Asia subregion, latitude, longitude, and elevation account for most of the observed variability in $\delta^{18}O$ ($R^2 = 0.79$), with a subregional $\delta^{18}O$-elevation gradient of -1.5 to -2.0 ‰/km calculated, similar in magnitude to the regional Liu model (-1.5 ‰/km). The variability in $\delta^{18}O$-elevation gradient magnitude in our analyses is dependent upon the inclusion of longitude in the regression model (Tables 2.1 and 2.2).

The Himalayan-South Tibet subregion analysis indicates latitude, longitude, and elevation are the dominant controls on and good predictors ($R^2 = 0.86$) of meteoric $\delta^{18}O$. The observed $\delta^{18}O$-elevation gradient for this subregion is -3.1‰/km, similar in magnitude to empirical meteoric water isotope-elevation gradients along the Himalayan front (Garzione et al., 2000), global averages (Poage and Chamberlain, 2001), and gradients for the Coast and Great Plains subregions of the western US derived in this study. Analysis of only the Himalayan region (i.e. without South Tibet) produces similar trends ($R^2 = 0.91$; $\delta^{18}O$-elevation gradient = -3.3‰/km) to the Himalaya-South Tibet analysis.

North-Central Tibetan Plateau $\delta^{18}O$ is modeled effectively ($R^2 = 0.71$) as a function of latitude and elevation alone with a corresponding $\delta^{18}O$-elevation gradient of -1.5 ‰/km. Analysis of all Tibetan Plateau (South Tibet and North-Central Tibet) results

in a significantly reduced model $R^2$ value (0.56) as well as a higher magnitude $\delta^{18}O$-elevation gradient of -2.5‰/km.

### 2.6 Calculating model uncertainty

Model uncertainties were calculated for all regions and subregions through comparison of actual $\delta^{18}O$ and elevation values with $\delta^{18}O$ and elevation values calculated using model-derived coefficients and intercepts. We also compared our modeled-derived uncertainties with those derived from predicted isotopic and elevation values using BW, Dutton and Liu model parameters. Predicted $\delta^{18}O$ values are calculated using all appropriate independent environmental parameter coefficients for each reduced model. Model-predicted elevations are calculated using the following equation:

$$Model\ Elevation\ (m) = \frac{(\delta^{18}O_{Actual} - \delta^{18}O_{Sea\ level})}{(\delta^{18}O/elevation)_{model}} \quad \text{(Eq. 2)}$$

where $\delta^{18}O_{sea\ level}$ is calculated using all model variables and coefficients except elevation, effectively calculating model $\delta^{18}O$ at zero elevation. The difference between actual $\delta^{18}O$ and model-predicted sea level $\delta^{18}O$ is thus assumed to be solely a function of site elevation which we calculate using the regional or subregional $\delta^{18}O$-elevation gradient [$(\delta^{18}O/elevation)_{model}$]. Table 2.3 lists and Figures 2.4 – 2.6 show model uncertainties at 95% (2σ) confidence intervals for predicted $\delta^{18}O$ and elevation values. Model-predicted $\delta^{18}O$ (Figure 2.4) and elevation (Figures 2.5 and 2.6) values consistently plot along a 1:1 line for all statistical models derived in this study, which is required by

**TABLE 2.3** – Regression model elevation uncertainties

| Subregion | Model | 2σ (± m) | Slope | Intercept |
|---|---|---|---|---|
| | ***WESTERN US*** | | | |
| *Western US ALL* | This Study | 1345 | 1.00 | 1 |
| | Dutton model | 1359 | 0.97 | 736 |
| | BW model | 2041 | 1.40 | 1130 |
| *Coast* | This Study | 898 | 1.00 | 3 |
| | Dutton model | 1168 | 1.09 | 692 |
| | BW model | 1675 | 1.53 | 1146 |
| *Basin and Range* | This Study | 1777 | 0.99 | 2 |
| | Dutton model | 974 | 0.65 | 1424 |
| | BW model | 1556 | 1.04 | 1931 |
| *RMCP* | This Study | 1964 | 1.00 | 0 |
| | Dutton model | 1688 | 0.58 | 1173 |
| | BW model | 2769 | 0.72 | 2091 |
| *Continental Interior* | This Study | 2156 | 1.00 | 9 |
| | Dutton model | 1195 | 0.59 | 1438 |
| | BW model | 1904 | 0.92 | 2019 |
| *Great Plains* | This Study | 1221 | 0.99 | 0 |
| | Dutton model | 1258 | 1.02 | 155 |
| | BW model | 2090 | 1.48 | 309 |
| *Coast-Gulf of CA* | This Study | 1059 | 1.00 | 3 |
| | Dutton model | 1177 | 0.97 | 888 |
| | BW model | 1683 | 1.40 | 1293 |
| | ***EASTERN ASIA*** | | | |
| *ASIA ALL* | This Study | 2285 | 1.00 | -7 |
| | Liu model | 3484 | 1.31 | -546 |
| | BW model | 2622 | 0.98 | 700 |
| *Eastern Asia* | This Study | 629 | 0.99 | 3 |
| | Liu model | 950 | 1.07 | -32 |
| | BW model | 747 | 0.79 | 1103 |
| *Himalaya- S. Tibet* | This Study | 1048 | 1.00 | 40 |
| | Liu model | 2625 | 1.83 | -1833 |
| | BW model | 1971 | 1.37 | -286 |
| *North-Central Tibet* | This Study | 2385 | 0.99 | 39 |
| | Liu model | 4073 | 1.35 | -1689 |
| | BW model | 3061 | 1.01 | -177 |

**Table 2.3 Notes** – 2σ elevation uncertainty values for all western US and east Asia subregions. Uncertainties derived from BW, Dutton and Liu regression models are included for comparison. 2σ values were calculated from linear regression of model-predicted elevations versus actual elevations (Figures 2.5 and 2.6). See text for discussion on how model-predicted elevations were calculated. Note that in some cases published regional or global models have lower 2σ uncertainty values than uncertainties derived from this analysis. However, in many of these cases the published regression model is typified by model vs. actual slopes significantly different than 1 due systematic over- or underpredictions of site elevations as reflected by intercept values significantly different than 0 (e.g. Dutton model for Basin and Range).

## Figure 2.4

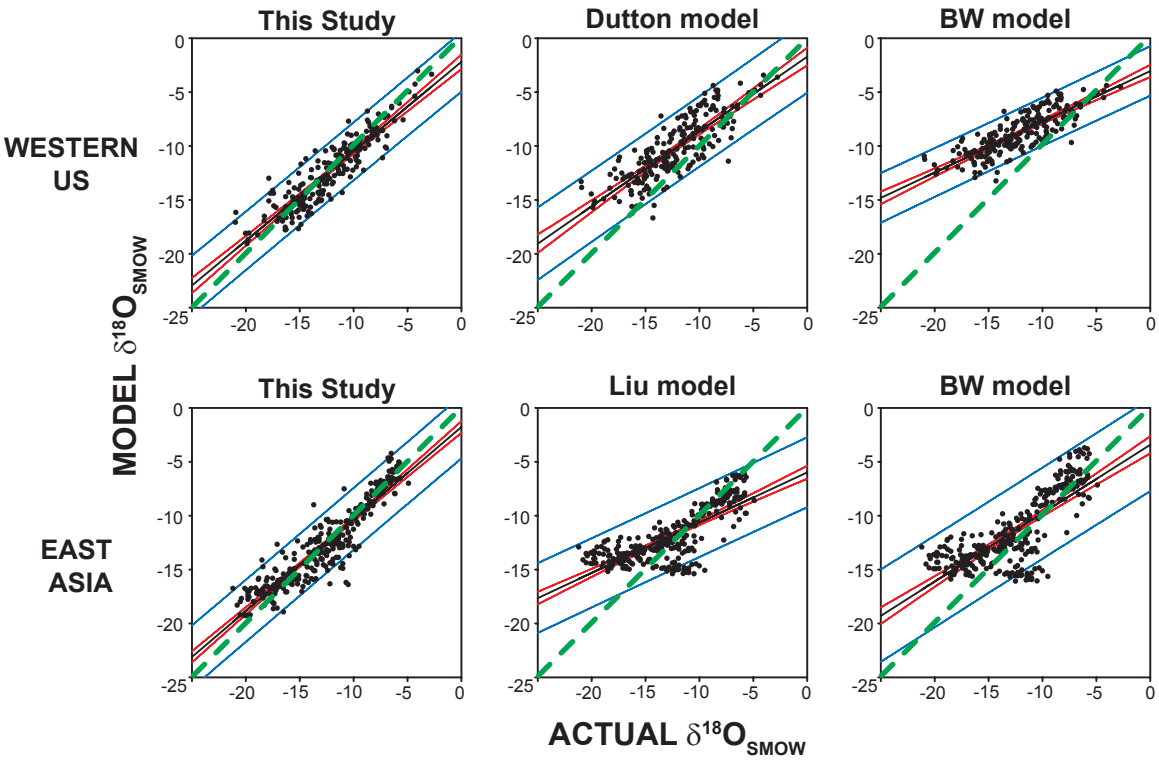


Figure 2.4 – Plots showing model predicted $\delta^{18}O$ versus actual site $\delta^{18}O$ values. Predicted values are calculated using multiple regression model coefficients derived in this study and are compared to predicted values calculated using regional (Dutton et al., 2005; Liu et al., 2008) and global (Bowen and Wilkinson, 2002) regression model coefficients. Red lines mark the 95% (2σ) confidence interval on the best-fit regression and blue lines mark the 95% (2σ) prediction interval for the regression. Dashed green line indicates 1:1 line (actual $\delta^{18}O$ = model-predicted $\delta^{18}O$). All models are plotted at the same scale for direct comparison.

our modeling approach as our statistical models are best fits to all data points in each region and subregion. Performance of the BW model and regional models (Dutton model for western US; Liu model for east Asia) is regionally variable and is discussed below. Figures 2.7 – 2.10 show contour maps for regional $\delta^{18}O$ and elevation residuals to highlight spatial trends in model (this study and published) predictive capabilities.

*2.6.1 $\delta^{18}O$ uncertainty*

Using the derived environmental parameter coefficients associated with the best-fit, reduced regression model for each subregion (Table 2.1), we calculate model-predicted $\delta^{18}O$ values at precipitation collection sites in the western US and east Asia. Average model $\delta^{18}O$ residuals (difference between model predicted and observed $\delta^{18}O$) are ±1.1‰ and ±1.2‰ for the western US and east Asia, respectively. Compiling subregional model-predicted $\delta^{18}O$ values to calculate average model residuals for the full region has the advantage of reducing average regional residual values in comparison to residuals calculated using a single best-fit regression model for the full regional dataset (±1.3‰ for western US; ±1.9‰ for east Asia), but the compilation of distinct, subregional regression models violates the assumption that all sites are fit equally well by the same model, resulting in slight deviations from a 1:1 line in plots of model-predicted $\delta^{18}O$ versus observed $\delta^{18}O$ (Figure 2.4; Western US slope = 0.83; East Asia slope = 0.85). High $R^2$ values for model versus predicted $\delta^{18}O$ values in both the western US ($R^2 = 0.82$) and east Asia ($R^2 = 0.85$) indicate that the regression models derived in this study account for a significant portion of the variability observed in modern $\delta^{18}O$ distributions in both regions. Additionally, our regression models consistently more

accurately predict modern $\delta^{18}O$ values in comparison to published regional (Dutton and Liu) and global (BW model) regression models (Figures 2.7 and 2.8). Application of regional model coefficients yields average model residuals of 2.3‰ for the western US (Dutton model) and 2.2‰ for east Asia (Liu model). In both regions, the BW model produces the highest absolute model residuals, with average values of 3.5‰ in the western US and 2.4‰ in east Asia. The BW model also consistently overpredicts $\delta^{18}O$ values, particularly for sites with low (< -15‰) weighted mean annual $\delta^{18}O$ values (Figure 2.4).

*2.6.2 Elevation uncertainty*

Similar to our $\delta^{18}O$ uncertainty analysis, the reduced regression models derived in this study consistently perform as well or better at predicting site elevations than existing regional and global predictive models in both the western US and east Asia (Table 2.3, Figures 2.5 and 2.6). Model accuracy, however, is subregion dependent. Elevation uncertainties ($2\sigma$) for regression models derived in this study are lowest for the Coast (±898 m), Great Plains (±1221 m), and Coast-Gulf of CA (±1059 m) subregions and highest for the Basin and Range (±1777 m), Rocky Mountain-Colorado Plateau (±1964 m), and joint Continental Interior (±2156 m) subregions in the western US. In east Asia, $2\sigma$ model uncertainties range from ±629 m for the eastern Asia subregion, to ±1048 m in the Himalayan-South Tibet subregion and up to ±2385 m in the North-Central Tibetan Plateau.

Regional (Dutton and Liu models) and global (BW model) regression models exhibit varying levels of accuracy at predicting site elevations depending on subregion

## Figure 2.5

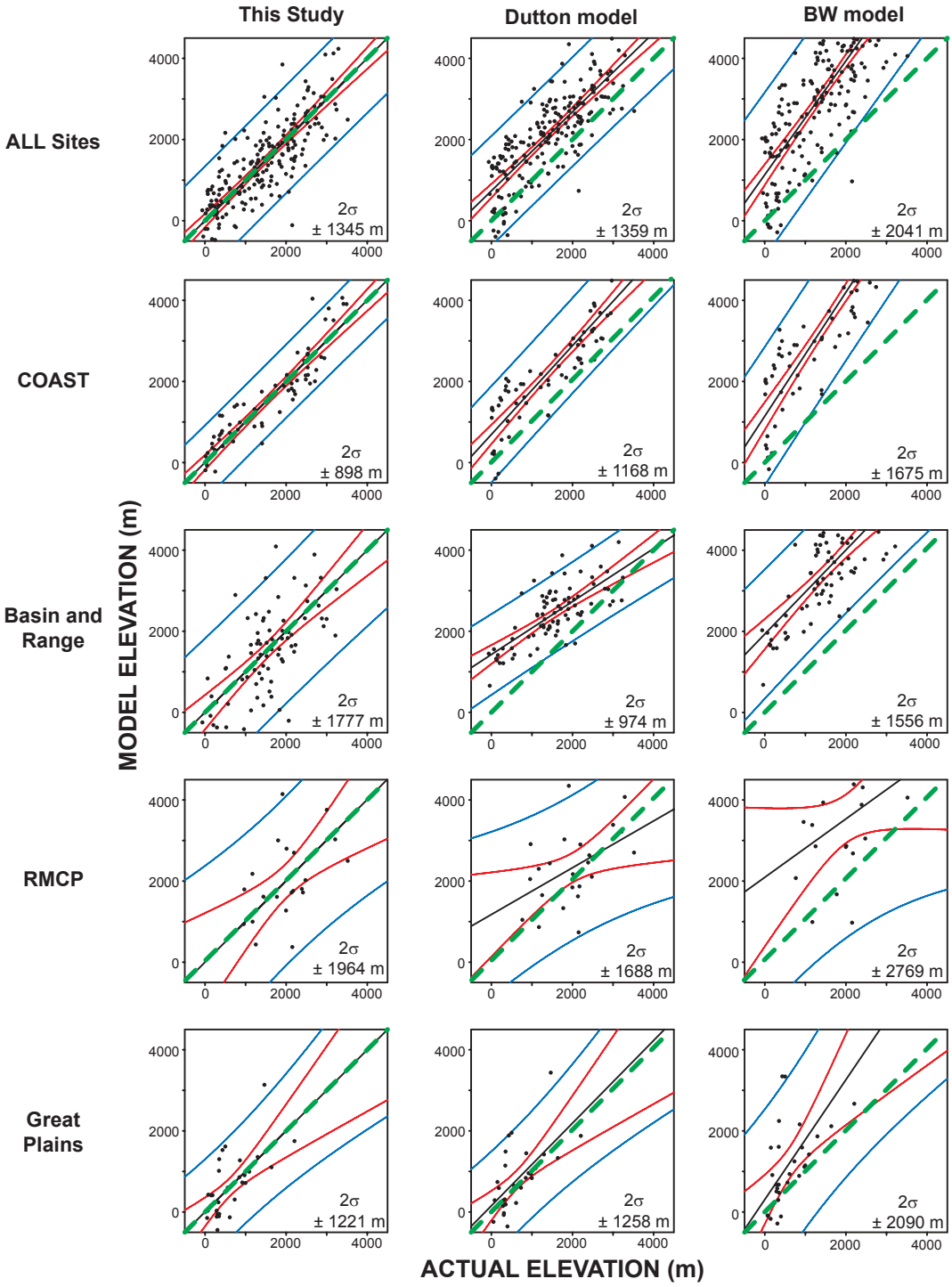


Figure 2.5 - Western US model predicted site elevations versus actual elevations. Calculated using regression coefficients of reduced linear models derived in this study (see text for discussion), as well as coefficients of published regional (Dutton et al., 2005) and global (Bowen and Wilkinson, 2002) regression models for comparison. Red lines mark the 95% (2σ) confidence interval on the best-fit regression and blue lines mark the 95% (2σ) prediction interval for the regression (2σ uncertainties also provided in Table 2.3). Dashed green line indicates 1:1 line (actual elevation = model-predicted elevation). All subregions and models are plotted at the same scale for direct comparison of model performance.

## Figure 2.6

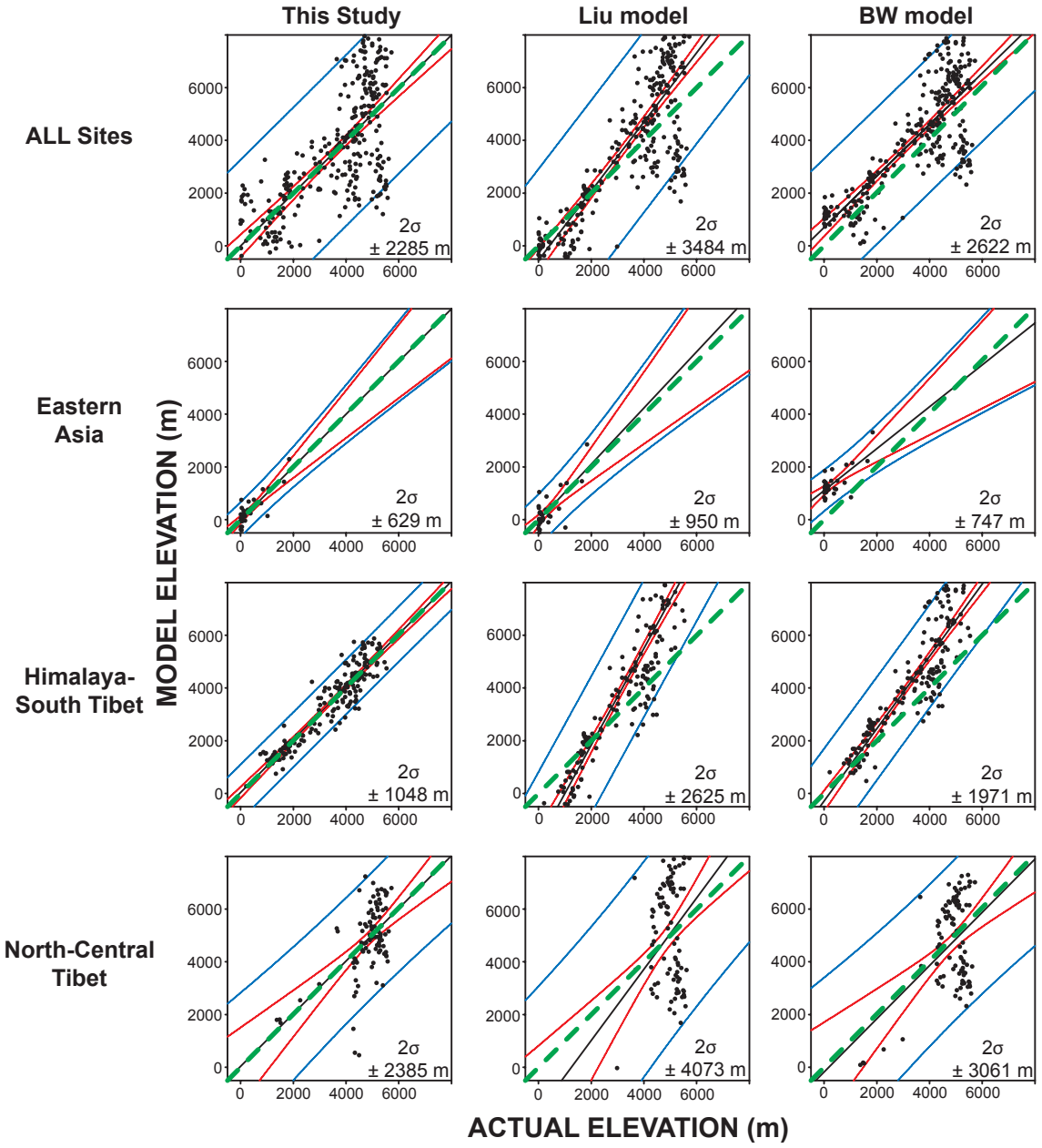


Figure 2.6 – East Asia model predicted elevations versus actual elevations. See Figure 2.5 caption for additional information on plots. In this region the relevant regional model is from Liu and others (2008). See Table 2.3 for uncertainty values.

## Figure 2.7

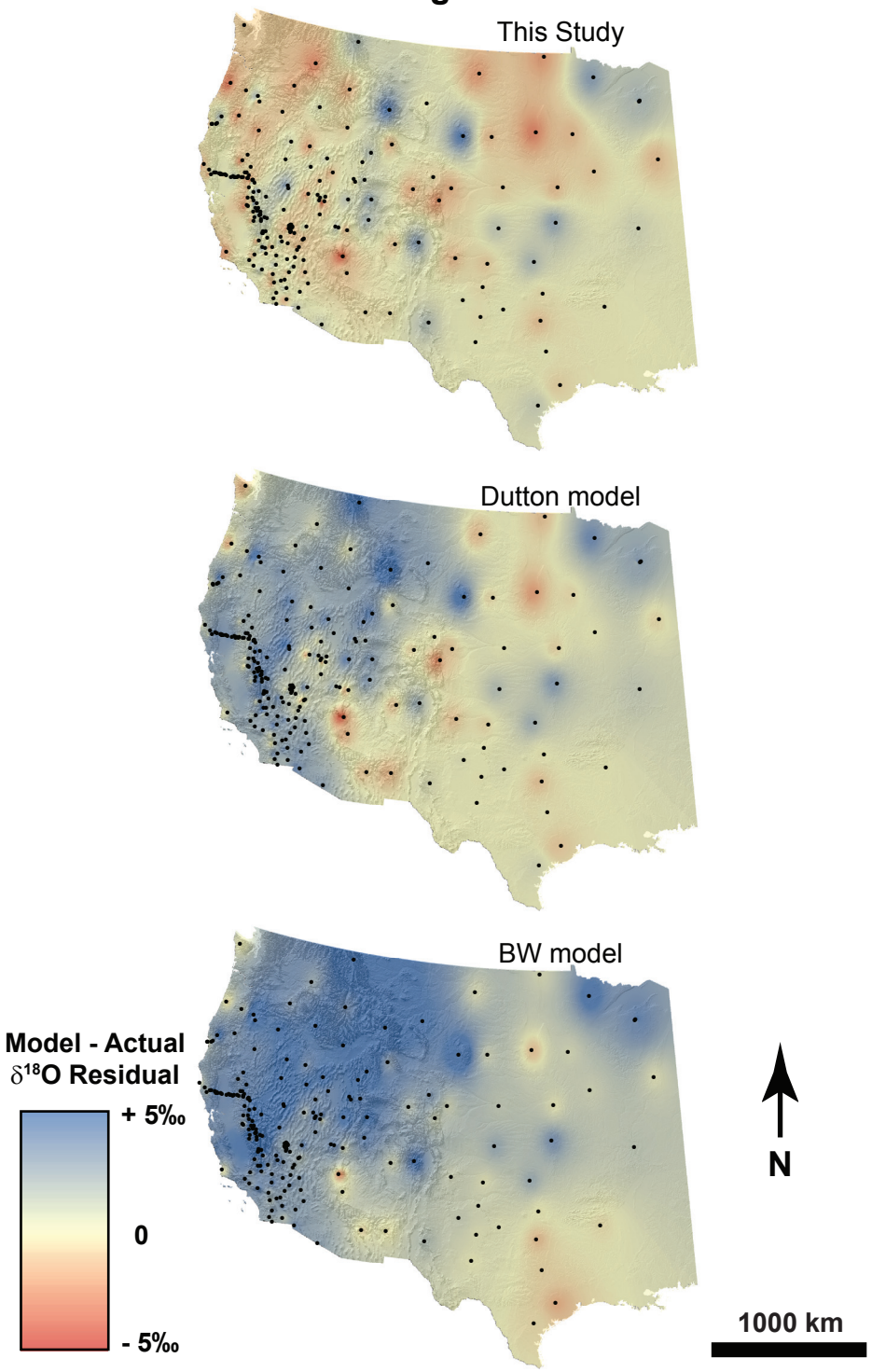


Figure 2.7 – Western US model $\delta^{18}O$ residuals contoured using ArcGIS Inverse Distance Weighted algorithm. Dutton and BW models are shown for comparison. All model residuals are plotted at the same color-scale, but note that some sites are characterized by model residuals with magnitudes greater than the ±5‰ cutoff, particularly the BW model for sites in the northern Basin and Range and RMCP subregions. The majority of western US sites have model residuals between -2 and +2‰ when calculated using our model coefficients. Site locations shown by black dots.

## Figure 2.8

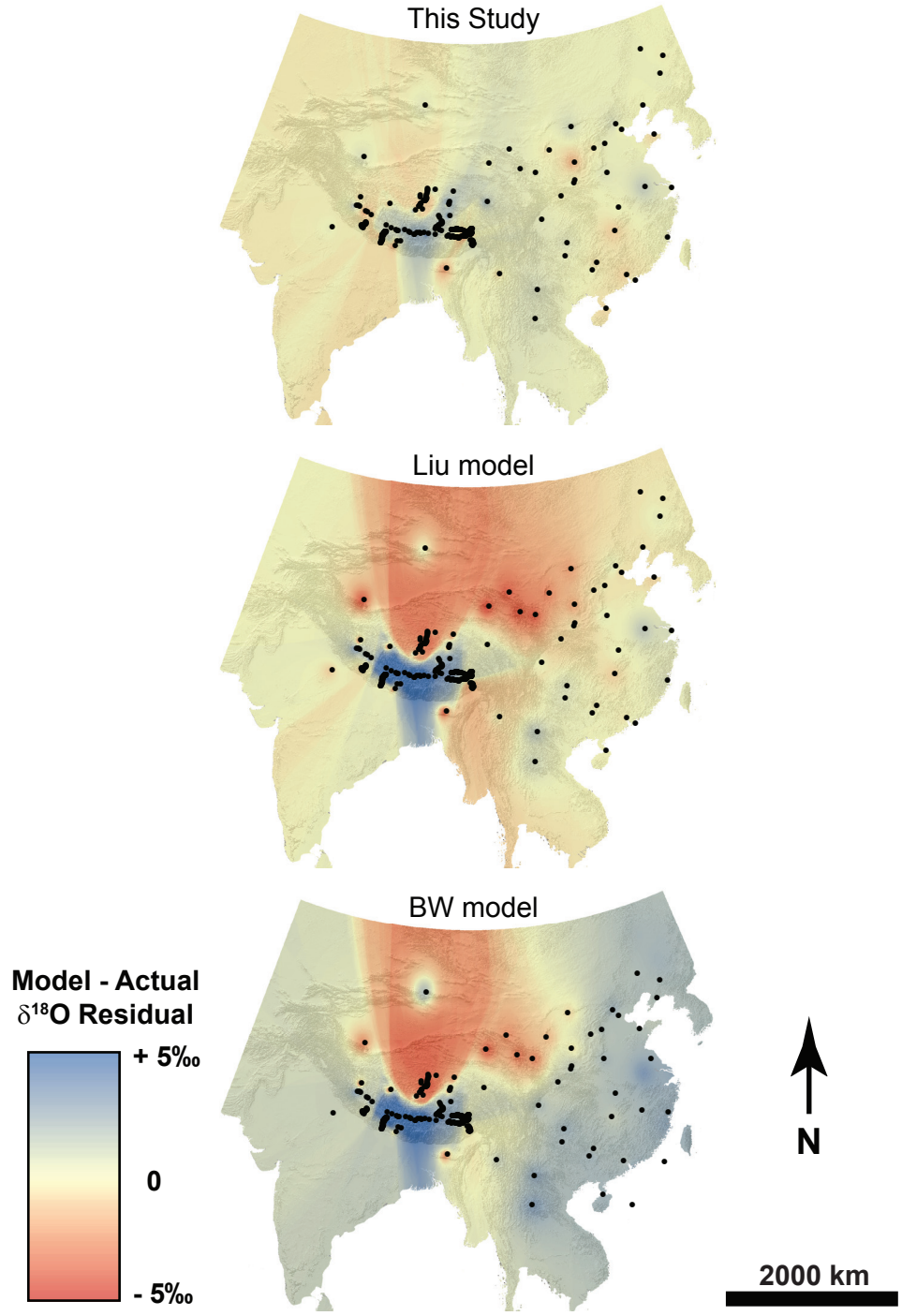


Figure 2.8 – Smoothed contour map of east Asia model $\delta^{18}O$ residuals. Liu and BW models are shown for comparison. The color patterns indicate that both the regional (Liu model) and global (BW model) regression models significantly underpredict meteoric $\delta^{18}O$ values at most central and northern Tibetan Plateau sites and overpredict $\delta^{18}O$ values for Himalaya and southern Tibetan Plateau locations. In some cases the color code is saturated at the extremes due to absolute residual values greater than ±5‰ (see Table 2.3 for uncertainty values). Site locations shown by black dots. Note that some regions (e.g. India, northern margin of Tibetan Plateau) have sparse data coverage. As a result, caution should be taken when interpreting contoured residual values in these regions.

## Figure 2.9

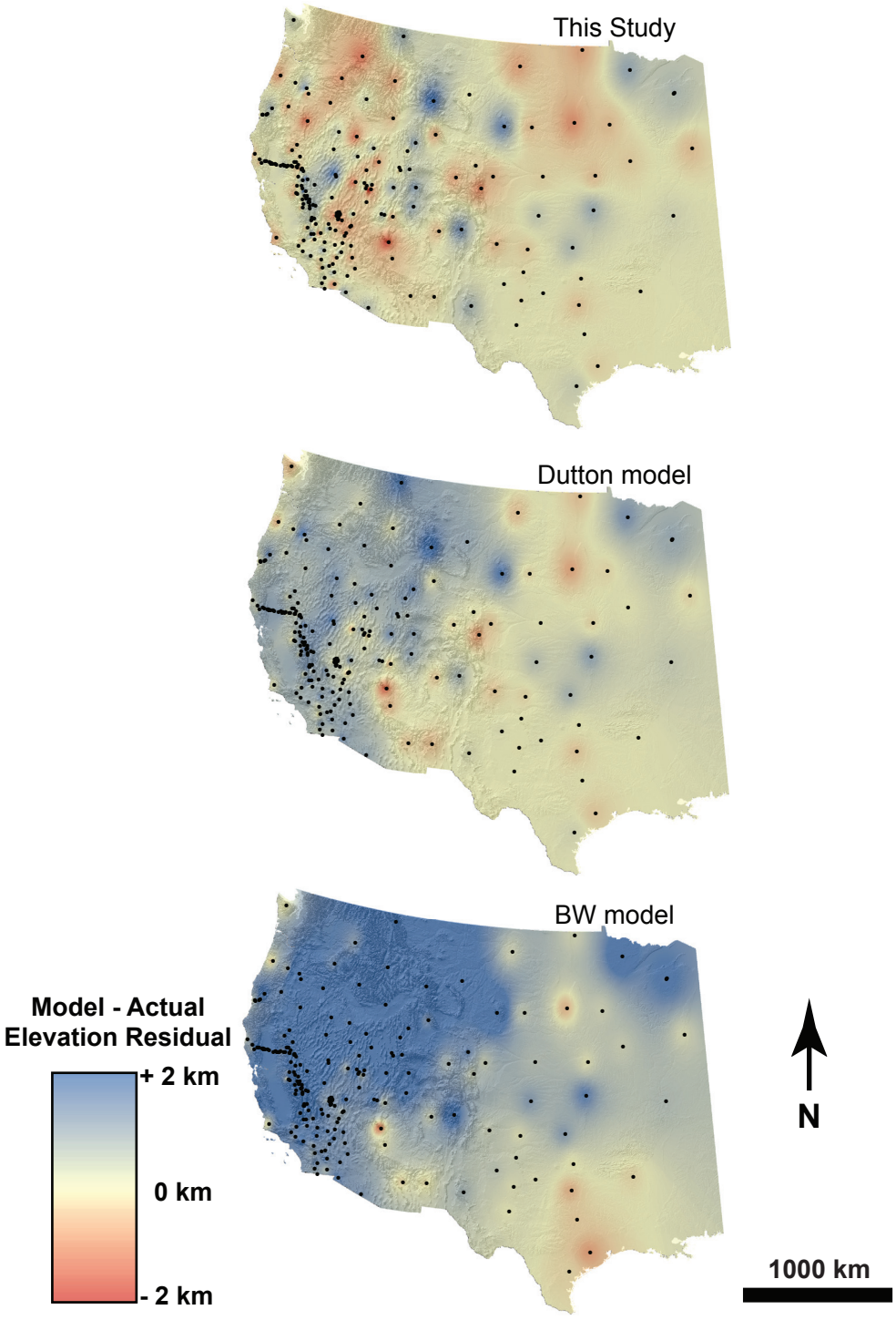


Figure 2.9 - Western US model-predicted elevation residuals. Dutton and BW models are shown for comparison. Some sites have elevation residuals > + 2km (darkest blues) and cannot be distinguished by the colorscale. Note that both the Dutton and BW models consistently overpredict site elevations in the Basin and Range and northern RMCP subregions with the BW model producing extreme overpredictions (> 2 km) at many of these sites (see Figure 2.5). Site locations shown by black dots.

## Figure 2.10

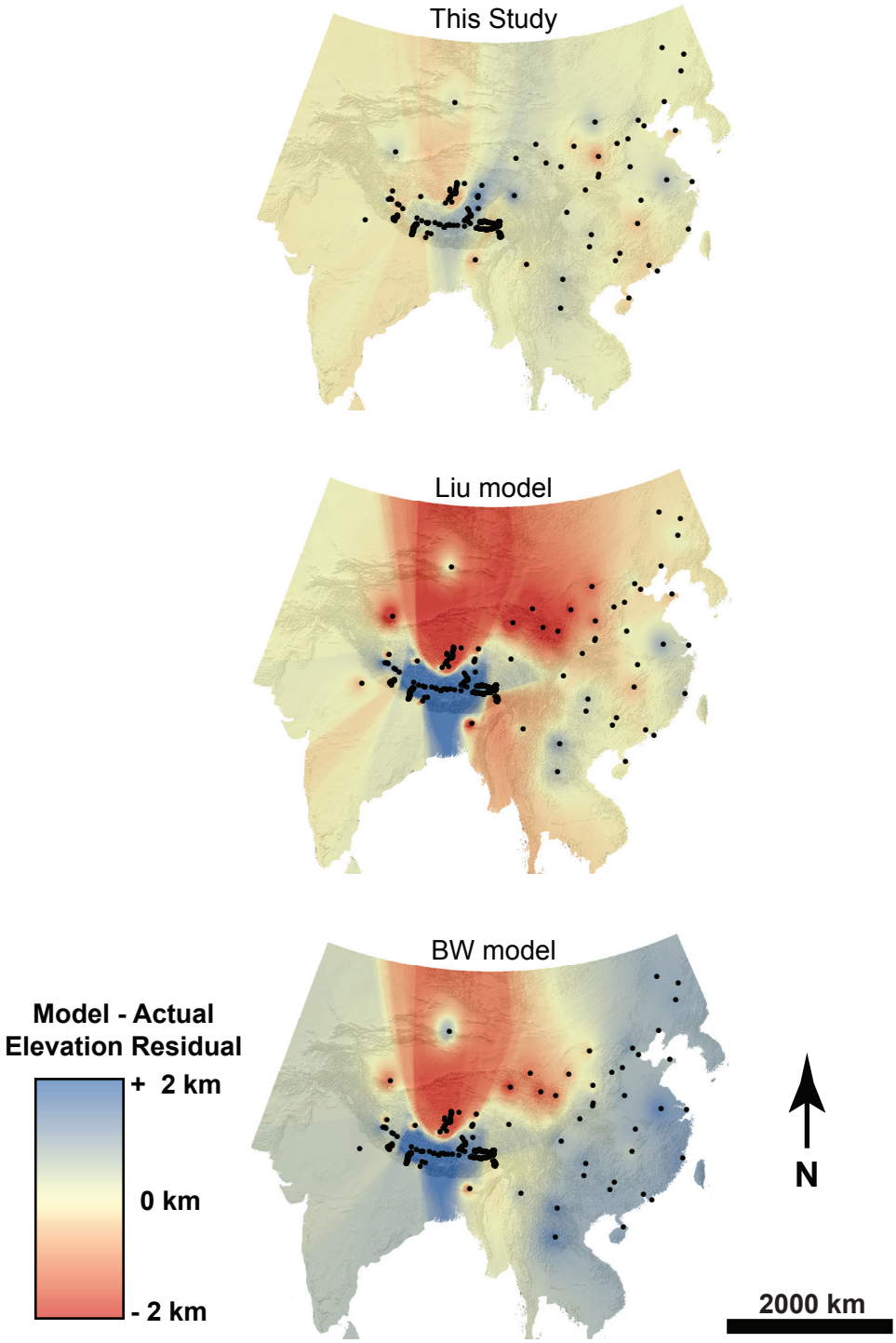


Figure 2.10 – East Asia model-predicted elevation residuals. Liu and BW models are shown for comparison. Model-predicted elevations of this study are consistently more accurate than either the Liu or BW model (see also Figure 2.6), particularly in the Tibetan Plateau and Himalaya where the Liu and BW models are characterized by extreme (> 2 km) elevation underestimates and overestimates, respectively. Black dots mark site locations. As with regional residual $\delta^{18}O$ (Figure 2.8), caution must be taken when interpreting residual contours in regions of sparse data.

(Figures 2.5 and 2.6). The BW model consistently overpredicts site elevations by more than 1500 m for most subregions in the western US and in the Himalaya-South Tibet subregion of east Asia. The Dutton model predicts site elevations to a similar degree of accuracy to that of our statistical analysis (2σ uncertainty < 1300 m) in the Coast, Great Plains and Coast-Gulf of CA subregions of the western US, but significantly overestimates (> 1500 m) elevations in the continental interior subregions. The Liu model predicts eastern Asia site elevations to within ± 1000 m, but is characterized by significant elevation residuals (-2000 m to +4000 m) in both the Himalaya and Tibet subregions (Figures 2.6 and 2.10).

## 2.7 Discussion and Implications

### *2.7.1 Regional and subregional trends*

Statistical analyses of modern precipitation $\delta^{18}O$ distributions in the western US and east Asia indicate a significant degree of variability in both type and magnitude of environmental controls on precipitation isotopic values for various physiographic and climatic subregions. In general, as proposed in earlier studies which deconvolved the temperature effect on precipitation isotopic compositions into geographic parameters alone (Bowen and Wilkinson, 2002; Bowen and Revenaugh, 2003; Dutton et al., 2005; Liu et al., 2008), we show that latitude and elevation are dominant controls on $\delta^{18}O$ distributions. The requirement of a polynomial function of latitude, however, appears to be region dependent, with the western US equally well fit by either a polynomial function of latitude or a strictly linear regression of environmental parameters. In contrast, some

subregions of east Asia are better fit by a polynomial function of latitude (Tables 2.1 and 2.2), in particular the eastern Asia subregion. This variability in the parameterization of latitude is likely related to the latitudinal distribution of precipitation and meteoric water sampling sites in the western US and east Asia regions. The east Asia dataset spans tropical to temperate latitudes (~20–50°N) while the western US dataset is exclusively contained within the temperate mid-latitudes (~30–50°N). Compilation of GNIP $\delta^{18}O$ records plotted as a function of latitude (Bowen and Wilkinson, 2002 Figure 1; Dutton et al., 2005 Figure 4a) reveals an approximate linear $\delta^{18}O$-latitude relationship for the mid-latitude range of western North America, whereas the relative lack of latitudinal dependence in the subtropics (20–30°N/S) requires a polynomial fit to latitude for regions spanning tropical to temperate latitudes (i.e. east Asia).

While latitude and elevation consistently act as dominant controls on modern meteoric $\delta^{18}O$ values, additional environmental parameters (e.g., longitude, MAT, MAP) also function as dominant isotopic controls depending on physiographic and climatic environment. In most cases, covariance of site MAT with latitude and elevation allows the influence of MAT on site $\delta^{18}O$ values to be sufficiently accounted for by latitude and elevation alone, whereas the influences of longitude and MAP are more likely to be independent of latitude and elevation effects. MAP acts as a dominant control, in addition to latitude and elevation, on $\delta^{18}O$ distributions in both the Coast and Coast-Gulf of CA subregions of the western US. Interestingly, though, the direct correlation between site elevation and $\delta^{18}O$ in these subregions (higher $\delta^{18}O$ with higher mean annual precipitation) is in contrast to the anticipated 'amount effect' which is known to be a major isotopic control in tropical and subtropical regions (Dansgaard, 1964; Rozanski et

al., 1993). The observed positive $\delta^{18}O$-MAP correlation in the coast subregion of the western US is likely due to the steep elevation gradient in this region in contrast to a relatively weak precipitation gradient (Figure 2.11). As a result, the altitude effect dominates over any influence from the amount effect, as reflected by the strong dependence of $\delta^{18}O$ on elevation in the Coast subregion ($R^2 = 0.76$). The observed positive correlation between MAP and $\delta^{18}O$, thus, likely reflects variability in $\delta^{18}O$ values at comparable elevations throughout this climatically diverse region. The influence of longitude in east Asia subregions is likely due to the variable influences of distinct moisture sources as a function of longitudinal position in this region. The Indian and East Asian monsoons are the dominant precipitation sources for Himalaya and eastern Asia subregions, respectively (Figure 2.3), with increasing influence of the East Asian monsoon to the east and vice versa. As a result, longitude reflects the relative contribution of each monsoonal system to annual precipitation $\delta^{18}O$ values in areas where both systems are influential.

### *2.7.2 $\delta^{18}O$-elevation and $\delta^{18}O$-latitude gradient variability*

One of the most important results derived from statistical analysis of modern precipitation $\delta^{18}O$ is the systematic variability observed in $\delta^{18}O$-elevation gradients. The Coast, Great Plains, and Coast-Gulf of CA subregions of the western US and the Himalaya-South Tibet subregion of east Asia are all characterized by $\delta^{18}O$-elevation gradients similar in magnitude to the global empirical average (-2.8‰/km; Poage and Chamberlain, 2001) and to linear fits to Rayleigh distillation model-derived gradients at elevations less than 4000 m (estimated from Rowley et al., 2001). Annual precipitation in

# Figure 2.11

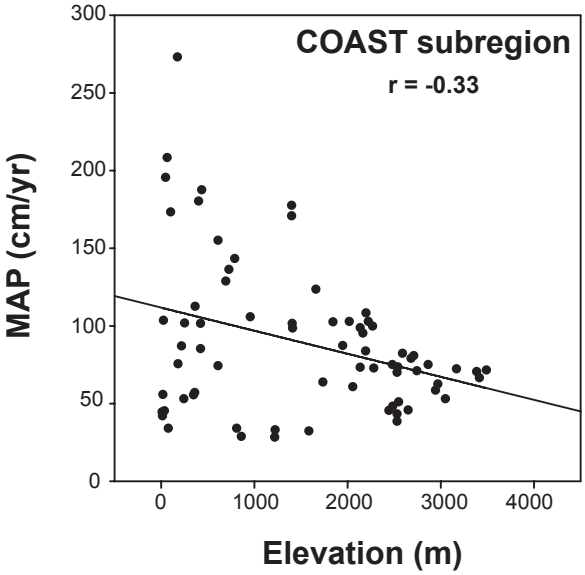


Figure 2.11 – Mean annual precipitation (MAP) plotted as a function of site elevation for the Coast subregion of the western US, indicating that maximum MAP occurs at low elevation coastal sites and generally decreases with increasing elevation in the Sierra Nevada.

each of these subregions is derived predominantly from storm systems sourced proximally from an oceanic moisture source (e.g., Pacific Ocean, Gulf of Mexico, or Indian Ocean) that undergo simple orographic lifting and rainout, consistent with Rayleigh distillation assumptions. In contrast, observed $\delta^{18}O$-elevation gradients in continental interior regions of the western US (Basin and Range, RMCP) and east Asia (North-Central Tibetan Plateau), as well as the eastern Asia subregion, are systematically lower in magnitude, approximately by a factor of two. Our modeled $\delta^{18}O$-elevation gradient for the eastern Asia subregion is consistent with the regional Liu model (-1.5‰/km); a result which is not surprising considering that the vast majority of sites analyzed in the Liu et al. (2008) study are located within the eastern Asia subregion.

The observed trend toward muted isotope-elevation gradients in continental interiors and continental interior rainshadows (e.g., the Basin and Range) is consistent with published isotopic records from similar settings (Blisniuk and Stern, 2005; Quade et al., 2007; Lechler and Niemi, *in revision*). This trend indicates that isotopic variability in these physiographic and climatic settings cannot be solely attributed to Rayleigh distillation processes, which require that moisture parcels are isolated, well-mixed, open-fractionation systems in isotopic equilibrium, such that isotopic evolution is only a function of the degree of rainout. The influence of the monsoonal systems that dominate east Asia precipitation (Fig. 2.3), and the associated increase in convective storm activity which violates the assumption of isotopic equilibrium throughout a contributing air mass, have been proposed as a possible mechanism for the reduction in $\delta^{18}O$-elevation gradients in this region (Liu et al., 2008). This hypothesis is consistent with studies of seasonal isotopic trends in monsoonal regions (Brown et al., 2008) and thus a plausible

cause for the reduced $\delta^{18}O$-elevation gradient observed in our statistical analysis of the eastern Asia subregion.

In addition to convective storm influence, the increased likelihood of mixing of moisture sources, continental moisture recycling, below-cloud evaporation ("pseudo-altitude effect"; Moser and Stichler, 1971; Friedman et al., 1992) and post-depositional evaporation of surface waters are also likely causes for increased variability of precipitation isotope relationships (Blisniuk and Stern, 2005) in continental interior settings. Many of these processes characterize the continental interior rainshadow (e.g., Basin and Range) and high elevation continental plateau (e.g., Tibet) regions where we observe a systematic reduction in $\delta^{18}O$-elevation gradient, thus providing probable causal mechanisms for the observed isotopic trends. The influence of complex moisture source interaction is clearly evident in the North-Central Tibetan Plateau subregion where latitude and $\delta^{18}O$ are positively correlated (i.e. increasing $\delta^{18}O$ to the north). This unique latitude-$\delta^{18}O$ relationship is the result of the increased influence of enriched isotopic moisture sources located north and west of the Tibetan Plateau (e.g., Tian et al., 2007) to sites in the central and northern Plateau (Figure 2.3), such that rainout progresses from the northern and western Plateau margin into the Plateau interior.

The increased complexity of rainout processes in continental interior settings is also reflected by poorer model fits (Tables 2.1 and 2.2) and increased elevation uncertainties (Table 2.3, Figures 2.5, 2.6, 2.9 and 2.10) in the Basin and Range, RMCP, Continental Interior, and North-Central Tibetan Plateau subregions. Region-dependent complexity in precipitation processes and moisture source interactions, as well as

variability in the covariance among independent environmental parameters, may also explain the variability observed in the absolute magnitude of the $\delta^{18}O$-latitude relationship (Table 2.2). For comparable linear models [i.e. $\delta^{18}O = \beta_0 + \beta_1(LAT) + \beta_2(ELEV)$], $\delta^{18}O$-latitude gradients tend to be shallower in subregions where elevation is the dominant control on $\delta^{18}O$ values (e.g., Coast, Himalaya-South Tibet) and steeper in regions where elevation control is minor (e.g., Basin and Range, RMCP), reflecting a tradeoff between elevation and latitude in controlling rainout processes. These trends appear to indicate that, like $\delta^{18}O$-elevation gradients, $\delta^{18}O$-latitude gradients may also directly relate to physiographic and climatic setting. It is important to note, however, that these trends can be complicated by variable latitudinal positions of dominant moisture sources such that rainout progresses in unique geographic directions yielding unsystematic isotope-latitude relationships (e.g., Tibet).

*2.7.3 Basin and Range case study*

Statistical analysis of modern meteoric $\delta^{18}O$ in the western US and east Asia indicates that simple orographic systems (i.e. single dominant moisture source, monotonic elevation increase) can be modeled well with Rayleigh distillation principles. Continental interior rainshadows, high elevation plateaus and areas dominated by monsoonal precipitation systems and associated convective storm activity, however, exhibit more complex isotopic relationships. The Basin and Range province of western North America is a good region to further explore and verify these systematic relationships as complexity of moisture source interaction and dominant moisture sources varies as a function of geographic position. Most of the Basin and Range is characterized

by complex moisture source interaction and significant variability in storm track trajectory and associated degree of rainout (Friedman et al., 2002a) with many of the contributing storm tracks forced to traverse orographic barriers along the western coast of North America (e.g., Sierra Nevada, Cascades, Coast Ranges) prior to reaching interior sites. This high degree of rainout prior to reaching the continental interior appears to result in the reduced isotope-elevation relationships discussed above. At positions farther south (south of ~37°N), however, the North American summer monsoon, which derives moisture from the Gulf of California, tropical Pacific Ocean and Gulf of Mexico (Adams and Comrie, 1997), acts as a dominant source of seasonal (summer) precipitation. These southerly moisture sources are not subject to the same degree of orographic rainout as central and northern Pacific sources prior to reaching the Basin and Range, and, as a result, precipitation in the areas influenced by the monsoon may be better approximated by Rayleigh distillation processes.

We explore the idea of spatial variability in Basin and Range isotope-environment relationships through analysis of geographic subsets of Basin and Range precipitation stations. Basin and Range sites influenced by the North American monsoon (Basin and Range – Gulf of CA) are characterized by steeper $\delta^{18}O$-elevation gradients (-1.9‰/km) and higher correlation between site elevation and $\delta^{18}O$ composition ($R^2 = 0.53$), whereas sites north of ~37°N (Basin and Range Interior) have muted $\delta^{18}O$-elevation gradients (-1.2‰/km) and are dominantly controlled by MAT ($R^2 = 0.56$) instead of elevation ($R^2 = 0.11$). These trends are also reflected in the Coast-Gulf of CA analysis discussed above with $\delta^{18}O$ at sites in the vicinity of the Gulf of CA being accurately modeled by Coast subregion environmental parameters and coefficients which appear to be consistent with

Rayleigh distillation processes. Statistical analysis of Basin and Range seasonal data subsets (Friedman et al., 1992; 2002b) also supports the idea of variable isotopic relationships depending on seasonal moisture source. $\delta^{18}O$-elevation gradients for winter season precipitation are reduced in magnitude (-0.8 to -1.2‰/km) compared to summer $\delta^{18}O$-elevation gradients (-1.8 to -2.2‰/km). This seasonal variability in isotope-elevation relationships appears to reflect the fact that winter precipitation is more likely to traverse the Sierra Nevada, and produce the characteristic rainshadow effects (i.e. low $\delta^{18}O$-elevation gradient), than summer storm systems derived from more southerly sources (e.g., Gulf of California). Winter season precipitation dominates over summer precipitation throughout much of the Basin and Range (average regional winter-summer ratio ~ 2–3; Friedman et al., 1992; 2002b). This seasonal trend is reflected in the reduced $\delta^{18}O$-elevation gradient observed in our statistical analysis of modern Basin and Range precipitation $\delta^{18}O$.

### *2.7.4 Implications for stable isotope paleoclimate, hydrologic and paleoelevation studies*

The increased uncertainty for isotopic relationships in continental interior settings acts as a fundamental limitation to estimating absolute magnitudes or magnitudes of change in stable isotope-based paleoclimate, hydrologic and paleoelevation studies utilizing paleo-meteoric water proxies from these settings. Despite this increased uncertainty, more accurate interpretations from meteoric water proxy records can be made by accounting for the systematic variations in isotopic relationships as a function of environmental setting. Table 2.4 lists regional and subregional $\delta^{18}O$-temperature relationships for statistical analyses where $\delta^{18}O$ was modeled solely as a function of

**TABLE 2.4** – Temperature Coefficients

| REGION | MAT(‰/°C) | Intercept | $R^2$ |
|---|---|---|---|
| | ***WESTERN US*** | | |
| *All Sites* | 0.49 | -17.4 | 0.55 |
| *Coast* | 0.59 | -18.4 | 0.66 |
| *Basin and Range*** | 0.44 | -9.1 | 0.76 |
| *RMCP*** | 0.64 | -17.7 | 0.66 |
| *Continental Interior* | 0.41 | -17.5 | 0.65 |
| *Great Plains* | 0.48 | -14.2 | 0.61 |
| *Coast-Gulf of CA* | 0.44 | -17.3 | 0.62 |
| | ***EAST ASIA*** | | |
| *All sites* | 0.34 | -12.9 | 0.44 |
| *Eastern Asia* | 0.07 | -8.5 | 0.26 |
| *Himalaya-S. Tibet* | 0.48 | -13.5 | 0.67 |
| *North-Central Tibet* | -0.05 | -14.3 | 0.01 |
| *Himalaya only* | 0.54 | -14.2 | 0.74 |
| *All Tibet* | 0.10 | -14.1 | 0.02 |

**Table 2.4 Notes** – Temperature coefficients for temperature-only regression models analyzed in this study. Variability of coefficient magnitude is discussed in the text. ** - indicates subregions where temperature-only models are acceptable reduced linear regression models.

MAT. With the exception of the Tibetan Plateau subregion, which is characterized by complex isotope-latitude and isotope-temperature relationships as a result of high $\delta^{18}O$ moisture sources north and west of the Plateau as discussed above, the observed trends in isotope-temperature relationships are similar to those documented in published studies (Rozanski et al., 1993; Vachon et al., 2010). Steep $\delta^{18}O$-temperature gradients are observed in high altitude and continental interior settings (e.g., Coast, RMCP, and Basin and Range Interior of the western US; Himalaya-South Tibet in east Asia) whereas reduced gradients and poorly defined isotope-temperature relationships are more commonly found in low elevation coastal regions (e.g., eastern Asia). The Coast subregion of the western US falls into the former category as a result of the inclusion of Sierra Nevada sites whose high elevations and seasonal variability in average daily temperatures make this region more akin to the RMCP subregion than eastern Asia from an isotope-temperature perspective.

It is important to note that interpretation of isotope-temperature relationships derived in this study must be made with caution as previous work has shown that temperature during precipitation event (Kohn and Welker, 2005) and at the moisture source location (Vachon et al., 2010) are also dominant controls on isotope-temperature relationships. Without the high temporal resolution temperature data (i.e. on an individual storm basis) needed to make these calculations, our calculated isotope-temperature relationships only serve to provide general physiographic and climatic trends. However, these trends still have important first order implications for stable isotope-based paleoclimate studies as interpretability of temperature signals in proxy isotopic records is shown to be location dependent. Isotope-temperature relationships in low elevation

coastal settings are generally poorly correlated and low in magnitude (≤ 0.3‰/°C), whereas isotope-temperature relationships are well defined and characterized by steep gradients (0.45 – 0.7‰/°C) in continental interior alpine settings and proxies formed in these settings should be assumed to reflect these phenomena.

Our statistical analyses also have far-reaching implications for stable isotope-based determinations of paleoelevations, both in terms of site of proxy formation and location of groundwater recharge. This work places quantitative constraints on the general isotope-elevation trends acknowledged in the literature (Blisniuk and Stern, 2005 and references therein) with reduced isotope-elevation relationships in arid, orographic rainshadows and high elevation continental plateaus. We show that the global empirical (Poage and Chamberlain, 2001) and Rayleigh distillation-derived average (e.g., Rowley et al., 2001) $\delta^{18}O$-elevation gradients characterize simple orographic settings with a single dominant moisture source and transport direction (e.g., Sierra Nevada, Himalaya). Regions characterized by complex moisture source interaction, continental moisture recycling, and below-cloud and surface evaporation (e.g., Basin and Range, Tibetan Plateau) exhibit a systematic reduction in $\delta^{18}O$-elevation gradients by approximately a factor of two (-1 to -1.5‰/km). As a result, stable isotope-based elevation determinations require that the paleogeographic environment in which paleo-meteoric water proxies formed is considered.

For example, contradicting stable isotope-based paleoelevation estimates for the northern Tibetan Plateau (e.g., Cyr et al., 2005; DeCelles et al., 2007) can be better reconciled as a result of our statistical analysis. Application of low magnitude $\delta^{18}O$-

elevation gradients that are comparable to modern gradients in the Plateau region suggest that high (> 4.5 km) regional paleoelevations have characterized the northern Tibetan Plateau since at least the Oligocene (DeCelles et al., 2007). In contrast, interpretation of proxy $\delta^{18}O$ records assuming Rayleigh distillation processes controlled northern Tibetan Plateau meteoric water isotopic compositions suggest that Paleocene-Eocene paleoelevations were significantly lower (≤ 2 km), requiring surface uplift in excess of 2 km since Oligocene time (Cyr et al., 2005). The systematic shift to reduced isotope-elevation gradients in continental interior plateau settings observed in our statistical analysis of modern precipitation $\delta^{18}O$ in the western US and east Asia suggests that reduced magnitude $\delta^{18}O$-elevation gradients (~ -1.5‰/km) should be applied to proxy records obtained from the plateau interior for paleoelevation calculations. As a result, this study provides additional support for high regional paleoelevations in the northern Tibetan Plateau since at least the Oligocene.

The consistent trend of reduced isotope-elevation gradients in continental interiors also has important implications for how high magnitude isotopic shifts can be interpreted in the proxy record. Such isotopic shifts (≥ 6‰) have been observed in multiple Cenozoic meteoric water proxy records from the Basin and Range (e.g., Horton and Chamberlain, 2006; Mix et al., 2011) and Rocky Mountain Cordillera (Carroll et al., 2008; Davis et al., 2008; Doebbert et al., 2010). Assuming the reduced $\delta^{18}O$-elevation gradient (~ -1.5‰/km) that characterizes these regions in the modern is also applicable through much of the Cenozoic, such high magnitude shifts are unlikely to reflect an elevation signal exclusively as changes of this magnitude would require implausible changes in elevation (≥ 4 km). Instead, these high magnitude isotopic shifts, especially when

concentrated over short timescales (e.g., Carroll et al., 2008), are more likely to reflect drainage reorganization (Carroll et al., 2008; Davis et al., 2008; Doebbert et al., 2010) or changes in moisture source through time (Horton and Chamberlain, 2006). Such a change in moisture source is a probable influence on Neogene isotopic records from the central and southern Basin and Range as late Miocene-early Pliocene opening of the Gulf of California (Oskin et al., 2001) likely introduced isotopically-distinct moisture sources to the annual precipitation cycle in this region. Accordingly, accurate interpretation of paleo-meteoric water isotopic records requires that the potential influence of variable moisture source contributions to the proxy record are estimated, possibly by constraining regional paleogeography at the site of proxy formation to hypothesize the associated influences on storm track trajectories.

Cases where large isotopic shifts in continental interior meteoric water proxies actually do reflect high magnitude elevation change are systems where a high elevation orographic barrier acts as a dominant control on leeward precipitation $\delta^{18}O$ (or $\delta D$). Precipitation $\delta^{18}O$ values for sites on the leeward side of, but proximal to, the Sierra Nevada in the western US and Himalaya in east Asia are consistently more depleted than would be predicted based on site parameters alone (Figures 2.7 and 2.8). This isotopic depletion is a direct result of the high degree of rainout occurring over the high elevations of the windward orographic barrier, making proximal leeward sites appear to be at high elevations (Figures 2.9 and 2.10). This effect supports the theory behind stable isotope-based paleoelevation studies using leeward side meteoric proxies to constrain orographic barrier elevations (Poage and Chamberlain, 2002; Mulch et al., 2006; Crowley et al., 2008; Mulch et al., 2008; Cassel et al., 2009), but caution has also been suggested for

using such an approach as varying climate and atmospheric states may result in (1) variability in the degree of rainout occurring over the orographic barrier (Molnar, 2010) and (2) the tendency for storm tracks to be blocked by or travel around rather than over a high elevation orographic barrier (Galewsky, 2009).

The works of Galewsky (2009) and Molnar (2010), as well as studies discussing the controls on the isotopic composition of precipitation (e.g., Dansgaard, 1964; Rozanski et al., 1993), indicate the need to account for climatic variability when interpreting isotopic records as isotopic relationships are climate state dependent. For example, isotope-elevation gradients may be expected to be greater in magnitude, possibly by a factor of 2 or more, in simple orographic settings (e.g., Sierra Nevada) under a warmer and more humid climate, conditions believed to have characterized early Paleogene climate (Molnar, 2010). This trend toward steeper isotope-elevation gradients is proposed to result simply from greater moisture carrying capabilities of the warmer air masses, allowing for increased amounts of rainout and associated isotopic fractionation for inland sites. Conversely, warmer climates might also act to reduce isotope-elevation gradients through either increased relative humidity of the contributing air mass (Rowley and Garzione, 2007) or the influence of isotopically heavy upper troposphere moisture to high elevation sites (Poulsen and Jeffery, 2011). In any case, meteoric isotopic compositions can change significantly without a change in elevation simply as a function of varying climate state. Accordingly, how climatic conditions during the time of proxy formation may have altered modern isotope-environment relationships must be accounted for in proxy-based studies, particularly when proxies formed under climatic conditions significantly different than modern. This fundamental limitation to proxy studies can be

addressed through the use of regional and global circulation models with stable isotopic monitoring capabilities such that constraints on the variability in isotopic relationships to specific environmental parameters can be quantified as a function of climatic or physiographic change (e.g., Insel et al., 2010).

Applicability of the modern isotopic relationships derived in this study are also proxy dependent as different forms of meteoric water (e.g., lakes, rivers, soil waters) have variable isotopic relationships with the original precipitation from which they were derived. For example, lacustrine and fluvial proxies reflect the integrated isotopic signal from throughout the contributing catchment, thus recording a range of site elevations and site temperatures in a single isotopic value. Pedogenic carbonates, in contrast, form in locally-derived soil waters that are more likely to reflect site $\delta^{18}O$ values (e.g., Sheldon and Tabor, 2009). In either case, proxy isotopic composition reflects all processes influencing isotopic composition during the transition from precipitation to integration into lake, river, or soil water system. A regional study of modern lake water isotopic compositions indicates that evaporative effects can lead to significantly higher isotopic compositions of lake waters in comparison to local precipitation in the arid, continental interior western US, particularly in closed basin systems (Henderson and Shuman, 2009). Similarly, soil waters can also be subject to significant evaporative influence (e.g., Quade et al., 2007). Proxies formed in these waters (e.g., lacustrine and pedogenic carbonates) may, thus, no longer preserve the isotopic signal of the original precipitation and its associated relationship to relevant environmental parameters. As a result, the degree of evaporative influence must be independently constrained for accurate interpretation of proxy records to be made.

## 2.8 Conclusions

Statistical analysis of modern precipitation $\delta^{18}O$ distributions in the western US and east Asia suggests that isotopic compositions can be accurately modeled as a function of geographic (latitude, longitude, elevation) and climatic (MAT, MAP) parameters. This work refines previous global (Bowen and Wilkinson, 2002; Bowen and Revenaugh, 2003) and regional (Dutton et al., 2005; Liu et al., 2008) statistical analyses by investigating the potential influence of a wider set of environmental parameters and constraining the influence of each parameter as part of single multiple regression model for a range of physiographic and climatic environments. Our analyses confirm that latitude and elevation act as dominant controls on precipitation $\delta^{18}O$ for nearly all regions and subregions, but the magnitude of the control, as well as the influence of other environmental parameters, varies on a subregional basis. In particular, $\delta^{18}O$-elevation gradients in simple orographic settings of the Coast and Great Plains subregions of the western US and Himalaya-South Tibet subregion of east Asia are in general agreement with global empirical averages (~ -2.8‰/km) and gradients characteristic of Rayleigh distillation rainout processes. A systematic reduction in the magnitude of $\delta^{18}O$-elevation gradients by approximately a factor of two (-1.5‰/km) is observed in arid, continental interior rainshadows (Basin and Range) and high elevation continental plateaus (Tibet), regions often characterized by complex moisture source interaction, increased continental moisture recycling and/or convective storm activity. Identifying the dominant environmental controls on, and the corresponding quantitative relationship with,

precipitation $\delta^{18}O$ greatly informs stable isotope-based estimates of terrestrial climate change, locations of groundwater recharge, and paleoelevations. In particular, with independent estimates of paleo-precipitation (e.g., Sheldon and Retallack, 2004) and paleogeographic position, the influence of altitude and/or temperature on meteoric $\delta^{18}O$ can be more accurately quantified for stable isotope proxy records, assuming the influence of changes in paleoenvironment and climate state can be constrained.

## 2.9 Acknowledgements

Boris Avdeev's guidance on effectively using the statistical program R was instrumental to this study. Mike Hren is thanked for insightful discussions about interpretations of isotopic patterns as well as for providing access to various isotopic datasets.

## 2.10 References cited


Adams, D. K., and Comrie, A. C., 1997, The North American monsoon: Bulletin of the American Meteorological Society, v. 78, no. 10, p. 2197-2213.

Allison, G. B., 1988, A review of some of the physical, chemical and isotopic techniques available for estimating groundwater recharge, *in* Simmers, I., ed., Estimation of Natural Groundwater Recharge: Dardrecht, D. Reidel Publishing Co., p. 509 pp.

Araguás-Araguás, L., Froehlich, K., and Rozanski, K., 1998, Stable isotope composition of precipitation over southeast Asia: Journal of Geophysical Research-Atmospheres, v. 103, no. D22, p. 28721-28742.

Blisniuk, P. M., and Stern, L. A., 2005, Stable istope paleoaltimetry: a critical review: American Journal of Science, v. 305, no. 10, p. 1033-1074.

Bowen, G. J., and Revenaugh, J., 2003, Interpolating the isotopic composition of modern meteoric precipitation: Water Resources Research, v. 39, no. 10, p. 9-1 - 9-13.

Bowen, G. J., and Wilkinson, B., 2002, Spatial distribution of delta $^{18}O$ in meteoric precipitation: Geology, v. 30, no. 4, p. 315-318.

Brown, D., Worden, J., and Noone, D., 2008, Comparison of atmospheric hydrology over convective continental regions using water vapor isotope measurements from space: Journal of Geophysical Research-Atmospheres, v. 113, no. D15124.

Carroll, A. R., Doebbert, A. C., Booth, A. L., Chamberlain, C. P., Rhodes-Carson, M. K., Smith, M. E., Johnson, C. M., and Beard, B. L., 2008, Capture of high-altitude precipitation by a low-altitude Eocene lake, Western US: Geology, v. 36, no. 10, p. 791-794.

Cassel, E. J., Calvert, A. T., and Graham, S. A., 2009, Age, geochemical composition, and distribution of Oligocene ignimbrites in the northern Sierra Nevada, California: implications for landscape morphology, elevation, and drainage divide geography of the Nevadaplano: International Geology Review, v. 51, no. 7-8, p. 723-742.

Cole, J. E., Rind, D., Webb, R. S., Jouzel, J., and Healy, R., 1999, Climatic controls on interannual variability of precipitation $\delta^{18}O$: Simulated influence of temperature, precipitation amount, and vapor source region: Journal of Geophysical Research-Atmospheres, v. 104, no. D12, p. 14223-14235.

Crowley, B. E., Koch, P. L., and Davis, E. B., 2008, Stable isotope constraints on the elevation history of the Sierra Nevada Mountains, California: Geological Society of America Bulletin, v. 120, no. 5-6, p. 588-598.

Cyr, A. J., Currie, B. S., and Rowley, D. B., 2005, Geochemical evaluation of Fenghuoshan Group lacustrine carbonates, North-Central Tibet: Implications for the paleoaltimetry of the Eocene Tibetan Plateau: Journal of Geology, v. 113, no. 5, p. 517-533.

Dansgaard, W., 1964, Stable Isotopes in Precipitation: Tellus, v. 16, no. 4, p. 436-468.

Davis, S. J., Wiegand, B. A., Carroll, A. R., and Chamberlain, C. P., 2008, The effect of drainage reorganization on paleoaltimetry studies: An example from the Paleogene Laramide foreland: Earth and Planetary Science Letters, v. 275, no. 3-4, p. 258-268.

DeCelles, P. G., Quade, J., Kapp, P., Fan, M. J., Dettman, D. L., and Ding, L., 2007, High and dry in central Tibet during the Late Oligocene: Earth and Planetary Science Letters, v. 253, no. 3-4, p. 389-401.

Doebbert, A. C., Carroll, A. R., Mulch, A., Chetel, L. M., and Chamberlain, C. P., 2010, Geomorphic controls on lacustrine isotopic compositions: Evidence from the Laney Member, Green River Formation, Wyoming: Geological Society of America Bulletin, v. 122, no. 1-2, p. 236-252.

Dutton, A., Wilkinson, B.H., Welker, J.M., Bowen, G.J., and Lohmann, K.C., 2005, Spatial distribution and seasonal variation in $^{18}O/^{16}O$ of modern precipitation and river water across the conterminous USA: Hydrological Processes, v. 19, p. 4121-4146.

Fredrickson, G. C. and Criss, R.E., 1999, Isotope hydrology and residence times of the unimpounded Meramec River basin, Missouri: Chemical Geology, v. 157, p. 303-317.

Friedman, I., Harris, J.M., Smith, G.I., Johnson, C.A., 2002a, Stable isotope composition of waters in the Great Basin, United States 1. Air-mass trajectories: Journal of Geophysical Research-Atmospheres, v. 107, p. 14 pp.

Friedman, I., and Smith, G. I., 1972, Deuterium Content of Snow as an Index to Winter Climate in Sierra-Nevada Area: Science, v. 176, no. 4036, p. 790-793.

Friedman, I., Smith, G. I., Gleason, J. D., Warden, A., and Harris, J. M., 1992, Stable Isotope Composition of Waters in Southeastern California .1. Modern Precipitation: Journal of Geophysical Research-Atmospheres, v. 97, no. D5, p. 5795-5812.

Friedman, I., Smith, G.I., Johnson, C.A., Moscati, R.J., 2002b, Stable isotope compositions of waters in the Great Basin, United States 2. Modern precipitation: Journal of Geophysical Research, v. 107, p. ACL 15-11 - ACL 15-21.

Galewsky, J., 2009, Orographic precipitation isotopic ratios in stratified atmospheric flows: Implications for paleoelevation studies: Geology, v. 37, no. 9, p. 791-794.

Garzione, C. N., Quade, J., DeCelles, P. G., and English, N. B., 2000, Predicting paleoelevation of Tibet and the Himalaya from $\delta^{18}O$ vs. altitude gradients in meteoric water across the Nepal Himalaya: Earth and Planetary Science Letters, v. 183, no. 1-2, p. 215-229.

Gat, J. R., 1996, Oxygen and hydrogen isotopes in the hydrologic cycle: Annual Review of Earth and Planetary Sciences, v. 24, p. 225-262.

Harvey, F. E., 2001, Use of NADP archive samples to determine the isotope composition of precipitation: Characterizing the meteoric input function for use in ground water studies: Ground Water, v. 39, no. 3, p. 380-390.

Harvey, F. E., 2005, Stable hydrogen and oxygen isotope composition of precipitation in northeastern Colorado: Journal of the American Water Resources Association, v. 41, no. 2, p. 447-459.

Henderson, A. K., and Shuman, B. N., 2009, Hydrogen and oxygen isotopic compositions of lake water in the western United States: Geological Society of America Bulletin, v. 121, no. 7-8, p. 1179-1189.

Horton, T. W., and Chamberlain, C. P., 2006, Stable isotopic evidence for Neogene surface downdrop in the central Basin and Range Province: Geological Society of America Bulletin, v. 118, no. 3-4, p. 475-490.

Horton, T. W., Sjostrom, D. J., Abruzzese, M. J., Poage, M. A., Waldbauer, J. R., Hren, M. T., Wooden, J. L., and Chamberlain, C. P., 2004, Spatial and temporal variation of Cenozoic surface elevation in the Great Basin and Sierra Nevada: American Journal of Science, v. 304, no. 10, p. 862-888.

Hren, M. T., Bookhagen, B., Blisniuk, P. M., Booth, A. L., and Chamberlain, C. P., 2009, $\delta^{18}O$ and $\delta D$ of streamwaters across the Himalaya and Tibetan Plateau: Implications for moisture sources and paleoelevation reconstructions: Earth and Planetary Science Letters, v. 288, no. 1-2, p. 20-32.

Ingraham, N. L., Lyles, B. F., Jacobson, R. L., and Hess, J. W., 1991, Stable isotopic study of precipitation and spring discharge in southern Nevada: Journal of Hydrology, v. 125, no. 3-4, p. 243-258.

Ingraham, N. L., and Taylor, B. E., 1991, Light stable isotope systematics of large-scale hydrologic regimes in California and Nevada: Water Resources Research, v. 27, no. 1, p. 77-90.

Insel, N., Poulsen, C. J., and Ehlers, T. A., 2010, Influence of the Andes Mountains on South American moisture transport, convection, and precipitation: Climate Dynamics, v. 35, no. 7-8, p. 1477-1492.

Johnson, K. R., and Ingram, B. L., 2004, Spatial and temporal variability in the stable isotope systematics of modern precipitation in China: implications for paleoclimate reconstructions: Earth and Planetary Science Letters, v. 220, no. 3-4, p. 365-377.

Jouzel, J., Alley, R. B., Cuffey, K. M., Dansgaard, W., Grootes, P., Hoffmann, G., Johnsen, S. J., Koster, R. D., Peel, D., Shuman, C. A., Stievenard, M., Stuiver, M., and White, J., 1997, Validity of the temperature reconstruction from water isotopes in ice cores: Journal of Geophysical Research-Oceans, v. 102, no. C12, p. 26471-26487.

Kent-Corson, M. L., Sherman, L. S., Mulch, A., and Chamberlain, C. P., 2006, Cenozoic topographic and climatic response to changing tectonic boundary conditions in western North America: Earth and Planetary Science Letters, v. 252, no. 3-4, p. 453-466.

Koch, P. L., Zachos, J. C., and Dettman, D. L., 1995, Stable-isotope stratigraphy and paleoclimatology of the Paleogene Bighorn Basin (Wyoming, USA): Palaeogeography Palaeoclimatology Palaeoecology, v. 115, no. 1-4, p. 61-89.

Kohn, M. J., and Welker, J. M., 2005, On the temperature correlation of $\delta^{18}O$ in modem precipitation: Earth and Planetary Science Letters, v. 231, no. 1-2, p. 87-96.

Krabbenhoft, D. P., Bowser, C. J., Anderson, M. P., and Valley, J. W., 1990, Estimating groundwater exchange with lakes : 1. The stable isotope mass balance method: Water Resources Research, v. 26, no. 10, p. 2445-2453.

Lechler, A. R., and Niemi, N. A., *in revision*, Topographic and environmental controls on terrestrial water isotopic compositions and isotope-elevation gradient variability in the southwestern United States: implications for stable isotope-based paleoaltimetry and hydrologic studies: Geological Society of America Bulletin.

Lee, J. E., and Fung, I., 2008, "Amount effect" of water isotopes and quantitative analysis of post-condensation processes: Hydrological Processes, v. 22, no. 1, p. 1-8.

Liu, Z. F., Tian, L. D., Chai, X. R., and Yao, T. D., 2008, A model-based determination of spatial variation of precipitation $\delta^{18}O$ over China: Chemical Geology, v. 249, no. 1-2, p. 203-212.

Marquardt, D. W., 1980, You should standardize the predictor variables in your regression models: Journal of the American Statistical Association, v. 75, p. 74-103.

Mix, H. T., Mulch, A., Kent-Corson, M. L., and Chamberlain, C. P., 2011, Cenozoic migration of topography in the North American Cordillera: Geology, v. 39, no. 1, p. 87-90.

Molnar, P., 2010, Deuterium and oxygen isotopes, paleoelevations of the Sierra Nevada, and Cenozoic climate: Geological Society of America Bulletin, v. 122, no. 7-8, p. 1106-1115.

Moser, H., and Stichler, W., 1971, Die Verwendung des Deuterium- und Sauerstoff-18-Gehalts bei hydrologischen Untersuchungen: Geologica Bavaria, v. 64, p. 7-35.

Mulch, A., Graham, S. A., and Chamberlain, C. P., 2006, Hydrogen isotopes in Eocene river gravels and paleoelevation of the Sierra Nevada: Science, v. 313, no. 5783, p. 87-89.

Mulch, A., Sarna-Wojcicki, A. M., Perkins, M. E., and Chamberlain, C. P., 2008, A Miocene to Pleistocene climate and elevation record of the Sierra Nevada (California): Proceedings of the National Academy of Sciences of the United States of America, v. 105, no. 19, p. 6819-6824.

Nativ, R. and Riggio, R., 1990, Precipitation in the southern High Plains: meteorologic and isotopic features: Journal of Geophysical Research, v. 95, p. 22559-22564.

O'Brien, R. M., 2007, A caution regarding rules of thumb for variance inflation factors: Quality & Quantity, v. 41, no. 5, p. 673-690.

Oskin, M., Stock, J., and Martin-Barajas, A., 2001, Rapid localization of Pacific-North America plate motion in the Gulf of California: Geology, v. 29, no. 5, p. 459-462.

Pandey, G. R., Cayan, D. R., and Georgakakos, K. P., 1999, Precipitation structure in the Sierra Nevada of California during winter: Journal of Geophysical Research-Atmospheres, v. 104, no. D10, p. 12019-12030.

Poage, M. A., and Chamberlain, C. P., 2001, Empirical relationships between elevation and the stable isotope composition of precipitation and surface waters: Considerations for studies of paleoelevation change: American Journal of Science, v. 301, no. 1, p. 1-15.

Poage, M. A., and Chamberlain, C. P., 2002, Stable isotopic evidence for a Pre-Middle Miocene rain shadow in the western Basin and Range: Implications for the paleotopography of the Sierra Nevada: Tectonics, v. 21, no. 4, 1034.

Poulsen, C. J. and Jeffery, L.M., 2011, Climate change imprinting on stable isotopic compositions of high-elevation meteoric water: Geology, *in press*.

Quade, J., Cerling, T. E., and Bowman, J. R., 1989, Development of Asian Monsoon Revealed by Marked Ecological Shift during the Latest Miocene in Northern Pakistan: Nature, v. 342, no. 6246, p. 163-166.

Quade, J., Garzione, C. N., and Eiler, J., 2007, Paleoelevation reconstruction using pedogenic carbonates: Reviews in Mineralogy and Geochemistry, v. 66, no. 1, p. 53-87.

Rowley, D. B., and Currie, B. S., 2006, Palaeo-altimetry of the late Eocene to Miocene Lunpola basin, central Tibet: Nature, v. 439, no. 7077, p. 677-681.

Rowley, D. B., and Garzione, C. N., 2007, Stable isotope-based paleoaltimetry: Annual Review of Earth and Planetary Sciences, v. 35, p. 463-508.

Rowley, D. B., Pierrehumbert, R. T., and Currie, B. S., 2001, A new approach to stable isotope-based paleoaltimetry: implications for paleoaltimetry and paleohypsometry of the High Himalaya since the Late Miocene: Earth and Planetary Science Letters, v. 188, no. 1-2, p. 253-268.

Rozanski, K., and Araguás-Araguás, L., 1995, Spatial and temporal variability of stable isotope composition of precipitation over the South American continent: Bull. Inst. Fr. Etudes Andines, v. 24, p. 379-390.

Rozanski, K. L., Araguás-Araguás, L., and Gonfiantini, R., 1993, Isotopic patterns in modern global precipitation, *in* al., P. K. S. e., ed., Climate Change in Continental Isotopic Records, Geophys. Monogr. Ser.: Washington D.C., AGU, p. 1-36.

Saylor, J. E., Quade, J., Dellman, D. L., DeCelles, P. G., Kapp, P. A., and Ding, L., 2009, The Late Miocene through present paleoelevation history of southwestern Tibet: American Journal of Science, v. 309, no. 1, p. 1-42.

Sheldon, N. D., and Retallack, G. J., 2004, Regional paleoprecipitation records from the late Eocene and Oligocene of North America: Journal of Geology, v. 112, no. 4, p. 487-494.

Sheldon, N. D., and Tabor, N. J., 2009, Quantitative paleoenvironmental and paleoclimatic reconstruction using paleosols: Earth-Science Reviews, v. 95, no. 1-2, p. 1-52.

Simpkins, W. W., 1995, Isotopic composition of precipitation in central Iowa: Journal of Hydrology, v. 172, no. 1-4, p. 185-207.

Stern, L. A. and Blisniuk, P. M., 2002, Stable isotope composition of precipitation across the southern Patagonia Andes: Journal of Geophysical Research, v. 107.

Thompson, L. G., Yao, T., Davis, M. E., Henderson, K. A., MosleyThompson, E., Lin, P. N., Beer, J., Synal, H. A., ColeDai, J., and Bolzan, J. F., 1997, Tropical climate instability: The last glacial cycle from a Qinghai-Tibetan ice core: Science, v. 276, no. 5320, p. 1821-1825.

Tian, L., Masson-Delmotte, V., Stievenard, M., Yao, T., and Jouzel, J., 2001, Tibetan Plateau summer monsoon northward extent revealed by measurements of water stable isotopes: Journal of Geophysical Research-Atmospheres, v. 106, no. D22, p. 28081-28088.

Tian, L. D., Yao, T. D., MacClune, K., White, J. W. C., Schilla, A., Vaughn, B., Vachon, R., and Ichiyanagi, K., 2007, Stable isotopic variations in west China: A consideration of moisture sources: Journal of Geophysical Research-Atmospheres, v. 112, no. D10.

Vachon, R. W., Welker, J. M., White, J. W. C., and Vaughn, B. H., 2010, Moisture source temperatures and precipitation $\delta^{18}O$-temperature relationships across the United States: Water Resources Research, v. 46.

Welker, J. M., 2000, Isotopic ($\delta^{18}O$) characteristics of weekly precipitation collected across the USA: an initial analysis with application to water source studies: Hydrological Processes, v. 14, no. 8, p. 1449-1464.

Yurtsever, Y., and Gat, J.R., 1981, Atmospheric waters, *in* Gat, J. R. a. G., R., ed., Stable Isotope Hydrology, p. 103-142.

Zhang, X., Nakawo, M., Yao, T., Han, J., and Xie, Z., 2002, Variations of stable isotopic compositions in precipitation on the Tibetan Plateau and its adjacent regions: Science in China Series D-Earth Sciences, v. 45, no. 6, p. 481-493.

# CHAPTER III

## Topographic and environmental controls on terrestrial water isotopic compositions and isotope-elevation gradient variability in the southwestern United States: implications for stable isotope-based paleoaltimetry and hydrologic studies[*]

### 3.1 Abstract

Meteoric water stable isotopic compositions (δD and $\delta^{18}O$) result from complex interactions among atmospheric processes that are active during precipitation and isotopic modification processes that occur following deposition. In stable isotope paleoaltimetry and hydrologic studies, accurate interpretation of paleo-meteoric water proxy records requires that the relative effect of each process that controls isotopic composition can be reliably constrained. Assessing the role of post-depositional processes is possible through comparison of regional precipitation $\delta^{18}O$ (or δD) values with those of regional terrestrial waters (e.g., ground- and surface waters), as increased influence of post-depositional processes produces terrestrial water isotopic compositions that differ significantly from those of the original precipitation from which the waters were derived.

[*] **Citation**: Lechler, A.R. and Niemi, N.A., *in revision*, Topographic and environmental controls on terrestrial water isotopic compositions and isotope-elevation gradients in the southwestern United States: implications for stable isotope-based paleoaltimetry and hydrologic studies: Geological Society of America Bulletin.

Comparison of the isotopic composition of precipitation with that of surface and spring waters from the southwestern United States along a latitudinal transect at ~36ºN from the southern Sierra Nevada, CA to the Spring Mountains, NV reveals that precipitation and surface waters from the orographic slope of the southern Sierra Nevada exhibit similar isotopic compositions and isotope-elevation relationships. In contrast, Basin and Range surface and spring waters are characterized by less depleted stable isotopic compositions and $\delta^{18}O$-elevation gradients that are a factor of 3–4 lower than those of the original precipitation from which these waters are derived. We demonstrate that altitude-dependent sublimation of the winter snowpack is a viable mechanism for the observed isotopic enrichment of spring and surface waters in the Basin and Range, as increased removal of light isotopes (H and $^{16}O$) from higher elevation snowpacks, sustained throughout the winter season, acts to reverse the isotopic depletion effects of Rayleigh distillation during precipitation. This suggests that atmospheric processes alone may be insufficient to explain globally observed variations in $\delta^{18}O$-elevation gradients, and that the geologic record of the $\delta^{18}O$ composition of paleo-meteoric waters may not accurately reflect the $\delta^{18}O$ compositions of paleoprecipitation, particularly in arid environments dominated by winter precipitation in the form of snow. Consideration of this effect, particularly as can be constrained by paleoclimate reconstructions, is necessary to accurately derive quantitative estimates of paleoaltitude and seasonal groundwater recharge.

## 3.2 Introduction

Paleo-meteoric water proxies (ice cores, lacustrine and pedogenic carbonates, fluid inclusions, etc.) are fundamental to a diverse array of geologic and paleoclimate studies. As such, understanding the controls on the stable isotopic composition (δD and $\delta^{18}O$) of meteoric waters is fundamental to accurate interpretation of these proxy records. Environmental variables such as temperature, distance from moisture source, seasonality of precipitation and elevation are all known to influence the isotopic composition of precipitation at a single site (Dansgaard, 1964; Rozanski et al., 1993; Gat, 1996; Jouzel et al., 1997, 2003; Insel et al., 2010), and, presumably, the meteoric waters derived from this precipitation. The combined effects of these variables can complicate interpretation of the proxy record, but when the influence of individual environmental parameters can be isolated, isotopic records can inform a wide-range of paleoclimate, hydrologic, and paleoelevation studies. Isotope-temperature relationships have been widely applied to paleoclimate studies of both terrestrial and marine proxy records (e.g., Koch et al., 1995; Zachos et al., 2001) over a range of timescales. Hydrologic studies often utilize seasonal differences in, or the elevation dependence of, the isotopic composition of meteoric waters to estimate the timing and location of groundwater recharge (Allison et al., 1988; de Vries and Simmers, 2002). Correlations between elevation and stable isotopic composition are also a tenet of stable isotope-based paleoelevation methodologies (e.g., Rowley et al, 2001; Poage and Chamberlain, 2001; Blisniuk and Stern, 2005; Rowley and Garzione, 2007). In all such cases, the relationship between the environmental control, whether temperature, seasonality, or elevation, and the isotopic composition of the

meteoric water proxy must be quantified in order to make accurate estimates of paleotemperature, recharge, or paleoelevation.

The relationship between elevation and isotopic composition is of particular interest, as the field of quantitative paleoaltimetry has garnered significant attention in recent decades due to the importance accurate elevation histories have for constraining the geodynamic, tectonic, and climatic evolution of major orogenic systems (Kohn, 2007). The basic theoretical framework of stable isotope-based paleoaltimetry is built on Rayleigh distillation principles where heavy water isotopes (D and $^{18}O$) are preferentially removed during condensation from an air mass as part of an open fractionation system (Rowley and Garzione, 2007). Thus, waters at higher elevations are expected to be characterized by lower $\delta^{18}O$ and $\delta D$ values than waters at lower elevations along a single moisture trajectory (Dansgaard, 1964; Rowley et al., 2001). In theory, paleoelevation histories can then be constrained as long as proxies for the stable isotopic composition of paleo-meteoric waters can be obtained.

Commonly used stable isotope paleoaltimetry proxies include fluvial, lacustrine and pedogenic carbonates; hydrous silicates; and fossil teeth and bone (Kohn, 2007 and references therein). In all cases, the conditions under which the proxy formed (i.e. seasonality, growth rates) and the type of water in which it formed (e.g., lakes, soil waters, animal body waters) must be known or assumed. For example, lacustrine proxies reflect water isotopic compositions integrated across an entire catchment; in contrast, pedogenic carbonates derive their isotopic composition from local soil and meteoric waters (Tabor and Montanez, 2005). As a result, accurate interpretation of proxy records requires understanding the processes that influence meteoric water compositions for each

proxy system, as each proxy records information about a unique set of hydrologic processes acting over specific spatial and temporal scales.

In addition to reliable proxy materials, paleoelevation reconstructions require that a quantitative relationship between isotopic composition of precipitation and elevation also be known or assumed. Commonly, an empirically-derived, global average $\delta^{18}O$-elevation gradient of ~ -2.8‰/km is used as a starting point for paleoelevation quantification (e.g., Chamberlain and Poage, 2000; Garzione et al., 2000; Horton et al., 2004; Blisniuk et al., 2005; Kent-Corson et al., 2006; Saylor et al., 2009). However, modern $\delta^{18}O$-elevation gradients exhibit significant regional variability (Clark and Fritz, 1997; Poage and Chamberlain, 2001), and, in particular, $\delta^{18}O$-elevation gradients appear to be significantly lower (< -2.8‰/km) over large, high-standing orogenic plateaus (Blisniuk and Stern, 2005; Quade et al., 2007; Lechler, 2011). Mechanisms that have been proposed to explain regional variability in $\delta^{18}O$-elevation gradients primarily consider the role of atmospheric processes, including (1) mixing of moisture sources (DeCelles et al., 2007), a process common in continental interiors, (2) the role of convective storms and their associated violation of open-system, Rayleigh distillation processes (Liu et al., 2008), (3) the re-evaporation and recycling of $^{18}O$-enriched continental waters (Tian et al., 2001) and (4) the "amount effect", which accounts for drop-size dependent isotopic equilibration times (Lee and Fung, 2008). Each of these processes may act to produce precipitation $\delta^{18}O$-elevation gradients that differ from those predicted by simple Rayleigh distillation rainout (Rowley et al., 2001), increasing the uncertainty of quantitative, stable isotope-based paleoaltimetry estimates.

Understanding the controls on meteoric water $\delta^{18}O$ and $\delta^{18}O$-elevation gradient variability is further complicated by processes that modify the isotopic composition of the original precipitation after deposition. For example, isotopic modification of seasonal and annual snowpacks is a well-documented, post-depositional phenomenon that has been shown to have important implications for paleoclimate studies utilizing these paleo-meteoric water reservoirs as terrestrial isotopic records (Epstein et al., 1965; Johnsen, 1977; Cuffey and Steig, 1998; Ekaykin et al., 2002; Neumann et al., 2005; Town et al., 2008). In the field of paleoaltimetry, the role of evaporative enrichment of $^{18}O$ and $^{2}H$ in meteoric waters, and the implications this has for paleoelevation reconstructions, is also well-established (Garzione et al., 2000; Horton et al., 2004; Blisniuk and Stern, 2005; Blisniuk et al., 2005; Cyr et al., 2005; DeCelles et al., 2007; Quade et al., 2007; Polissar et al., 2009) with empirical evidence suggesting paleoelevation estimates can be underestimated by >2 km in regions of significant evaporative influence (Quade et al., 2007).

The dramatic influence that post-depositional isotopic modification processes can have on meteoric water isotopic compositions points to the need to understand the controls on the isotopic composition and isotope-elevation relationships of both precipitation (rain and snow) and terrestrial waters (groundwater, lakes, rivers, late season snowpack and snowmelt). In this study we investigate the regional variability of meteoric water $\delta^{18}O$ and associated $\delta^{18}O$-elevation relationships through modern spring and surface water sampling from the orographic slope to the orographic rainshadow of the Sierra Nevada mountains of the southwestern United States (Fig. 3.1). Comparison of $\delta^{18}O$ values and $\delta^{18}O$-elevation gradients for terrestrial waters with those of published

precipitation datasets elucidates the role that regionally-specific, post-depositional processes play in controlling the stable isotopic composition of modern terrestrial waters in this region. We demonstrate that understanding and quantifying these processes is important for any stable isotope-based paleoaltimetry, paleoclimate and hydrologic study utilizing isotopic records subject to post-depositional isotopic modification.

## 3.3 Study area

### *3.3.1 Physiographic and climatic setting*

In the western United States, south of ~42ºN, the Sierra Nevada acts as the primary orographic barrier and first order control on regional precipitation patterns. Annual precipitation amounts range from ~10 cm in the San Joaquin Valley on the western margin of the orogen up to ~250 cm at the highest elevation regions of the northern Sierra Nevada (PRISM Climate Group, www.prism.oregonstate.edu; accessed October 2010). Winter-season, Pacific-sourced storms deliver the majority of annual precipitation to the Sierra Nevada region (winter/summer ratio ≥ 5; Friedman and Smith, 1972; Friedman et al., 1992), in the form of both rain and snow, with increased snow accumulation at higher latitudes and elevations (Sierran winter snowline ~ 1500 m; Dahlgren et al., 1997). The influence of summer season precipitation, primarily sourced in the eastern tropical Pacific Ocean and Gulf of California, increases to the south with a minimum regional winter/summer precipitation ratio (W:S) of ~0.9 southeast of the southernmost Sierra Nevada in Goldstone, CA (Friedman et al., 1992). Due to the predominance of winter precipitation in the annual precipitation budget, spring snowmelt

and runoff leads to peak discharges during the spring in the Sierra Nevada and adjacent Basin and Range fluvial and groundwater systems.

Topographically, the Sierra Nevada is characterized by an asymmetric profile with peak elevations located along the eastern range front, resulting in a series of major, west-flowing, moderate gradient fluvial systems on the western (windward) slope of the orogen. The low elevation (< 200 m) San Joaquin Valley forms the western boundary of the Sierra Nevada and is base level for many of these fluvial systems (Fig. 3.1). Fluvial headwaters range in elevation from > 4000 m in the central Sierra Nevada (in the vicinity of Mt. Whitney) to 1500–2500 m in the southern and northern Sierra Nevada.

In the orographic rainshadow of the southern Sierra Nevada, late Cenozoic central Basin and Range extension has created a region characterized by a series of alternating low elevation basins and high elevation ranges producing high local relief (Fig. 3.1). West of Death Valley, CA, the Panamint Mountains expose a sequence of metamorphosed Proterozoic basement gneisses and schists overlain by upper Precambrian siliciclastic units (Labotka et al., 1980) that reach a maximum elevation at Telescope Peak (3369 m). Below- and near-sea-level basins (< 300 m) in the surrounding Panamint and Death valleys provide local relief exceeding 3000 m (Fig. 3.1C). This region has an arid climate with annual precipitation amounts ranging from ~5 cm in the valleys to < 38 cm at the highest peaks (Webb et al., 1987). The majority of annual precipitation falls during the winter season, with snow dominating the precipitation budget at high range elevations (> 2000 m).

Farther to the east, the Spring Mountains of southern Nevada are another high relief range formed as a result of Basin and Range extension. The range exhibits

topographic relief exceeding 2500 meters, from elevations of ~1000 m in the adjacent Pahrump and Las Vegas valleys to 3632 m at Mt. Charleston. Faulted and fractured Paleozoic carbonates comprise the vast majority of the Spring Mountains bedrock (Burchfiel et al., 1974). The fractured nature of the bedrock is a dominant control on regional hydrology, as the Spring Mountains act as a primary water source for the metropolitan areas of the Las Vegas Valley, in addition to feeding the Pahrump Valley to the west. The Spring Mountains are an arid to semiarid region with annual precipitation ranging from 20 cm in the foothills to > 60 cm at the range crest (Winograd and Thordarson, 1975). Winter season precipitation comprises approximately two-thirds of the annual precipitation budget in the Spring Mountains, yet accounts for ~90% of groundwater recharge (Winograd et al., 1998).

*3.3.2 Modern water sampling*

Spring and surface waters were collected from four elevation transects at a latitude of ~ 36°N in the southern Sierra Nevada and central Basin and Range region of the southwestern United States (Table 3.1, Fig. 3.1). Springs, streams and tributaries with small upstream drainage areas (< 5 $km^2$; Table 3.1), as determined from GIS-based hydrologic grids, were targeted for sampling in order to approximate a point source as closely as possible. In some cases, larger drainage area basins (up to ~2600 $km^2$; e.g., the Kern River, Table 3.1) were also sampled in order to test these point source approximations. The latitudinal range of sampling was also minimized in order to eliminate or reduce any latitudinal influence on the stable isotopic composition of meteoric waters. In this study, two surface water transects (Tule River and Southern Sierra, Fig. 3.1B) were sampled within the southern Sierra Nevada in order to constrain

## Figure 3.1

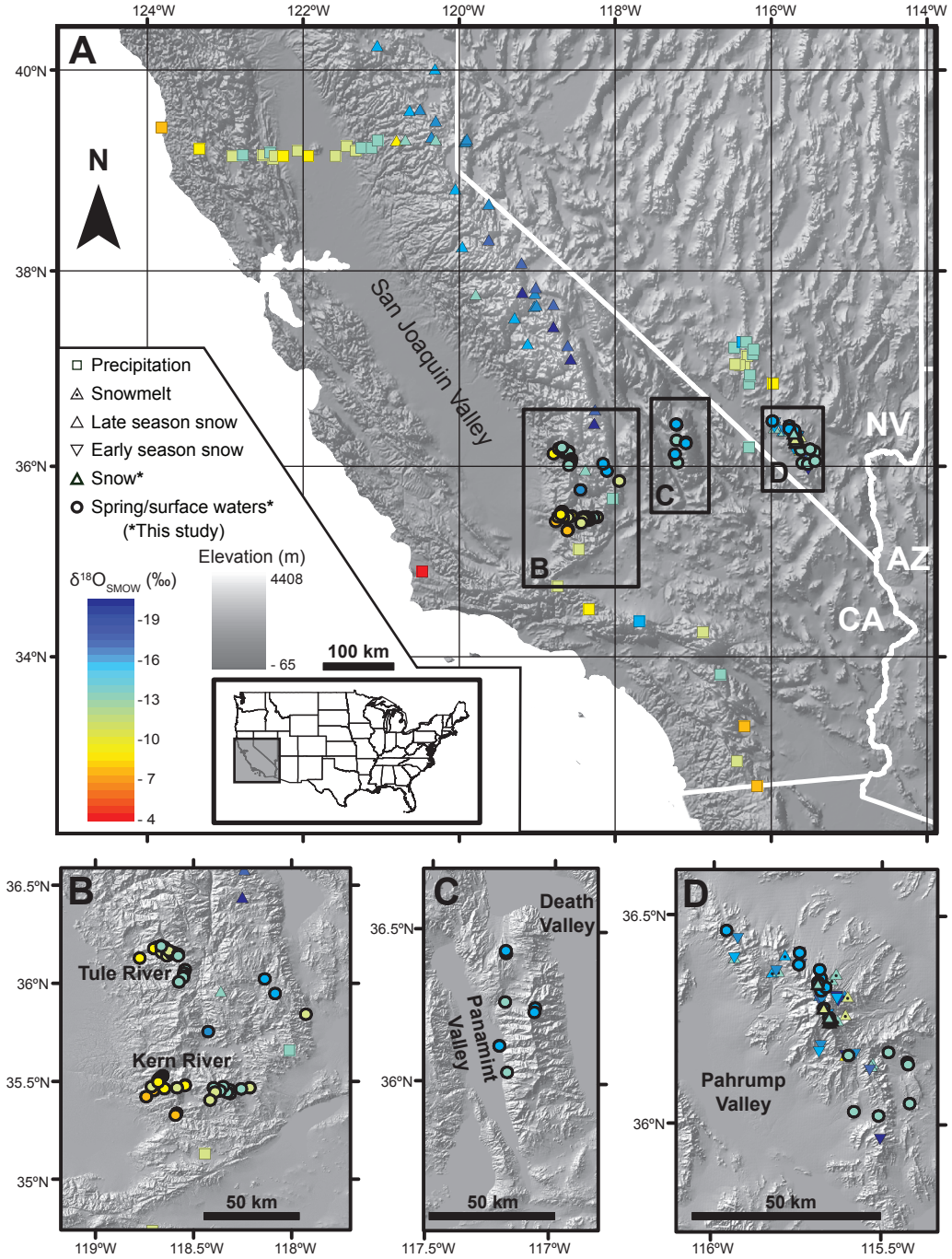


Figure 3.1 - (A) Digital elevation model (DEM) of the southwestern United States with locations of precipitation (central and northern Sierra Nevada: Ingraham and Taylor, 1991; southern Sierra Nevada and Basin and Range: Ingraham et al., 1991; Friedman et al., 1992), early season snowpack (Basin and Range: Hershey, 1989; Winograd et al., 1998), snowmelt (Basin and Range: Hershey, 1989; Winograd et al., 1998), spring and surface water (this study), and late season snowpack (central and northern Sierra Nevada: Friedman and Smith, 1972; Ingraham and Taylor, 1991; Basin and Range: this study) samples, color coded by $\delta^{18}O$ value. Samples collected as part of this study are denoted by heavy outline. Inset map shows approximate DEM extent. (B) DEM of southern Sierra Nevada region showing location of snow, precipitation and surface water samples. (C) DEM of Panamint Mountains, CA showing location of spring water samples. (D) DEM of Spring Mountains, NV showing snow, snowmelt, and spring water sample locations. B, C, and D have same color code as (A).

the isotope-elevation relationships of terrestrial waters across this orographic slope. Within the Sierran rainshadow, spring and surface waters were collected from the Panamint Mountains, ~75 km to the east of the southern Sierra Nevada (Fig. 3.1C), and in the Spring Mountains, which are located ~30 km northwest of Las Vegas, NV (Fig. 3.1D). Additionally, six late season (May 2009) snowpack samples were collected from the Spring Mountains over an elevation range of ~ 2500–3000 m for comparison with the sampled spring waters.

In order to investigate the relationships between isotopic composition and elevation, and the degree to which this relationship varies, we calculated the mean elevation of the contributing drainage basin for each water sample using GIS-based hydrologic analysis. Previous studies have shown that precipitation-weighted mean basin elevations are the most accurate representations of mean recharge elevations for surface waters (Rowley and Garzione, 2007), but with small drainage basin areas (< 250 $km^2$) the influence of uneven precipitation distributions appears to be negligible (Hren et al., 2009). As all of our sampled waters have small upstream drainage areas (<< 250 $km^2$), with the exception of the Kern River, mean basin elevation calculations using basin hypsometry alone are presumed to be sufficient. It is important to note that basin elevation calculations can be complicated for bedrock spring systems where surface topography may not accurately reflect the source areas for sampled waters, as discussed later. However, most of our collected springs were characterized by minimal flow rates, often only minor trickles and areas of ponding, in contrast to documented bedrock springs which are easily identifiable based on high discharges and mismatches between isotopic compositions and GIS-derived mean basin elevations. As such, the majority of springs

sampled in this study are likely locally sourced and thus surface hydrology-based calculations provide accurate estimates of the mean elevation of contributing drainage areas.

Isotopic measurements were completed at the University of Michigan Stable Isotope Laboratory. $\delta^{18}O$ values were measured via a Thermo Finnigan Gas Bench II coupled to the inlet of a Thermo Finnigan Delta V Plus mass spectrometer. δD measurements were performed using a continuous flow via a Thermo Finnigan High Temperature Conversion Elemental Analyzer (TC-EA) device coupled to the inlet of a Thermo Finnigan Delta V Plus mass spectrometer through a Thermo Finnigan ConFlo IV interface. Isotopic values were calculated based on isotopic analyses of lab standards (SLAP, Ann Arbor snow, evaporated $H_2O$), and most sample waters (~80% of the 98 analyzed waters) were subject to replicate analysis. Replicate and internal standard isotopic analyses constrained accuracy and precision of reported isotopic values to ± 0.1‰ for $\delta^{18}O$ and ± 2‰ for δD. All $\delta^{18}O$ and δD values are reported relative to Vienna Standard Mean Ocean Water (VSMOW).

## 3.4 Southwestern US meteoric water $\delta^{18}O$

### *3.4.1 Spring and stream water isotopic results*

*Orographic slope data*

Low elevation sample sites in both the Tule River and Southern Sierra sample transects (orographic slope) exhibit the highest $\delta^{18}O$ values of all analyzed samples. Tule River $\delta^{18}O$ values range from -9.6‰ to -12.5‰ over an elevation range of 1132–2403 m, yielding a mean $\delta^{18}O$-elevation gradient of -2.1‰/km (Fig. 3.2). For the Southern Sierra

transect, $\delta^{18}O$ values exhibit a wider $\delta^{18}O$ range of -7.6‰ to -14.6‰ for an elevation range of 881–2612 m resulting in a slightly higher magnitude, mean $\delta^{18}O$-elevation gradient of -3.1‰/km (Fig. 3.2). If the North and South Fork Kern River samples (drainage basin areas > 500 $km^2$; Table 3.1) are removed from the calculation, the mean $\delta^{18}O$-elevation gradient reduces to -2.8‰/km.

*Basin and Range data*

Compared to Tule River and Southern Sierra waters, maximum $\delta^{18}O$ values (i.e. low elevation values) are lower (by 2–5‰) in the Panamint Mountains and Spring Mountains transects, both of which are located within the Sierra Nevada orographic rainshadow. Panamint Mountains spring waters range from -12.6‰ to -14.1‰ over an elevation range of 1360–2579 m, resulting in a mean $\delta^{18}O$-elevation gradient of -0.9‰/km (Fig. 3.2). Spring waters in the Spring Mountains exhibit a similar magnitude $\delta^{18}O$-elevation gradient of -0.8‰/km, derived from a $\delta^{18}O$ range of -11.7‰ to -13.8‰ over elevations of 1106–3041 m (Fig. 3.2). Spring Mountains snow samples consistently exhibit higher $\delta^{18}O$ values (-10.0 to -12.5‰) compared to equal elevation spring waters, and show a trend of increasing $\delta^{18}O$ values with elevation (+3.6‰/km, Fig. 3.2), in contrast to the inverse $\delta^{18}O$-elevation relationships expected based on Rayleigh distillation processes.

*3.4.2 $\delta D$-$\delta^{18}O$ results*

All field samples were also analyzed for deuterium concentration ($\delta D$). Both the Tule River and Southern Sierra transects are characterized by highly correlated ($R^2 > 0.8$; Figure 3.3) $\delta D$-$\delta^{18}O$ relationships in general agreement with the Global Meteoric Water Line (GMWL: $\delta D = 8*\delta^{18}O + 10$; Craig, 1961). Our two Basin and Range datasets

(Spring Mountains and Panamint Mountains), however, exhibit a poor correlation between δD and $\delta^{18}O$ ($R^2 < 0.3$) with variable δD-$\delta^{18}O$ slopes (Fig. 3.3).

### *3.4.3 Comparison to published southwestern US precipitation $\delta^{18}O$ data*

In order to assess how accurately surface and spring waters preserve the isotopic composition of precipitation and the degree to which post-depositional isotopic modification occurs in the southwestern US study area, we compare our stream and spring water isotopic records to published regional isotopic records of both terrestrial waters (springs, late season snowpack, surface waters) and precipitation (rain and snow). For this comparison, we compiled published datasets for the northern and central Sierra Nevada (Friedman and Smith, 1972; Ingraham and Taylor, 1991), the southern Sierra Nevada (Friedman et al., 1992) and the Basin and Range (Hershey, 1989; Ingraham et al., 1991; Winograd et al., 1998) of the southwestern US (Fig. 3.2).

In the orographic slope region of the southwestern US (central and northern Sierra Nevada, southern Sierra Nevada), both precipitation and terrestrial waters (published and this study) exhibit a similar range in $\delta^{18}O$ values as well as similar magnitude $\delta^{18}O$-elevation gradients, whereas systematic differences are observed between precipitation and terrestrial $\delta^{18}O$ values and $\delta^{18}O$-elevation gradients derived from the Basin and Range (orographic rainshadow) datasets (Fig. 3.2). Specifically, Basin and Range spring water $\delta^{18}O$-elevation gradients (-0.8‰/km and -0.9‰/km) are a factor of 2–3 lower in magnitude compared to published regional precipitation isotopic gradients (-2.1‰/km; Ingraham et al., 1991; Fig. 3.2) and are also a factor of 3–4 lower than $\delta^{18}O$-elevation gradients observed for surface waters collected from the Sierra Nevada orographic slope

# Figure 3.2

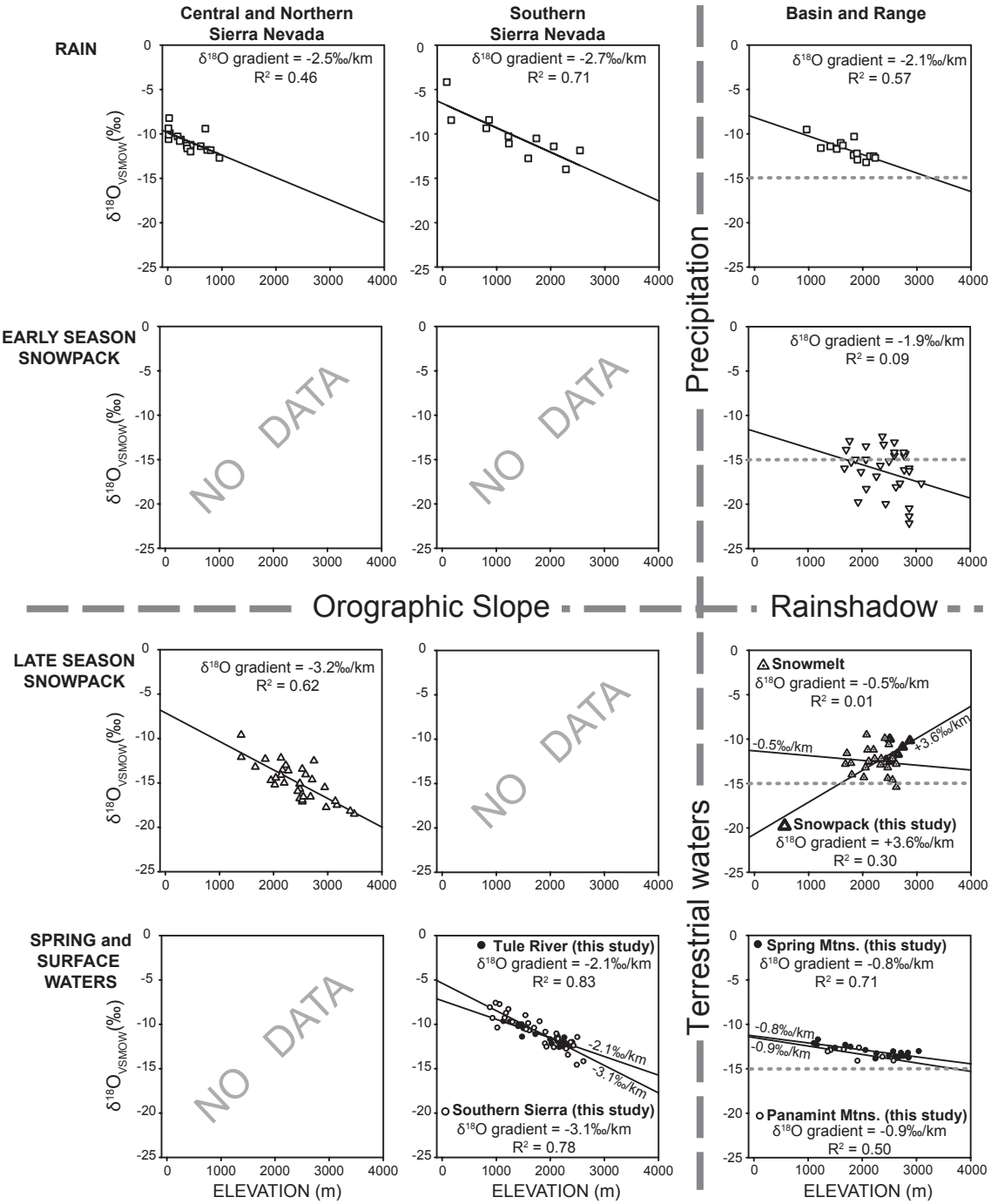


Figure 3.2 - $\delta^{18}O$ versus elevation for precipitation (rain, early season snowpack) and terrestrial waters (late season snowpack, springs, surface waters) in the orographic slope (central and northern Sierra Nevada, southern Sierra Nevada), and orographic rainshadow (Basin and Range) regions of the southwestern US. See Figure 3.1 caption for references and data sources. $\delta^{18}O$-elevation gradients and associated $R^2$ values are included for each dataset. Note the reduction in $\delta^{18}O$-elevation gradients for terrestrial waters in the Basin and Range by a factor of 3-4 compared with isotopic gradients of regional precipitation as well as in comparison to both precipitation and terrestrial waters in the orographic slope region. Dotted line at -15‰ included for Basin and Range datasets to highlight isotopic differences between early season snowpack and snowmelt-derived spring waters.

## Figure 3.3

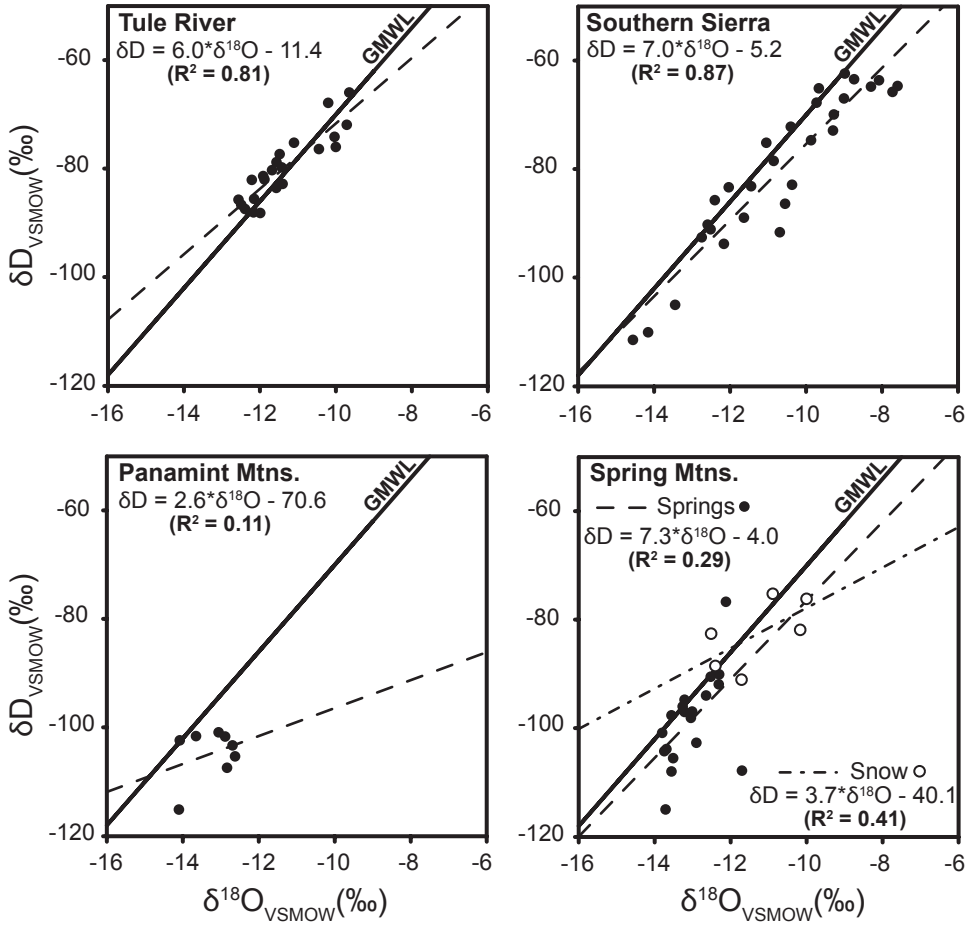


Figure 3.3 - δD versus $\delta^{18}O$ for terrestrial water transects of this study. Best-fit regression shown for each dataset relative to the Global Meteoric Water Line (GMWL): $\delta D = 8 \times \delta^{18}O + 10$ (Craig, 1961). δD-$\delta^{18}O$ slopes derived from Tule River and Southern Sierra surface water transects and Spring Mountains spring waters approximate GMWL. Panamint Mountains spring waters and Spring Mountains late season snow samples show significant deviation from GMWL.

(-2.1‰/km and -3.1‰/km). This systematic reduction in $\delta^{18}O$-elevation gradient is observed not only in our spring and surface water datasets, but also in published datasets from the Spring Mountains (Winograd et al., 1998) where snowmelt samples are characterized by a low $\delta^{18}O$-elevation gradient (-0.5‰/km) and snowmelt $\delta^{18}O$ values are on average > 2‰ higher than equal-elevation snowcore values (Fig. 3.2; Hershey, 1989; Winograd et al., 1998). Snowmelt values, however, closely approximate the isotopic composition of spring waters from the Spring Mountains at comparable elevations (Fig. 3.2).

It is important to note that there is a statistically poor ($R^2 < 0.1$) correlation between $\delta^{18}O$ and elevation for published Spring Mountains early season snowpack and snowmelt data (Fig. 3.2; Winograd et al., 1998), complicating the discussion of $\delta^{18}O$-elevation gradients and their relationship to spring water isotopic values. However, these snowpack and snowmelt samples were unsystematically collected in terms of both time and location during the early snow season (December–March; Winograd et al., 1998) and, as a result, provide only point source $\delta^{18}O$ data that likely reflects the $\delta^{18}O$ variability of individual precipitation events (Ingraham and Taylor, 1991) rather than the integrated isotopic value for each corresponding elevation. Spring waters are more likely to integrate over seasons or even years of precipitation and, thus, are more reliable indicators of $\delta^{18}O$-elevation relationships, as suggested by the relatively good correlation between $\delta^{18}O$ and elevation ($R^2 = 0.71$) for our Spring Mountains spring water samples. Even with these limitations, Spring Mountains snowcore and snowmelt datasets inform our interpretation of spring water isotopic compositions, as there is a clear shift to higher $\delta^{18}O$ values (> -15‰) in the snowmelt and spring water datasets relative to early season

snowcore $\delta^{18}O$ values, which are consistently lower (often < -15‰ (VSMOW)), particularly at elevations greater than 2000 m (Fig. 3.2).

### 3.5 Controls on meteoric water $\delta^{18}O$

Southwestern US terrestrial water isotopic datasets, both published and derived from this study, exhibit systematic regional differences in isotopic compositions and isotope-elevation relationships. Additionally, similarity in isotopic trends across all compiled datasets (Fig. 3.2), which span ~ 40 years of meteoric water sampling, suggests that, despite the limited duration of sampling for this study (1–2 seasons; Table 3.1), the observed isotopic trends in our southwestern US meteoric water datasets are representative on at least the decadal scale. The observed ranges in $\delta^{18}O$ values for Basin and Range transects (Spring and Panamint mountains) are reduced by a factor of 2–4 relative to $\delta^{18}O$ ranges for transects with comparable relief from the orographic slope (Tule River and Southern Sierra). Maximum $\delta^{18}O$ values (i.e. lowest elevations) in the Spring and Panamint mountains are 2–5‰ lower than Tule River and Southern Sierra maximums, simply due to orographic rainout over the Sierra Nevada prior to reaching the continental interior. However, minimum $\delta^{18}O$ values are comparable among all spring and surface water transects (~ -15 to -13‰), resulting in lower magnitude $\delta^{18}O$-elevation gradients for Basin and Range transects (Fig. 3.2). These results point to region-specific and elevation-dependent processes controlling the isotopic composition of Basin and Range terrestrial waters. Precipitation and terrestrial water $\delta^{18}O$ values and $\delta^{18}O$-elevation gradients are similar for all of the orographic slope datasets, suggesting that the processes influencing the isotopic composition of Basin and Range terrestrial waters are

not significant in the orographic slope region. As discussed previously, a number of mechanisms have been proposed to account for variability in $\delta^{18}O$-elevation gradients, but many of these are only relevant to depositional (i.e. atmospheric) processes and, thus, are unlikely to account for the isotopic shifts observed for the spring and surface waters relative to precipitation values in the continental interior of the western US.

Evaporation is one process that affects the isotopic composition of meteoric waters after deposition by systematically removing light isotopes (H and $^{16}O$), thereby increasing $\delta D$ and $\delta^{18}O$ values of the remaining water. However, in order to reduce $\delta^{18}O$-elevation gradients, the evaporative processes must be elevation dependent, with increased evaporative isotopic enrichment at higher elevations needed to reduce the isotopic gradient between low and high elevation sites. In the southwestern US, such an evaporation-elevation relationship is unlikely as peak evaporation commonly occurs in low elevation basins where temperature and aridity are at a maximum (e.g., Death Valley).

Snow sublimation is a process similar to, but distinct from, evaporation, which influences the isotopic composition of late season snowpacks and snowpack-derived meteoric waters (e.g., snowmelt, integrated spring and surface waters). Like evaporation, sublimation driven mass loss of snow after deposition will change the isotopic composition of the remaining snowpack to higher $\delta^{18}O$ values (Moser and Stichler, 1975; Stichler et al., 2001; Konishchev et al., 2003; Ekaykin et al., 2009). It has been proposed that snowpack sublimation would result in no net isotopic change to the remnant snowpack (Friedman et al., 1991); however this view is limited to only whole-grain, ice-vapor transitions and layer by layer mass loss from the snowpack. In an alpine snowpack,

however, the ice-vapor transition often involves an intermediate step of local melting and associated evaporation of this minor liquid phase, thus producing a similar isotopic effect to that of standard water evaporation (Neumann et al., 2008). Accordingly, the use of the term 'snow sublimation' in the remainder of this work encompasses the inter-snowpack ice-water-vapor phase changes occurring and is not limited to only whole-grain, ice-vapor transitions.

The effect of post-depositional isotopic modification due to snow sublimation has been studied extensively due to its relevance to paleoclimate reconstructions (Moser and Sitchler, 1975; Sommerfeld et al., 1991; Cooper, 1998; Stichler et al., 2001; Konishchev et al., 2003; Sinclair and Marshall, 2008; Ekaykin et al., 2009; Sokratov and Golubev, 2009), but has been largely ignored in the field of paleoaltimetry. Due to the fact that high elevation snowpacks are sustained later into the melt season than those at lower elevations, it is likely that snowpack mass loss due to sublimation is altitude dependent (e.g., Vuille, 1996). As a result, higher elevation snowpacks will experience increased sublimation-induced enrichment of $^{18}O$, which reduces the isotopic gradient between low and high elevation snowpacks, ultimately producing a decreased $\delta^{18}O$-elevation gradient across the remnant snowpack. The isotopic composition of meltwater derived from a sublimated snowpack will thus record a $\delta^{18}O$-elevation gradient that is substantially lower than that of the original precipitation, as observed in the Panamint Mountains and Spring Mountains datasets of this study (Fig. 3.2).

The influence of sublimation on the isotopic composition of meteoric waters is also likely to be region-dependent, as sublimation requires a specific set of environmental conditions, namely, high radiation input, low relative humidity, low vapor pressure, and

high wind speeds, all of which characterize mountain ranges in the Basin and Range, and high relief continental interiors, in general. This, along with the fact that annual precipitation in the Basin and Range is dominated by winter season precipitation in the form of snow, suggests that sublimation may be a primary influence on the isotopic evolution of meteoric waters in this region. If so, sublimation may account for the systematic isotopic differences between precipitation and terrestrial waters in our Basin and Range transects. Sublimation is unlikely to be as dominant of a process in the orographic slope of the Sierra Nevada, due to the high relative humidity of this region in comparison to the continental interior, and as reflected in the lack of net isotopic change in Sierran snowpacks over the course of the winter season (Taylor et al., 2001). The reduced sublimation potential in the Sierra Nevada may explain the similarity between precipitation and terrestrial water $\delta^{18}O$-elevation gradients in the orographic slope region as well as the difference between orographic slope and Basin and Range spring and surface water $\delta^{18}O$-elevation gradients.

The wealth of meteoric water isotopic datasets from the Spring Mountains, in addition to the spring water sampling of this study (Fig. 3.2), makes this a key region to investigate the role of snow sublimation in post-depositional isotopic enrichment and modification of $\delta^{18}O$-elevation gradients. The > +2‰ shift for snowmelt samples compared to early season (December–March) snowcores (Fig. 3.2; Hershey, 1989; Winograd et al., 1998), suggests that processes specific to snowpack isotopic modification exert a primary influence on meteoric water isotopic values. A shift of even greater magnitude (~ +3–5‰) is observed in the six late-season (May) snowpack samples collected as part of this study, further supporting the idea of post-depositional isotopic

modification of the snowpack throughout the winter season. Similarity of snowmelt (Winograd et al., 1998) and spring water (this study) $\delta^{18}O$ values and $\delta^{18}O$-elevation gradients (Fig. 3.2) suggests that winter season precipitation and the processes affecting this precipitation following deposition are the primary influences on the isotopic composition of meteoric waters recharged in this region (Winograd et al., 1998). Using the data and evidence presented above, in combination with a range of reasonable environmental parameters, we use a Rayleigh distillation snow sublimation model to calculate the effects of sublimation processes on the isotopic composition of snowmelt-derived spring and surface waters.

### 3.6 Rayleigh distillation modeling of $\delta^{18}O$

We assess the plausibility of snow sublimation as a primary driver for the isotopic composition of snowmelt-derived meteoric waters through a Rayleigh distillation model, which quantifies the isotopic evolution of snowpacks as a function of elevation. Initial (early season) snowpack $\delta^{18}O$ value is controlled by the isotopic composition of individual precipitation events that occur at a given site. The $\delta^{18}O$ value of these individual precipitation events can be quite variable at a single location and early season snowpacks often preserve this initial variability. Over the course of the winter season, however, the snowpack undergoes $\delta^{18}O$ homogenization due to snowpack metamorphism and a variety of isotopic exchange processes (Friedman et al., 1991; Cooper, 1998; Taylor et al., 2001; Unnikrishna et al., 2002; Earman et al., 2006; Neumann et al., 2008). As a result, seasonal snowpacks evolve to a uniform, average $\delta^{18}O$ value that correlates to site elevation (Fig. 3.2; Friedman and Smith, 1972). In the Basin and Range, compiled

early season snowpack $\delta^{18}O$-elevation gradients, albeit poorly constrained (Winograd et al., 1998), are similar to regional precipitation (rain) gradients and are of a similar magnitude (~ -2‰/km) to Rayleigh distillation-derived gradients (Rowley et al., 2001).

Initial parameters of the Rayleigh distillation model are based on published data from southern Nevada, including an initial $\delta^{18}O$ value of -11‰ at 1000 m (Friedman et al., 2002) and a precipitation $\delta^{18}O$-elevation gradient of -2.0‰/km (Fig. 3.2; Ingraham et al., 1991; Winograd et al., 1998). We apply an experimentally determined snow-vapor fractionation factor (Neumann et al., 2008) and assume that the fraction of mass loss due to sublimation increases linearly with elevation, consistent with available observational constraints (Vuille, 1996, Hood et al., 1999; Schulz and de Jong, 2004). Rayleigh distillation applies to open fractionation systems such that sublimated snow is completely removed from the system after phase change. In real world settings, this sublimated vapor may interact with the remaining snowpack at a later time or position downwind. For the sake of model simplicity, we assume that the influence of vapor-snowpack isotopic exchange is minor but the possible implications of these interactions are discussed later. The applied, experimentally-derived fractionation factor (Neumann et al., 2008) assumes snowpack temperature is held constant at -5°C, independent of elevation. Inclusion of an adiabatic lapse rate would only serve to increase isotopic fractionation with altitude (i.e. increased $^{16}O$ removal at colder temperatures and higher elevations), thus amplifying the effects of altitude-dependent sublimation on $\delta^{18}O$-elevation gradients. The isotopic evolution of snow with increasing fraction of sublimation-derived mass loss is shown by a suite of Rayleigh distillation curves (gray lines in Fig. 3.4A) described by the following function:

$$\delta^{18}O_{final} = (\delta^{18}O_{initial} + 1000) \times (1 - f)^{\left(\frac{1}{\alpha} - 1\right)} - 1000 \quad \textbf{(Eq. 3.1)}$$

where $f$ is the fraction of the snowpack sublimated and $\alpha$ is 1.013, the snow-vapor fractionation factor at -5°C (Neumann et al., 2008).

The isotopic evolution of discrete points undergoing altitude-dependent sublimation is shown by suites of colored dots (Fig. 3.4), assuming sublimation is 0% at 1500 m (the approximate winter snow line in the Spring Mountains) and increases linearly with elevation (Fig. 3.4A). For example, navy blue dots represent the evolution of the original snowpack at 500-m increments for an altitude-dependent sublimation gradient of 5%/km (Fig. 3.4A). The suite of dots from black to light blue along the 4500 m distillation curve represent the final isotopic composition of the snowpack at 4500 m with increasing sublimation gradients (e.g., 0, 5, 10, 20, and 30%/km) representing 0, 15, 30, 60, and 90% total mass loss due to sublimation (Fig. 3.4A). The effect of sublimation on $\delta^{18}$O-elevation gradient is shown by plotting the final (late season) isotopic composition of the snowpack versus elevation for our range of modeled sublimation gradients (Fig. 3.4B). Black dots (0% sublimation) represent the original $\delta^{18}$O-elevation gradient of the snowpack, -2‰/km (Fig. 3.4B). With increasing sublimation amounts, the $\delta^{18}$O-elevation gradient of the snowpack is reduced (Fig. 3.4B). If sublimation gradients are high enough (> 15%/km), the $\delta^{18}$O-elevation gradient may actually invert at higher elevations (> 3000 m), and the snowpack will exhibit increasing $\delta^{18}$O with elevation, similar to that observed in our late season snow samples (Fig. 3.2) and documented in the European Alps (Moser and Stichler, 1975).

# Figure 3.4

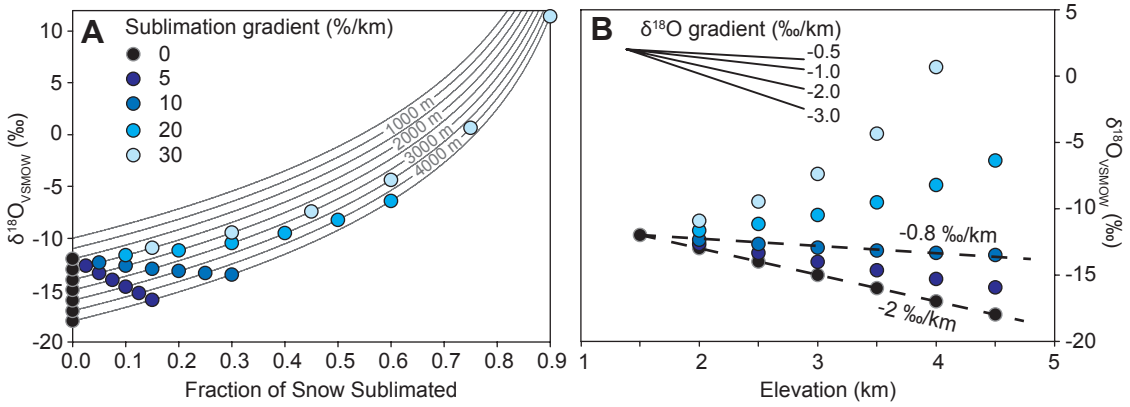


Figure 3.4 - (A) Rayleigh distillation curves (gray lines at elevations of 500-4500 m) for a theoretical snowpack undergoing mass loss due to sublimation with a $\delta^{18}O$ composition of -11‰ at 1000 m and a precipitation $\delta^{18}O$-elevation gradient of -2.0‰/km. Dots indicate the $\delta^{18}O$ isotopic shifts for discrete elevations on the snowpack with increasing gradients of altitude-dependent mass loss due to sublimation (see text for discussion). (B) $\delta^{18}O$ composition of snowpack after sublimation-derived mass loss versus elevation, colored to match models in (A). The slope of a line through each group of colored dots represents the $\delta^{18}O$-elevation gradient resulting from isotopic evolution due to sublimation, with black dots representing the original, unmodified $\delta^{18}O$-elevation gradient of -2.0‰/km. A sublimation gradient of 10‰/km (medium blue dots) results in a shift in post-depositional $\delta^{18}O$-elevation gradient similar to that observed in the Spring and Panamint mountains (from -2.0‰/km to ~ -0.8‰/km).

In the Spring Mountains, spring water and snowmelt $\delta^{18}O$-elevation gradients are a factor of 3–4 lower than rain and early season snowpack gradients (Fig. 3.2). Modeling results indicate that such a reduction of $\delta^{18}O$-elevation gradient magnitudes can be achieved with a sublimation gradient of ~10%/km. Snowpack $\delta^{18}O$ datasets are not available from the Panamint Mountains, but the similarity of Panamint Mountains spring water $\delta^{18}O$ values and $\delta^{18}O$-elevation gradients to Spring Mountains datasets suggests a sublimation gradient of ~10%/km may also apply to the Panamint Mountains. Although compelling observational constraints on sublimation rates and gradients are scarce, such a sublimation gradient is consistent with field-based estimates of sublimation in other regions of the western US. Detailed calculations using measurements of latent heat fluxes from Niwot Ridge, CO estimate annual snowpack mass loss due to sublimation is ~15% at elevations of 3500 m (Hood et al., 1999). A field-based study monitoring the evolution of snowpacks in the Magdalena Mountains in central New Mexico provides another estimate, with observed sublimation amounts of ~13% at an elevation of 2560 m (Earman et al., 2006). Thus, despite a lack of hard constraints on regional sublimation amounts in the Spring and Panamint mountains, expected sublimation rates based on observed $\delta^{18}O$-elevation gradient evolution are of a reasonable magnitude when compared to available constraints from throughout the western United States.

### 3.7 $\delta D$-$\delta^{18}O$ relationships

Regional $\delta D$-$\delta^{18}O$ trends observed for our sampled spring and stream waters (Fig. 3.3) provide additional support for sublimation influence on Basin and Range meteoric waters. Sublimation, like evaporation, is a kinetically influenced process, and, as such,

will tend to drive $\delta D$-$\delta^{18}O$ relationships away from the GMWL. Both field (Stichler et al., 2001; Earman et al., 2006) and experimental (Lee et al., 2009) studies suggest that $\delta D$-$\delta^{18}O$ slopes of ~5–6 characterize snowpacks undergoing sublimation. Late season snowpack samples from the Spring Mountains, collected as part of this study, have a $\delta D$-$\delta^{18}O$ slope of 3.7 (Fig. 3.3), consistent with significant post-depositional isotopic modification by kinetic processes. Spring water samples from the Spring Mountains, however, are characterized by a $\delta D$-$\delta^{18}O$ slope of ~7.3, similar to that of the GMWL (Fig. 3.3). One possible explanation for this higher than expected $\delta D$-$\delta^{18}O$ slope for sublimation-influenced waters is that sampled spring waters integrate meltwaters from throughout the melt season, not just from the late season snowpacks most heavily influenced by sublimation. Based on our Rayleigh distillation models, the total mass loss necessary to sufficiently alter $\delta^{18}O$ compositions and produce the reduced $\delta^{18}O$-elevation gradients observed in Spring Mountains spring and meltwaters is quite modest ($\leq$ 15%). As such, the total kinetic effects of sublimation on the isotopic compositions should also be modest and result in only minor deviations from the GMWL for meltwaters, as observed (Fig. 3.3).

The very low $\delta D$-$\delta^{18}O$ gradient observed for Panamint Mountains waters (~ 2.6; Fig. 3.3) is also consistent with significant influence from kinetic processes, but interpretations of this dataset should be made with caution as the regression is constrained by a small sample population (n = 8) and the best-fit regression is poorly constrained ($R^2$ = 0.11). Published meteoric water datasets from neighboring Death Valley exhibit similarly low $\delta D$-$\delta^{18}O$ gradients (~ 3.5; Jahren and Sanford, 2002) suggesting that post-depositional kinetic processes exert a dominant influence on regional

meteoric water isotopic compositions. The Jahren and Sanford (2002) dataset also provides additional support for our proposal of sublimation influence to regional snowpack isotopic compositions as snowpacks that showed clear evidence for sublimation-derived mass loss had $\delta^{18}O$ values 3–4‰ higher than those for recent accumulations of fresh snow at the same site.

It is important to note, however, that sublimation alone is unlikely to account for all of the observed regional variability in $\delta D$-$\delta^{18}O$ trends. Continental moisture recycling, seasonal variability in moisture source and below cloud evaporation of rain and snow can all lead to deviations from the GMWL (Araguás-Araguás et al., 2000). Each of these processes may account for at least part of the increased variability in $\delta D$-$\delta^{18}O$ relationships for the Basin and Range waters observed in this and published (e.g., Jahren and Sanford, 2002) studies, as high regional aridity promotes increased moisture recycling as well as both depositional and post-depositional evaporation, and the seasonal influence of multiple moisture sources (Pacific Ocean, Gulf of California) complicates isotopic relationships for precipitation and associated meteoric waters in the Basin and Range. Unraveling the effects of each of these individual processes on $\delta D$-$\delta^{18}O$ relationships in the Basin and Range is complex and requires highly-controlled field and lab-based methodologies that are beyond the scope of this study.

## 3.8 Additional mechanisms for $\delta^{18}O$-elevation gradient variability

### *3.8.1 Alternative sources of $\delta^{18}O$ evolution in a snowpack*

While sublimation can plausibly explain the alteration of the isotopic composition of a snowpack and resulting $\delta^{18}O$-elevation gradients, the roles of other isotopic

exchange processes also need to be considered. Temperature-gradient metamorphism and partial melting and refreezing (Colbeck, 1987) serve to homogenize the isotopic composition of a snowpack, but generally do not lead to isotopic exchange with external reservoirs, and thus would not alter net snowpack $\delta^{18}O$, or change $\delta^{18}O$-elevation gradients. One process that could account for relative $^{16}O$ depletion ($^{18}O$ enrichment) through isotopic exchange with an external reservoir is the condensation of atmospheric water vapor onto, or into, the snowpack (Moser and Stichler, 1975; Cooper, 1998). This process dominates over sublimation during the late spring and early summer when regional relative humidity and atmospheric temperature increase. Atmospheric water vapor during these seasons tends to be characterized by higher $\delta^{18}O$ values than that of winter snow, and, as a result, condensation of this vapor onto the snowpack would result in an increase in snowpack $\delta^{18}O$ value. However, the importance of condensation of atmospheric moisture vapor to modifying snowpack $\delta^{18}O$ compositions appears minor, as net mass gain due to condensation is often insignificant in comparison to annual mass loss due to sublimation (Hood et al., 1999; Earman et al., 2006), particularly in regions characterized by low relative humidity, such as the Basin and Range.

Isotopic exchange between snow and atmospheric water vapor is another mechanism that may contribute to the observed isotopic enrichment of a snowpack, as demonstrated in a controlled experiment monitoring the isotopic evolution of snow in the presence of an isotopically distinct (low $\delta^{18}O$ value) brine (Earman et al., 2006). Snow-atmospheric water vapor exchange is most likely to occur during the spring as the snowpack warms (Fred Phillips, pers. comm., 2008) and when atmospheric water vapor is characterized by higher $\delta^{18}O$ values than that of the snow. The significance of this

process to modifying the $\delta^{18}O$ composition of snow remains poorly constrained (Earman et al., 2006), and thus fully quantifying this effect on $\delta^{18}O$-elevation gradients is not possible at present, but the applicability of this mechanism to the reduction of $\delta^{18}O$-elevation gradients can be assessed from a theoretical perspective. If the rate, or amount, of isotopic exchange is not altitude dependent, the effect will be to shift snowpack $\delta^{18}O$ to higher values but not to reduce $\delta^{18}O$-elevation gradients. However, snowpacks at higher elevations are sustained later into the spring or early summer than at lower elevations, and, as a result, are subject to longer exposure times and associated atmospheric isotopic exchange. Thus, it is possible that in some cases the amount of isotopic exchange would be elevation dependent, and, as seen with elevation-dependent mass loss via sublimation, could lead to a reduction in snowpack $\delta^{18}O$-elevation gradient through the melt season. In order to fully validate this mechanism, the magnitude of isotopic enrichment in late season snowpacks as a function of seasonal variability of $\delta^{18}O$ (i.e. the difference in isotopic composition between warm and cool season precipitation and atmospheric water vapor) must be quantified through future study.

*3.8.2 Complications from bedrock springs*

Meteoric water samples collected from the Spring and Panamint mountains were obtained from bedrock springs, in contrast with surface water (runoff) samples obtained from the orographic slope of the southern Sierra Nevada. Collecting from bedrock springs can potentially complicate the interpretation of isotope-elevation relationships due to the possible deep infiltration and transport of high elevation (low $\delta^{18}O$ value) waters to low elevation springs, which would reduce the apparent $\delta^{18}O$ gradient between low and high elevation sites. Such transport may account for the slightly lower $\delta^{18}O$

values (1–2‰) for the lowest elevation Spring and Panamint mountains spring water samples when compared to precipitation $\delta^{18}O$ values from comparable elevations in nearby regions (Fig. 3.2). However, this bedrock spring effect cannot account for all of the observed variability in isotopic compositions and isotope-elevation relationships because transport of high elevation waters will lead to decreased $\delta^{18}O$ values at lower elevation sites, but will have no effect on high elevation water $\delta^{18}O$ values. The observation that the highest elevation spring samples ($\delta^{18}O$ ~ -14 to -13‰; Fig. 3.2) of this study exhibit the greatest deviation from equal elevation winter precipitation $\delta^{18}O$ values (-22 to -15‰; Fig. 3.2) suggests that complications from bedrock hydrology are a secondary influence on $\delta^{18}O$-elevation gradients and that elevation dependent processes, such as altitude-dependent snow sublimation, act as a first order control on the isotopic composition of our sampled Basin and Range spring waters. While uncertainty in recharge locations for bedrock springs cannot account for the observed isotopic trends at high elevations in Spring and Panamint mountains spring waters, it can alter the absolute magnitude of $\delta^{18}O$-elevation gradients. Thus, constraining the amount of regional sublimation using isotopic proxies will be subject to increased uncertainty in areas where regional hydrology is poorly understood.

## 3.9 Implications of snow sublimation on stable isotope-based hydrologic and paleoelevation studies

### *3.9.1 Hydrologic studies*

An understanding of the processes that modify the isotopic composition of precipitation after deposition is important for any paleoaltimetry, paleoclimate, or

hydrologic study utilizing the stable isotopic composition of meteoric water proxies. Modern spring and surface waters collected for this study suggest significant post-depositional isotopic modification of terrestrial waters in the continental interior of the southwestern US has occurred. Specifically, the process of altitude-dependent snow sublimation in the mountain environments of the continental interior appears to be a primary control on isotopic composition, a finding with implications for future hydrologic studies in this region, especially in the context of current global warming trends. For example, groundwater isotopic compositions are commonly used to determine the seasonality and location of annual recharge in mountain settings (e.g., Winograd et al., 1998). Hydrologic studies often consider only the depositional isotopic compositions of winter and summer season precipitation, and apply two-component (warm and cool season) mixing models to estimate seasonal influence on groundwater recharge. Snowpack sublimation, however, leads to increased meltwater $\delta^{18}O$ values, yielding an isotopic signature that modifies winter precipitation to become more "summer-like". This effect leads to an underestimate of the contribution of winter season precipitation to groundwater recharge (Earman et al., 2006), which can potentially misrepresent regional hydrologic processes. In the continental interior western US, average winter season precipitation $\delta^{18}O$ values are ~3–6‰ lower than those of summer rain (Friedman et al., 1992; Friedman et al., 2002). This seasonal difference can be at least partially erased through sublimation or other post-depositional processes, as indicated by the observed ~2–5‰ shift between precipitation and terrestrial continental interior waters of this study (Fig. 3.2), an effect that will complicate quantification of seasonal influence to groundwater recharge. In the Spring Mountains, observation of the ≥+2‰ shift in the

$\delta^{18}O$ of spring snowmelt relative to mean winter snowpack, has led to more accurate quantification of seasonal recharge amounts, specifically the increased influence of winter season recharge (~90%) to the annual groundwater budget (Winograd et al., 1998). Future hydrologic studies must also be aware of the likelihood of post-depositional increases in $\delta^{18}O$ values, particularly for winter season snowpacks, in order to avoid significantly underestimating the contribution of winter season recharge.

Accurate assessment of the timing and location of groundwater recharge is also fundamental to proper water resource management in the arid, continental interior of the western United States. The results of this study indicate that altitude-dependent snow sublimation exerts a first order influence on the stable isotopic compositions of the terrestrial meteoric waters that ultimately feed regional groundwater systems. Understanding the isotopic evolution of snowpack systems is especially important considering snowpacks are often the largest reservoirs for annual precipitation, and spring season snowmelt is the dominant source of water recharge, in the water-stressed western US (e.g., Mote et al., 2005; Henderson and Shuman, 2010). Recent trends of declining mountain snowpack and earlier onset of spring snowmelt as a result of global climate warming have been well-documented throughout the western US (Mote et al., 2005; Knowles et al., 2006; Clow, 2010; Kapnick and Hall, 2010; Minder, 2010). In combination with the isotopic effects of snowpack sublimation, these trends of declining snowpack and earlier onset of snowmelt have important implications for hydrologic studies utilizing stable isotopic compositions to understand recharge processes. With shorter snow seasons, and associated increases in the percentage of annual precipitation falling as rain instead of snow, the magnitude of isotopic modification due to snow

sublimation will likely be reduced. Accordingly, the isotopic signatures of winter precipitation and their difference relative to those of summer precipitation may be better preserved under these new climatic conditions. Since sublimation leads to increased $\delta^{18}O$ (and $\delta D$), if current warming trends continue, it follows that, in mountain catchments where snowmelt is a dominant groundwater contributor, there may be a shift to more negative $\delta^{18}O$ and $\delta D$ values of meteoric waters, independent of a change in seasonal precipitation amounts or timing and location of groundwater recharge. For accurate hydrologic assessments, these possible climate change-induced shifts must not be interpreted as a change to higher elevation sources or increased contribution of winter season precipitation to the groundwater budget.

*3.9.2 Stable isotope paleoaltimetry*

Paleoaltimetry reconstructions often utilize isotopic relationships from modern precipitation to constrain paleoelevation histories (Rowley et al., 2001; Currie et al., 2005; Garzione et al., 2006; Mulch et al., 2006; DeCelles et al., 2007). As the results of this study indicate, however, meteoric water proxies subject to post-depositional isotopic modification may not accurately reflect the isotopic composition of the precipitation from which they are derived. Specifically, the process of snow sublimation systematically increases the $\delta^{18}O$ and $\delta D$ composition of the snowpack, and the meteoric waters derived from it, throughout the snow and snowmelt seasons. The elevation-dependent behavior of snow sublimation leads to reduced isotopic differences between high and low elevations, thus reversing the effects of Rayleigh distillation processes and ultimately leading to underestimates of paleoelevation. The degree to which these isotopic shifts influence paleoelevation estimates depends on the amount of sublimation-derived mass loss

occurring over the course of the snow season. Using the same Rayleigh distillation equation above (Eq. 3.1), the net snowpack isotopic change for a corresponding sublimation amount can be calculated. Combining this isotopic shift with commonly-applied $\delta^{18}O$-elevation gradients of -2 to -3‰/km, a resulting paleoelevation underestimate can be calculated (the difference between elevation calculated using post-depositional $\delta^{18}O$ value and 'actual' elevation; Fig. 3.5).

Estimates for seasonal sublimation mass losses in alpine environments are highly variable, ranging from 10–90% (Strasser et al., 2008). In most empirical studies of the continental interior western US, however, observed annual sublimation mass loss is generally moderate, on the order of 5–40% (Hood et al, 1999; Earman et al., 2006; Strasser et al., 2008). Corresponding maximum paleoelevation underestimates for these sublimation amounts would be ~ 2 and 3 km for applied $\delta^{18}O$-elevation gradients of -3‰/km and -2‰/km, respectively (Fig. 3.5), which are similar to underestimates resulting from significant evaporative influence (Quade et al., 2007). It should be noted that these calculations assume sublimated snowpacks are the only contributor to terrestrial waters and, thus, provide maximum paleoelevation underestimates. Surface and groundwater contributions that are not influenced by post-depositional isotopic change (e.g., cool season rain) will reduce the isotopic impact of snowpack sublimation and, as a result, the degree to which paleoelevations would be underestimated. The fact that winter season precipitation, primarily in the form of snow, is the dominant contributor to groundwater recharge in the mountainous, continental interior US, however, suggests that these calculations provide good first order approximations of the impact sublimation-induced isotopic change can have on paleoelevation quantification. The magnitude of

these underestimates highlights the need to constrain the influence of snow sublimation on the isotopic composition of terrestrial waters in order to make accurate estimates of paleoelevation. As a specific example, attempts to estimate the "paleoelevation" of the Spring Mountains using the $\delta^{18}O$ composition of present-day spring and surface waters in combination with either the modern precipitation $\delta^{18}O$-elevation gradient (-2.0‰/km) or a global average $\delta^{18}O$-elevation gradient (-2.8‰/km; Poage and Chamberlain, 2001) would result in an underestimate of range elevations (or relief) by a factor of 3 to 4.

The influence of sublimation isotopic modification processes to paleoelevation reconstructions will also be proxy-dependent as each proxy system informs about regional hydrology in a unique way. As this study indicates, paleo-terrestrial water (e.g., lakes, rivers, springs) proxy records (e.g., lacustrine carbonates, fossil shells and teeth deriving their isotopic signatures from lake, river, and/or spring waters) are likely to be directly affected by sublimation effects, particularly in meteoric water systems where seasonal snowpack is a dominant contributor to the annual hydrologic cycle. Lake, river and spring waters integrate the isotopic signal from throughout the contributing catchment. Contributions from upstream water sources (i.e. higher elevations, lower $\delta^{18}O$ values) often result in terrestrial water $\delta D$ and $\delta^{18}O$ values that are lower than those of equal elevation precipitation (e.g., Dutton et al., 2005). As a result, lacustrine and fluvial proxies more reliably inform about basin hypsometry than about elevations at the site of proxy formation (e.g., Dettman and Lohmann, 2000; Rowley et al., 2001; Rowley and Garzione, 2007). In cases where lacustrine and fluvial proxy systems are subject to significant sublimation influence, paleoelevation reconstructions using these proxy records will be prone to errors in paleo-hypsometric calculations, specifically

underestimation of catchment relief and maximum elevations. In contrast, pedogenic carbonates, and similar paleo-precipitation proxies (e.g., weathered volcanic ashes), are less likely to be influenced by sublimation processes as they more reliably record paleo-precipitation isotopic compositions and thus are subject to reduced post-depositional isotopic modification. Sublimation influence to pedogenic carbonate proxy records is also expected to be significantly reduced due to the tendency for soil carbonates to form exclusively during summer months when temperature, evaporation and soil degassing rates are at a maximum (Quade et al., 2007) and when local soil waters are more likely to be derived from warm season precipitation characterized by minimal or no snowfall.

Sublimation can significantly increase stable isotope-based paleoelevation uncertainties (Fig. 3.5), but these uncertainties can be constrained due to the fact that snow sublimation requires a specific set of environmental conditions in order to significantly influence the stable isotopic composition of terrestrial waters. As a result, sublimation influence can be estimated, at least to a first degree, by characterizing the paleo-environment from which isotopic records are derived. In general, sublimation will be most influential in areas dominated by winter season precipitation in the form of snow, where regional meteoric water recharge is derived primarily from spring season snowmelt, and in regions of high aridity, high wind speeds, high solar radiation and low vapor pressure. This combination of environmental characteristics is common in a number of modern orogenic systems subject to current paleoaltimetry debate, such as the arid, continental interior of the western US (Houghton, 1969), the South American Altiplano (Houston and Hartley, 2003) and portions of Tibet (Wu and Qian, 2003; Shreve et al., 2009). Continued work to better quantify modern annual sublimation amounts,

# Figure 3.5

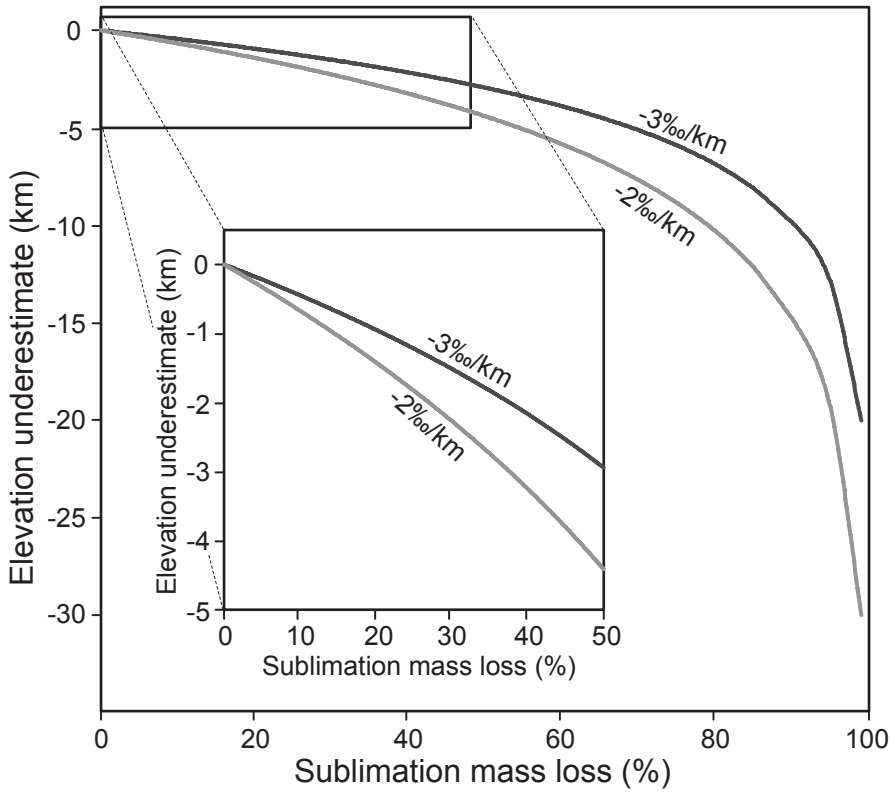


Figure 3.5 - Stable isotope-based elevation underestimates calculated as a function of sublimation-derived mass loss from a seasonal snowpack. Elevation values are calculated using Rayleigh distillation model-derived $\delta^{18}O$ increases for a sublimated snowpack (see text for discussion) in combination with commonly applied $\delta^{18}O$-elevation gradients. Inset plot limits focus to sublimation rates (0-50%) that are characteristic of modern, continental interior montane settings, particularly in the western US Cordillera.

particularly in arid, continental interior montane and high-standing plateau regions, will greatly aid the interpretation of sublimation-influenced isotopic records in future studies.

*3.9.3 Isotopic relationships over continental plateaus*

Interior continental plateaus are commonly the focus of paleoaltimetry study (e.g., Western US, Tibet, Altiplano) as their paleoelevation histories are integral to constraining the geodynamic and climatic evolution of major orogenic systems. Often, though, these interior plateaus are characterized by complex isotope-elevation relationships that complicate standard stable isotope approaches (e.g., Blisniuk and Stern, 2005; Quade et al., 2007). Figure 6 shows meteoric water $\delta^{18}O$ compositions as a function of elevation and distance from the major regional orographic barrier across the Himalayan-Tibetan Plateau orogen (Fig. 3.6A, see caption for references) and in the western US at a latitude of ~36°N (Fig. 3.6B, this study). In both regions, there is a well-defined relationship between $\delta^{18}O$ and elevation along the orographic slope (Sierra Nevada for the western US; Himalaya for the Tibetan Plateau) with $\delta^{18}O$ mimicking topography (low $\delta^{18}O$ values at high elevations). In the continental interior, however, $\delta^{18}O$-elevation relationships are less straightforward. As discussed, in the western US, continental interior meteoric water $\delta^{18}O$-elevation relationships are muted relative to the orographic slope, which we propose here results, at least partially, from post-depositional, altitude-dependent isotopic modification processes, such as snow sublimation. In the Tibetan Plateau, a similar disconnect between $\delta^{18}O$ and elevation is observed, with increasing $\delta^{18}O$ values correlating with increasing distance from the Himalayan front.

It is important to point out that the spatial scale over which the Tibetan Plateau $\delta^{18}O$-elevation relationships are shown is significantly greater than that for the

southwestern US (Fig. 3.6), introducing additional influences to regional $\delta^{18}O$ patterns. The increase in $\delta^{18}O$ as a function of distance from the Himalayan front (i.e. latitude) is believed to be largely due to the complex interaction of multiple moisture sources over northern Tibet (Liu et al., 2008) as well as the increased influence of continental moisture recycling over the Tibetan Plateau (Tian et al., 2001), but this increase may at least partially result from isotopic modification of meteoric waters through either evaporation or snowpack sublimation in this high elevation, arid region. The influence of sublimation may have been even more important in the Tibetan Plateau region during the geologic past when winter season snow was a more dominant contributor to the annual precipitation budget. For example, the Tibetan Plateau is presently dominated by summer precipitation (W:S precipitation ratios of ~0.25), but has experienced periods of greater winter precipitation in the recent geologic past (e.g., W:S ratios of ~0.75; Wang et al., 2001), as well as arid, and potentially winter-dominated precipitation conditions, in early Cenozoic time (DeCelles et al., 2007).

Lacustrine carbonates from the northern Tibetan Plateau provide estimates for the $\delta^{18}O$ values of regional Eocene-Oligocene meteoric waters of ~-10‰ (VSMOW). Using Rayleigh distillation-derived $\delta^{18}O$-elevation gradients (~-2.8‰/km), an Eocene paleoelevation of $\leq$ 2 km has been proposed for the basin in which these lacustrine carbonates formed (Cyr et al., 2005). In contrast, application of a more modest $\delta^{18}O$-elevation gradient of ~-1.5‰/km, characteristic of modern precipitation in this region, yields paleoelevation estimates indistinguishable from modern Tibetan Plateau elevations (~ 4.5─5 km; DeCelles et al., 2007). If the early Cenozoic physiographic and climatic environment of the Tibetan Plateau was comparable to modern (i.e. arid, continental

## Figure 3.6

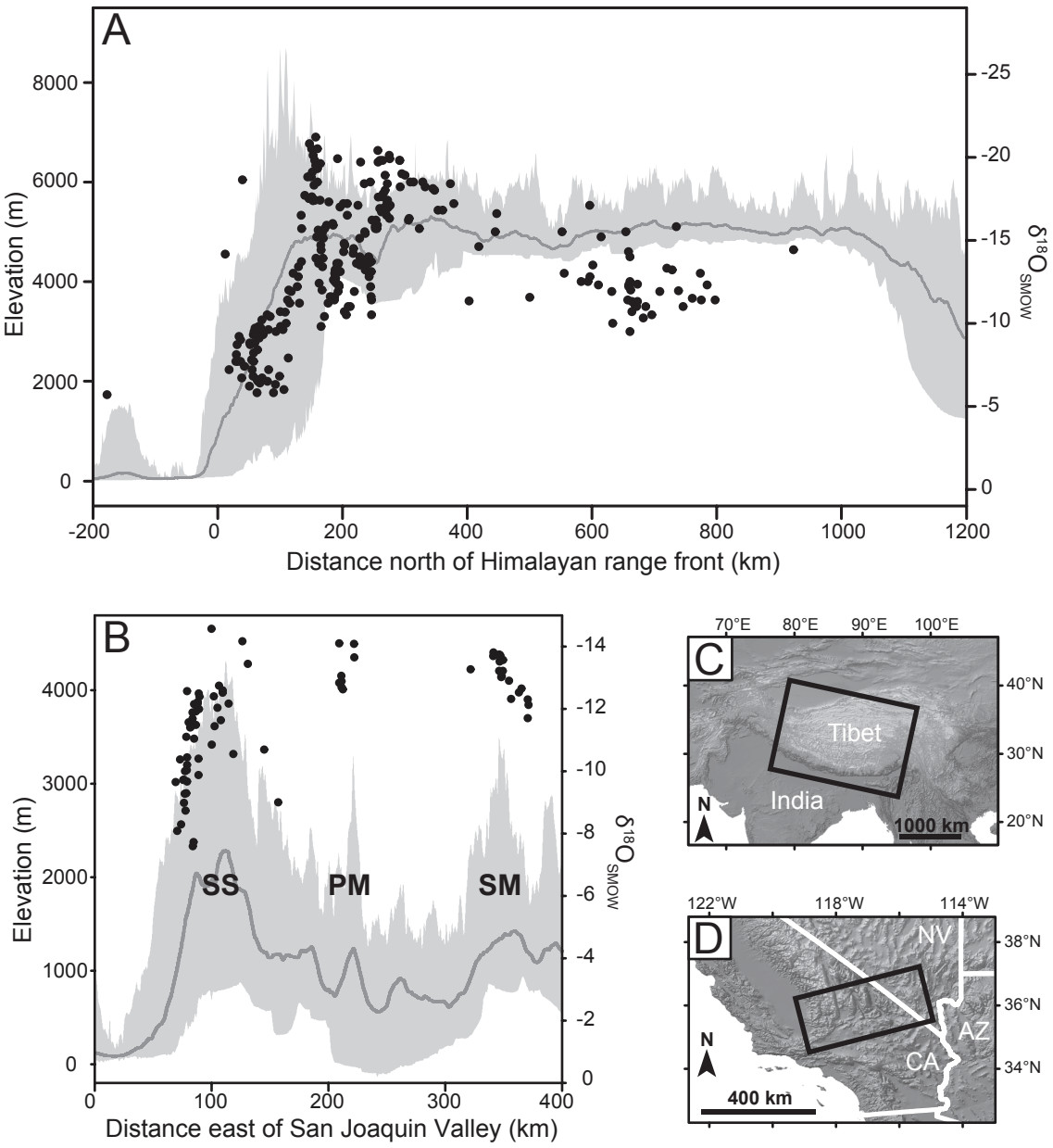


Figure 3.6 - Meteoric $\delta^{18}O$ in the southwestern US and east Asia. Topographic swath profiles (left y-axis) and meteoric water $\delta^{18}O$ (right y-axis) plotted as a function of distance from the major regional orographic barrier for the (A) Himalaya-Tibetan Plateau ($\delta^{18}O$ values compiled from Araguás-Araguás et al., 1998; Tian et al., 2007; and Hren et al., 2009) and (B) western US at ~36°N (this study; SS = Southern Sierra; PM = Panamint Mountains; SM = Spring Mountains) . Maximum and minimum elevations marked by upper and lower bounds of the gray swath, respectively. Dark gray lines mark mean elevations. (A) and (B) plotted with the same vertical exaggeration (V:H ~ 80). (C) and (D) Location maps for east Asia (C) and the western US (D). Black boxes outline the extent of topographic swath profile and $\delta^{18}O$ data coverage.

interior), the work presented in this study suggests that Eocene-Oligocene meteoric water $\delta^{18}O$-elevation gradients were likely low in magnitude and paleo-meteoric water $\delta^{18}O$ values calculated from Tibetan proxies provide only minimum elevation estimates, particularly if snowmelt was a dominant contributor to Tibetan meteoric water systems. Thus, measured and calculated $\delta^{18}O$ values are consistent with high regional paleoelevations in northern Tibet since the Late Eocene (e.g., DeCelles et al., 2007).

In order to quantify accurately regional paleoelevations, all possible influences on the depositional (i.e. precipitation) and post-depositional isotopic compositions of meteoric waters and the associated modification of isotope-elevation relationships must be taken into account. Altitude-dependent snowpack sublimation is only one such process, but its systematic behavior (i.e. reduction in $\delta^{18}O$-elevation gradients correlative with sublimation amount) makes its influence relatively straightforward to constrain. This, along with the fact that snowmelt contribution to groundwater recharge is often greater than suggested solely by the relative proportion of winter snow to annual precipitation amounts (Earman et al. 2006, and references therein), points to the need to consider these post-depositional effects, much as evaporative effects are considered, in constraining paleoelevation histories using stable isotope proxies. To the extent that contributions from snowmelt to paleo-meteoric waters can be inferred on the basis of $\delta^{18}O$ compositions (Norris et al., 1996; Dettman and Lohmann, 2000), it can be assumed that paleoelevations determined from these proxies using a globally-averaged, precipitation $\delta^{18}O$-elevation gradient are minimum estimates.

## 3.10 Conclusions

Modern spring and surface water transects from the Sierra Nevada orographic slope and the Basin and Range in the Sierran rainshadow reveal that altitude-dependent snow sublimation reduces $\delta^{18}O$-elevation gradients by a factor of 3–4 in snowmelt and spring waters of the Panamint and Spring mountains relative to regional precipitation (rain, early season snowpack) isotopic gradients. This reduction in $\delta^{18}O$-elevation gradient is not observed in Tule River and Southern Sierra surface water transects along the Sierran orographic slope, likely due to high relative humidity limiting the role of snow sublimation in this region. The results of this study indicate that snow sublimation may be a first order influence on the isotopic composition of meteoric waters in arid regions dominated by winter precipitation in the form of snow. As a result, snowmelt-derived waters in these regions are unlikely to preserve the isotopic composition of the original precipitation from which they were derived. Common seasonal sublimation amounts of 5–40% in continental interior, montane settings will result in 0.5–6.5‰ increases in snowpack $\delta^{18}O$ values throughout the winter season. Such isotopic shifts can lead to significant underestimates of both paleoelevation and the contribution of winter season precipitation to groundwater recharge. This study points to the need to constrain post-depositional influences on the isotopic composition of meteoric waters and associated proxies, as the isotopic compositions of these waters and proxies are fundamental data for a wide-range of paleoclimate, hydrologic, and paleoaltimetry applications.

**TABLE 3.1** - Sampled spring and surface water isotopic data and drainage basin characteristics

| Description | Latitude (°N) | Longitude (°W) | Sample Elevation (m) | Drainage Area ($km^2$) | Mean Basin Elevation (m) | Sample ID | Date | δD (‰ VSMOW) | $\delta^{18}O$ (‰ VSMOW) | d-excess (‰ VSMOW) |
|---|---|---|---|---|---|---|---|---|---|---|
| ***Tule River*** | | | | | | | | | | |
| Cow spring | 36.12879 | 118.77326 | 418 | 4.69 | 1132 | TR-01-09 | May-09 | -66 | -9.6 | 11.3 |
| Wishon Camp 1 | 36.19200 | 118.66520 | 1226 | 0.29 | 1407 | TR-02-09 | May-09 | -74 | -10.0 | 6.2 |
| Wishon Camp 2 | 36.19168 | 118.66492 | 1217 | 0.29 | 1406 | TR-03-09 | May-09 | -68 | -10.2 | 13.8 |
| N. fork Tule River | 36.19042 | 118.66475 | 1196 | 86.20 | 2164 | TR-04-09 | May-09 | -86 | -12.6 | 14.9 |
| Meadow Creek | 36.18828 | 118.67084 | 1163 | 2.89 | 1723 | TR-05-09 | May-09 | -75 | -11.1 | 13.7 |
| Wishon Rd. 1 | 36.18656 | 118.68448 | 1059 | 0.60 | 1469 | TR-06-09 | May-09 | -76 | -10.0 | 4.2 |
| Wishon Rd. 2 | 36.17766 | 118.70116 | 955 | 0.91 | 1253 | TR-07-09 | May-09 | -72 | -9.7 | 5.9 |
| Hossack Creek | 36.18361 | 118.64916 | 1480 | 4.17 | 2142 | TR-08-09 | May-09 | -79 | -11.6 | 13.9 |
| Soda Creek tributary | 36.15749 | 118.66212 | 1202 | 3.76 | 1501 | TR-09-09 | May-09 | -76 | -10.4 | 7.3 |
| Unnamed spring Hwy 190 | 36.14083 | 118.63349 | 1363 | 0.13 | 1476 | TR-10-09 | May-09 | -83 | -11.4 | 8.5 |
| Nelson Creek 1 | 36.15031 | 118.61178 | 1590 | 2.19 | 1996 | TR-11-09 | May-09 | -80 | -11.7 | 13.3 |
| Belknap Creek | 36.15358 | 118.59712 | 1701 | 4.35 | 2184 | TR-12-09 | May-09 | -86 | -12.2 | 11.8 |
| Nelson Creek 2 | 36.15662 | 118.61267 | 1753 | 1.35 | 2115 | TR-13-09 | May-09 | -84 | -11.6 | 9.1 |
| Nelson Creek 3 | 36.16058 | 118.61015 | 1947 | 0.70 | 2246 | TR-14-09 | May-09 | -82 | -11.9 | 13.2 |
| unnamed spring | 36.16564 | 118.62455 | 2008 | 0.51 | 2141 | TR-16-09 | May-09 | -80 | -11.4 | 11.7 |
| Cedar Slope stream | 36.14928 | 118.57729 | 1828 | 1.44 | 2258 | TR-18-09 | May-09 | -77 | -11.5 | 14.7 |
| Boulder Creek | 36.14173 | 118.56031 | 1983 | 7.13 | 2305 | TR-19-09 | May-09 | -82 | -12.2 | 15.7 |
| Dome Creek | 36.06958 | 118.54215 | 2193 | 1.27 | 2397 | TR-20-09 | May-09 | -87 | -12.4 | 11.8 |
| Horse Canyon stream | 36.05282 | 118.54752 | 2052 | 0.29 | 2403 | TR-22-09 | May-09 | -88 | -12.0 | 7.9 |
| Ice Creek | 36.03746 | 118.55011 | 1976 | 0.36 | 2237 | TR-23-09 | May-09 | -87 | -12.5 | 13.4 |
| Alder Creek | 36.02987 | 118.55924 | 1974 | 0.13 | 2022 | TR-24-09 | May-09 | -88 | -12.2 | 9.4 |
| Last Chance meadow | 36.00718 | 118.57408 | 1832 | 2.25 | 2133 | TR-25-09 | May-09 | -81 | -11.9 | 14.1 |
| ***Southern Sierra*** | | | | | | | | | | |
| Big Pine Meadow | 35.94821 | 118.08332 | 2173 | 8.33 | 2326 | SS-01-09 | May-09 | -105 | -13.4 | 2.7 |
| S. fork Kern River | 36.02233 | 118.13599 | 1823 | 543.89 | 2612 | SS-02-09 | May-09 | -110 | -14.2 | 3.4 |
| Nine Mile Creek | 35.84314 | 117.92664 | 1055 | 27.24 | 1611 | SS-03-09 | May-09 | -92 | -10.7 | -6.0 |
| quail feeder | 35.44221 | 117.78847 | 1111 | 0.00 | 1111 | SS-06-09 | May-09 | -67 | -9.0 | 5.1 |
| Kelso feeder | 35.46699 | 118.21153 | 1313 | 17.02 | 1553 | SS-07-09 | May-09 | -86 | -10.6 | -1.8 |

**TABLE 3.1** - Sampled spring and surface water isotopic data and drainage basin characteristics

| Description | Latitude (°N) | Longitude (°W) | Sample Elevation (m) | Drainage Area ($km^2$) | Mean Basin Elevation (m) | Sample ID | Date | δD (‰ VSMOW) | $\delta^{18}O$ (‰ VSMOW) | d-excess (‰ VSMOW) |
|---|---|---|---|---|---|---|---|---|---|---|
| Burning Moscow spring | 35.46110 | 118.25563 | 1778 | 1.80 | 1900 | SS-08-09 | May-09 | -94 | -12.2 | 3.6 |
| Lander station camp | 35.45512 | 118.31295 | 1928 | 0.25 | 1928 | SS-09-09 | May-09 | -91 | -12.5 | 9.2 |
| Waterhole Mine spring | 35.43845 | 118.31215 | 1940 | 5.02 | 2064 | SS-10-09 | May-09 | -90 | -12.6 | 10.6 |
| Claraville | 35.44392 | 118.32789 | 1915 | 5.06 | 2142 | SS-11-09 | May-09 | -89 | -11.6 | 4.2 |
| French Meadow | 35.47240 | 118.34864 | 2104 | 3.32 | 2294 | SS-12-09 | May-09 | -93 | -12.7 | 9.5 |
| Piute Mtn. Rd. | 35.45220 | 118.36290 | 2210 | 0.78 | 2376 | SS-13-09 | May-09 | -83 | -12.0 | 13.0 |
| Cold spring | 35.46699 | 118.39651 | 2436 | 0.10 | 2429 | SS-14-09 | May-09 | -86 | -12.4 | 13.6 |
| Piute Spring seep | 35.44644 | 118.38935 | 2461 | 0.08 | 2499 | SS-15-09 | May-09 | -83 | -11.4 | 8.5 |
| Setimo Creek tributary | 35.40483 | 118.41469 | 1525 | 2.52 | 1908 | SS-16-09 | May-09 | -78 | -10.9 | 8.5 |
| Dutchman Creek 1 | 35.48048 | 118.54194 | 1244 | 1.87 | 1700 | SS-17-09 | May-09 | -72 | -10.4 | 11.1 |
| Dutchman Creek 2 | 35.47910 | 118.54234 | 1264 | 2.74 | 1590 | SS-18-09 | May-09 | -75 | -9.9 | 4.4 |
| Breckenridge campground | 35.46696 | 118.58256 | 2052 | 0.47 | 2115 | SS-19-09 | May-09 | -75 | -11.0 | 13.3 |
| Breckenridge Mtn. 1 | 35.46443 | 118.64740 | 1571 | 0.21 | 1801 | SS-20-09 | May-09 | -65 | -9.7 | 12.3 |
| Breckenridge Mtn. 2 | 35.45417 | 118.70407 | 855 | 13.41 | 1225 | SS-21-09 | May-09 | -65 | -8.3 | 1.7 |
| Rock spring | 35.42256 | 118.74075 | 717 | 1.15 | 881 | SS-22-09 | May-09 | -64 | -8.1 | 1.1 |
| Dougherty Creek | 35.47277 | 118.71334 | 488 | 4.21 | 1019 | SS-23-09 | May-09 | -83 | -10.4 | 0.2 |
| Cow Flat spring 1 | 35.52734 | 118.65671 | 765 | 0.10 | 931 | SS-24-09 | May-09 | -73 | -9.3 | 1.6 |
| Cow Flat spring 2 | 35.52116 | 118.66420 | 887 | 0.45 | 1180 | SS-25-09 | May-09 | -63 | -8.7 | 6.5 |
| Cow Flat seep | 35.51620 | 118.67181 | 911 | 0.27 | 1156 | SS-26-09 | May-09 | -70 | -9.3 | 4.3 |
| Democrat spring | 35.50673 | 118.67870 | 987 | 0.78 | 1300 | SS-27-09 | May-09 | -68 | -9.7 | 10.1 |
| Cow Flat spring 3 | 35.49623 | 118.67915 | 964 | 6.30 | 1540 | SS-28-09 | May-09 | -62 | -9.0 | 9.5 |
| N. fork Kern River | 35.75367 | 118.42381 | 808 | 2613.43 | 2490 | SS-29-09 | May-09 | -111 | -14.6 | 5.2 |
| Wik spring | 35.33745 | 118.58460 | 817 | 2.39 | 1062 | SS-30-09 | May-09 | -66 | -7.7 | -3.9 |
| Dead Horse spring | 35.32743 | 118.59135 | 690 | 5.33 | 989 | SS-31-09 | May-09 | -65 | -7.6 | -3.9 |
| ***Panamint Mtns.*** | | | | | | | | | | |
| Pleasant Canyon | 36.03383 | 117.18084 | 807 | 31.08 | 1938 | PM-04 | May-09 | -105 | -12.6 | -4.2 |
| Warm Sulphur Springs | 36.12042 | 117.21437 | 605 | 53.34 | 1659 | PM-05 | May-09 | -107 | -12.8 | -4.6 |
| unnamed Wildrose spring 1 | 36.12130 | 117.21397 | 605 | 75.37 | 1913 | PM-06 | May-09 | -115 | -14.1 | -2.2 |
| unnamed Wildrose spring 2 | 36.26575 | 117.19341 | 1246 | 0.32 | 1413 | PM-07 | May-09 | -103 | -12.7 | -1.7 |

**TABLE 3.1** - Sampled spring and surface water isotopic data and drainage basin characteristics

| Description | Latitude (°N) | Longitude (°W) | Sample Elevation (m) | Drainage Area ($km^2$) | Mean Basin Elevation (m) | Sample ID | Date | δD (‰ VSMOW) | $\delta^{18}O$ (‰ VSMOW) | d-excess (‰ VSMOW) |
|---|---|---|---|---|---|---|---|---|---|---|
| Charcoal Kilns spring | 36.24758 | 117.07172 | 2208 | 0.13 | 2372 | PM-08 | May-09 | -102 | -13.7 | 7.8 |
| Wildrose Canyon spring | 36.23435 | 117.07452 | 2397 | 0.40 | 2579 | PM-09 | May-09 | -102 | -14.1 | 10.4 |
| Upper Emigrant spring | 36.42560 | 117.19353 | 1244 | 0.53 | 1414 | PM-10 | May-09 | -102 | -12.9 | 1.5 |
| Emigrant spring | 36.43497 | 117.19533 | 1158 | 0.36 | 1360 | PM-11 | May-09 | -101 | -13.1 | 3.6 |
| ***Spring Mtns.*** | | | | | | | | | | |
| Mazie spring | 36.24487 | 115.65451 | 2769 | 0.01 | 2766 | SM-07-08 | Oct-08 | | -13.6 | |
| Mule spring | 36.03129 | 115.58093 | 1463 | 0.61 | 1685 | SM-19-09 | May-09 | -92 | -12.3 | 6.7 |
| Cave spring | 36.16594 | 115.59797 | 1911 | < 0.01 | 1964 | SM-20-09 | May-09 | -103 | -12.9 | 0.7 |
| Warner spring | 36.02110 | 115.50747 | 1621 | 0.03 | 1664 | SM-21-09 | May-09 | -91 | -12.5 | 9.8 |
| | | | | | | SM-17-08 | Oct-08 | | -12.6 | |
| Wheeler Camp spring | 36.05277 | 115.41686 | 1010 | 0.07 | 1105 | SM-22-09 | May-09 | -77 | -12.1 | 20.4 |
| | | | | | | SM-01-08 | Oct-08 | | -11.8 | |
| White Rock spring | 36.17380 | 115.47982 | 1439 | 0.04 | 1496 | SM-23-09 | May-09 | -94 | -12.6 | 7.3 |
| | | | | | | SM-02-08 | Oct-08 | | -12.6 | |
| Red spring | 36.14446 | 115.42045 | 1089 | 0.04 | 1154 | SM-24-09 | May-09 | -90 | -12.3 | 8.5 |
| | | | | | | SM-03-09 | Oct-08 | | -12.4 | |
| Calico spring | 36.14991 | 115.42203 | 1073 | 0.01 | 1117 | SM-25-09 | May-09 | -108 | -11.7 | -14.1 |
| | | | | | | SM-04-08 | Oct-08 | | -11.9 | |
| Little Falls | 36.25604 | 115.65536 | 2430 | 0.23 | 2842 | SM-30-09 | May-09 | -95 | -13.2 | 11.1 |
| | | | | | | SM-05-08 | Oct-08 | | -13.1 | |
| Mary Jane Falls | 36.27913 | 115.67147 | 2871 | 0.67 | 3041 | SM-32-09 | May-09 | -97 | -13.0 | 7.3 |
| | | | | | | SM-08-08 | Oct-08 | | -13.1 | |
| Edna Grey spring | 36.32057 | 115.67999 | 2558 | 0.19 | 2710 | SM-34-09 | May-09 | -108 | -13.6 | 0.7 |
| | | | | | | SM-09-08 | Oct-08 | | -13.4 | |
| Lee Canyon | 36.32867 | 115.66611 | 2515 | 0.05 | 2572 | SM-35-09 | May-09 | -98 | -13.0 | 6.4 |
| | | | | | | SM-10-08 | Oct-08 | | -13.5 | |

**TABLE 3.1** - Sampled spring and surface water isotopic data and drainage basin characteristics

| Description | Latitude (°N) | Longitude (°W) | Sample Elevation (m) | Drainage Area ($km^2$) | Mean Basin Elevation (m) | Sample ID | Date | δD (‰ VSMOW) | $\delta^{18}O$ (‰ VSMOW) | d-excess (‰ VSMOW) |
|---|---|---|---|---|---|---|---|---|---|---|
| Mack Canyon 1 | 36.34974 | 115.67990 | 2512 | 0.44 | 2666 | SM-36-09 | May-09 | -115 | -13.7 | -5.1 |
| | | | | | | SM-11-08 | Oct-08 | | -13.8 | |
| Mack Canyon 3 | 36.33723 | 115.68835 | 2644 | 0.62 | 2856 | SM-37-09 | May-09 | -104 | -13.7 | 5.9 |
| Mack Canyon 2 | 36.34095 | 115.68882 | 2611 | 0.01 | 2692 | SM-39-09 | May-09 | -97 | -13.2 | 8.9 |
| Mud Springs | 36.37150 | 115.68424 | 2267 | 0.40 | 2508 | SM-40-09 | May-09 | -106 | -13.5 | 2.7 |
| | | | | | | SM-13-08 | Oct-08 | | -13.4 | |
| Whisky spring | 36.38289 | 115.74559 | 2340 | < 0.01 | 2380 | SM-41-09 | May-09 | -104 | -13.7 | 5.9 |
| | | | | | | SM-14-08 | Oct-08 | | -13.6 | |
| Cold Creek spring | 36.41176 | 115.74418 | 1905 | 1.07 | 2249 | SM-42-09 | May-09 | -101 | -13.8 | 9.7 |
| | | | | | | SM-15-08 | Oct-08 | | -13.8 | |
| Gold spring | 36.46330 | 115.96174 | 2060 | 0.23 | 2261 | SM-43-09 | May-09 | -96 | -13.3 | 10.2 |
| | | | | | | SM-16-08 | Oct-08 | | -13.2 | |
| ***Snow Samples*** | | | | | | | | | | |
| | 36.24589 | 115.65355 | 2737 | | | SM-26-09 | May-09 | -75 | -10.9 | 12.1 |
| | 36.25036 | 115.65020 | 2521 | | | SM-27-09 | May-09 | -83 | -12.5 | 17.7 |
| | 36.25051 | 115.64822 | 2500 | | | SM-29-09 | May-09 | -76 | -10.0 | 4.0 |
| | 36.25604 | 115.65536 | 2430 | | | SM-31-09 | May-09 | -89 | -12.4 | 10.8 |
| | 36.27913 | 115.67147 | 2871 | | | SM-33-09 | May-09 | -82 | -10.2 | -0.4 |
| | 36.33723 | 115.68835 | 2644 | | | SM-38-09 | May-09 | -91 | -11.7 | 2.8 |

**Table 3.1** - Geographic coordinates, drainage basin characteristics, and isotopic data for all spring/surface water and late season snowpack samples collected and analyzed as part of this study. 'Description' column provides either the official name of the sampled spring, stream or tributary or an unofficial name given by the authors of this study to distinguish individual samples. Spring Mountains spring waters were sampled in two separate field seasons (October 2008 and May 2009). Where available, isotopic data from each field season is included. Similarity of paired October 2008 and May 2009 isotopic values suggests spring waters are integrated over multiple seasons of meteoric water recharge and not significantly influenced by a single (winter) recharge season.

### 3.11 Acknowledgements

Kacey Lohmann and Lora Wingate are thanked for help with stable isotope analyses and sample collection strategies. David Azzolini assembled GIS databases that were instrumental to this study. Hope Jahren and Fred Longstaffe are thanked for thoughtful and insightful reviews, and Nathan Sheldon provided comments that improved the presentation of this work. The isotopic analyses were funded in part by a grant from the Turner Fund at the University of Michigan to ARL.

### 3.12 References cited

Allison, G. B., 1988, A review of some of the physical, chemical and isotopic techniques available for estimating groundwater recharge, *in* Simmers, I., ed., Estimation of Natural Groundwater Recharge: Dardrecht, D. Reidel Publishing Co., 509 pp.

Araguás-Araguás, L., Froehlich, K., and Rozanski, K., 1998, Stable isotope composition of precipitation over southeast Asia: Journal of Geophysical Research-Atmospheres, v. 103, no. D22, p. 28721-28742.

Araguás-Araguás, L., Froehlich, K., and Rozanski, K., 2000, Deuterium and oxygen-18 isotope composition of precipitation and atmospheric moisture: Hydrological Processes, v. 14, no. 8, p. 1341-1355.

Blisniuk, P. M., and Stern, L. A., 2005, Stable isotope paleoaltimetry; a critical review: American Journal of Science, v. 305, no. 10, p. 1033-1074.

Blisniuk, P. M., Stern, L. A., Chamberlain, C. P., Idleman, B., and Zeitler, P. K., 2005, Climatic and ecologic changes during Miocene surface uplift in the southern Patagonian Andes: Earth and Planetary Science Letters, v. 230, no. 1-2, p. 125-142.

Burchfiel, B. C., Fleck, R. J., Secor, D. T., Vincelette, R. R., and Davis, G. A., 1974, Geology of the Spring Mountains, Nevada: Geological Society of America Bulletin, v. 85, no. 7, p. 1013-1022.

Chamberlain, C. P., and Poage, M. A., 2000, Reconstructing the paleotopography of mountain belts from the isotopic composition of authigenic minerals: Geology, v. 28, no. 2, p. 115-118.

Clark, I. D., and Fritz, P., 1997, Environmental isotopes in hydrogeology: Boca Raton, FL, Lewis Publishers, 328 p.

Clow, D. W., 2010, Changes in the timing of snowmelt and streamflow in Colorado: a response to recent warming: Journal of Climate, v. 23, no. 9, p. 2293-2306.

Colbeck, S. C., 1987, Snow metamorphism and classification, *in* Jones, H. G., and Orville-Thomas, W. J., eds., Seasonal Snowcovers: Physics, Chemistry, Hydrology: New York, Springer, p. 1-35.

Cooper, L. W., 1998, Isotopic fractionation in snow cover, *in* Kendall, C., and McDonnell, J. J., eds., Isotope Tracers in Catchment Hydrology: New York, Elsevier, p. 119-136.

Craig, H., 1961, Isotopic variations in meteoric waters: Science, v. 133, no. 3465, p. 1702-1703.

Cuffey, K. M., and Steig, E. J., 1998, Isotopic diffusion in polar firn: implications for interpretation of seasonal climate parameters in ice-core records, with emphasis on central Greenland: Journal of Glaciology, v. 44, no. 147, p. 273-284.

Currie, B. S., Rowley, D. B., and Tabor, N. J., 2005, Middle Miocene paleoaltimetry of southern Tibet; implications for the role of mantle thickening and delamination in the Himalayan Orogen: Geology, v. 33, no. 3, p. 181-184.

Cyr, A. J., Currie, B. S., and Rowley, D. B., 2005, Geochemical evaluation of Fenghuoshan Group lacustrine carbonates, north-central Tibet; implications for the paleoaltimetry of the Eocene Tibetan Plateau: Journal of Geology, v. 113, no. 5, p. 517-533.

Dahlgren, R. A., Boettinger, J. L., Huntington, G. L., and Amundson, R. G., 1997, Soil development along an elevational transect in the western Sierra Nevada, California: Geoderma, v. 78, no. 3-4, p. 207-236.

Dansgaard, W., 1964, Stable Isotopes in Precipitation: Tellus, v. 16, no. 4, p. 436-468.

de Vries, J. J., and Simmers, I., 2002, Groundwater recharge: an overview of processes and challenges: Hydrogeology Journal, v. 10, no. 1, p. 5-17.

DeCelles, P. G., Quade, J., Kapp, P., Fan, M., Dettman, D. L., and Ding, L., 2007, High and dry in central Tibet during the late Oligocene: Earth and Planetary Science Letters, v. 253, no. 3-4, p. 389-401.

Dettman, D. L., and Lohmann, K. C., 2000, Oxygen isotope evidence for high-altitude snow in the Laramide Rocky Mountains of North America during the Late Cretaceous and Paleogene: Geology, v. 28, no. 3, p. 243-246.

Dutton, A., Wilkinson, B.H., Welker, J.M., Bowen, G.J., and Lohmann, K.C., 2005, Spatial distribution and seasonal variation in $^{18}O/^{16}O$ of modern precipitation and river water across the conterminous USA: Hydrological Processes, v. 19, p. 4121-4146.

Earman, S., Campbell, A. R., Phillips, F. M., and Newman, B. D., 2006, Isotopic exchange between snow and atmospheric water vapor; estimation of the snowmelt component of groundwater recharge in the Southwestern United States: Journal of Geophysical Research, v. 111, p. D09302.

Ekaykin, A. A., Hondoh, T., Lipenkov, V.Y., and Miyamoto, A., 2009, Post-depositional changes in snow isotope content: preliminary results of laboratory experiments, *in* Climate of the Past Discussions, p. 2239-2267.

Ekaykin, A. A., Lipenkov, V.Y., Barkov, N.I., Petit, J.R., and Masson-Delmotte, V., 2002, Spatial and temporal variability in isotope composition of recent snow in the vicinity of Vostok station, Antarctica: implications for ice-core record interpretation: Annals in Glaciology, v. 35, p. 181-186.

Epstein, S., Sharp, R. P., and Gow, A. J., 1965, 6-year record of oxygen and hydrogen isotope variations in South Pole firn: Journal of Geophysical Research, v. 70, no. 8, p. 1809-1814.

Friedman, I., Benson, C., and Gleason, J., 1991, Isotopic changes during snow metamorphism, *in* Taylor Jr., H.P., O'Neil, J.R., and Kaplan, I.R., eds., Stable Isotope Geochemistry: A Tribute to Samuel Epstein: The Geochemical Society Special Publication No. 3, p. 211-221.

Friedman, I., Smith, G.I., Johnson, C.A., Moscati, R.J., 2002, Stable isotope compositions of waters in the Great Basin, United States 2. Modern precipitation: Journal of Geophysical Research, v. 107, p. ACL 15-11 - ACL 15-21.

Friedman, I., and Smith, G. I., 1972, Deuterium content of snow as an index to winter climate in Sierra Nevada area: Science, v. 176, no. 4036, p. 790-793.

Friedman, I., Smith, G. I., Gleason, J. D., Warden, A., and Harris, J. M., 1992, Stable isotope composition of waters in southeastern California .1. Modern Precipitation: Journal of Geophysical Research, v. 97, no. D5, p. 5795-5812.

Garzione, C. N., Quade, J., DeCelles, P. G., and English, N. B., 2000, Predicting paleoelevation of Tibet and the Himalaya from $\delta^{18}O$ vs. altitude gradients in meteoric water across the Nepal Himalaya: Earth and Planetary Science Letters, v. 183, no. 1-2, p. 215-229.

Garzione, C. N., Molnar, P., Libarkin, J. C., and MacFadden, B. J., 2006, Rapid late Miocene rise of the Bolivian Altiplano; evidence for removal of mantle lithosphere: Earth and Planetary Science Letters, v. 241, no. 3-4, p. 543-556.

Gat, J. R., 1996, Oxygen and hydrogen isotopes in the hydrologic cycle: Annual Review of Earth and Planetary Sciences, v. 24, p. 225-262.

Henderson, A. K., and Shuman, B.N., 2010, Differing controls on river- and lake-water hydrogen and oxygen isotopic values in the western United States: Hydrological Processes.

Hershey, R. L., 1989, Hydrogeology and hydrogeochemistry of the Spring Mountains, Clark County, Nevada [M.S. thesis]: Las Vegas, University of Nevada at Las Vegas, 236 p.

Hood, E., Williams, M., and Cline, D., 1999, Sublimation from a seasonal snowpack at a continental, mid-latitude alpine site: Hydrological Processes, v. 13, p. 1781-1797.

Horton, T. W., Sjostrom, D. J., Abruzzese, M. J., Poage, M. A., Waldbauer, J. R., Hren, M. T., Wooden, J. L., and Chamberlain, C. P., 2004, Spatial and temporal variation of Cenozoic surface elevation in the Great Basin and Sierra Nevada: American Journal of Science, v. 304, no. 10, p. 862-888.

Houghton, J., 1969, Characteristics of rainfall in the Great Basin: University of Nevada, Reno, 205 p.

Houston, J., and Hartley, A. J., 2003, The central Andean west-slope rainshadow and its potential contribution to the origin of hyper-aridity in the Atacama desert: International Journal of Climatology, v. 23, no. 12, p. 1453-1464.

Hren, M. T., Bookhagen, B., Blisniuk, P. M., Booth, A. L., and Chamberlain, C. P., 2009, $\delta^{18}O$ and $\delta D$ of streamwaters across the Himalaya and Tibetan Plateau: Implications for moisture sources and paleoelevation reconstructions: Earth and Planetary Science Letters, v. 288, no. 1-2, p. 20-32.

Ingraham, N. L., Lyles, B. F., Jacobson, R. L., and Hess, J. W., 1991, Stable isotopic study of precipitation and spring discharge in southern Nevada: Journal of Hydrology, v. 125, no. 3-4, p. 243-258.

Ingraham, N. L., and Taylor, B. E., 1991, Light stable isotope systematics of large-scale hydrologic regimes in California and Nevada: Water Resources Research, v. 27, no. 1, p. 77-90.

Insel, N., Poulsen, C. J., and Ehlers, T. A., 2010, Influence of the Andes Mountains on South American moisture transport, convection, and precipitation: Climate Dynamics, v. 35, no. 7-8, p. 1477-1492.

Jahren, A. H., and Sanford, K. L., 2002, Ground-water is the Ultimate Source of the Salt Creek Pupfish Habitat, Death Valley, USA: Journal of Arid Environments, v. 51, no. 3, p. 401-411.

Johnsen, S. J., 1977, Stable isotope homogenization of polar firn and ice, *in* Proceedings of the Symposium on Isotopes and Impurities in Snow and Ice, I.U.G.G. XVI, General Assembly, Grenoble, 1975, p. 210-219.

Jouzel, J., Froehlich, K., and Schotterer, U., 1997, Deuterium and oxygen-18 in present-day precipitation: data and modelling: Hydrological Sciences Journal-Journal Des Sciences Hydrologiques, v. 42, no. 5, p. 747-763.

Jouzel, J., Vimeux, F., Caillon, N., Delaygue, G., Hoffmann, G., Masson-Delmotte, V., and Parrenin, F., 2003, Magnitude of isotope/temperature scaling for interpretation of central Antarctic ice cores: Journal of Geophysical Research, v. 108, 4361, 10 p.

Kapnick, S., and Hall, A., 2010, Observed climate-snowpack relationships in California and their implications for the future: Journal of Climate, v. 23, no. 13, p. 3446-3456.

Kent-Corson, M. L., Sherman, L. S., Mulch, A., and Chamberlain, C. P., 2006, Cenozoic topographic and climatic response to changing tectonic boundary conditions in western North America: Earth and Planetary Science Letters, v. 252, no. 3-4, p. 453-466.

Knowles, N., Dettinger, M. D., and Cayan, D. R., 2006, Trends in snowfall versus rainfall in the Western United States: Journal of Climate, v. 19, no. 18, p. 4545-4559.

Koch, P. L., Zachos, J. C., and Dettman, D. L., 1995, Stable isotope stratigraphy and paleoclimatology of the Paleogene Bighorn Basin (Wyoming, USA): Palaeogeography Palaeoclimatology Palaeoecology, v. 115, no. 1-4, p. 61-89.

Kohn, M. J., 2007, Paleoaltimetry: Geochemical and Thermodynamic Approaches, Reviews in Mineralogy and Geochemistry: Mineralological Society of America, v.66, 278 p.

Konishchev, V. N., Golubev, V. N., and Sokratov, S. A., 2003, Sublimation from a seasonal snow cover and an isotopic content of ice wedges in the light of a palaeoclimate reconstruction: International Conference on Permafrost, Proceedings, v. 8, p. 585-590.

Labotka, T. C., Albee, A. L., Lanphere, M. A., and McDowell, S. D., 1980, Stratigraphy, structure, and metamorphism in the central Panamint Mountains (Telescope Peak

Quadrangle), Death Valley Area, California - Summary: Geological Society of America Bulletin, v. 91, no. 3, p. 125-129.

Lechler, A. R., 2011, The Cenozoic paleoelevation and paleogeographic history of the southwestern US Cordillera: a combined sedimentologic and isotopic approach [PhD thesis]: University of Michigan, Ann Arbor, 245 p.

Lee, J. E., and Fung, I., 2008, "Amount effect" of water isotopes and quantitative analysis of post-condensation processes: Hydrological Processes, v. 22, no. 1, p. 1-8.

Lee, J. H., Feng, X. H., Posmentier, E. S., Faiia, A. M., and Taylor, S., 2009, Stable isotopic exchange rate constant between snow and liquid water: Chemical Geology, v. 260, no. 1-2, p. 57-62.

Liu, Z., Tian, L., Chai, X., and Yao, T., 2008, A model-based determination of spatial variation of precipitation $\delta^{18}O$ over China: Chemical Geology, v. 249, no. 1-2, p. 203-212.

Minder, J. R., 2010, The sensitivity of mountain snowpack accumulation to climate warming: Journal of Climate, v. 23, no. 10, p. 2634-2650.

Moser, H., and Stichler, W., 1975, Deuterium and oxygen-18 contents as an index of the properties of snow covers, *in* Snow Mechanics Symposium, Grindelwald, Bernese Oberland (Switzerland), p. 122-135.

Mote, P. W., Hamlet, A. F., Clark, M. P., and Lettenmaier, D. P., 2005, Declining mountain snowpack in western North America: Bulletin of the American Meteorological Society, v. 86, no. 1, p. 39-49.

Mulch, A., Graham, S. A., and Chamberlain, C. P., 2006, Hydrogen isotopes in Eocene river gravels and paleoelevation of the Sierra Nevada: Science, v. 313, no. 5783, p. 87-89.

Neumann, T. A., Albert, M. R., Lomonaco, R., Engel, C., Courville, Z., and Perron, F., 2008, Experimental determination of snow sublimation rate and stable-isotope exchange: Annals of Glaciology, v. 49, p. 1-6.

Neumann, T. A., Waddington, E. D., Steig, E. J., Grootes, P. M., 2005, Non-climate influences on stable isotopes at Taylor Mouth, Antarctica: Journal of Glaciology, v. 51, no. 173, p. 248-258.

Norris, R. D., Jones, L. S., Corfield, R. M., and Cartlidge, J. E., 1996, Skiing in the Eocene Uinta Mountains? Isotopic evidence in the Green River Formation for snow melt and large mountains: Geology, v. 24, no. 5, p. 403-406.

Poage, M. A., and Chamberlain, C. P., 2001, Empirical relationships between elevation and the stable isotope composition of precipitation and surface waters: considerations for studies of paleoelevation change: American Journal of Science, v. 301, no. 1, p. 1-15.

Polissar, P. J., Freeman, K. H., Rowley, D. B., McInerney, F. A., and Currie, B. S., 2009, Paleoaltimetry of the Tibetan Plateau from D/H ratios of lipid biomarkers: Earth and Planetary Science Letters, v. 287, p. 64-76.

Quade, J., Garzione, C. N., and Eiler, J., 2007, Paleoelevation reconstruction using pedogenic carbonates: Reviews in Mineralogy and Geochemistry, v. 66, no. 1, p. 53-87.

Rowley, D. B., and Garzione, C. N., 2007, Stable isotope-based paleoaltimetry: Annual Review of Earth and Planetary Sciences, v. 35, p. 463-508.

Rowley, D. B., Pierrehumbert, R. T., and Currie, B. S., 2001, A new approach to stable isotope-based paleoaltimetry; implications for paleoaltimetry and paleohypsometry of the High Himalaya since the late Miocene: Earth and Planetary Science Letters, v. 188, no. 1-2, p. 253-268.

Rozanski, K. L., Araguás-Araguás, L., and Gonfiantini, R., 1993, Isotopic patterns in modern global precipitation, *in* Swart, P.K., Lohmann, K.C., McKenzie, J., and Savin, S., eds., Climate Change in Continental Isotopic Records, Geophysics Monograph Series No. 78: Washington D.C., American Geophysical Union, p. 1-36.

Saylor, J. E., Quade, J., Dettman, D. L., DeCelles, P. G., Kapp, P. A., and Ding, L., 2009, The late Miocene through present paleoelevation history of southwestern Tibet: American Journal of Science, v. 309, no. 1, p. 1-42.

Schulz, O., and de Jong, C., 2004, Snowmelt and sublimation: field experiments and modelling in the High Atlas Mountains and Morocco: Hydrology and Earth System Sciences, v. 8, no. 6, p. 1076-1089.

Shreve, C. M., Okin, G. S., and Painter, T. H., 2009, Indices for estimating fractional snow cover in the western Tibetan Plateau: Journal of Glaciology, v. 55, no. 192, p. 737-745.

Sinclair, K. E., Marshall, S.J., 2008, Post-depositional modification of stable water isotopes in winter snowpacks in Canadian Rocky Mountains: Annals of Glaciology, v. 49, p. 96-106.

Sokratov, S. A. and Golubev, V.N., 2009, Snow isotopic content change by sublimation: Journal of Glaciology, v. 55, no. 193, p. 823-828.

Sommerfeld, R. A., Judy, C., and Friedman, I., 1991, Isotopic changes during the formation of depth hoar in experimental snowpacks: Special Publication - Geochemical Society, v. 3, p. 205-209.

Stichler, W., Schotterer, U., Froehlich, K., Ginot, P., Kull, C., Gaeggeler, H., and Pouyaud, B., 2001, Influence of sublimation on stable isotope records recovered from high-altitude glaciers in the tropical Andes: Journal of Geophysical Research, v. 106, no. D19, p. 22,613-22,620.

Strasser, U., Bernhardt, M., Weber, M., Liston, G. E., and Mauser, W., 2008, Is snow sublimation important in the alpine water balance?: Cryosphere, v. 2, no. 1, p. 53-66.

Tabor, N. J., and Montanez, I. P., 2005, Oxygen and hydrogen isotope compositions of Permian pedogenic phyllosilicates: Development of modem surface domain arrays and implications for paleotemperature reconstructions: Palaeogeography Palaeoclimatology Palaeoecology, v. 223, no. 1-2, p. 127-146.

Taylor, S., Feng, X., Kirchner, J. W., Osterhuber, R., Klaue, B., and Renshaw, C. E., 2001, Isotopic evolution of a seasonal snowpack and its melt: Water Resources Research, v. 37, no. 3, p. 759-769.

Tian, L., Masson-Delmotte, V., Stievenard, M., Yao, T., and Jouzel, J., 2001, Tibetan Plateau summer monsoon northward extent revealed by measurements of water stable isotopes: Journal of Geophysical Research, v. 106, no. D22, p. 28,081-28,088.

Town, M. S., Warren, S. G., Walden, V. P., and Waddington, E.D., 2008, Effect of atmospheric water vapor on modification of stable isotopes in near-surface snow on ice sheets: Journal of Geophysical Research, v. 113, p. 1-16.

Unnikrishna, P. V., McDonnell, J. J., and Kendall, C., 2002, Isotope variations in a Sierra Nevada snowpack and their relation to meltwater: Journal of Hydrology, v. 260, no. 1-4, p. 38-57.

Vuille, M., 1996, Zur raumleitlichen dynamik von schneefall und ausaperung im bereich des sudlichen Altiplano, Sudamerika: Geographica Bernensia, v. G45, 118 p.

Wang, Y. J., Cheng, H., Edwards, R. L., An, Z. S., Wu, J. Y., Shen, C. C., and Dorale, J. A., 2001, A high-resolution absolute-dated Late Pleistocene monsoon record from Hulu Cave, China: Science, v. 294, no. 5550, p. 2345-2348.

Webb, R. H., Steiger, J. W., and Turner, R. M., 1987, Dynamics of Mojave desert shrub assemblages in the Panamint Mountains, California: Ecology, v. 68, no. 3, p. 478-490.

Winograd, I. J., Riggs, A. C., and Coplen, T. B., 1998, The relative contributions of summer and cool-season precipitation to groundwater recharge, Spring Mountains, Nevada, USA: Hydrogeology Journal, v. 6, no. 1, p. 77-93.

Winograd, I. J., and Thordarson, W., 1975, Hydrogeologic and hydrochemical framework, south-central Great Basin, Nevada-California, with special reference to the Nevada test site: U. S. Geological Survey Professional Paper 712-C, Reston, VA, 126 p.

Wu, T. W., and Qian, Z. A., 2003, The relation between the Tibetan winter snow and the Asian summer monsoon and rainfall: An observational investigation: Journal of Climate, v. 16, no. 12, p. 2038-2051.

Zachos, J., Pagani, M., Sloan, L., Thomas, E., and Billups, K., 2001, Trends, rhythms, and aberrations in global climate 65 Ma to present: Science, v. 292, no. 5517, p. 686-693.

# CHAPTER IV

## Sedimentologic and isotopic constraints on the Paleogene paleogeography and paleotopography of the southern Sierra Nevada, California[*]

### 4.1 Abstract

Detrital zircon U-Pb provenance and stable isotopic studies of three Paleogene southern Sierra Nevada (California) basins place new constraints on the paleoelevation history of the region. Age spectra from the Paleocene Witnet Formation within the southernmost Sierra Nevada link these sediments to source terranes that were at or near sea-level in the early Cenozoic, while age spectra from the Paleocene Goler Formation, east of the Sierra Nevada, demonstrate isolation of southern Sierra Nevada basins from the continental interior and tapping of Jurassic and Triassic arc flank sources during the Paleocene. West of the Sierra Nevada, strata of the Eocene Tejon Formation are dominated by Cretaceous zircons sourced from the Sierran batholith. Goler Formation carbonate $\delta^{18}O$ suggests Paleocene paleoelevations of 1–2 km for the central and southern Sierra Nevada. Taken together, these data indicate a Paleogene southern Sierra

[*] **Citation:** Lechler, A.R., and Niemi, N.A., 2011, Sedimentologic and isotopic constraints on the Paleogene paleogeography and paleotopography of the southern Sierra Nevada, California: *Geology*, v. 39, no. 4, p. 379-382.

Nevada with modest elevations, locally dissected to sea-level by rift basins formed by Late Cretaceous lithospheric collapse. These results place new limits on the amount of regional mid- to late Cenozoic elevation gain that may have resulted from the loss of dense, mantle lithosphere from below the central and southern Sierra Nevada and point to possible north-south variations in the topographic evolution of the Sierra Nevada.

## 4.2 Introduction

The topographic evolution of the Sierra Nevada (California) is a key constraint on tectonic and geodynamic models of the southwest United States; however, various elevation histories have been proposed. At one end of the spectrum, geomorphic evidence has been used to argue for a low elevation (< 1 km) northern (north of the San Joaquin River) and moderate elevation (2–2.5 km) central Sierra Nevada (Mt. Whitney region) throughout much of the Cenozoic, with modern elevations achieved by 1.5–2 km of Late Miocene-Early Pliocene uplift (Unruh, 1991; Wakabayashi and Sawyer, 2001). At the other end, low temperature thermochronologic data has been interpreted as requiring a high-standing (~ 4.5 km) central Sierra since the Late Cretaceous (House et al., 1998), while in the northern Sierra, stable isotope and molecular proxies suggest Eocene range elevations comparable to the modern (2–2.5 km; Mulch et al., 2006; Hren et al., 2010). A multi-stage evolution for the central Sierra Nevada, based on thermochronometric and geomorphic evidence, has also been proposed in which early Cenozoic surfaces (~ 1.5 km) experienced >2 km of uplift sometime between 32.5 and 3.5 Ma, raising the central Sierra to its modern (~ 4 km) elevations (Clark et al., 2005).

The contrasting elevation histories for the central and northern Sierra Nevada may

in part be the result of along-strike variations (e.g., Busby and Putirka, 2009). Validation of this idea is limited, however, due to a lack of robust paleoelevation constraints for the Sierra Nevada south of Mt. Whitney. This region has experienced a unique tectonic evolution including early Cenozoic lithospheric collapse (e.g., Saleeby et al., 2007) and late Cenozoic loss of a dense lithospheric root (the seismically imaged 'Isabella anomaly', e.g., Zandt et al., 2004; Fig. 4.1). Recent thermochronologic and structural data suggest the southern Sierra Nevada experienced a multi-stage uplift history consistent with the Clark et al. (2005) model for the central Sierra (Maheo et al., 2009), but the magnitude and timing of regional uplift is poorly constrained. We present new detrital zircon U-Pb dates and $\delta^{18}O$ data from southern Sierra Nevada Paleogene basins (Fig. 4.1) to provide constraints on early Cenozoic regional paleogeography and paleotopography.

### 4.3 Early Cenozoic basins

The Sierra Nevada magmatic arc formed in response to Mesozoic subduction along the western margin of North America (Evernden and Kistler, 1970). A shift to low-angle subduction during the latest Cretaceous-early Paleogene led to widespread oblique extension throughout much of the arc and arc flank that resulted in a sequence of local rift basins that preserve early Cenozoic sediments in the southern Sierra Nevada region (Wood and Saleeby, 1997). East of the Sierra Nevada, these sediments are represented by the Paleocene Goler Formation, a 4-km-thick, fossil-bearing, continental clastic sequence best exposed in the El Paso Mountains (Fig. 4.1). The early Paleocene lower Goler Formation (Members 1–3; Cox, 1982) is interpreted as a sequence of alluvial fan conglomerates and sandstones derived primarily from local Triassic plutonic rocks (Cox,

# Figure 4.1

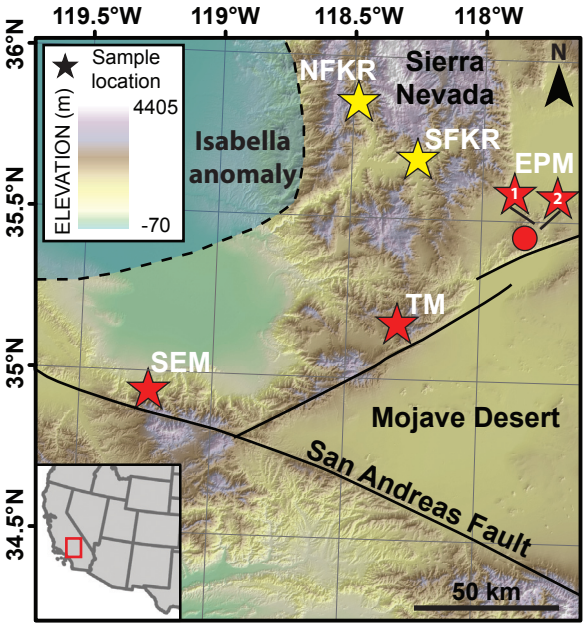


Figure 4.1 - Color digital elevation model (DEM) with sandstone (red stars), modern sand (yellow stars), and micrite (red circle) sample locations (see Figure A4.1 in appendix for local geology of sample sites). Goler Formation samples are marked by numbered stars. Blue swath shows approximate position of Isabella anomaly imaged at ~150 km depth (Zandt et al., 2004). Inset map of southwest United States shows approximate DEM extent. **NFKR**- North Fork Kern River, **SFKR** - South Fork Kern River, **EPM** - El Paso Mtns., **TM** - Tehachapi Mtns., **SEM** - San Emigdio Mtns.

1982). Middle Paleocene upper Goler Formation (Members 4a–d) fluvial sandstones and conglomerates contain a diverse clast assemblage of plutonic, volcanic, and siliciclastic cobbles indicative of a more distal source (Cox, 1982). Marine mollusks in Member 4d, along with ray teeth, turtle and crocodilian fossils in Members 3, 4a and 4b, require the Goler basin to have been alternately inundated by or adjacent to the paleo-Pacific Ocean during the Paleocene (e.g., Lofgren et al., 2008).

Within the southernmost Sierra Nevada, the Witnet Formation comprises the oldest preserved Cenozoic sediments (Fig. 4.1). This sequence of plutonic- and volcanic-cobble conglomerates and sandstones (Buwalda, 1954) is lithologically indistinguishable from the lower Goler Formation (Members 1 and 2). This similarity has led to speculation that the two units are correlative (Cox, 1982). However, poor age control on the Witnet Formation, with estimates spanning from latest Cretaceous (Wood and Saleeby, 1997) to Oligocene (Buwalda, 1954), preclude a definitive correlation.

West of the southern Sierra Nevada, the oldest Cenozoic sediments preserved are the Middle Eocene Tejon Formation, which was deposited in a shallow marine basin directly on top of crystalline basement rocks now exposed in the San Emigdio Mountains (Fig. 4.1). Like the Witnet and Goler formations, the siliciclastic Tejon Formation contains abundant plutonic and volcanic detritus. Sandstone petrology suggests Tejon sediments were derived from sources in the southern Sierra Nevada, northern Mojave Desert, and basement rocks of the San Emigdio and Tehachapi Mountains (Critelli and Nilsen, 2000).

### 4.4 Detrital zircon U-Pb and carbonate $\delta^{18}O$ data

Six medium- to coarse-grained, arkosic to lithic sand and sandstone samples from the southern Sierra Nevada region (Fig. 4.1) were analyzed at the University of Arizona LaserChron Center (see Table A4.1 in the appendix for the complete U-Pb dataset). In total, 578 analyses satisfied concordance and reproducibility requirements (Table A4.1) and were incorporated into age-probability plots for each basin (Fig. 4.2A).

In order to constrain the amount of Sierran detritus deposited in early Cenozoic basins, U-Pb age spectra were compiled from two modern river sand samples collected from the Kern River, which drains the southern Sierra Nevada batholith (Fig. 4.1). Both North (NFKR) and South (SFKR) Fork samples are dominated by mid-Cretaceous and Late Jurassic zircons with subordinate Middle Jurassic age peaks. A minor Early Jurassic age peak is also evident in the SFKR sample (Fig. 4.2A).

Two sandstone samples were collected from the fluvial portion of the Goler Formation (EPM-1 from Member 4d, EPM-2 from Member 4b; Fig. A4.1 in the Appendix). Both Goler samples are dominated by Middle and Late Jurassic ages, with a minor peak of Late Triassic-Early Jurassic ages (Fig. 4.2A). A shift to younger ages is observed in the upper Goler sample (EPM-1), which also contains a well-defined peak of mid-Cretaceous zircons not observed in EPM-2.

Age spectra from the Witnet (TM-1) and Tejon (SEM-1) formations are distinct from the upper Goler Formation. Witnet sediments are dominated by mid-Cretaceous and Early Triassic zircons, while mid-Cretaceous zircons are the only significant population in the Tejon sample (Fig. 4.2A).

All samples display a paucity of pre-Mesozoic zircons (Fig. A4.2 in the

# Figure 4.2

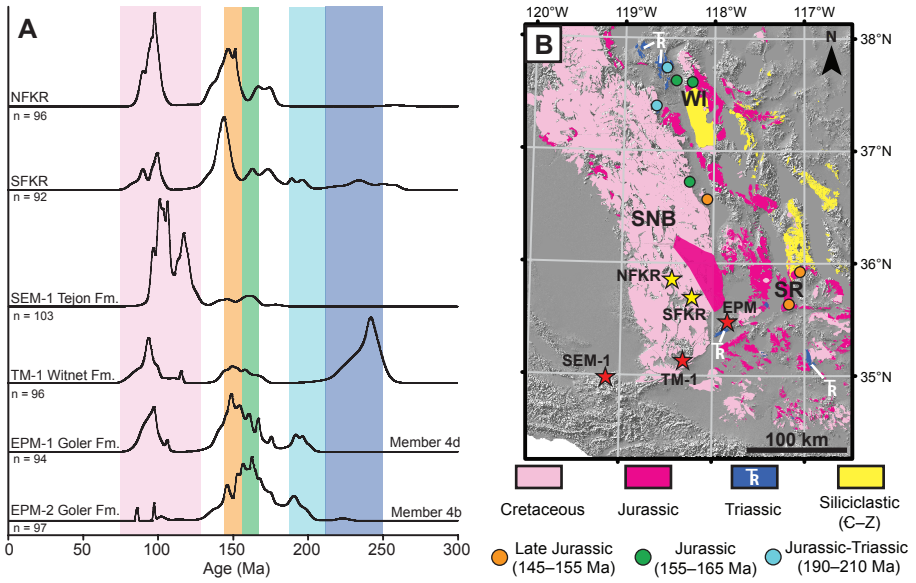


Figure 4.2 - (A) 0-300 Ma detrital zircon U-Pb age-probability plots (see Appendix Figure A4.2 for full age spectra). Colored swaths highlight diagnostic age populations. (B) digital elevation model (DEM) of Sierra Nevada region with modern distribution of igneous and siliciclastic rocks, color-coded by age (compiled from various sources, see Appendix Fig. A4.3). Location of diagnostic ages denoted by colored dots with same color-code as (A). Stars mark sample locations. **WI** - White-Inyo Mtns.; **SR** - Slate Range; **SNB** - Sierra Nevada batholith.

Appendix). Proterozoic and Paleozoic ages comprise ~9% of the Goler samples, and are even rarer in the Witnet (4%) and Tejon (2%) samples.

Lacustrine micrite sampled from Goler Formation Member 4a (Cox, 1982) provides isotopic ($\delta^{18}O$) constraints on Goler basin waters. The micrite has an average $\delta^{18}O_{PDB}$ value of -12.3‰ (Table A4.2 in the Appendix). The $\delta^{18}O$ of the water in which the micrite precipitated was calculated (O'Neil et al., 1969) using a regional Eocene sea level temperature range of 20–25 °C (Yapp, 2008; Hren et al., 2010). Corresponding $\delta^{18}O_{SMOW}$ values of -10.1‰ to -11.2‰ are presumed to represent Goler basin waters at the time of micrite deposition.

**4.5 Sedimentary provenance**

We identify prospective source regions for each Paleogene basin using the modern distribution of igneous and siliciclastic rocks in the Sierra Nevada region (Fig. 4.2B). This approach is limited by the assumption that modern distributions are representative of early Cenozoic exposures, but the uniqueness of detrital age spectra (Fig. 4.2A) and the systematic age distribution of igneous rocks in this region (Fig. 4.2B) permit this approach.

The Sierran batholith is discounted as a major source for Goler sediments based on the dominance of Middle to Late Jurassic zircon U-Pb ages over Cretaceous ages and the presence of a mixed plutonic and volcanic clast assemblage in the upper Goler Formation, an interpretation consistent with the observation that Sierran detritus is a minor component of El Paso basin sediments prior to 8 Ma (Loomis and Burbank, 1988). Middle and Late Jurassic plutonic and volcanic rocks are currently exposed east of the

Sierra Nevada (Fig. 4.2B) in the White-Inyo Mountains (Dunne et al., 1998) and the Slate Range (Dunne and Walker, 2004). The Slate Range has been proposed as a source region for the upper Goler Formation, based on west-directed paleocurrent indicators and clast lithologies (Cox, 1982). Our data do not preclude the Slate Range as a sedimentary source for the upper Goler Formation, but observed 190–210 Ma and 155–165 Ma zircon age populations have no known source in the Slate Range. The 190–210 Ma zircon population is perhaps most diagnostic, as igneous rocks of this age are scarce in the Sierra Nevada region. The most viable source for 190–210 Ma zircons, as well as 155–165 Ma and Proterozoic populations, is west of the northern White Mountains (Fig. 4.2B).

Witnet Formation U-Pb ages require a sedimentary source distinct from that of the upper Goler Formation (Fig. 4.2A). Mid-Cretaceous zircons in the Witnet Formation are likely derived from local Sierran basement sources (Fig. A4.1). The prominent peak of Early Triassic ages, however, must be derived from a more distal source. The most likely sources are Triassic plutons in the basement of the El Paso Mountains and northern Mojave Desert (Fig. 4.2B; Cox, 1982). These plutons were also the primary source for locally-derived sediments in the lower Goler Formation (Cox, 1982), which supports proposed correlations of the lower Goler and Witnet formations, and suggests both were part of the same sedimentary system, with proximal Goler alluvial fans supplying sediment to the Witnet basin via a west-flowing, trans-Sierran river. This interpretation places new bounds on the age and paleoelevation of the Witnet Formation, constraining deposition to early Paleocene time, at elevations at or below those of the near-sea-level Goler basin.

The dominance of mid-Cretaceous zircons in the Tejon Formation indicates that

the Tejon basin was fed by a fluvial system with headwaters in the Sierran batholith, and was isolated from the arc flank regions sourcing the Goler and Witnet Formations. Thus, the Paleocene rivers transecting the southernmost Sierra Nevada appear to have been cutoff or redirected during the Eocene.

The small proportion of pre-Mesozoic zircons in all detrital samples (≤ 9%) places additional constraints on sedimentary provenance. Paleo- and Mesoproterozoic zircon ages dominate Neoproterozoic and Paleozoic quartzite-rich strata in the Great Basin (e.g., Gehrels et al., 1995). As a result, Proterozoic zircons and associated quartzite clasts would have been abundant in continental interior-sourced Paleogene fluvial systems, as observed in Amargosa paleoriver deposits (Fig. 4.3A; Howard, 1996; Wernicke, 2011). Quartzite is subordinate to igneous clasts throughout the upper Goler Formation (Cox, 1982). This, along with the relative lack of pre-Mesozoic zircons in the Goler, Witnet and Tejon formations, suggests that southern Sierra Nevada fluvial systems were isolated from the continental interior during the early Paleogene (Fig. 4.3A), a result consistent with observed endemism of Goler fossil species (Lofgren et al., 2008).

## 4.6 Early Cenozoic paleotopography and paleogeography of the southern Sierra Nevada

Our provenance work on southern Sierra Nevada Paleogene basins places important constraints on the early Cenozoic paleoelevation history of the region. Paleontologic evidence puts the Goler basin at or near sea level during deposition (Lofgren et al., 2008). As Witnet sediments appear to be coeval with, lie downstream from, and share a common source with the lower Goler Formation, the Witnet Formation

must have also been deposited at or near sea level, ~1500 m lower than modern exposure elevations.

Water $\delta^{18}O_{SMOW}$ values of -10.1‰ to -11.2‰ derived from Goler Formation lacustrine micrites are significantly depleted relative to Eocene sea level $\delta^{18}O_{SMOW}$ estimates of -6.7‰ to -8.9‰ (Yapp, 2008; Hren et al., 2010). Goler Formation paleosol carbonate nodules from the same stratigraphic interval as the micrite (Member 4a) exhibit remarkably similar $\delta^{18}O_{SMOW}$ values (-10.5 to -11.6%, calculated from Torres, 2010) to the micrite. Paleosol carbonate $\delta^{18}O$ reflects local precipitation falling directly into the basin, whereas lacustrine carbonates integrate the isotopic signal from throughout the contributing catchment. The observed isotopic depletion in each proxy system suggests that all waters falling (precipitation) and transported (fluvial) into the Goler basin were subject to orographic rainout over a topographic barrier on the windward side of the Goler basin and White-Inyo Mtn. source region, likely in the Paleocene central and southern Sierra Nevada. With early Cenozoic $\delta^{18}O$-elevation gradients of ~-2‰/km (Mulch et al., 2006; Hren et al., 2010), a $\delta^{18}O$ depletion of -1.2‰ to -4.5‰ for Goler waters relative to Eocene sea level indicates that the Paleocene central and southern Sierra Nevada had paleoelevations of 1–2 km.

In combination, the provenance and isotopic data suggest that the Paleocene southern Sierra Nevada had modest elevations, in agreement with estimates derived for the Paleocene-Eocene central Sierra Nevada (~1.5 km; Clark et al., 2005); however, on a local scale, near-sea-level basins transected the range. These basins likely developed in response to Late Cretaceous orogenic collapse of the southernmost Sierra Nevada (Saleeby et al., 2007). Localization of the source terranes for Goler sediments adjacent to

the position of Late Cretaceous dextral shear zones associated with Sierran orogenic collapse further underscores the apparent tectonic control on the paleogeographic evolution of the early Cenozoic southern Sierra (Fig. 4.3A; Bartley et al., 2007). During the Eocene, the west-directed fluvial systems feeding the Goler and Witnet basins appear to have been cutoff or redirected. This truncation may record a phase of regional Eocene uplift (e.g., Goodman and Malin, 1992); however, based on similarities between the net post-Paleocene uplift of the Witnet Formation (~1500 m), and the proposed post-Eocene uplift of the central and southern Sierra Nevada (~2000 m; Clark et al., 2005), the amount of early Eocene uplift was presumably minor.

The results presented here provide a coherent Cenozoic uplift history for the central and southern Sierra Nevada, consistent with previous models (Clark et al., 2005; Maheo et al., 2009). The applicability of this history to the entire orogen, however, depends on whether the northern Sierra Nevada is a long-lived (e.g., Mulch et al., 2006) or young (e.g., Wakabayashi and Sawyer, 2001) topographic feature. Additionally, the work presented here, along with existing paleontologic (Lofgren et al., 2008) and sedimentologic (Cecil et al., 2011) evidence, suggests that Sierra Nevada coastal basins were isolated from continental interior drainages in Paleocene-Eocene time (Fig. 4.3A). This contrasts with Oligocene reconstructions in which fluvial systems rising in the Great Basin traversed the Sierra Nevada (north of 38ºN), connecting the high-standing continental interior to the coast (e.g. Henry and Faulds, 2010) and calls into question models in which a high-standing orogenic plateau over present-day Nevada extended as far south as the latitude (~36ºN) of the southern Sierra (e.g., Ernst, 2010).

# Figure 4.3

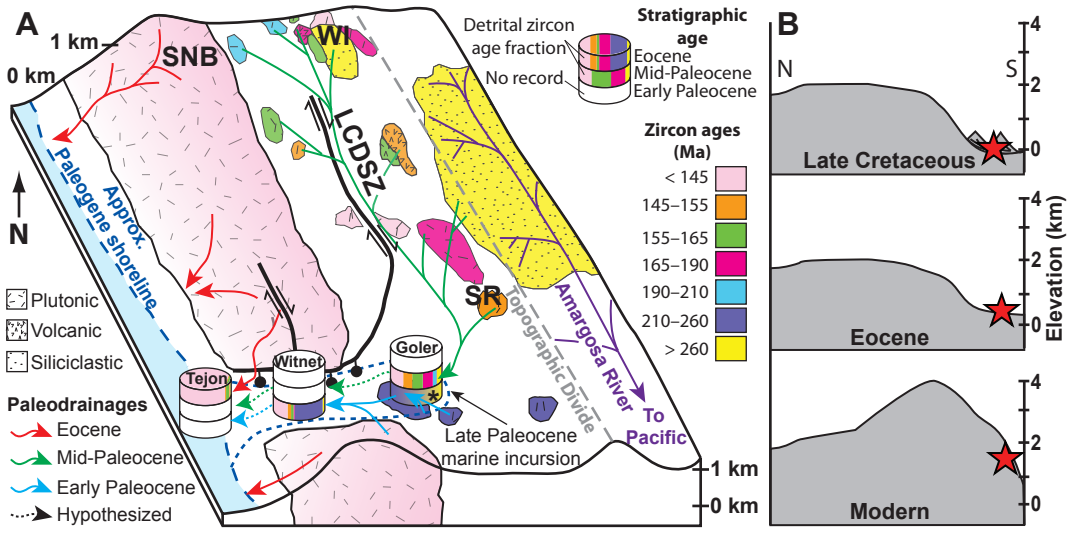


Figure 4.3 - (A) Diagram of early Paleogene southern Sierra Nevada regional paleotopography and paleogeography constrained by detrital zircon U-Pb age spectra and correspondence with plutonic, volcanic, and siliciclastic source terranes (Fig. 4.2B). Late Cretaceous dextral shear zones (LCDSZ) and rift basins provided fluvial pathways and depocenters for Paleogene sediment transport and deposition. Amargosa River paleogeography from Howard (1996) and Wernicke (2011). * - Lower Goler Formation detrital composition constrained by clast and sandstone point counts (Cox, 1982), not through detrital zircon U-Pb dating. (B) Schematic north-south cross-sections showing the Late Cretaceous to modern mean elevation distributions of the Sierra Nevada. Red star marks position of Witnet basin through time.

## 4.7 Conclusions

Combined zircon U-Pb provenance and $\delta^{18}O$ data constrain the Paleocene paleoelevation of the southern Sierra Nevada to be modest (1–2 km), with local dissection by low elevation basins and fluvial systems tapping the eastern arc flank region. Near-sea-level deposition of the Witnet Formation requires ~1500 m of absolute uplift of the southern Sierra Nevada since the Paleocene. Most of this uplift is likely post-Eocene, given similarities to published uplift estimates of the central and southern Sierra Nevada based on geomorphic criteria (Clark et al., 2005), and may be the result of the loss of a dense lithospheric root. These results contrast with models of a topographically stable northern Sierra Nevada (e.g., Mulch et al., 2006), thus underscoring the possibility of spatial variability in Cenozoic Sierra Nevada paleogeography, and highlighting the roles that local tectonic events have played in controlling the topographic and geodynamic evolution of the Cordilleran margin.

## 4.8 Acknowledgements

We thank G. Gehrels and A. Pullen at the University of Arizona LaserChron Center for assistance with U-Pb analyses, and K. Lohmann and L. Wingate at the University of Michigan Stable Isotope Lab for collaboration on isotopic analyses. C. Henry, E. Nadin, and K. Putirka are thanked for thoughtful reviews. U-Pb analysis was supported by National Science Foundation grants EAR-0310252 (NAN) and EAR-0607458 (M. K. Clark) and a University of Michigan Turner Award (ARL).

## 4.9 References cited


Bartley, J.M., Glazner, A.F., Coleman, D.S., Kylander-Clark, A., Mapes, R., and Friedrich, A.M., 2007, Large Laramide dextral offset across Owens Valley, California, and its possible relation to tectonic unroofing of the southern Sierra Nevada, *in* Till, A.B., Roeske, S.M., Sample, J.C., and Foster, D.A., eds., Exhumation Associated with Continental Strike-Slip Fault Systems: Boulder, Colorado, Geological Society of America, p. 129–148.

Busby, C.J., and Putirka, K., 2009, Miocene evolution of the western edge of the Nevadaplano in the central and northern Sierra Nevada: palaeocanyons, magmatism, and structure: International Geology Review, v. 51, p. 670–701, doi:10.1080/00206810902978265.

Buwalda, J.P., 1954, Geology of the Tehachapi Mountains, California: Bulletin - California. Division of Mines and Geology, v. 170, p. 131–142.

Cecil, M.R., Ducea, M., Mulch, A., Allen, C., and Campbell, I., 2011, Provenance of Eocene river sediments from the central-northern Sierra Nevada and implications for paleotopography: Tectonics, v. 30, doi:10.1029/2010TC002717.

Clark, M.K., Maheo, G., Saleeby, J., and Farley, K.A., 2005, The non-equilibrium landscape of the southern Sierra Nevada, California: GSA Today, v. 15, p. 4–10, doi:10.1130/1052-5173(2005)015[4:TNLOTS]2.0.CO;2.

Cox, B.F., 1982, Stratigraphy, sedimentology, and structure of the Goler Formation (Paleocene), El Paso Mountains, California: Implications for Paleogene tectonism on the Garlock Fault Zone [Ph.D. Thesis]: Riverside, University of California, 248 p.

Critelli, S., and Nilsen, T.H., 2000, Provenance and stratigraphy of the Eocene Tejon Formation, Western Tehachapi Mountains, San Emigdio Mountains, and Southern San Joaquin Basin, California: Sedimentary Geology, v. 136, p. 7–27, doi:10.1016/S0037-0738(00)00080-4.

Dunne, G.C., Garvey, T.P., Oborne, M., Schneidereit, D., Fritsche, A.E., and Walker, J.D., 1998, Geology of the Inyo Mountains Volcanic Complex: Implications for Jurassic paleogeography of the Sierran magmatic arc in eastern California: Geological Society of America Bulletin, v. 110, p. 1376–1397, doi:10.1130/0016-7606(1998)110<1376:GOTIMV>2.3.CO;2.

Dunne, G.C., and Walker, J.D., 2004, Structure and evolution of the East Sierran thrust system, east central California: Tectonics, v. 23, p. TC4012, doi:10.1029/2002TC001478.

Ernst, W.G., 2010, Young convergent-margins, climate, and crustal thickness - A Late Cretaceous-Paleogene Nevadaplano in the American Southwest?: Lithosphere, v. 2,

p. 67–75, doi:10.1130/L84.1.

Evernden, J.F., and Kistler, R.W., 1970, Chronology of emplacement of Mesozoic batholithic complexes in California and western Nevada: U.S. Geological Survey Professional Paper 623, 42 p.

Gehrels, G.E., Dickinson, W.R., Ross, G.M., Stewart, J.H., and Howell, D.G., 1995, Detrital zircon reference for Cambrian to Triassic miogeoclinal strata of western North America: Geology, v. 23, p. 831–834, doi:10.1130/0091-7613(1995)023<0831:DZRFCT>2.3.CO;2.

Goodman, E.D., and Malin, P.E., 1992, Evolution of the southern San Joaquin basin and mid-Tertiary transitional tectonics, central California: Tectonics, v. 11, p. 478–498, doi:10.1029/91TC02871.

Henry, C.D., and Faulds, J.E., 2010, Ash-flow tuffs in the Nine Hill, Nevada, paleovalley and implications for tectonism and volcanism of the western Great Basin, USA: Geosphere, v. 6, p. 339–369, doi:10.1130/GES00548.1.

House, M.A., Wernicke, B.P., and Farley, K.A., 1998, Dating topography of the Sierra Nevada, California, using apatite (U-Th)/He ages: Nature, v. 396, p. 66–69, doi:10.1038/23926.

Howard, J.L., 1996, Paleocene to Holocene paleodeltas of ancestral Colorado River offset by the San Andreas fault system, southern California: Geology, v. 24, p. 783–786, doi:10.1130/0091-7613(1996)024<0783:PTHPOA>2.3.CO;2.

Hren, M.T., Pagani, M., Erwin, D.M., and Brandon, M., 2010, Biomarker reconstruction of the early Eocene paleotopography and paleoclimate of the northern Sierra Nevada: Geology, v. 38, p. 7–10, doi:10.1130/G30215.1.

Lofgren, D.L., Honey, J.G., McKenna, M.C., Zondervan, R.L., and Smith, E.E., 2008, Paleocene primates from the Goler Formation of the Mojave Desert in California, *in* Wang, X., and Barnes, L.G., eds., Geology and Vertebrate Paleontology of Western and Southern North America, Contributions in Honor of David P. Whistler, Volume Science Series 41, National History Museum of Los Angeles County, p. 11–28.

Loomis, D.P., and Burbank, D.W., 1988, The stratigraphic evolution of the El Paso basin, southern California: Implications for the Miocene development of the Garlock Fault and uplift of the Sierra Nevada: Geological Society of America Bulletin, v. 100, p. 12–28, doi:10.1130/0016-7606(1988)100<0012:TSEOTE>2.3.CO;2.

Maheo, G., Saleeby, J., Saleeby, Z., and Farley, K.A., 2009, Tectonic control on southern Sierra Nevada topography, California: Tectonics, v. 28, p. TC6006, doi:10.1029/2008TC002340.

Mulch, A., Graham, S.A., and Chamberlain, C.P., 2006, Hydrogen isotopes in Eocene river gravels and paleoelevation of the Sierra Nevada: Science, v. 313, p. 87–89, doi:10.1126/science.1125986.

O'Neil, J.R., Clayton, R.N., and Mayeda, T.K., 1969, Oxygen isotope fractionation in divalent metal carbonates: The Journal of Chemical Physics, v. 51, p. 5547–5558, doi:10.1063/1.1671982.

Saleeby, J., Farley, K.A., Kistler, R.W., and Fleck, R.J., 2007, Thermal evolution and exhumation of deep-level batholithic exposures, southernmost Sierra Nevada, California: Geological Society of America Special Paper, v. 419, p. 39–66.

Torres, M., 2010, Paleoclimatic and paleoenvironmental interpretations of the Paleocene Goler Formation of southern California [B.S. Thesis]: Pitzer College, 77 p.

Unruh, J.R., 1991, The uplift of the Sierra Nevada and implications for Late Cenozoic epeirogeny in the Western Cordillera: Geological Society of America Bulletin, v. 103, p. 1395–1404, p. 1395–1404, doi:10.1130/0016-7606(1991)103<1395:TUOTSN>2.3.CO;2.

Wakabayashi, J., and Sawyer, T.L., 2001, Stream incision, tectonics, uplift, and evolution of topography of the Sierra Nevada, California: The Journal of Geology, v. 109, p. 539–562, doi:10.1086/321962.

Wernicke, B., 2011, The California River and its role in carving the Grand Canyon: Geological Society of America Bulletin, v. 123, doi: 10.1130/B30274.1.

Wood, D., and Saleeby, J., 1997, Late Cretaceous-Paleocene extensional collapse and disaggregation of the southernmost Sierra Nevada batholith: International Geology Review, v. 39, p. 973–1009, doi:10.1080/00206819709465314.

Yapp, C.J., 2008, O-18/O-16 and D/H in goethite from a North American oxisol of the Early Eocene climatic optimum: Geochimica et Cosmochimica Acta, v. 72, p. 5838–5851, doi:10.1016/j.gca.2008.09.002.

Zandt, G., Gilbert, H., Owens, T.J., Ducea, M., Saleeby, J., and Jones, C.H., 2004, Active foundering of a continental arc root beneath the southern Sierra Nevada in California: Nature, v. 431, p. 41–46, doi:10.1038/nature02847

# CHAPTER V

## Carbonate clumped isotope paleotemperature evidence for a high elevation Paleocene-Eocene 'Nevadaplano' in the Western US Cordillera[*]

### 5.1 Abstract

Accurate paleoelevation histories for the western US Cordillera provide first order constraints on the climatic, tectonic, and geodynamic evolution of the region. It has long been speculated that a high elevation 'Nevadaplano' dominated much of the interior Cordillera in late Cretaceous-early Paleogene time, but at present direct and absolute estimates of regional paleoelevation are generally lacking or limited to paleobotanical studies limited by high inherent uncertainties. Measurement of lacustrine carbonate growth temperatures using the clumped isotope paleothermometry analytical technique reveals significant temperature differences between carbonate proxies formed within and external to the proposed high elevation plateau. Clumped isotope temperatures for

[*] **Citation:** Lechler, A.R., Niemi, N.A., Hren, M.T., and Lohmann, K.C., *in prep*., Carbonate clumped isotope paleotemperature evidence for a high elevation Paleocene-Eocene 'Nevadaplano' in the Western US Cordillera

lacustrine carbonates in the Paleocene Goler Formation, known to be deposited at a paleoelevation at or near sea level, are ~ 16°C warmer than clumped isotope temperatures of lacustrine carbonates and *Unionid* bivalve shells collected from the Late Cretaceous-Eocene Sheep Pass Formation in east-central Nevada. Using both modern and ancient lake water temperature lapse rates, the observed temperature difference indicates that the Sheep Pass basin of the Cordilleran interior was part of a high elevation (≥ 2.6 km) orogenic plateau that collapsed during subsequent Tertiary Basin and Range extension. This study provides direct evidence for high paleoelevations in the interior western US and thus supports models ascribing widespread crustal extension to internal buoyancy forces associated with excess gravitational potential energy of a high elevation continental plateau. Carbonate clumped isotope temperatures at multiple stratigraphic intervals in the Paleocene-Eocene section of the Sheep Pass Formation also constrain the amount of climate warming (~ 5ºC) that occurred in the interior western US during the Early Eocene Climatic Optimum. Together, these results illustrate the utility of clumped isotope paleothermometry to paleoaltimetry and paleoclimate studies, particularly in regions where paleo-meteoric water proxy records are subject to significant evaporative influence.

## 5.2 Introduction

Quantitative paleoelevation histories are vital to the development and validation of tectonic and geodynamic models of orogen development. In the Western US Cordillera, accurate elevation histories are particularly relevant to resolving the driving forces for widespread Tertiary extension and the mechanism(s) by which this extension

occurred. Competing models for the Cenozoic evolution of the Basin and Range are commonly characterized by unique topographic histories, thus providing testable predictions for the topographic evolution of the region (Clark, 2007). As a result, the relative influences of plate boundary, internal buoyancy, and basal normal forces on Basin and Range extension can be better understood if elevation distributions both prior to and concomitant with regional crustal extension and magmatism can be constrained (e.g., Sonder and Jones, 1999).

Excess gravitational potential energy of a high elevation (> 3 km) continental plateau with a crustal thickness > 50 km is commonly cited as a primary driver for Basin and Range extension (Coney and Harms, 1984; Jones et al., 1996, 1998; Dilek and Moores, 1999; Sonder and Jones, 1999; Flesch et al., 2007). In such a scenario, long-lived Mesozoic and early Cenozoic convergence and subduction of the Farallon oceanic plate off the western margin of North America is speculated to have created a high elevation orogenic plateau in the hinterland of the active Sierra Nevada magmatic arc that was flanked on its eastern margin by the Sevier fold-thrust belt (Coney and Harms, 1984; Jones et al., 1998; Dilek and Moores, 1999; DeCelles, 2004). This orogenic plateau has been termed the 'Nevadaplano' (DeCelles, 2004) due to proposed similarity with the Altiplano-Puna Plateau of the South American Andes and would have been a dominant physiographic feature in the Cordilleran interior during the Late Cretaceous-early Cenozoic. Beyond analogy, however, evidence for such high regional paleoelevations is generally restricted to indirect estimates derived from mass balance calculations that assume pre-extension crustal thicknesses in excess of 50 km are required to account for the ~ 30 km thick crust that characterizes much of the highly extended, modern Basin and

Range Province (e.g., Coney and Harms, 1984; Gans, 1987; Wernicke et al., 1996; Best et al., 2009; Ernst, 2010). Assuming the pre-extended crust of the Cordilleran interior was isostatically compensated, the proto-Basin and Range plateau would have been characterized by high regional paleoelevations (≥ 3km; e.g., DeCelles, 2004; Ernst, 2010).

More direct measures of paleoelevations in the Paleogene 'Nevadaplano' region have been produced using stable isotope and paleobotanical paleoaltimetry techniques, but interpretation of these paleoelevation histories must be made with caution due to the inherent assumptions and uncertainties associated with each technique. Stable isotopic records derived from Basin and Range lacustrine paleo-meteoric water proxies exhibit high magnitude isotopic shifts in $\delta^{18}O$ values that are proposed to reflect surface uplift > 2km from the middle Eocene to early Oligocene (Horton et al., 2004), followed by 1 – 3 km of surface lowering since the middle Miocene (Horton et al., 2004; Horton and Chamberlain, 2006). This surface uplift history implies that the Cordilleran interior had high paleoelevations (> 3 km) prior to Neogene extension, but these records do not provide absolute paleoelevation estimates and instead potentially constrain only relative changes in surface elevations through time. Isolating the elevation signal in these meteoric water proxy records is further complicated by uncertainty in how changes in climate, moisture source, and storm track trajectory influence proxy isotopic records, as well as how the evolution of regional paleofluvial systems in the western US Cordillera might account for the observed large isotopic shifts, independent of elevation change at the site of proxy formation (Carroll et al., 2008; Davis et al., 2008; Davis et al., 2009). Paleoelevation estimates for the 'Nevadaplano' have also been derived from

paleobotanical studies utilizing the physiognomy of fossil leaf assemblages to propose high regional elevations (≥ 2.5 km) throughout much of the region during the early Paleogene (e.g., Wolfe et al., 1997; Gregory-Wodzicki, 1997). Recent work, however, reveals that accurate quantification of paleoelevation uncertainties using the leaf physiognomy paleoaltimetry technique is subject to debate (Peppe et al., 2010; Spicer et al., 2010) and that uncertainties may be excessively high (≥ 2 km; Peppe et al., 2010).

In this study, we use clumped isotope paleothermometry of early Paleocene-Middle Eocene lacustrine micrites and *Unionid* bivalve shells collected from sites that would have been located within and external to the proposed 'Nevadaplano' to add constraints on the paleoelevation history of this region prior to widespread Tertiary extension. The carbonate sample site external to the 'Nevadaplano' has a known paleoelevation near sea level during the time of carbonate deposition. This sea level reference makes quantification of the relative temperature difference between sea level and the early Cenozoic 'Nevadaplano' possible, and, as a result, allows for direct inference of absolute paleoelevations. This work provides some of the first direct estimates of continental interior paleoelevations in the proto-Basin and Range Province during a time of relative tectonic quiescence following the end of the Sevier Orogeny when the proposed orogenic plateau may have attained a limiting crustal thickness and elevation (McQuarrie and Chase, 2000; DeCelles, 2004). As a result, this work has the potential to elucidate the probable driving mechanisms for the widespread Tertiary extension that controls the modern physiography of the region.

### 5.3 Clumped isotope paleothermometry and paleoaltimetry applications

Carbonate clumped isotope paleothermometry utilizes the temperature dependence of $^{13}C$-$^{18}O$ bond abundance (degree of 'clumping') in the carbonate crystal lattice to constrain temperatures of carbonate formation, independent of the carbonate stable isotopic composition (e.g., Ghosh et al., 2006). The higher bond energies of these multiply-substituted isotopologues (i.e. molecules with more than one rare isotope) result in a higher degree of 'clumping' (i.e. more $^{13}C$-$^{18}O$ bonds) at colder formation temperatures. In practice, carbonate clumped isotope analysis focuses on measuring the abundance of mass-47 isotopologues in $CO_2$ gas (primarily $^{13}C^{18}O^{16}O$) derived from phosphoric acid digestion of carbonate material. The measured enrichment of mass-47 isotopologues relative to a stochastic mass-47 distribution in $CO_2$ with equivalent isotopic compositions ($\delta^{18}O$ and $\delta^{13}C$), termed the $\Delta_{47}$ value, is then used for temperature determinations through application of the empirically derived 'clumping'-temperature relationship of Ghosh et al. (2006): $\Delta_{47} = 59200/T^2 - 0.02$, where T is in Kelvin (see Huntington et al., 2009 for additional details on the method).

Obtaining independent measures of temperature for carbonate growth and/or diagenetic resetting is a powerful tool for paleoclimate, hydrologic, and paleoelevation studies utilizing carbonate proxies for the stable isotopic composition of paleo-meteoric waters. For many of these studies, and particularly in stable isotope paleoaltimetry, the environmental parameter of interest is the isotopic composition of the water in which the carbonate proxy precipitated, as this water is assumed to reflect meteoric precipitation and/or surface water isotopic compositions at the time of proxy formation. Quantifying the relationship between water and carbonate isotopic compositions can be complicated,

however, due to temperature-dependent fractionation between the two phases (e.g., Kim and O'Neil, 1997). As a result, significant uncertainties in the temperature of lacustrine carbonate formation lead to significant uncertainties in the calculation of water isotopic compositions. With independent measures of the temperature of carbonate formation, the $\delta^{18}O$ value of the original water can be directly calculated, and, as a result, these carbonate proxy records can be more reliably interpreted.

Quantification of carbonate formation temperatures can also function as a powerful tool in paleoaltimetry studies independent of calculated water $\delta^{18}O$ values due to the covariance of surface temperature with elevation. This covariance leads to the testable hypothesis that carbonates precipitated at high elevation sites will be characterized by colder carbonate growth temperatures than contemporaneous carbonates formed at lower elevations, assuming carbonate growth occurs over equivalent times of the year and local climatic variations don't supersede elevation effects. This temperature-based paleoaltimetry application of clumped isotope paleothermometry can be an especially powerful tool in settings where the violation of Rayleigh distillation rainout processes significantly limits the application of standard stable isotope paleoaltimetry techniques. For example, regions with complex isotope-elevation relationships [e.g., continental interior of the western US (Ingraham and Taylor, 1991; Friedman et al., 2002; Lechler and Niemi, *in revision*, Chapter 2 of this thesis); Tibetan Plateau (Tian et al., 2007; Hren et al., 2009; this thesis)] and areas where surface waters are subject to evaporative influence are prone to producing stable isotope-based paleoelevation estimates with significant uncertainties (e.g., Quade et al., 2007; this thesis).

Huntington et al. (2010) used carbonate clumped isotope analysis of modern and ancient lacustrine carbonates collected over an elevation range of ~ 2 km in the Colorado Plateau region to suggest that middle Miocene paleoelevations and paleotopographic gradients were comparable to the modern, as well as to constrain a regional climatic change of ~7°C cooling since the late Miocene. Here we apply an analogous approach to address the paleotopographic and paleoclimatic evolution of the proto-Basin and Range during the Late Cretaceous-early Paleogene. If an orogenic plateau with elevations in excess of 3 km did characterize the western US interior in early Cenozoic time, we expect significant differences in carbonate growth temperatures between sites internal and external to the high elevation plateau, a hypothesis that can be directly tested with clumped isotope paleothermometry.

**5.4 Geologic setting and sample locations**

The Western US Cordillera was subject to oceanic subduction and associated compressive stresses throughout much of the Mesozoic and early Cenozoic Sevier and Laramide orogenies, resulting in a spatially extensive orogenic system bounded on its western margin by the Sierra Nevada magmatic arc. During the latest Cretaceous-early Paleogene synconvergent extension in both the magmatic arc region (e.g., Wood and Saleeby, 1997) and the Sevier-Laramide orogen (e.g., Wells et al., 1990; Hodges and Walker, 1992; Wells and Hoisch, 2008) created a series of local rift basins that preserve some of the oldest Cenozoic sediments in the region. Immediately east of the southernmost Sierra Nevada, these early Cenozoic sediments are represented by the Paleocene Goler Formation which outcrops in the El Paso Mountains of southeastern CA

(Figure 5.1). The Goler Formation is a > 4 km thick continental clastic sequence of dominantly alluvial and fluvial sandstones and conglomerates that has been subdivided into four lithologic members (Cox, 1982). The lower Goler Formation (Members 1 and 2) consists of pebble and cobble conglomerates proposed to have been locally derived from the Triassic plutonic basement of the Goler basin (Cox, 1982). Sedimentary provenance studies of the quartzite-cobble-rich and volcanic-cobble-rich strata in Members 4a and 4c indicates that upper Goler Formation sediments were sourced within the arc flank regions of the eastern Sierra Nevada (Chapter 4; Lechler and Niemi, 2011). A diverse fossil assemblage (ray teeth, crocodiles, turtles, primates, conodonts) throughout Members 3 and 4, in combination with the presence of marine mudstones and molluscs in the uppermost Goler Formation (Member 4d), suggests that the Goler basin resided at or near sea level throughout the early Paleogene (e.g., Lofgren et al., 2008). This fossil assemblage also provides depositional age constraints, indicating that the upper Goler Formation was deposited during the middle and late Paleocene (Torrejonian and Tiffanian North American Land Mammal Ages [NALMA]; Lofgren et al., 2008). Recent magnetostratigraphic study places more definitive bounds of ~ 62 – 57.5 Ma for the timing of Goler Formation deposition (Albright et al., 2009).

Late Cretaceous-early Paleogene synconvergent extension also produced a series of extensional basins within the interior of the Cordilleran orogen (Wells and Hoisch, 2008; Druschke et al., 2009b). The late Cretaceous-Eocene Sheep Pass Formation is an alluvial, fluvial, and lacustrine sedimentary sequence deposited on the hanging wall of one of these actively subsiding rift basins. The > 1 km thick Sheep Pass Formation currently outcrops in the Pancake, Grant and southern Egan ranges of east-central Nevada

(Figure 5.1) and provides one of the earliest records of extension-related sedimentary basin formation in the continental interior of the western US (Druschke et al., 2009a and b). Previous workers have subdivided the Sheep Pass Formation into six lithologic members (A–F) (Figure 5.2B; Fouch, 1979; Druschke et al., 2009b). Clastic-dominated alluvial fan and distal alluvial fan/marginal lacustrine environments characterize Members A and C, respectively, whereas carbonate-dominated sediments in Members B and D–F are interpreted to have been deposited in lacustrine environments (e.g., Fouch, 1979; Druschke et al., 2009b). Abundant molluscan specimens throughout Members B, C, and E suggest the Sheep Pass basin evolved from a single, regionally extensive lake environment into a series of isolated and ephemeral ponds in a wetland terrain through the early Paleogene (Good, 1987). Recent U-Pb detrital zircon dating provides a maximum depositional age of 81.3 ± 3.7 Ma in the middle of Sheep Pass Member A and a minimum age for the Sheep Pass Formation of 37.7 Ma ± 0.6 Ma based on U-Pb dating in the Stinking Springs Conglomerate member of the overlying Garrett Ranch Group volcanics (Druschke et al., 2009b). U-Pb carbonate dating at the base of Member B (Druschke et al., 2009a), in combination with biostratigraphic study of molluscan fossil assemblages in Members B and C (Good, 1987), suggests a late Campanian through Early Paleocene (~ 71.5 – 61 Ma) age for Member B. Molluscan biostratigraphy (Good, 1987) also constrains the depositional ages of Members C (middle to late Paleocene, ~ 61 – 55 Ma), D (early Eocene, ~ 55 – 50 Ma) and E (Bridgerian NALMA: 50.3 – 46.2 Ma).

Samples were collected from both the Goler and Sheep Pass Formations for clumped isotope paleothermometry analysis (Figures 5.1 and 5.2). Clastic sediments dominate much of the Goler sedimentary sequence but a single micritic limestone lens

# FIGURE 5.1

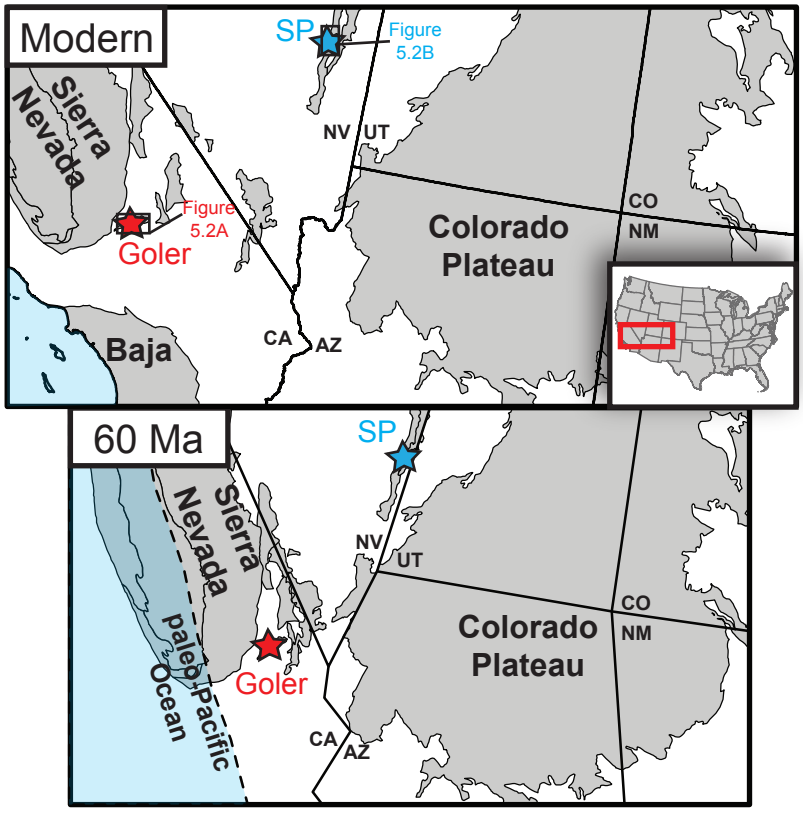


Figure 5.1 – Map of sample locations. Upper map shows carbonate sample locations (stars) in modern geographic coordinates with major physiographic provinces of the western US shown in gray. Inset map of the continental US indicates map extent. Lower map shows sample site locations in their Paleocene paleogeographic positions prior to Tertiary Basin and Range extension. Paleocene sample locations and paleogeography of retrodeformed state boundaries and physiographic provinces are based on palinspastic reconstructions of McQuarrie and Wernicke (2005). SP = Sheep Pass Formation; Goler = Goler Formation.

# FIGURE 5.2

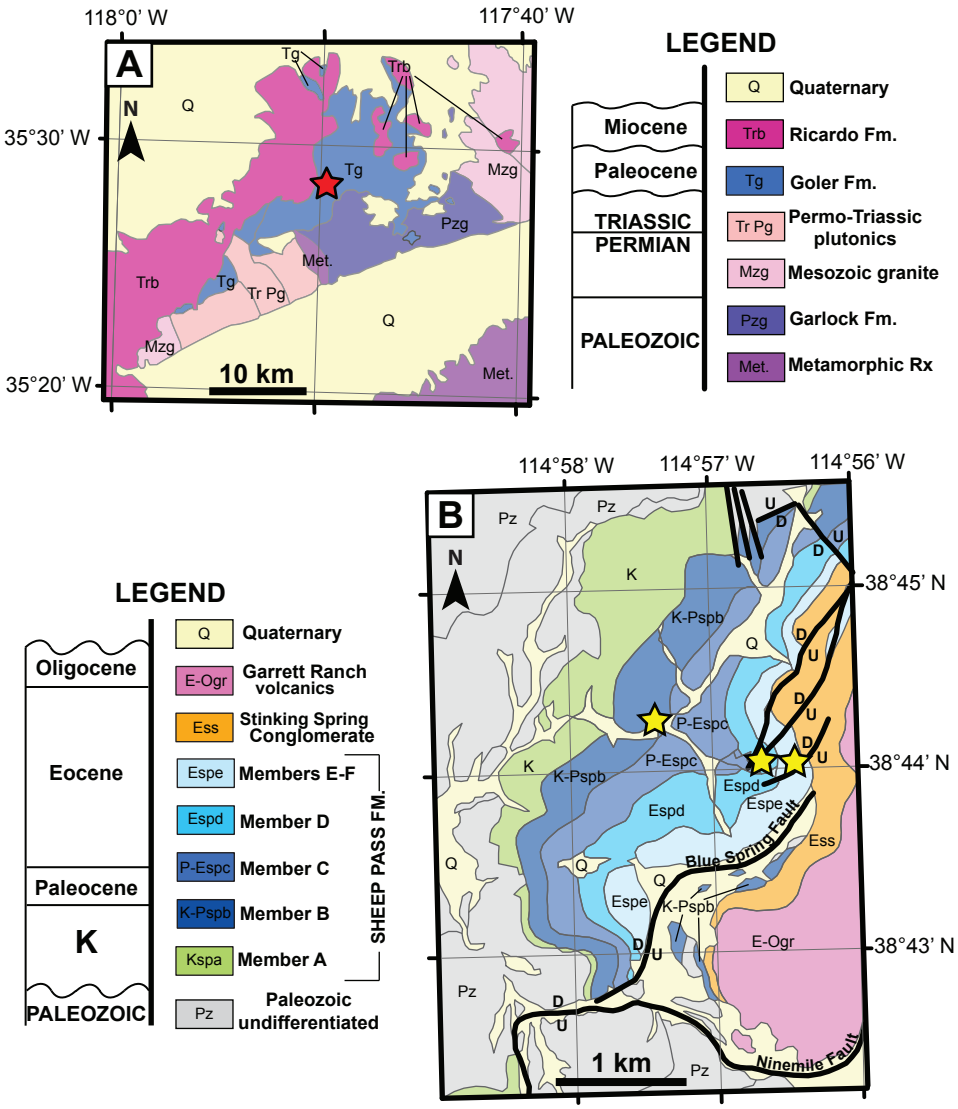


Figure 5.2 – Geologic setting of carbonate sample locations. (A) Geologic map of the El Paso Mountains of southeastern California, modified from Cox (1982). The Paleocene Goler Formation unconformably overlies metamorphic rocks of the Paleozoic Garlock Formation and Mesozoic plutonic rocks associated with the onset of regional Sierra Nevada arc magmatism and is unconformably overlain by Miocene Ricardo Formation volcanics. Red star marks location of micritic carbonate sampling from Member 4a. (B) Detailed geology of Sheep Pass Canyon, southern Egan Range, Nevada where the type section of the late Cretaceous-Eocene Sheep Pass Formation is exposed (modified from Druschke et al., 2009b). Yellow stars mark Sheep Pass carbonate sample locations. Both lacustrine carbonate and fossil mollusc shells were collected from the same location within Member B (K-Pspb). The E-W striking Ninemile Fault is a proposed synconvergent normal fault that was active throughout the deposition of the Sheep Pass Formation (Druschke et al., 2009a and b). See Figure 5.1 for additional location information for (A) and (B).

(1–2 m thick), believed to represent a small pond formed in the floodplain of a braided river system that traversed the Goler basin (Cox, 1982), is found within Member 4a and was sampled as part of this study (Figure 5.2A). The dominance of lacustrine environments and associated carbonate throughout much of the Sheep Pass Formation afforded the opportunity to collect carbonate samples at multiple stratigraphic intervals. All Sheep Pass Formation samples were collected from the type section, which is exposed in Sheep Pass Canyon in the southern Egan Range (Figure 5.2B). Lacustrine micrite samples were collected from Sheep Pass Members B, D and E. The sample from Member B also contained abundant fossil molluscs (*Unionid* bivalves), that were analyzed as part of this study.

**5.5 Analytical techniques**

Carbonate sample preparation and isotopic analysis was completed at the University of Michigan Stable Isotope Lab. All samples were analyzed for both standard stable ($\delta^{18}O$ and $\delta^{13}C$) and clumped ($\Delta_{47}$) isotopic compositions. Stable isotopic analyses were completed in October 2010 and isotopologue measurements were made in January 2011. Carbonate samples were drilled following standard micromilling procedures (Dettman and Lohmann, 1995). For $\delta^{18}O$ and $\delta^{13}C$ measurements, ~ 1 mg of drilled carbonate powder for each sample was placed under vacuum at 200°C for one hour to remove volatile contaminants and water. Samples were then placed in individual borosilicate reaction vessels and reacted at 77°C ± 1°C with 4 drops of anhydrous phosphoric acid for 8 minutes in a Finnigan MAT Kiel IV preparation device coupled

directly to the inlet of a Finnigan MAT 253 triple collector isotope ratio mass spectrometer. Measured precision is < 0.1‰ for both $\delta^{18}O$ and $\delta^{13}C$.

For clumped isotope analyses, a specific $CO_2$ extraction procedure is required in order to ensure purity of analyte $CO_2$ gas (Huntington et al., 2009). Approximately 5 mg of drilled carbonate powder was loaded into a rotary, multisample carousel that dropped individual powder samples into a common acid bath composed of ~ 20 ml of anhydrous phosphoric acid that was held at a constant temperature of 75°C using a circulating water bath. $CO_2$ was produced by reacting carbonate powders for 1 hour at 75°C. The $CO_2$ purification process followed the cryogenic procedures under vacuum conditions outlined in Ghosh et al. (2006) and Huntington et al. (2009), to remove residual water vapor and other contaminants. To eliminate hydrocarbon and halocarbon contaminants, $CO_2$ gas was entrained in a He carrier gas that flowed at a rate of 2 ml/min through a HP 5890 gas chromatograph (GC) column (Supel-Q-PLOT with 530 μm i.d., 30 m long) held at -20°C for 40 minutes. After flowing through the GC column, $CO_2$ was frozen out in a cold trap using liquid $N_2$ and He carrier gas was pumped away. $CO_2$ pressure was measured prior to and following the GC purification step in order to ensure consistent yields. Purified $CO_2$ then went through two subsequent cryogenic purification cycles and was eventually trapped in an evacuated glass vessel and transferred for isotopologue analysis.

$CO_2$ masses 45–49 were measured on a dual-inlet Thermo-Finnigan MAT 253 mass spectrometer following the methods of Eiler and Schauble (2004). Normalized $\Delta_{47}$ values were calculated using the stochastic reference heated gas line for the January 2011 analysis period. Heated gases with stochastic isotopologue distributions were produced by heating $CO_2$ gases of variable isotopic compositions in a muffle furnace at 1000°C for

2 hours. The heated gas reference line for our analysis period is shown in Figure 5.3. Each isotopologue analysis requires ~ 3 hours of mass spectrometer time in order to achieve precisions on the order of $10^{-6}$ for $\Delta_{47}$ and each carbonate sample was subject to at least triplicate analysis in order to reduce temperature uncertainties to values as low as ~ ±1.5°C (1 S.E.). Final temperature values were corrected for empirically-determined acid fractionation factors at 75°C and calculated following the methods of Ghosh et al. (2006) using both intralab (Huron River mussel, Jolters ooids) and interlab (Carrara marble) carbonate standards.

The small size of bivalve shells in Sheep Pass Member B (≤ 5 mm in diameter) prevented high resolution temporal (i.e. seasonal) sampling of individual shells. Thus, only bulk isotopic and temperature values are presented in this study. Depending on the growth habits of these organisms, these bulk values likely integrate over multiple seasons and/or years of carbonate precipitation, similar to the lacustrine carbonates analyzed as part of this work.

**5.6 Isotopic and isotopologue results**

Table 5.1 summarizes isotopic ($\delta^{18}O$, $\delta^{13}C$) and isotopologue ($\Delta_{47}$) analyses for all Goler and Sheep Pass carbonate samples. Detailed isotopic and isotopologue results ($\delta_{47}$, $\delta_{48}$, $\delta_{49}$, $\Delta_{47}$, $\Delta_{48}$, $\Delta_{49}$) are provided in Appendix Table A5.1. $\delta^{18}O$ and $\delta^{13}C$ values are reported relative to the Peedee Belemnite standard (PDB).

Goler Formation micrite (EP0803) is characterized by highly reproducible $\delta^{18}O$ and $\delta^{13}C$ values of -12.3‰ (± 0.1) and -3.2‰ (± 0.2), respectively. Sheep Pass

# FIGURE 5.3

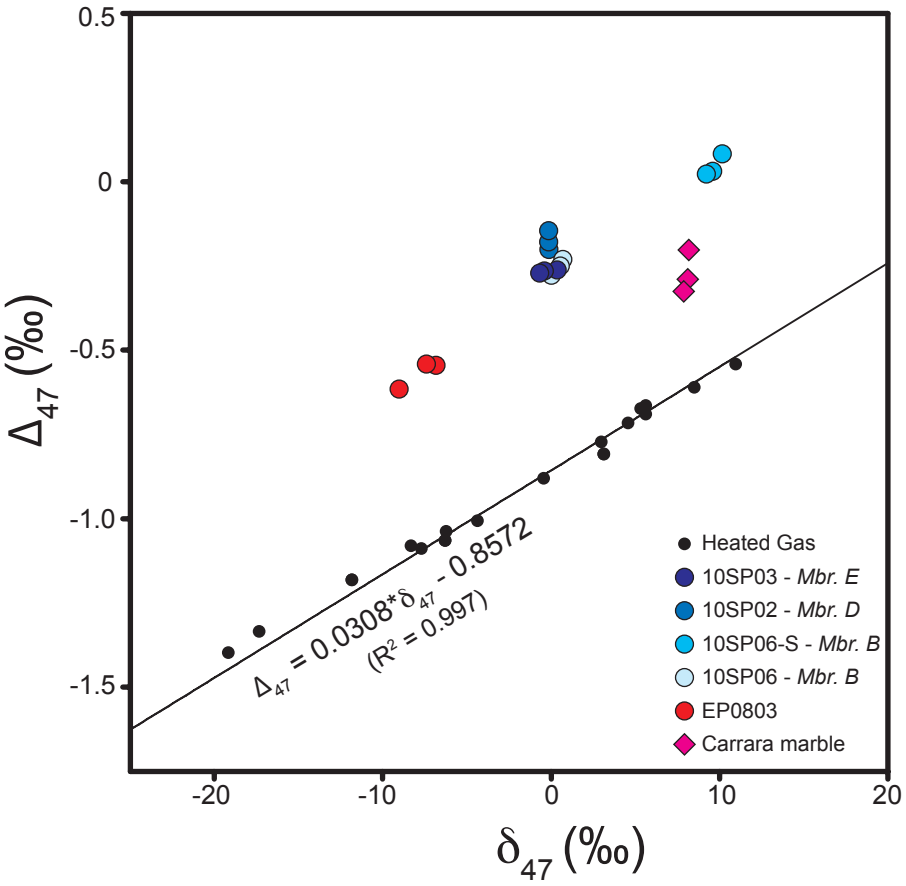


Figure 5.3 – Heated gas line and isotopologue data. $\Delta_{47}$ versus $\delta_{47}$ for Goler and Sheep Pass carbonate samples, the Carrara marble interlab carbonate standard, and heated $CO_2$ gases. See text for discussion of heated gas line. Linear regression of heated gas isotopologue values includes analyses of heated $CO_2$ gases with $\delta_{47}$ values ranging from -54 to +10‰. Temperature values for carbonate samples are determined by normalizing measured $\Delta_{47}$ values using stochastic heated gas compositions at equal $\delta_{47}$ values. See Table 5.1 for detailed analytical results and calculated temperatures.

carbonates exhibit a higher degree of variability in $\delta^{18}O$ and $\delta^{13}C$ values depending on the type of carbonate material (i.e. micrite, bivalve shell) and stratigraphic position (Table 5.1). Despite this variability, Sheep Pass carbonate $\delta^{13}C$ and $\delta^{18}O$ values are characterized by higher $\delta^{18}O$ and $\delta^{13}C$ values than those measured in the Goler Formation, except in cases where easily identifiable diagenetic calcite spar was analyzed (e.g., Sample 10SP03). Carbonate (10SP06) and bivalve shell (10SP06-S) samples from Sheep Pass Member B have high $\delta^{13}C$ values of 4.2‰ and 9.0‰, respectively, and distinct average $\delta^{18}O$ compositions of -11.4‰ for the carbonate matrix and -5.9‰ for bivalve shells. The Member D carbonate sample (10SP02) has an average $\delta^{13}C$ value of 0.5‰ and an average $\delta^{18}O$ value of -4.2‰. Isotopic values for our Member E sample (10SP03) are -0.3‰ ($\delta^{13}C$) and -6.9‰ ($\delta^{18}O$).

The results of clumped isotope analyses, including both individual analyses and sample averaged $\Delta_{47}$ values, are listed in Table 5.1. In addition to investigating mass-47 compositions, plots of $\Delta_{48}$ versus $\delta_{48}$ were analyzed for all carbonate samples to identify contaminated analyte $CO_2$ gases (following the method of Huntington et al., 2009). Only analyses that exhibited $\Delta_{48}$-$\delta_{48}$ relationships in agreement with heated gas values were accepted for subsequent temperature calculations and inclusion in Table 5.1. All reported uncertainties are ± one standard error (S.E.) since final sample temperature magnitudes are averages of individual $\Delta_{47}$ values which are themselves derived from multiple measurement cycle averages. The average carbonate clumped isotope temperature for Goler Formation micrite (39.9 ± 1.9°C) is consistently higher than those observed throughout the Sheep Pass Formation. The average clumped isotope temperature for Sheep Pass Formation Member B (24.9 ± 1.5°C) is statistically indistinguishable from

temperatures derived from the bivalve shells collected from the same stratigraphic level (22.1 ± 2.2°C). Member D carbonate exhibits a warmer average temperature (29.5°C) and is also characterized by a higher degree of scatter in individual temperature analyses (S.E. = 3.9°C). Member E carbonate has an average carbonate clumped isotope temperature (24.0 ± 1.7°C) indistinguishable from Member B carbonates.

### 5.7 Assessment of diagenetic influence

Petrographic analysis of carbonate samples suggests all analyzed samples are primary in origin and not significantly recrystallized or altered by diagenetic processes. Most analyzed carbonates preserve a cryptocrystalline, micritic texture with minimal evidence for major recrystallization or calcite spar formation. This is particularly true for micrite samples collected from the Goler Formation and Sheep Pass Members D and E. Sheep Pass Member B carbonate exhibits a higher degree of crystallinity, similar to that observed in bivalve shell material at the same stratigraphic interval, but we suggest this crystallinity does not significantly alter our isotopic or clumped isotope temperature results as primary stable isotopic values and carbonate temperatures appear to be preserved. Member B bivalve shells exhibit distinct isotopic compositions from those of the corresponding carbonate matrix (Table 5.1). If major resetting had influenced Member B carbonates we expect all affected material will exhibit similar, reset isotopic values. The preservation of distinct isotopic compositions supports interpretations that the primary isotopic signature is preserved in Member B carbonates and bivalve shells.

Member B carbonate clumped isotope temperatures are also inconsistent with diagenetic resetting during burial, as calculated formation temperatures are consistent

**Table 5.1** – Summary of clumped isotope thermometry and stable isotopic results

| Sample | $\Delta_{47}$ (‰) | Corrected $\Delta_{47}$† (‰) | Summary $\delta^{13}C_{PDB}$ (‰) | Summary $\delta^{18}O_{PDB}$ (‰) | Summary Avg. Corrected $\Delta_{47}$ (‰) ± 1 S.E. | Summary Temperature (°C) ± 1 S.E. |
|---|---|---|---|---|---|---|
| ***Paleocene Goler Formation*** | | | | | | |
| **EP0803** | 0.5226 | 0.5885 | -3.2 ± 0.2 | -12.3 ± 0.1 | 0.5948 ± 0.008 | 39.9 ± 1.9 |
| *35.4640°N* | 0.5198 | 0.5858 | | | | |
| *117.8539°W* | 0.5442 | 0.6102 | | | | |
| ***Late Cretaceous-Eocene Sheep Pass Formation*** | | | | | | |
| **10SP06** ***(Mbr. B)*** | 0.6052 | 0.6712 | 4.2 ± 0.4 | -11.4 ± 0.8 | 0.6585 ± 0.007 | 24.9 ± 1.5 |
| *38.7376°N* | 0.5819 | 0.6479 | | | | |
| *114.9570°W* | 0.5905 | 0.6565 | | | | |
| **10SP06-S** ***(Mbr. B)*** | 0.5927 | 0.6587 | 9.0 ± 1.2 | -5.9 ± 0.5 | 0.6713 ± 0.011 | 22.1 ± 2.2 |
| *38.7376°N* | 0.6265 | 0.6925 | | | | |
| *114.9570°W* | 0.5969 | 0.6628 | | | | |
| **10SP02** ***(Mbr. D)*** | 0.5345 | 0.6005 | 0.5 ± 0.4 | -4.2 ± 0.9 | 0.6388 ± 0.017 | 29.5 ± 3.9 |
| *38.7335°N* | 0.6048 | 0.6708 | | | | |
| *114.9438°W* | 0.5543 | 0.6203 | | | | |
| | 0.5975 | 0.6635 | | | | |
| **10SP03** ***(Mbr. E)*** | 0.5815 | 0.6475 | -0.3 ± 0.6 | -6.9 ± 0.7 | 0.6626 ± 0.008 | 24.0 ± 2.9 |
| *38.7339°N* | 0.6023 | 0.6683 | | | | |
| *114.9409°W* | 0.6061 | 0.6721 | | | | |
| *Spar* | ---- | ---- | -2.8 ± 0.1 | -16.4 ± 0.1 | | |

**Table 5.1 Notes***:* Isotopic and isotopologue data for analyzed carbonates from the Goler and Sheep Pass Formations. Samples that exhibited evidence for significant contamination of analyte $CO_2$, based on measured $\Delta_{48}$ and $\delta_{48}$ ratios, were omitted from this analysis. Reported $\delta^{13}C$ and $\delta^{18}O$ values are averages of analyses performed in October 2010. Clumped isotope analyses were conducted in January 2011. † - $\Delta_{47}$ values were corrected for empirically derived acid fractionation factors for anhydrous phosphoric acid reaction at 75°C (Hren et al., *in prep*.) prior to calculation of clumped isotope temperatures. Geographic coordinates for sample site locations provided below sample ID. Corresponding Sheep Pass Member noted in parentheses.

with near surface conditions and are very similar to those derived from Member E which exhibits minimal petrographic evidence for diagenetic recrystallization. A final piece of evidence for preservation of primary signatures in Sheep Pass carbonates is the low $\delta^{18}O$ value observed for easily identifiable calcite spar in sample 10SP03 collected from Member E (Table 5.1). This crystalline calcite spar is indicative of late-stage diagenetic alteration which is consistent with measured low $\delta^{18}O$ values that likely reflect later-stage equilibration with isotopically depleted meteoric waters. This degree of crystallinity and isotopic depletion is not observed in any other Sheep Pass sample analyzed in this study.

Carbonate formation temperatures in the Goler Formation (~ 40°C) are significantly warmer than modern surface temperatures, particularly for mid-latitude regions. As a result, caution must be taken to ensure that we are reliably recording temperatures of carbonate formation and not resetting during burial diagenesis. In addition to petrographic analysis suggesting analyzed carbonate is primary, the paleogeographic and paleoclimatic setting of the Goler basin is also consistent with the proposed interpretation that the measured temperatures accurately reflect near surface conditions during Paleocene carbonate formation. Abundant evidence indicates that the Goler basin resided at or near sea level throughout the Paleocene (e.g., Lofgren et al., 2008), but throughout much of its existence it appears to have been cutoff from direct marine influences based on the lack of contemporaneous marine deposits elsewhere in the surrounding region. As a low elevation, inland continental site, the Goler basin would have been subject to greater seasonal temperature extremes than coastal sites where temperature is moderated by direct marine influence. Modern mean monthly air temperatures can reach 33–35°C at inland sites in southern California (e.g., Blythe, CA;

Huntington et al., 2010). Similarly, surface water temperatures in excess of 30°C are commonly observed in the Salton Sea during summer months (Huntington et al., 2010). Marine isotope (e.g., Zachos et al., 1994) and paleobotanical (Wolfe, 1994) records indicate that coastal regions of western North America were ≥ 7°C (and possibly up to 12°C) warmer than the modern during the early Paleogene. These proposals of warm early Cenozoic climates are consistent with independent evidence from fossil assemblages (Lofgren et al., 2008) and geochemical analysis of paleosols (Torres, 2010) in the Goler Formation that suggests a tropical climate characterized the Paleocene Goler basin. Taken together, modern trends in air and surface water temperatures in combination with proposed temperature changes since Paleocene time indicate that surface water temperatures of ~ 40°C for the shallow, ephemeral floodplain lake in which Goler micrite precipitated are quite plausible, especially considering the tendency for lacustrine calcite to precipitate during spring/summer months when air and lake water temperatures are at a maximum (e.g., Leng and Marshall, 2004; Huntington et al., 2010).

### 5.8 Discussion of clumped isotope results

Carbonate clumped isotopic study of Paleocene-Eocene carbonates from multiple sites in the western US Cordillera indicate that carbonate formation temperatures in the continental interior Sevier-Laramide orogen are significantly lower than temperatures from contemporaneous proxies formed in near sea level basins in the vicinity of the paleo-Pacific coast. Average carbonate formation temperatures in Sheep Pass Members B and E are consistently in the range of 22–25°C, whereas analyzed carbonate from Member D has a significantly higher average temperature of 29.5°C (Table 5.1).

Cenozoic carbonate material is limited to a single stratigraphic interval in the Goler Formation (middle Paleocene Member 4a), so a similar time-temperature history is not possible for the Goler basin. Thus, it is important to identify the causes for the observed temperature fluctuation in Sheep Pass Member D and whether this temperature shift reflects changes in elevation or simply changes in regional/global climate through time.

Sheep Pass Formation Member D deposition is constrained to the early-middle Eocene based on molluscan fossil assemblages in the overlying and underlying conformable members (Good, 1987). This time of deposition coincides with the well documented Early Eocene Climatic Optimum when deep marine $\delta^{18}O$ values (VPDB) decreased by > 1‰, reflecting a period of significant climate warming (~ 5–7°C; Zachos et al., 2001). Direct comparison of the time-temperature history of Sheep Pass carbonates with the Cenozoic marine $\delta^{18}O$ record reveals a high degree of correlation between measured temperatures and marine isotopic trends (Figure 5.4), suggesting that the increase in temperature observed in Member D simply reflects the influence of continental climate change during the Early Eocene. The observed ~ 5°C increase in Sheep Pass carbonate temperatures between Members B and D is consistent with estimates of temperature change during this time (Zachos et al., 2001), but interpretation of the magnitude of the temperature change observed in the Sheep Pass carbonate record must be made with caution as Member D samples exhibit a high degree of variability in measured $\Delta_{47}$ values and associated calculated temperatures (Table 5.1).

If the influence of continental climate change is accounted for in our clumped isotope temperature record, we observe a 15–17°C shift between Goler Formation micrites and contemporaneous Sheep Pass carbonates. The observed difference in

# FIGURE 5.4

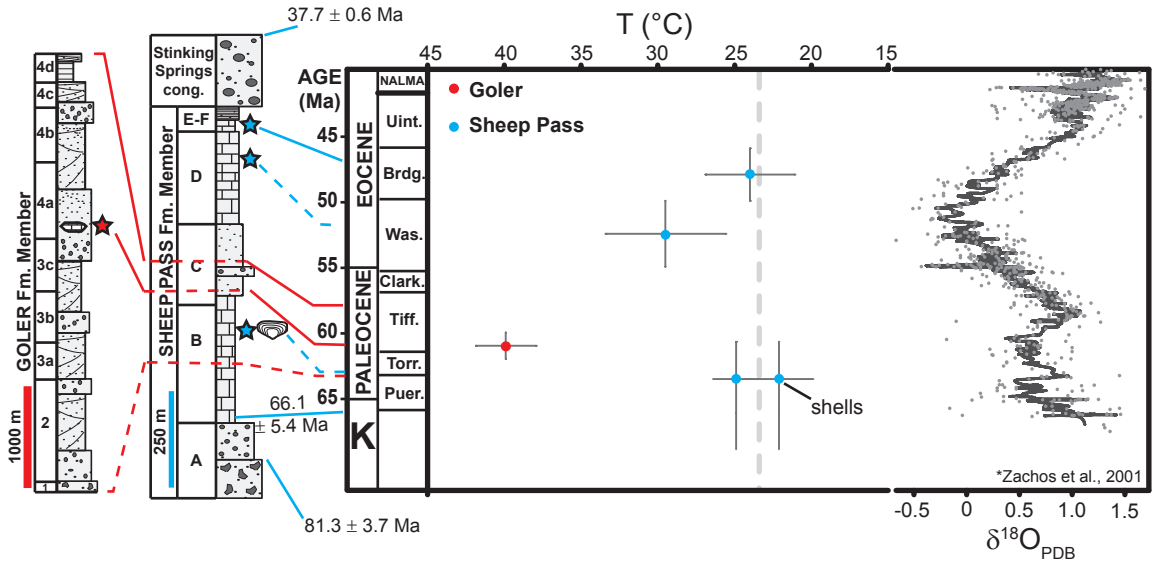


Figure 5.4 – Carbonate clumped isotope temperature record. Age-temperature plot for Goler and Sheep Pass carbonate samples. Dashed gray line marks average carbonate clumped isotope temperature for Sheep Pass Formation Members B and E (~ 23.5ºC). Zachos et al. (2001) marine $\delta^{18}O$ record is shown for reference. Simplified stratigraphic columns (Goler Fm. - Cox, 1982; Sheep Pass - Fouch, 1979; Druschke et al., 2009b) are included to provide stratigraphic correlation of the Goler (red lines) and Sheep Pass (blue lines) Formations. Dashed lines indicate approximate correlations. Stars mark approximate stratigraphic position of analyzed carbonate samples. Sampled molluscs from Sheep Pass Member B also shown. North American Land Mammal Age (NALMA) assignments and age uncertainties are based on Sheep Pass molluscan biostratigraphy (Good, 1987) and radiometric dating (Druschke et al., 2009b) and Goler Formation biostratigraphy (e.g. Lofgren et al., 2008) and magnetostratigraphy (Albright et al., 2009). NALMA abbreviations: Puer. = Puercan, Torr. = Torrejonian, Tiff. = Tiffanian, Clark. = Clarkforkian, Was. = Wasatchian, Brdg. = Bridgerian, Uint. = Uintan.

carbonate formation temperatures implies significant differences in elevation between the two sites. In order to calculate the absolute elevation difference the regional lake water temperature-elevation relationship during the early Cenozoic must be known or assumed. Modern mean annual temperature (MAT) lapse rates in the western US vary between 6.8 and 8.1°C/km (Meyer, 1992). Regional modern lake surface water temperature (LST) as well as modern and middle to late Miocene lake water carbonate temperature (LCT) lapse rates are lower in magnitude (LST = -5.6°C/km; LCT = -4.2°C/km) and more closely approximate the moist adiabat for the atmosphere (Huntington et al., 2010). Since our sampled lacustrine systems are analogous to the study sites of Huntington et al. (2010), we expect a temperature lapse rate of -4 to -6°C/km characterized Paleocene-Eocene lacustrine systems of the western US.

*5.8.1 Paleoelevation of the Paleocene-Eocene 'Nevadaplano'*

To isolate the elevation signal in our carbonate temperature records, we must first account for environmental variables, such as latitude, that influence lake water temperatures independent of elevation. During the early Paleogene, the Sheep Pass basin was located ~3°N of the Goler basin (Figure 5.1, Table 5.1). Using the modern latitudinal temperature gradient for mid-latitude western North America (-0.33°C/°N; Gregory and Chase, 1992) this latitudinal difference equates to a temperature difference of ~1°C, which is likely an upper limit as latitudinal-temperature gradients are expected to have been reduced during the Paleogene (e.g., Zachos et al., 1994). Thus, the influence of latitude effects on the observed temperature difference appears to be quite minor, suggesting that elevation acts as a primary control on the measured carbonate formation temperatures. Accounting for latitudinal effects, the temperature difference between

Goler micrite (39.9 ± 1.9°C) and the average clumped isotope temperature for Sheep Pass carbonate and bivalve shells from the approximately contemporaneous Member B (23.5 ± 2.0°C) is 15.4 ± 2.7°C. Applying temperature lapse rates of -4 and -6°C/km, this equates to elevation differences of 3.9 ± 0.7 km and 2.6 ± 0.5 km, respectively.

For these calculations, we assume that Goler and Sheep Pass carbonates precipitated and/or grew during the same time of the year. If timing of carbonate precipitation was highly variable among Goler and Sheep Pass carbonate samples, some of the observed temperature difference could be the result of seasonal fluctuations in lake temperature. For example, if Goler micrite precipitation was restricted to only summer months whereas Sheep Pass carbonates formed throughout the year, Goler temperatures would be biased toward higher values and elevation differences would be overestimated, and vice versa. Even with this uncertainty, the plausible shift in temperatures due to seasonal bias is not sufficient to account for the high magnitude temperature difference (15–17°C) observed between Goler and Sheep Pass carbonates in its entirety. Thus, this significant temperature difference is likely to reflect differences in basin elevations. Furthermore, we are confident in the assumption that measured Goler and Sheep Pass carbonates are equivalent temperature proxies due to abundant evidence suggesting lacustrine carbonate precipitation is promoted during, or even restricted to, summer months (e.g., Leng and Marshall, 2004; Huntington et al., 2010) when water temperatures and $CO_2$ outgassing rate are at a maximum. Accordingly, we expect that the calculated elevation differences reliably reflect topographic distributions during the time of carbonate proxy formation.

With a known sea level elevation datum for the Goler basin, calculated elevation differences of 2.6 – 3.9 km indicate the Sheep Pass basin was located at high elevations during Paleocene carbonate deposition of Member B. The similarity of carbonate growth temperatures and marine $\delta^{18}O$ values during the early Paleocene (Member B) and earliest middle Eocene (Member E; Figure 5.4) further suggests these high regional elevations were maintained at least into the middle Eocene, suggesting a sustained period of tectonic quiescence in the 'Nevadaplano' during the early Paleogene.

Calculated elevation difference is sensitive to the choice of temperature lapse rate due the linearity of the temperature-elevation gradient, but application of either end-member lapse rate (-4 or -6°C/km) suggests the Sheep Pass basin was part of a high elevation (≥ 2.6 km) orogenic plateau ('Nevadaplano') system in the Paleocene-Eocene western US Cordilleran interior. As a result, this study provides direct estimates for early Cenozoic paleoelevations of the Sevier orogenic plateau ('Nevadaplano') and confirms proposed models for high regional elevations in the western US Cordillera prior to widespread Tertiary extension (e.g., Dilek and Moores, 1999; Sonder and Jones, 1999; DeCelles, 2004; Ernst, 2010). High elevations in the Sheep Pass basin predate the commencement of regional volcanism and tectonism in the Sheep Pass region during the late Eocene-early Oligocene (e.g., Armstrong and Ward, 1991; Best and Christiansen, 1991; Axen et al., 1993; Mueller and Snoke, 1993; Best et al., 2009). If regional uplift of ~ 2 km occurred concurrently with the southward sweep of magmatism that progressed through the US Cordillera during the Paleogene as has been proposed (Horton et al., 2004), regional mean elevations ≥ 5 km were attained immediately prior to Basin and Range extension. Such elevation magnitudes are at the upper limits of elevation estimates

based on crustal shortening amounts and proposed crustal thicknesses (e.g., DeCelles, 2004; Ernst, 2010). Thus, we think it is unlikely that the southward sweep in magmatism was associated with significant changes in surface uplift, at least in the Sheep Pass region of the Cordillera.

*5.8.2 Calculation of water $\delta^{18}O$ values*

Independent measure of carbonate growth temperatures provides the capability to directly calculate water $\delta^{18}O$ values which also have potential applications for paleoelevation determinations (e.g., Chamberlain and Poage, 2000; Rowley and Garzione, 2007). Water $\delta^{18}O$ values (VSMOW) were calculated using the fractionation equations of Kim and O'Neil (1997) along with corresponding carbonate $\delta^{18}O$ and temperature values. A plot of water $\delta^{18}O$ as a function of age is shown in Figure 5.5. Water $\delta^{18}O$ generally mirrors the pattern of carbonate $\delta^{18}O$ (Table 5.1) with Sheep Pass carbonates consistently having higher $\delta^{18}O$ values than the Goler micrite. Rayleigh distillation principles predict precipitation at high elevation sites, such as the early Paleogene 'Nevadaplano', will be characterized by low $\delta^{18}O$ values as a result of increased rainout, and associated preferential removal of heavy isotopes (D, $^{18}O$) from the contributing airmass (Rowley et al., 2001; Chapters 2 and 3 of this thesis). The observed high $\delta^{18}O$ values in the Sheep Pass formation are inconsistent with these Rayleigh distillation trends. We interpret this inconsistency as evidence for significant evaporative enrichment of Sheep Pass basin waters. Independent sedimentologic and fossil evidence for hypersaline conditions in Member D of the Sheep Pass Formation (e.g., Good, 1987) is consistent with the high water $\delta^{18}O$ values -1.0‰, VSMOW) observed in this stratigraphic interval. Bivalve shells in Member B and lacustrine micrite in Member E

# FIGURE 5.5

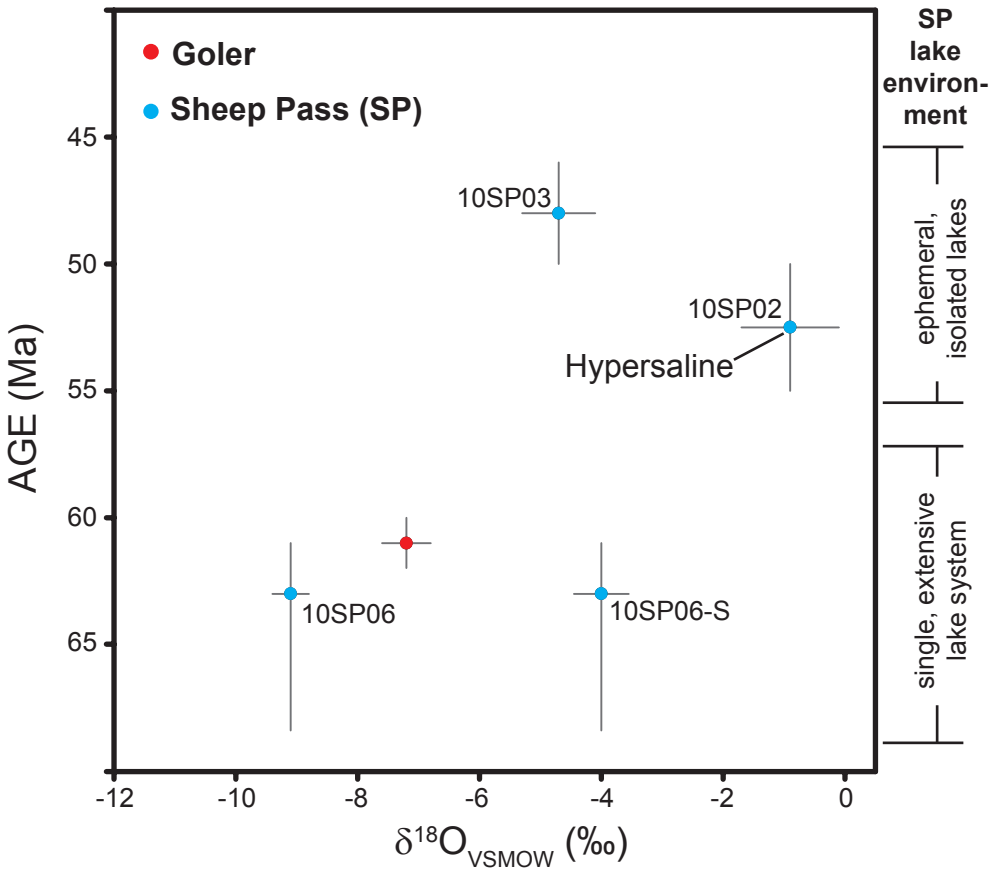


Figure 5.5 – Calculated water $\delta^{18}O$ values for Goler and Sheep Pass carbonates. Age assignments described in Figure 5.4 caption. Sheep Pass water $\delta^{18}O$ values are labeled by sample ID (Table 5.1) for clarification. Evolution of Sheep Pass (SP) lacustrine environments ('SP lake environment') during the early Cenozoic is constrained by molluscan biostratigraphy (Good, 1987); Sheep Pass Member D hypersaline lake conditions are noted.

exhibit similar high $\delta^{18}O$ values (-4.0 and -4.7‰, VSMOW). The very high $\delta^{13}C$ values (~ 9‰, VPDB) of Member B bivalve shells are also consistent with formation from evaporative lake waters as $\delta^{18}O$ and $\delta^{13}C$ are known to covary in closed basin, evaporative lake systems (Talbot, 1990). High shell $\delta^{13}C$ values may also indicate that bivalve growth periods were restricted to times of high photosynthetic activity and rapid lake vegetation production, and associated $^{12}C$ removal from surface waters, which is likely to dominate lacustrine systems during summer months when evaporative water loss is at a maximum.

The utility of clumped isotope paleothermometry for paleoaltimetry studies is clearly evident in light of calculated water $\delta^{18}O$ values. Without independent estimates of temperature, it would be difficult to discern the degree of evaporative influence on measured $\delta^{18}O$ values. A simple interpretation of the stable isotopic results would suggest that the high $\delta^{18}O$ values for Sheep Pass carbonates reflect formation in a low elevation basin system deriving precipitation from a nearby, marine source. Inclusion of carbonate clumped isotope temperatures, however, provides definitive evidence that the Sheep Pass basin was located at high elevations during the early Paleogene, indicating that the observed stable isotopic trends are heavily influenced by lake water evaporation.

## 5.9 Conclusions

Clumped isotope paleothermometry studies of lacustrine carbonates from the Goler Formation of southeastern California and the Sheep Pass Formation of east-central Nevada provides direct and robust evidence for a Late Cretaceous-Eocene high elevation (2.6 – 3.9 km) orogenic plateau in the western US Cordilleran interior. This high

elevation ‘Nevadaplano’ formed in response to crustal shortening and associated crustal thickening during the Sevier and Laramide orogenies of western North America and likely acted, in conjunction with changes in plate boundary forces and basal normal stresses, to drive the mid-Tertiary Basin and Range extension that collapsed the plateau to its modern mean elevations of ~ 1.5 km. Questions on the southward extent of this orogenic plateau still remain (e.g., Lechler and Niemi, 2011; Chapter 4 of this thesis), but the results of this study are consistent with proposals of an externally-drained plateau system characterized by trans-Sierran fluvial systems that connected the ‘Nevadaplano’ to the paleo-Pacific coast during the Oligocene (Cassel et al., 2009; Henry and Faulds, 2010). Combined clumped isotope paleothermometry and stable isotopic analysis of carbonate proxies also highlights the importance of constraining evaporative influence on paleo-meteoric proxies for paleoelevation studies as proxy records derived from ephemeral and/or closed lacustrine systems are prone to producing significant paleoelevation underestimates.

## 5.10 Acknowledgements

This work was supported by a University of Michigan Turner Grant to ARL. We thank Lora Wingate for her assistance with isotopic analyses. Will Defliese contributed to clumped isotope analyses and provided beneficial discussion on the clumped isotope technique.

## 5.11 References cited


Albright, L. B., Lofgren, D.L., and McKenna, M.C., 2009, Magnetostratigraphy, mammalian biostratigraphy, and refined age assessment of the Goler Formation (Paleocene), California, *in* L. B. Albright, *ed.*, Papers on Geology, Vertebrate Paleontology, and Biostratigraphy in Honor of Michael O. Woodburne, 65, p. 259-278.

Armstrong, R. L. and Ward, P., 1991, Evolving geographic patterns of Cenozoic magmatism in the North American Cordillera - the temporal and spatial association of magmatism and metamorphic core complexes: Journal of Geophysical Research-Solid Earth and Planets, v. 96, B8, 13201-13224.

Axen, G. J., Taylor, W. J., and Bartley, J. M., 1993, Space-time patterns and tectonic controls of Tertiary extension and magmatism in the Great Basin of the western United States: Geological Society of America Bulletin, v. 105, no. 1, p. 56-76.

Best, M. G., Barr, D. L., Christiansen, E. H., Gromme, S., Deino, A. L., and Tingey, D. G., 2009, The Great Basin Altiplano during the middle Cenozoic ignimbrite flareup: insights from volcanic rocks: International Geology Review, v. 51, no. 7-8, p. 589-633.

Best, M. G., and Christiansen, E. H., 1991, Limited extension during peak Tertiary volcanism, Great Basin of Nevada and Utah: Journal of Geophysical Research-Solid Earth and Planets, v. 96, no. B8, p. 13509-13528.

Carroll, A. R., Doebbert, A. C., Booth, A. L., Chamberlain, C. P., Rhodes-Carson, M. K., Smith, M. E., Johnson, C. M. and Beard, B. L., 2008, Capture of high-altitude precipitation by a low-altitude Eocene lake, Western US: Geology, v. 36, no. 10, p. 791-794.

Cassel, E. J., Calvert, A. T. and Graham, S. A., 2009, Age, geochemical composition, and distribution of Oligocene ignimbrites in the northern Sierra Nevada, California: implications for landscape morphology, elevation, and drainage divide geography of the Nevadaplano: International Geology Review, v. 51, no. 7-8, p. 723-742.

Chamberlain, C. P. and Poage, M. A., 2000, Reconstructing the paleotopography of mountain belts from the isotopic composition of authigenic minerals: Geology, v. 28, no. 2, p. 115-118.

Clark, M. K., 2007, The significance of paleotopography: Reviews in Mineralogy and Geochemistry, v. 66, no. 1, p. 1-21.

Coney, P. J. and Harms, T. A., 1984, Cordilleran metamorphic core complexes - Cenozoic extensional relics of Mesozoic compression: Geology, v. 12, no. 9, p. 550-554.

Cox, B. F., 1982, Stratigraphy, sedimentology, and structure of the Goler Formation (Paleocene), El Paso Mountains, California: implications for Paleogene tectonism on the Garlock Fault Zone: [Ph.D. Thesis]: Riverside, University of California, 248 p.

Davis, S. J., Mix, H. T., Wiegand, B. A., Carroll, A. R. and Chamberlain, C. P., 2009, Synorogenic evolution of large-scale drainage patterns: isotope paleohydrology of sequential Laramide basins: American Journal of Science, v. 309, no. 7, p. 549-602.

Davis, S. J., Wiegand, B. A., Carroll, A. R. and Chamberlain, C. P., 2008, The effect of drainage reorganization on paleoaltimetry studies: An example from the Paleogene Laramide foreland: Earth and Planetary Science Letters, v. 275, no. 3-4, p. 258-268.

DeCelles, P. G., 2004, Late Jurassic to Eocene evolution of the Cordilleran thrust belt and foreland basin system, western USA: American Journal of Science, v. 304, no. 2, p. 105-168.

Dettman, D. L. and Lohmann, K. C., 1995, Microsampling carbonates for stable isotope and minor element analysis - physical separation of samples on a 20 micrometer scale: Journal of Sedimentary Research Section a-Sedimentary Petrology and Processes, v. 65, no. 3, p. 566-569.

Dilek, Y., and Moores, E. M., 1999, A Tibetan model for the early Tertiary western United States: Journal of the Geological Society, v. 156, p. 929-941.

Druschke, P., Hanson, A. D., Wells, M. L., Rasbury, T., Stockli, D. F. and Gehrels, G., 2009a, Synconvergent surface-breaking normal faults of Late Cretaceous age within the Sevier hinterland, east-central Nevada: Geology, v. 37, no. 5, p. 447-450.

Druschke, P., Hanson, A. D. and Wells, M. L., 2009b, Structural, stratigraphic, and geochronologic evidence for extension predating Palaeogene volcanism in the Sevier hinterland, east-central Nevada: International Geology Review, v. 51, no. 7-8, p. 743-775.

Eiler, J. M. and Schauble, E., 2004, $^{18}O^{13}C^{16}O$ in Earth's atmosphere: Geochemica et Cosmochemica Acta, v. 68, no. 23, p. 4767-4777.

Ernst, W. G., 2010, Young convergent-margin orogens, climate, and crustal thickness - A Late Cretaceous-Paleogene Nevadaplano in the American Southwest?: Lithosphere, v. 2, no. 2, p. 67-75.

Flesch, L. M., Holt, W. E., Haines, A. J., Wen, L. X. and Shen-Tu, B., 2007, The dynamics of western North America: stress magnitudes and the relative role of gravitational potential energy, plate interaction at the boundary and basal tractions: Geophysical Journal International, v. 169, no. 3, p. 866-896.

Fouch, T. D., 1979, Character and paleogeographic distribution of Upper Cretaceous(?) and Paleogene nonmarine sedimentary rocks in east-central Nevada, *in* J. M. Armentrout, Cole, M.R., and Terbest, H., *eds.*, Cenozoic paleogeography of the western United States: Pacific Coast Paleogeographic Symposium 3: Pacific Section, SEPM, p. 97-111.

Friedman, I., Smith, G.I., Johnson, C.A., Moscati, R.J., 2002, Stable isotope compositions of waters in the Great Basin, United States 2. Modern precipitation: Journal of Geophysical Research, 107 ACL 15-11 - ACL 15-21.

Gans, P. B., 1987, An open-system, 2-layer crustal stretching model for the eastern Great Basin: Tectonics, v. 6, no. 1, p. 1-12.

Ghosh, P., Adkins, J., Affek, H., Balta, B., Guo, W. F., Schauble, E. A., Schrag, D. and Eller, J. M., 2006, $^{13}C$-$^{18}O$ bonds in carbonate minerals: A new kind of paleothermometer: Geochimica Et Cosmochimica Acta, v. 70, no. 6, p. 1439-1456.

Good, S. C., 1987, Mollusc-based interpretations of lacustrine paleoenvironments of the Sheep Pass Formation (Latest Cretaceous to Eocene) of east central Nevada: Palaios, v. 2, no. 5, p. 476-478.

Gregory, K. M. and Chase, C. G., 1992, Tectonic significance of paleobotanically estimated climate and altitude of the Late Eocene erosion surface, Colorado: Geology, v. 20, no. 7, p. 581-585.

Gregory-Wodzicki, K. M., 1997, The Late Eocene House Range flora, Sevier Desert, Utah: paleoclimate and paleoelevation: Palaios, v. 12, no. 6, p. 552-567.

Henry, C. D., Faulds, J. E., 2010, Ash-flow tuffs in the Nine Hill, Nevada, paleovalley and implications for tectonism and volcanism of the western Great Basin, USA: Geosphere, v. 6, p. 339-369.

Hodges, K. V. and Walker, J. D., 1992, Extension in the Cretaceous Sevier Orogen, North American Cordillera: Geological Society of America Bulletin, v. 104, no. 5, p. 560-569.

Horton, T. W. and Chamberlain, C. P., 2006, Stable isotopic evidence for Neogene surface downdrop in the central Basin and Range Province: Geological Society of America Bulletin, v. 118, no. 3-4, p. 475-490.

Horton, T. W., Sjostrom, D. J., Abruzzese, M. J., Poage, M. A., Waldbauer, J. R., Hren, M. T., Wooden, J. L. and Chamberlain, C. P., 2004, Spatial and temporal variation of Cenozoic surface elevation in the Great Basin and Sierra Nevada: American Journal of Science, v. 304, no. 10, p. 862-888.

Hren, M. T., Bookhagen, B., Blisniuk, P. M., Booth, A. L., and Chamberlain, C. P., 2009, $\delta^{18}O$ and $\delta D$ of streamwaters across the Himalaya and Tibetan Plateau: Implications for moisture sources and paleoelevation reconstructions: Earth and Planetary Science Letters, v. 288, no. 1-2, p. 20-32.

Hren, M. T., Sheldon, N.D., Grimes, S.T., Collinson, M.E., Hooker, J.J., Bugler, M., and Lohmann, K., Coupled $CO_2$ and temperature declines across the Eocene-Oligocene transition, *in prep*.

Huntington, K. W., Eiler, J. M., Affek, H. P., Guo, W., Bonifacie, M., Yeung, L. Y., Thiagarajan, N., Passey, B., Tripati, A., Daeron, M. and Came, R., 2009, Methods and limitations of 'clumped' $CO_2$ isotope ($\Delta_{47}$) analysis by gas-source isotope ratio mass spectrometry: Journal of Mass Spectrometry, v. 44, no. 9, p.1318-1329.

Huntington, K. W., Wernicke, B. P. and Eiler, J. M., 2010, Influence of climate change and uplift on Colorado Plateau paleotemperatures from carbonate clumped isotope thermometry: Tectonics, v. 29.

Ingraham, N. L. and Taylor, B. E., 1991, Light stable isotope systematics of large-scale hydrologic regimes in California and Nevada: Water Resources Research, v. 27, no. 1, p. 77-90.

Jones, C. H., Sonder, L. J. and Unruh, J. R., 1998, Lithospheric gravitational potential energy and past orogenesis: Implications for conditions of initial basin and range and Laramide deformation: Geology, v. 26, no. 7, p. 639-642.

Jones, C. H., Unruh, J. R. and Sonder, L. J., 1996, The role of gravitational potential energy in active deformation in the southwestern United States: Nature, v. 381, no. 6577, p. 37-41.

Kim, S. T. and O'Neil, J. R., 1997, Equilibrium and nonequilibrium oxygen isotope effects in synthetic carbonates: Geochimica Et Cosmochimica Acta, v. 61, no. 16, p. 3461-3475.

Lechler, A. R., and Niemi, N.A., 2011, Sedimentologic and isotopic constraints on the Paleogene paleogeography and paleotopography of the southern Sierra Nevada, California: Geology, v. 39, no. 4, p. 379-382.

Leng, M. J. and Marshall, J. D., 2004, Palaeoclimate interpretation of stable isotope data from lake sediment archives: Quaternary Science Reviews, v. 23, no. 7-8, p. 811-831.

Lofgren, D. L., Honey, J.G., McKenna, M.C., Zondervan, R.L., Smith, E.E., 2008, Paleocene primates from the Goler Formation of the Mojave Desert in California, *in* X. Wang, and Barnes, L.G., *eds.*, Geology and Vertebrate Paleontology of Western and Southern North America, Contributions in Honor of David P. Whistler:Science Series 41, p. 11-28.

McQuarrie, N. and Chase, C. G., 2000, Raising the Colorado Plateau: Geology, v. 28, no. 1, p. 91-94.

McQuarrie, N. and Wernicke, B. P., 2005, An animated tectonic reconstruction of southwestern North America since 36 Ma: Geosphere, v. 1, no. 3, p. 147-172.

Meyer, H. W., 1992, Lapse rates and other variables applied to estimating paleoaltitudes from fossil floras: Palaeogeography Palaeoclimatology Palaeoecology, v. 99, no. 1-2, p. 71-99.

Mueller, K. J., and Snoke, A. W., 1993, Progressive overprinting of normal fault systems and their role in Tertiary exhumation of the East Humboldt-Wood Hills metamorphic complex northeast Nevada: Tectonics, v. 12, no. 2, p. 361-371.

Peppe, D. J., Royer, D. L., Wilf, P., and Kowalski, E. A., 2010, Quantification of large uncertainties in fossil leaf paleoaltimetry: Tectonics, v. 29.

Quade, J., Garzione, C. N. and Eiler, J., 2007, Paleoelevation reconstruction using pedogenic carbonates: Reviews in Mineralogy and Geochemistry, v. 66, no. 1, p. 53-87.

Rowley, D. B. and Garzione, C. N., 2007, Stable isotope-based paleoaltimetry: Annual Review of Earth and Planetary Sciences, v. 35, p. 463-508.

Rowley, D. B., Pierrehumbert, R. T. and Currie, B. S., 2001, A new approach to stable isotope-based paleoaltimetry: implications for paleoaltimetry and paleohypsometry of the High Himalaya since the Late Miocene: Earth and Planetary Science Letters, v. 188, no. 1-2, p. 253-268.

Sonder, L. J. and Jones, C. H., 1999, Western United States extension: How the West was widened: Annual Review of Earth and Planetary Sciences, v. 27, p. 417-462.

Spicer, R. A., and Yang, J. A., 2010, Quantification of uncertainties in fossil leaf paleoaltimetry: Does leaf size matter?: Tectonics, v. 29.

Talbot, M. R., 1990, A review of the paleohydrological interpretation of carbon and oxygen isotopic ratios in primary lacustrine carbonates: Chemical Geology, v. 80 no. 4, p. 261-279.

Tian, L. D., Yao, T. D., MacClune, K., White, J. W. C., Schilla, A., Vaughn, B., Vachon, R. and Ichiyanagi, K., 2007, Stable isotopic variations in west China: A consideration of moisture sources: Journal of Geophysical Research-Atmospheres, v. 112, D10112.

Torres, M., 2010, Paleoclimatic and Paleoenvironmental Interpretations of the Paleocene Goler Formation of Southern California, [B.S. thesis]: Claremont, California, Pitzer College, 77 p.

Wells, M. L., Dallmeyer, R. D. and Allmendinger, R. W., 1990, Late Cretaceous extension in the hinterland of the Sevier thrust belt, northwestern Utah and southern Idaho: Geology, v. 18, no. 10, p. 929-933.

Wells, M. L. and Hoisch, T. D., 2008, The role of mantle delamination in widespread Late Cretaceous extension and magmatism in the Cordilleran orogen, western United States: Geological Society of America Bulletin, v. 120, no. 5-6, p. 515-530.

Wernicke, B., Clayton, R., Ducea, M., Jones, C. H., Park, S., Ruppert, S., Saleeby, J., Snow, J. K., Squires, L., Fliedner, M., Jiracek, G., Keller, R., Klemperer, S., Luetgert, J., Malin, P., Miller, K., Mooney, W., Oliver, H., and Phinney, R., 1996, Origin of high mountains in the continents: The southern Sierra Nevada: Science, v. 271, no. 5246, p. 190-193.

Wolfe, J. A., 1994, Tertiary climatic changes at middle latitudes of western North America: Palaeogeography Palaeoclimatology Palaeoecology, v. 108, no. 3-4, p. 195-205.

Wolfe, J. A., Schorn, H. E., Forest, C. E. and Molnar, P., 1997, Paleobotanical evidence for high altitudes in Nevada during the Miocene: Science, v. 276, no. 5319, p. 1672-1675.

Wood, D., and Saleeby, J., 1997, Late Cretaceous-Paleocene extensional collapse and disaggregation of the southernmost Sierra Nevada batholiths: International Geology Review, v. 39, no. 11, p. 973-1009.

Zachos, J., Pagani, M., Sloan, L., Thomas, E. and Billups, K., 2001, Trends, rhythms, and aberrations in global climate 65 Ma to present: Science, v. 292, no. 5517, p. 686-693.

Zachos, J. C., Stott, L. D. and Lohmann, K. C., 1994, Evolution of early Cenozoic marine temperatures: Paleoceanography, v. 9, no. 2, p. 353-387.

# CHAPTER VI

## Summary and Conclusions

### 6.1 Summary of results

This dissertation presents new results and interpretations for two primary research themes. Part I (Chapters 2 and 3) aims to critically evaluate standard stable isotope paleoaltimetry methodologies and assumptions. Stable isotope paleoaltimetry techniques have served as the foundation for the vast majority of recent paleoelevation studies due to the relative ubiquity of paleo-meteoric water proxies in the geologic record, but the technique is potentially significantly limited by fundamental assumptions and inherent uncertainties that require further study. The studies presented in Part II (Chapters 4 and 5) utilize the implications of the work discussed in Part I to investigate the Cenozoic paleoelevation history of the western US Cordillera. Application of standard stable isotope paleoaltimetry techniques, in conjunction with U-Pb detrital zircon provenance (Chapter 4) and carbonate clumped isotope paleothermometry (Chapter 5) studies, provides new and robust paleoelevation estimates for the early Cenozoic southern Sierra Nevada region (Chapter 4) and Cordilleran interior 'Nevadaplano' (Chapter 5).

*6.1.1 Chapter 2 summary*

Multivariate statistical analysis of a dense compilation of modern precipitation $\delta^{18}O$ records from the western US and east Asia reveals that precipitation isotopic relationships with individual environmental parameters (i.e. latitude, longitude, elevation, MAT, MAP) are dependent on physiographic and climatic setting. As proposed in published models for global (Bowen and Wilkinson, 2002) and regional (Dutton et al., 2005; Liu et al., 2008) $\delta^{18}O$ distributions, latitude and elevation are dominant controls on modern precipitation $\delta^{18}O$ values. However, additional environmental controls (i.e. longitude and mean annual precipitation) are also shown to be primary controls on $\delta^{18}O$ distributions in specific subregions (e.g., Himalaya, Coast subregion of western US).

Furthermore, the magnitude of individual environmental parameter-$\delta^{18}O$ relationships is also shown to be setting-dependent. $\delta^{18}O$-elevation gradients in continental interior rainshadow (e.g., Basin and Range) and orogenic plateau regions (e.g., Tibetan Plateau) are a factor of two lower (~ -1.5‰/km) than gradients observed in 'simple' orographic settings that are characterized by relatively straightforward storm track trajectories derived from a single, dominant moisture source (e.g., western US Coast, Himalaya-South Tibet). The magnitude of observed isotope-elevation gradients in these simple orographic settings are in agreement with gradients predicted by Rayleigh distillation models (e.g., Rowley and Garzione, 2007), suggesting violation of basic Rayleigh distillation assumptions is the dominant cause for the observed isotopic variability in continental interior settings. This finding has important implications for stable isotope paleoaltimetry studies as changes in elevation in continental interior regions are likely to be more difficult to discern from the proxy record. This work also

has immediate relevance to stable isotope-based studies of paleoclimate and hydrology. In all cases, the physiographic and climatic setting in which the proxy originally formed must be taken into account in order to improve accuracy of paleoelevation, paleotemperature and paleo-groundwater recharge determinations.

*6.1.2 Chapter 3 summary*

Modern stream and spring water sampling from the orographic slope and orographic rainshadow of the southern Sierra Nevada region confirms the trends observed in the multivariate statistical analysis discussed in Chapter 2. The magnitude of $\delta^{18}O$-elevation gradients for spring water transects collected from the Panamint and Spring mountains are significantly reduced in comparison to surface water transects along the western slope of the Sierra Nevada. The low magnitudes of Spring and Panamint mountains' $\delta^{18}O$-gradients (~ -0.8‰/km) cannot be accounted for by atmospheric processes alone, suggesting that post-depositional isotopic change has further modified meteoric water isotopic compositions in these rainshadow regions. Altitude-dependent snow sublimation is shown to be a viable mechanism for the reduced isotopic gradients, as high elevation snowpacks that are sustained later in the year are likely subject to more extensive isotopic fractionation and associated $^{18}O$ enrichment than snowpacks at lower elevation. This variable isotopic enrichment reverses the effects of initial Rayleigh distillation rainout effects and leads to the observed low magnitude $\delta^{18}O$-elevation gradients. Accordingly, influence of snowmelt-derived meteoric waters to proxy systems must be constrained, especially in arid, mountainous regions where sublimation is a dominant ablation mechanism. This work also provides reference data

for future hydrologic studies investigating the influence of changing climatic conditions on the evolution of groundwater systems in the arid, western US.

### *6.1.3 Chapter 4 summary*

Combined sedimentologic and isotopic study of early Cenozoic sedimentary basin systems in the southernmost Sierra Nevada region places new constraints on the paleotopographic and paleogeographic evolution of the region. Zircon U-Pb provenance study of the early Paleocene Witnet Formation, the Paleocene Goler Formation and the Eocene Tejon Formation provides robust evidence that the southernmost Sierra Nevada was located at near sea level paleoelevations during the early Paleogene. Isotopic study of lacustrine micrite collected from the upper Goler Formation suggests that Goler basin waters were subject to orographic rainout over a moderate elevation (1 – 2 km) topographic barrier, constrained to be located in the central Sierra Nevada based on sedimentary provenance study of contemporaneous siliciclastic Goler sediments. Taken together, these data constrain post-Eocene surface uplift in the central and southern Sierra Nevada to be on the order of 1.5 – 2 km, a finding in agreement with independent thermochronologic study in the region (Clark et al., 2005). Additionally, zircon U-Pb ages suggest that early Cenozoic sedimentary basins in the southern Sierra Nevada region were isolated from continental interior sediment source regions, in contrast to Oligocene basins in the northern Sierra Nevada region that appear to have been fluvially connected to the continental interior (e.g., Cassel et al., 2009). This finding provides evidence for along-strike variations in the topographic development of the Sierra Nevada and calls into question whether a high elevation (> 3 km), orogenic plateau extended as far south as the

latitudes of the southernmost Sierra Nevada (~ 36°N) during the early Cenozoic (e.g., Ernst et al., 2010).

### *6.1.4 Chapter 5 summary*

Carbonate clumped isotope paleothermometry study of Late Cretaceous-Eocene lacustrine carbonates provides absolute paleoelevation estimates for the proposed early Cenozoic 'Nevadaplano' orogenic plateau. Carbonate formation temperatures were significantly warmer in the near sea level Goler basin in comparison to carbonate formation temperatures in the continental interior Sheep Pass Formation. The observed temperature difference (~ 16°C) indicates that a high elevation (≥ 2.6 km) continental plateau dominated the western US Cordilleran interior prior to widespread Basin and Range extension. In addition to providing absolute paleoelevation constraints for the early Cenozoic western US Cordillera, this study also highlights the utility of clumped isotope paleothermometry for paleoelevation studies, particularly in regions where meteoric water proxies are subject to significant evaporative influence.

## 6.2 Conclusions

In recent decades, the development of stable isotope paleoaltimetry techniques has greatly enhanced our capability to make quantitative estimates of paleoelevations in orogenic systems. Variability in isotope-elevation relationships, as well as influence from post-depositional isotopic fractionation processes, changes in climate, and complex moisture source interactions, however, significantly limit paleoelevation determinations derived from paleo-meteoric proxy records. These uncertainties and limitations have been

particularly impactful for paleoelevation studies in continental interior rainshadows and high elevation orogenic plateaus where fundamental Rayleigh distillation processes are often violated. This dissertation enhances the capability for accurate paleoelevation determinations through critical evaluation of the technique. Multivariate statistical analysis of modern precipitation $\delta^{18}O$ distributions indicates that isotopic relationships are dependent on physiographic and climatic setting. Proxy-based studies in continental interior regions and high elevation orogenic plateaus must acknowledge that isotope-elevation gradients are systematically reduced in these regions in comparison to orographic settings where Rayleigh distillation processes dominate. If empirical global average or Rayleigh distillation-derived isotope elevation gradients are incorrectly applied to continental interior proxy records, paleoelevations are likely to be significantly underestimated. Significant paleoelevation uncertainties can also result from the influences of post-depositional isotopic fractionation processes (e.g., evaporation, snowpack sublimation) to the proxy record. Accordingly, these post-depositional processes must also be accounted for in stable isotope paleoaltimetry studies.

The investigation of isotopic relationships in modern meteoric water systems presented in Chapters 2 and 3 of this dissertation also has direct implications for applications of stable isotope paleoaltimetry to the Cenozoic paleoelevation history of the western US Cordillera. In light of the systematic trends and variability in $\delta^{18}O$-elevation gradients observed in modern records, models citing significant decreases in proxy $\delta^{18}O$ values (~ 8‰) since middle Miocene time as evidence for widespread surface downdrop (2–3 km) in the Basin and Range (e.g., Horton and Chamberlain, 2006) must be reconsidered. Such large isotopic shifts equate to unreasonable estimates of regional

elevation change (> 5 km surface downdrop) when more accurate $\delta^{18}O$-elevation gradients for continental interior settings (~ -1.5‰/km) are applied. A more likely cause for large magnitude isotopic shifts are changes in the relative contribution of moisture source through time or reorganization of regional drainage systems (e.g., Davis et al., 2008). As a result, many of the published estimates for Cenozoic Basin and Range paleoelevations are subject to significant uncertainties that challenge their reliability.

The complications inherent to stable isotope paleoaltimetry calls for the application of complimentary and independent techniques in order to more reliably interpret proxy records. One such approach is pairing zircon U-Pb provenance techniques with standard stable isotope methodologies to elucidate isotopic records by providing independent constraints on the source regions for not only basin sediments, but basin waters as well. Provenance study can also be utilized to investigate how regional paleogeography and paleo-fluvial systems evolved through time. Accordingly, shifts in the proxy isotopic record resulting from drainage reorganization are more readily identifiable, which, in turn, allows for the elevation signal in the proxy record to be more reliably quantified.

Carbonate clumped isotope paleothermometry is additional powerful analytical tool to pair with stable isotopic study of meteoric water proxies as it allows for more accurate interpretation of the proxy record in two primary ways. First, carbonate formation temperatures can be used for paleoelevation determinations independent of proxy stable isotopic compositions through straightforward applications of temperature lapse rates. Furthermore, in cases where a contemporaneous near sea level temperature value can be obtained, absolute paleoelevation calculations are even possible (e.g.,

Chapter 5). Second, knowing the temperature of carbonate formation also allows for direct calculation of water $\delta^{18}O$ values, which can themselves be used for paleoelevation determinations through comparison with modern meteoric water $\delta^{18}O$ distributions. Independent and reliable measures of water isotopic compositions also enhances our ability to identify evaporative influences to the proxy record, which without independent sedimentologic evidence, are often difficult to quantify.

As part of the work presented in this dissertation, application of zircon U-Pb provenance and carbonate clumped isotope paleothermometry techniques in conjunction with standard stable isotope paleoaltimetry methodologies provides new and robust paleoelevation estimates for the early Cenozoic southern Sierra Nevada and continental interior regions of the western US Cordillera. Near sea level paleoelevations in the southernmost Sierra Nevada during the early Paleogene indicate that regional surface uplift of 1.5 – 2 km has occurred since Eocene time. These surface uplift estimates are consistent with published estimates for the central and southern Sierra Nevada derived from independent geomorphic and thermochronologic studies (e.g., Clark et al., 2005) and, thus, provide additional support for models attributing late Cenozoic uplift to delamination of mantle lithosphere form below the central and southern Sierran arc (e.g., Jones et al., 2004; Zandt et al., 2004). Clumped isotope paleotemperature estimates for lacustrine carbonates of the continental interior Sheep Pass Formation indicate that high regional elevations ($\geq$ 2.6 km) characterized the Cordilleran interior prior to Basin and Range extension. Direct evidence for high regional paleoelevations during the early Cenozoic validates models citing excess gravitational potential energy of a high elevation, continental plateau as the primary driver for Tertiary extension (e.g., Jones et

al., 1996; Dilek and Moores, 1999), at least in the Northern Basin and Range where the direct estimates of regional paleoelevations presented in this dissertation have been made.

Integration of the primary findings present in this dissertation produces a clearer picture of early Cenozoic western US paleotopography (Figure 6.1). Long-lived Mesozoic-early Cenozoic convergence and subduction of the Farallon oceanic plate constructed a spatially extensive, high elevation continental plateau in the hinterland of the Sierra Nevada magmatic arc. The southward extent of this high topography, however, remains poorly constrained. Near sea level rift basins in the southern Sierra Nevada region appear to have been cut off from continental interior sediment sources during the early Paleogene, suggesting that the early Cenozoic high elevation, orogenic plateau did not extend to the latitude of the southern Sierra Nevada, and that, instead, this region of the continental interior was characterized by a gradual topographic gradient with elevations decreasing to the south (Figure 6.1). As a result, central Basin and Range extension is unlikely to have been driven by buoyancy forces alone, suggesting that plate boundary and/or basal normal forces played a significant role in the late Cenozoic tectonic evolution of this region. At present this proposal of driving forces for central Basin and Range extension is highly speculative. Future work should center on constraining the paleoelevation history of the central Basin and Range prior to the middle Miocene onset of crustal extension in order to assess whether dominant driving mechanisms for Basin and Range extension varied in time and space.

# Figure 6.1

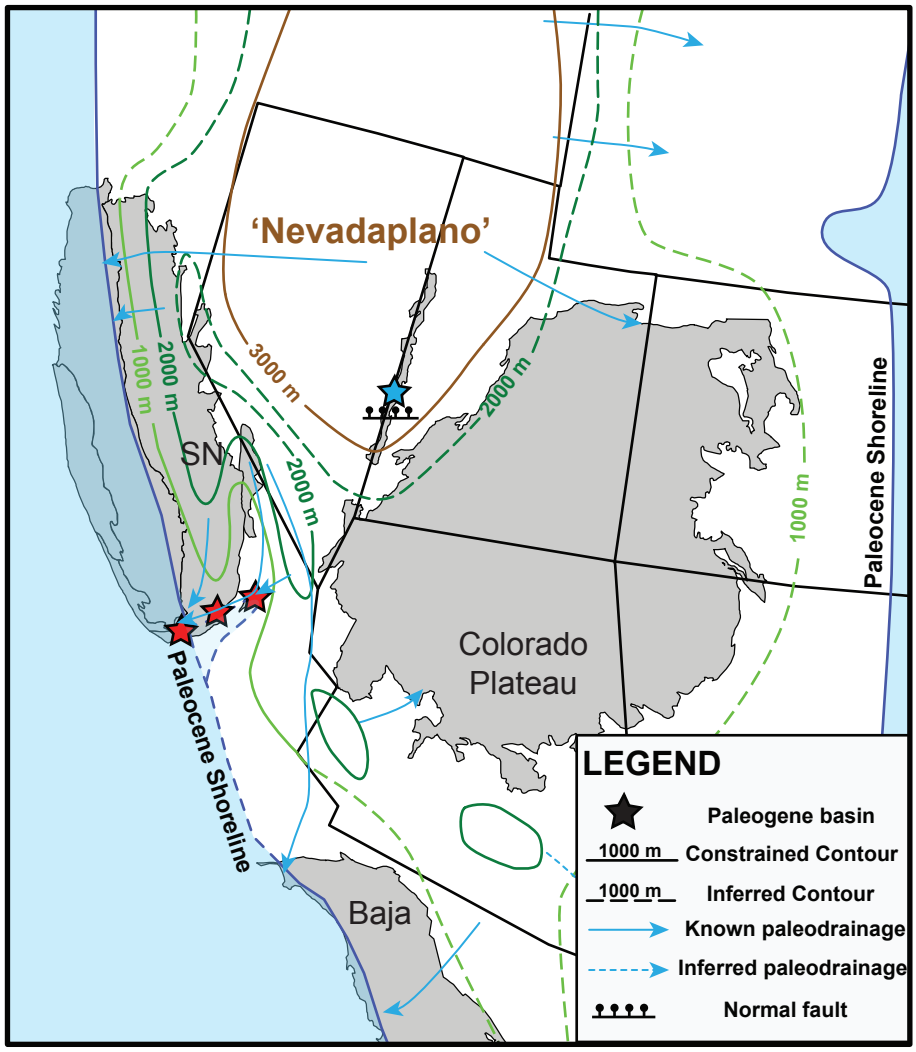


Figure 6.1 – Early Cenozoic paleotopography and paleogeography of the western US Cordillera. Paleocene paleogeographic and paleotopographic map of the western US with retrodeformed state boundaries. Locations of reference physiographic provinces (gray polygons) from McQuarrie and Wernicke, 2005. Paleotopographic contours and paleodrainages for the southern Sierra Nevada and 'Nevadaplano' region are based on peleoelevation studies presented in this thesis (Lechler and Niemi, 2011; Chapters 4 and 5). Remaining contours and paleodrainages compiled from various sources (**Sierra Nevada**: Mulch et al., 2006; Cassel et al., 2009; Hren et al., 2010; Cecil et al., 2011; **southern Basin and Range**: Abbott and Smith, 1989; Howard, 2000; Wernicke, 2011; **Sevier orogen**: Henry, 2008; Fan and Dettman, 2009). SN = Sierra Nevada.

## 6.3 References cited


Abbott, P. L., and Smith, T. E., 1989, Sonora, Mexico, source for the Eocene Poway Conglomerate of southern California: Geology, v. 17, no. 4, p. 329-332.

Bowen, G. J., and Wilkinson, B., 2002, Spatial distribution of $\delta^{18}O$ in meteoric precipitation: Geology, v. 30, no. 4, p. 315-318.

Cassel, E. J., Calvert, A. T., and Graham, S. A., 2009, Age, geochemical composition, and distribution of Oligocene ignimbrites in the northern Sierra Nevada, California: implications for landscape morphology, elevation, and drainage divide geography of the Nevadaplano: International Geology Review, v. 51, no. 7-8, p. 723-742.

Cecil, M.R., Ducea, M., Mulch, A., Allen, C., and Campbell, I., 2011, Provenance of Eocene river sediments from the central-northern Sierra Nevada and implications for paleotopography: Tectonics, v. 30, doi:10.1029/2010TC002717.

Clark, M. K., Maheo, G., Saleeby, J., Farley, K.A., 2005, The non-equilibrium landscape of the southern Sierra Nevada, California: GSA Today, v. 15, no. 9, p. 4-10.

Davis, S. J., Wiegand, B. A., Carroll, A. R., and Chamberlain, C. P., 2008, The effect of drainage reorganization on paleoaltimetry studies: An example from the Paleogene Laramide foreland: Earth and Planetary Science Letters, v. 275, no. 3-4, p. 258-268.

Dilek, Y., and Moores, E. M., 1999, A Tibetan model for the early Tertiary western United States: Journal of the Geological Society, v. 156, p. 929-941.

Dutton, A., Wilkinson, B.H., Welker, J.M., Bowen, G.J., and Lohmann, K.C., 2005, Spatial distribution and seasonal variation in $^{18}O/^{16}O$ of modern precipitation and river water across the conterminous USA: Hydrological Processes, v. 19, p. 4121-4146.

Ernst, W. G., 2010, Young convergent-margin orogens, climate, and crustal thickness-A Late Cretaceous-Paleogene Nevadaplano in the American Southwest?: Lithosphere, v. 2, no. 2, p. 67-75.

Fan, M. J., and Dettman, D. L., 2009, Late Paleocene high Laramide ranges in northeast Wyoming: Oxygen isotope study of ancient river water: Earth and Planetary Science Letters, v. 286, no. 1-2, p. 110-121.

Henry, C. D., 2008, Ash-flow tuffs and paleovalleys in northeastern Nevada: Implications for Eocene paleogeography and extension in the Sevier hinterland, northern Great Basin: Geosphere, v. 4, no. 1, p. 1-35.

Horton, T. W., and Chamberlain, C. P., 2006, Stable isotopic evidence for Neogene surface downdrop in the central Basin and Range Province: Geological Society of America Bulletin, v. 118, no. 3-4, p. 475-490.

Howard, J. L., 2000, Provenance of quartzite clasts in the Eocene-Oligocene Sespe Formation: Paleogeographic implications for southern California and the ancestral Colorado River: Geological Society of America Bulletin, v. 112, no. 11, p. 1635-1649.

Hren, M.T., Pagani, M., Erwin, D.M., and Brandon, M., 2010, Biomarker reconstruction of the early Eocene paleotopography and paleoclimate of the northern Sierra Nevada: Geology, v. 38, p. 7-10, doi:10.1130/G30215.1

Jones, C. H., Farmer, G. L., and Unruh, J., 2004, Tectonics of Pliocene removal of lithosphere of the Sierra Nevada, California: Geological Society of America Bulletin, v. 116, no. 11-12, p. 1408-1422.

Jones, C. H., Unruh, J. R., and Sonder, L. J., 1996, The role of gravitational potential energy in active deformation in the southwestern United States: Nature, v. 381, no. 6577, p. 37-41.

Lechler, A. R., and Niemi, N.A., 2011, Sedimentologic and isotopic constraints on the Paleogene paleogeography and paleotopography of the southern Sierra Nevada, California, Geology, v. 39, no. 4, p. 379-382.

Liu, Z. F., Tian, L. D., Chai, X. R., and Yao, T. D., 2008, A model-based determination of spatial variation of precipitation $\delta^{18}O$ over China: Chemical Geology, v. 249, no. 1-2, p. 203-212.

Mulch, A., Graham, S.A., and Chamberlain, C.P., 2006, Hydrogen isotopes in Eocene river gravels and paleoelevation of the Sierra Nevada: Science, v. 313, p. 87-89, doi:10.1126/science.1125986.

Rowley, D. B., and Garzione, C. N., 2007, Stable isotope-based paleoaltimetry: Annual Review of Earth and Planetary Sciences, v. 35, p. 463-508.

Wernicke, B., The California River and its role in carving the Grand Canyon: Geological Society of America Bulletin, v. 123, doi: 10.1130/B30274.1.

Zandt, G., Gilbert, H., Owens, T. J., Ducea, M., Saleeby, J., and Jones, C. H., 2004, Active foundering of a continental arc root beneath the southern Sierra Nevada in California: Nature, v. 431, no. 7004, p. 41-46.

# APPENDIX

This appendix contains additional data tables, maps and figures for Chapters 2, 4, and 5 of this dissertation (see individual chapters for additional information). Tables A2.1 and A2.2 list geographic, isotopic, and climatic information for all precipitation and surface water collection sites in the western US and east Asia, respectively, that were compiled for statistical analysis of modern meteoric water $\delta^{18}O$ (Chapter 2).

Supplementary information for Chapter 4 includes a full U-Pb data table (Table A4.1) for zircon analyses performed at the University of Arizona LaserChron Center in January 2010. Figure A4.1 shows simplified geologic maps for the detrital zircon sample sites in the southern Sierra Nevada region. Figure A4.2 shows the full U-Pb age spectra, highlighting the fact that early Cenozoic basins in the southern Sierra Nevada region have a scarcity of zircon U-Pb ages older than 300 Ma (see text for discussion). Table A4.2 lists isotopic data for Goler Formation micrite. Figure A4.3 is a map indicating the relevant data sources for the igneous and siliciclastic zircon-age source regions shown in Figure 4.2B. Table A4.3 provides geographic coordinates and lithologic descriptions for the samples collected for U-Pb and isotopic analysis.

Table A5.1 provides detailed isotopic and isotopologue data for the clumped isotope paleothermometry analysis of carbonates collected and analyzed from the Goler and Sheep Pass formations (Chapter 5).

## Table A2.1 – Compilation of western US precipitation $\delta^{18}O$ records

| Location | Subregion | LAT (º) | LON (º) | ELEV (m) | MAT (ºC) | MAP (cm) | W:S | Wgt. $\delta^{18}O$ (‰ SMOW) | Reference | Sample Period | Number of seasons |
|---|---|---|---|---|---|---|---|---|---|---|---|
| Agua Dulce, CA | COAST | 34.5033 | -118.3100 | 810 | 16.1 | 34.1 | 9.02 | -9.4 | Friedman et al., 1992 | 1982-1989 | 4 (dD); 1 (d18O) |
| Alsea Guard Station, OR | COAST | 44.3900 | -123.6200 | 104 | 11.6 | 173.4 | 4.10 | -7.0 | USNIP | 1989-2001 | NR |
| Badger Flat | COAST | 37.2650 | -119.1083 | 2530 | 5.3 | 70.1 | 5.02 | -15.1 | Friedman and Smith, 1972 | 1969-71 | 3 |
| Big Bear, CA | COAST | 34.2633 | -116.8533 | 2055 | 7.9 | 60.8 | 4.72 | -11.4 | Friedman et al., 1992 | 1982-1989 | 5 (dD); 2 (d18O) |
| Big Whitney Meadow | COAST | 36.4400 | -118.2550 | 2970 | 2.2 | 62.6 | 4.00 | -18.3 | Friedman and Smith, 1972 | 1969-71 | 3 |
| Bishop Park | COAST | 37.2433 | -118.5967 | 2530 | 1.5 | 38.4 | 3.25 | -16.9 | Friedman and Smith, 1972 | 1970-71 | 2 |
| Bishop Pass | COAST | 37.1000 | -118.5567 | 3415 | 0.2 | 66.7 | 3.36 | -19.8 | Friedman and Smith, 1972 | 1969-71 | 3 |
| Center Mountain | COAST | 38.1500 | -119.4667 | 2865 | 2.2 | 75.0 | 3.78 | -16.3 | Friedman and Smith, 1972 | 1971 | 1 |
| Clover Meadow | COAST | 37.5283 | -119.2750 | 2135 | 7.9 | 73.2 | 5.36 | -14.0 | Friedman and Smith, 1972 | 1970-71 | 3 |
| Cottonwood Lakes 2 | COAST | 36.4833 | -118.2167 | 3385 | 2.9 | 70.5 | 3.63 | -19.7 | Friedman and Smith, 1972 | 1970 | 1 |
| Deadman Summit | COAST | 37.7750 | -119.0150 | 2445 | 4.9 | 45.6 | 3.38 | -16.6 | Friedman and Smith, 1972 | 1969-71 | 3 |
| Echo Summit | COAST | 38.8283 | -120.0367 | 2270 | 5.6 | 99.8 | 4.47 | -14.4 | Friedman and Smith, 1972 | 1969-71 | 3 |
| Fred Meadow | COAST | 37.0383 | -119.0800 | 2195 | 6.7 | 83.9 | 6.36 | -12.9 | Friedman and Smith, 1972 | 1969, 1971 | 2 |
| Gem Pass | COAST | 37.7800 | -119.1700 | 3170 | 4.0 | 72.4 | 3.57 | -18.9 | Friedman and Smith, 1972 | 1969-71 | 3 |
| Gin Flat | COAST | 37.7650 | -119.7733 | 2135 | 8.6 | 98.9 | 5.90 | -13.2 | Friedman and Smith, 1972 | 1969-71 | 3 |
| Herring Creek | COAST | 38.2417 | -119.9417 | 2225 | 7.6 | 102.8 | 5.15 | -13.0 | Friedman and Smith, 1972 | 1970-71 | 2 |
| HJ Andrews Exp. Forest, OR | COAST | 44.2100 | -122.2500 | 436 | 9.3 | 187.4 | 3.34 | -9.8 | USNIP | 1989-2001 | NR |
| Hopland, CA | COAST | 39.0000 | -123.0800 | 253 | 14.4 | 101.6 | 8.53 | -7.7 | USNIP | 1989-2001 | NR |
| Ingraham_Taylor_1 | COAST | 41.8070 | -124.1447 | 50 | 11.7 | 195.6 | 4.49 | -7.3 | Ingraham&Taylor, 1991 | Jan-March 1985 | 1 |
| Ingraham_Taylor_10 | COAST | 39.1629 | -122.7536 | 955 | 13.8 | 105.9 | 7.68 | -12.7 | Ingraham&Taylor, 1991 | Jan-March 1985 | 1 |
| Ingraham_Taylor_11 | COAST | 39.1629 | -122.4921 | 610 | 15.0 | 74.4 | 7.94 | -11.4 | Ingraham&Taylor, 1991 | Dec 1984 - March 1985 | 1 |
| Ingraham_Taylor_12 | COAST | 39.1213 | -122.3639 | 349 | 16.0 | 55.6 | 7.86 | -11.3 | Ingraham&Taylor, 1991 | Nov 1984-March 1985 | 1 |
| Ingraham_Taylor_13 | COAST | 39.1792 | -122.4010 | 360 | 15.6 | 57.1 | 7.81 | -11.6 | Ingraham&Taylor, 1991 | Nov 1984-March 1985 | 1 |
| Ingraham_Taylor_14 | COAST | 39.1502 | -122.3454 | 245 | 16.1 | 53.0 | 7.73 | -10.6 | Ingraham&Taylor, 1991 | Nov 1984 - Jan 1985 | 1 |
| Ingraham_Taylor_15 | COAST | 39.1502 | -122.2342 | 37 | 16.1 | 45.3 | 7.39 | -9.9 | Ingraham&Taylor, 1991 | Nov 1984-March 1985 | 1 |
| Ingraham_Taylor_16 | COAST | 39.2011 | -122.0507 | 14 | 16.1 | 42.1 | 6.94 | -10.0 | Ingraham&Taylor, 1991 | Nov - Dec 1984 | 1 |
| Ingraham_Taylor_17 | COAST | 39.1502 | -121.9191 | 12 | 16.1 | 44.5 | 7.07 | -9.4 | Ingraham&Taylor, 1991 | Nov 1984-March 1985 | 1 |
| Ingraham_Taylor_18 | COAST | 39.1502 | -121.5669 | 18 | 16.1 | 55.7 | 7.54 | -10.1 | Ingraham&Taylor, 1991 | Nov 1984-March 1985 | 1 |
| Ingraham_Taylor_19 | COAST | 39.2444 | -121.4181 | 180 | 16.1 | 75.6 | 8.18 | -10.3 | Ingraham&Taylor, 1991 | Nov 1984-March 1985 | 1 |
| Ingraham_Taylor_2 | COAST | 41.7924 | -124.0873 | 66 | 11.7 | 208.2 | 4.78 | -7.9 | Ingraham&Taylor, 1991 | Jan-March 1985 | 1 |
| Ingraham_Taylor_20 | COAST | 39.2011 | -121.3065 | 218 | 16.1 | 87.0 | 7.83 | -10.8 | Ingraham&Taylor, 1991 | Nov 1984-March 1985 | 1 |
| Ingraham_Taylor_21 | COAST | 39.2299 | -121.2321 | 422 | 15.4 | 101.5 | 7.39 | -12.0 | Ingraham&Taylor, 1991 | Nov 1984-March 1985 | 1 |
| Ingraham_Taylor_22 | COAST | 39.2299 | -121.1018 | 728 | 14.2 | 136.3 | 7.52 | -11.8 | Ingraham&Taylor, 1991 | Dec 1984 - March 1985 | 1 |
| Ingraham_Taylor_23 | COAST | 39.3021 | -121.0274 | 792 | 13.7 | 143.2 | 7.38 | -11.8 | Ingraham&Taylor, 1991 | Dec 1984 - March 1985 | 1 |
| Ingraham_Taylor_24 | COAST | 39.3021 | -120.7855 | 1400 | 11.9 | 177.4 | 6.41 | -9.6 | Ingraham&Taylor, 1991 | Winter 1985 | 1 |
| Ingraham_Taylor_25 | COAST | 39.3097 | -120.6708 | 1401 | 10.3 | 170.9 | 6.15 | -12.1 | Ingraham&Taylor, 1991 | Winter 1985 | 1 |
| Ingraham_Taylor_26 | COAST | 39.5988 | -120.6147 | 1660 | 7.7 | 123.4 | 4.96 | -13.2 | Ingraham&Taylor, 1991 | Winter 1985 | 1 |
| Ingraham_Taylor_27 | COAST | 39.6132 | -120.4840 | 2021 | 6.6 | 102.7 | 4.36 | -15.2 | Ingraham&Taylor, 1991 | Winter 1985 | 1 |
| Ingraham_Taylor_28 | COAST | 39.3388 | -120.3348 | 2197 | 5.2 | 108.3 | 4.58 | -15.0 | Ingraham&Taylor, 1991 | Winter 1985 | 1 |
| Ingraham_Taylor_29 | COAST | 39.4986 | -120.2792 | 1950 | 5.5 | 87.3 | 4.20 | -14.7 | Ingraham&Taylor, 1991 | Winter 1985 | 1 |
| Ingraham_Taylor_3 | COAST | 41.8799 | -123.8191 | 402 | 11.6 | 180.2 | 5.41 | -10.1 | Ingraham&Taylor, 1991 | Jan-March 1985 | 1 |
| Ingraham_Taylor_4 | COAST | 41.9660 | -123.7492 | 610 | 10.4 | 155.0 | 5.25 | -11.4 | Ingraham&Taylor, 1991 | Jan-March 1985 | 1 |
| Ingraham_Taylor_5 | COAST | 42.7151 | -122.2362 | 1410 | 6.6 | 98.6 | 3.44 | -13.0 | Ingraham&Taylor, 1991 | Jan-March 1985 | 1 |
| Ingraham_Taylor_6 | COAST | 42.3672 | -123.5326 | 366 | 11.8 | 112.6 | 5.00 | -13.3 | Ingraham&Taylor, 1991 | Jan-March 1985 | 1 |
| Ingraham_Taylor_7 | COAST | 39.4336 | -123.7944 | 26 | 11.7 | 103.6 | 6.14 | -6.9 | Ingraham&Taylor, 1991 | Nov 1984-March 1985 | 1 |
| Ingraham_Taylor_8 | COAST | 39.2174 | -123.3095 | 695 | 13.5 | 128.9 | 7.80 | -9.4 | Ingraham&Taylor, 1991 | Nov 1984 - Jan 1985 | 1 |
| Ingraham_Taylor_9 | COAST | 39.1484 | -122.8843 | 426 | 13.9 | 85.3 | 8.50 | -11.2 | Ingraham&Taylor, 1991 | Dec 1984 - March 1985 | 1 |

## Table A2.1 – Compilation of western US precipitation $\delta^{18}O$ records

| Location | Subregion | LAT (º) | LON (º) | ELEV (m) | MAT (ºC) | MAP (cm) | W:S | Wgt. $\delta^{18}O$ (‰ SMOW) | Reference | Sample Period | Number of seasons |
|---|---|---|---|---|---|---|---|---|---|---|---|
| Jacumba, CA | COAST | 32.6167 | -116.1633 | 860 | 16.0 | 28.8 | 3.56 | -8.4 | Friedman et al., 1992 | 1982-1989 | 4 (dD); 2 (d18O) |
| Kingvale, CA | COAST | 39.3167 | -120.2833 | 1845 | 5.1 | 102.4 | 4.93 | -12.3 | Friedman and Smith, 1972 | 1970-71 | 2 |
| Mammoth Lakes | COAST | 37.6533 | -118.9900 | 2485 | 4.7 | 48.2 | 3.59 | -15.0 | Friedman and Smith, 1972 | 1970-71 | 2 |
| Mammoth Mid Station | COAST | 37.6417 | -119.0283 | 2945 | 4.7 | 58.4 | 3.53 | -16.3 | Friedman and Smith, 1972 | 1969-71 | 3 |
| Mono Craters, South | COAST | 37.8367 | -119.0000 | 2530 | 5.5 | 43.3 | 3.17 | -17.1 | Friedman and Smith, 1972 | 1970-71 | 2 |
| Mono Pass | COAST | 37.4383 | -118.7733 | 3490 | -0.3 | 71.5 | 3.24 | -19.9 | Friedman and Smith, 1972 | 1969-71 | 3 |
| Mount Dyer No. 1 | COAST | 40.2433 | -121.0350 | 2165 | 7.2 | 95.2 | 3.57 | -13.9 | Friedman and Smith, 1972 | 1969-71 | 3 |
| Mount Laguna, CA | COAST | 32.8817 | -116.4267 | 1735 | 11.6 | 63.8 | 4.65 | -10.5 | Friedman et al., 1992 | 1982-1989 | 4 (dD); 2 (d18O) |
| Mount Rose A-2 | COAST | 39.2983 | -119.9183 | 2590 | 3.9 | 82.2 | 3.46 | -14.9 | Friedman and Smith, 1972 | 1969-71 | 3 |
| Mount Rose C-1 | COAST | 39.3017 | -119.8983 | 2710 | 4.6 | 80.7 | 3.40 | -15.1 | Friedman and Smith, 1972 | 1969-71 | 3 |
| Mount Rose G | COAST | 39.3267 | -119.8850 | 2480 | 5.3 | 75.1 | 3.33 | -15.7 | Friedman and Smith, 1972 | 1969-71 | 3 |
| Mount San Jacinto, CA | COAST | 33.8150 | -116.6383 | 2540 | 13.3 | 73.6 | 4.12 | -11.9 | Friedman et al., 1992 | 1982-1989 | 4 (dD); 2 (d18O) |
| Olympic Nat'l Park, WA | COAST | 47.8600 | -123.9200 | 176 | 9.3 | 272.9 | 3.10 | -8.8 | USNIP | 1989-2001 | NR |
| Quail Lake, CA | COAST | 34.7433 | -118.7117 | 1225 | 14.1 | 33.1 | 9.01 | -11.1 | Friedman et al., 1992 | 1982-1989 | 5 (dD); 2 (d18O) |
| Rock Creek 1 | COAST | 37.4917 | -118.7167 | 2650 | 3.8 | 45.9 | 3.09 | -21.0 | Friedman and Smith, 1972 | 1969-70 | 2 |
| Rock Creek 3 | COAST | 37.4500 | -118.7417 | 3050 | 1.9 | 53.0 | 3.22 | -20.0 | Friedman and Smith, 1972 | 1969-70 | 2 |
| Round Meadow | COAST | 35.9650 | -118.3600 | 2745 | 7.0 | 70.9 | 5.09 | -14.0 | Friedman and Smith, 1972 | 1969-71 | 3 |
| Santa Maria, CA | COAST | 34.9000 | -120.4500 | 79 | 14.1 | 34.0 | 11.58 | -5.4 | GNIP | 1963-1965, 1973-1975 | 6 |
| Sonora Pass | COAST | 38.3133 | -119.6067 | 2680 | 2.8 | 79.1 | 3.94 | -16.6 | Friedman and Smith, 1972 | 1970-71 | 2 |
| Table Mountain, CA | COAST | 34.3750 | -117.6750 | 2280 | 10.3 | 72.9 | 7.13 | -14.0 | Friedman et al. 1992 | 1982-1989 | 4 (dD); 1 (d18O) |
| Tehachapi, CA | COAST | 35.1383 | -118.4417 | 1220 | 12.3 | 28.1 | 6.04 | -10.3 | Friedman et al. 1992 | 1982-1989 | 5 (dD); 2 (d18O) |
| Walker Pass, CA | COAST | 35.6600 | -118.0183 | 1585 | 14.3 | 32.4 | 5.27 | -12.8 | Friedman et al. 1992 | 1982-1989 | 6 (dD); 2 (d18O) |
| Whitney Portal | COAST | 36.5867 | -118.2400 | 2550 | 4.5 | 51.1 | 3.96 | -16.5 | Friedman and Smith, 1972 | 1970-71 | 2 |
| Yosemite Nat'l Park | COAST | 37.8000 | -119.8600 | 1408 | 10.6 | 101.4 | 6.44 | -9.1 | USNIP | 1989-2001 | NR |
| Alamo, NV | BR* | 37.3633 | -115.1933 | 1134 | 14.0 | 17.6 | 1.18 | -12.5 | Friedman et al., 2002 | 1991-1997 | 4 (dD); 1 (d18O) |
| Amboy, CA | BR* | 34.5650 | -115.7500 | 205 | 21.3 | 6.7 | 0.92 | -8.3 | Friedman et al., 1992 | 1982-1989 | 5 (dD); 2 (d18O) |
| Austin, NV | BR | 39.4683 | -117.1950 | 1747 | 8.3 | 24.3 | 1.21 | -17.5 | Friedman et al., 2002 | 1991-1997 | 4 (dD); 2 (d18O) |
| Baker, CA | BR* | 35.2850 | -116.0800 | 280 | 20.4 | 6.4 | 1.13 | -9.5 | Friedman et al., 1992 | 1982-1989 | 5 (dD); 2 (d18O) |
| Bear Lake, ID | BR | 42.2467 | -111.3383 | 1807 | 5.0 | 35.1 | 0.97 | -17.2 | Friedman et al., 2002 | 1991-1997 | 3 (dD); 1 (d18O) |
| Bend, OR | BR | 44.0933 | -121.1983 | 1052 | 8.3 | 25.3 | 1.63 | -17.4 | Friedman et al., 2002 | 1991-1997 | 4 (dD); 1 (d18O) |
| Big Creek, NV | BR | 39.3217 | -117.1217 | 2204 | 6.2 | 30.7 | 1.19 | -16.3 | Friedman et al., 2002 | 1991-1997 | 4 (dD); 3 (d18O) |
| Bishop, CA | BR* | 37.3733 | -118.3650 | 1256 | 13.7 | 15.3 | 2.92 | -13.9 | Friedman et al., 2002 | 1991-1997 | 5 (dD); 4 (d18O) |
| Blackcap Pass | BR | 37.6667 | -118.7700 | 3140 | 7.5 | 34.8 | 3.15 | -17.9 | Friedman and Smith, 1972 | 1969-71 | 3 |
| Blythe, CA | BR* | 33.6200 | -114.7183 | 120 | 22.8 | 7.6 | 1.24 | -8.3 | Friedman et al., 1992 | 1982-1989 | 6 (dD); 2 (d18O) |
| Borrego, CA | BR* | 33.2583 | -116.3233 | 160 | 21.0 | 14.5 | 3.14 | -8.5 | Friedman et al., 1992 | 1982-1989 | 4 (dD); 2 (d18O) |
| Brawley, CA | BR* | 32.9900 | -115.5150 | -40 | 22.8 | 5.9 | 1.69 | -6.2 | Friedman et al., 1992 | 1982-1989 | 5 (dD); 1 (d18O) |
| Burns, OR | BR | 43.5917 | -118.9533 | 1263 | 7.2 | 29.2 | 1.71 | -14.8 | Friedman et al., 2002 | 1991-1997 | 4 (dD); 2 (d18O) |
| Carson City, NV | BR | 39.1917 | -119.7350 | 1432 | 9.4 | 24.4 | 2.44 | -14.7 | Friedman et al., 2002 | 1991-1997 | 6 (dD); 4 (d18O) |
| Cave Mountain, NV | BR | 39.1583 | -114.6083 | 3246 | 6.9 | 57.3 | 1.25 | -15.8 | Friedman et al., 2002 | 1991-1997 | 4 (dD); 2 (d18O) |
| Cedar City, UT | BR | 37.7017 | -113.0967 | 1714 | 9.9 | 30.6 | 1.05 | -13.1 | Friedman et al., 2002 | 1991-1997 | 6 (dD); 4 (d18O) |
| Cherry Creek Range, NV | BR | 40.1217 | -114.8750 | 2880 | 6.7 | 48.4 | 1.25 | -15.3 | Friedman et al., 2002 | 1991-1997 | 5 (dD); 3 (d18O) |
| Chiriaco Summit, CA | BR* | 33.6650 | -115.7083 | 520 | 19.8 | 11.6 | 1.28 | -9.7 | Friedman et al., 1992 | 1982-1989 | 5 (dD); 2 (d18O) |
| Clark Mountain, CA | BR* | 35.5033 | -115.5633 | 1645 | 13.9 | 26.4 | 1.41 | -11.5 | Friedman et al., 1992 | 1982-1989 | 5 (dD); 2 (d18O) |
| Connors Pass, NV | BR | 39.0250 | -114.6417 | 2522 | 7.0 | 37.2 | 1.01 | -15.3 | Friedman et al., 2002 | 1991-1997 | 6 (dD); 4 (d18O) |
| Conway Summit | BR | 38.0883 | -119.1833 | 2480 | 5.6 | 47.7 | 3.12 | -17.7 | Friedman and Smith, 1972 | 1969-71 | 3 |
| Craters of the Moon, ID | BR | 43.4600 | -113.5500 | 1807 | 5.6 | 37.2 | 1.40 | -15.8 | USNIP | 1989-2001 | NR |
| Daggett, CA | BR* | 34.8550 | -116.7867 | 585 | 19.4 | 9.3 | 1.81 | -10.9 | Friedman et al., 1992 | 1982-1989 | 6 (dD); 2 (d18O) |
| Dantes View, CA | BR* | 36.2167 | -116.7183 | 1575 | 15.8 | 18.1 | 1.90 | -13.3 | Friedman et al. 1992, 2002 | 1983-1988; 1991-1997 | 12 (dD); 5 (d18O) |

## Table A2.1 – Compilation of western US precipitation $\delta^{18}O$ records

| Location | Subregion | LAT (º) | LON (º) | ELEV (m) | MAT (ºC) | MAP (cm) | W:S | Wgt. $\delta^{18}O$ (‰ SMOW) | Reference | Sample Period | Number of seasons |
|---|---|---|---|---|---|---|---|---|---|---|---|
| Darwin, CA | BR* | 36.2633 | -117.8267 | 1435 | 10.6 | 33.4 | 3.65 | -11.4 | Friedman et al., 1992 | 1982-1989 | 5 (dD); 1 (d18O) |
| Death Valley, CA | BR* | 36.4600 | -116.8800 | -65 | 22.7 | 5.2 | 2.25 | -9.5 | Friedman et al. 1992, 2002 | 1982-1997 | 11 (dD); 5 (d18O) |
| Delta, UT | BR | 39.3833 | -112.5083 | 1449 | 9.7 | 20.2 | 1.18 | -14.9 | Friedman et al., 2002 | 1991-1997 | 5 (dD); 3 (d18O) |
| Elko, NV | BR | 40.8233 | -115.7900 | 1937 | 7.2 | 26.3 | 1.38 | -15.6 | Friedman et al., 2002 | 1991-1997 | 4 (dD); 2 (d18O) |
| ELY, NV | BR | 39.3000 | -114.8417 | 1907 | 8.0 | 24.9 | 0.83 | -14.4 | Friedman et al., 2002 | 1991-1997 | 5 (dD); 3 (d18O) |
| Goldstone, CA | BR* | 35.3467 | -116.8883 | 920 | 16.8 | 11.1 | 1.92 | -10.4 | Friedman et al., 1992 | 1982-1989 | 4 (dD); 2 (d18O) |
| Hawthorne, NV | BR | 38.5450 | -118.6333 | 1298 | 11.8 | 13.9 | 1.14 | -13.9 | Friedman et al., 2002 | 1991-1997 | 4 (dD); 2 (d18O) |
| Hayford Peak, NV | BR* | 36.6583 | -115.1950 | 2999 | 9.5 | 50.7 | 1.52 | -13.3 | Friedman et al., 2002 | 1991-1997 | 3 (dD); 1 (d18O) |
| Inyokern, CA | BR* | 35.6583 | -117.8267 | 750 | 18.0 | 11.1 | 3.90 | -13.6 | Friedman et al., 1992 | 1982-1989 | 6 (dD); 1 (d18O) |
| Jackpot, NV | BR | 41.4717 | -114.6583 | 1590 | 7.0 | 26.8 | 0.91 | -15.6 | Friedman et al., 2002 | 1991-1997 | 4 (dD); 3 (d18O) |
| Joshua Tree, CA | BR* | 34.0200 | -116.1900 | 1280 | 15.0 | 30.9 | 2.36 | -10.8 | Friedman et al., 1992 | 1982-1989 | 6 (dD); 2 (d18O) |
| Lakeview, OR | BR | 42.1617 | -120.3983 | 1441 | 7.2 | 39.8 | 1.99 | -13.3 | Friedman et al., 2002 | 1991-1997 | 4 (dD); 2 (d18O) |
| Lehman Caves, NV | BR | 39.0100 | -114.2200 | 2067 | 8.0 | 32.2 | 0.93 | -11.0 | USNIP | 1989-2001 | NR |
| Leviathan Peak | BR | 38.6733 | -119.6067 | 2485 | 6.8 | 69.3 | 3.44 | -15.7 | Friedman and Smith, 1972 | 1970-71 | 2 |
| Logan, UT | BR | 41.6600 | -111.9000 | 1370 | 8.3 | 47.5 | 1.27 | -14.8 | USNIP | 1989-2001 | NR |
| Lone Pine, CA | BR* | 36.5900 | -118.0517 | 1130 | 14.7 | 18.0 | 3.79 | -12.3 | Friedman et al., 1992 | 1982-1989 | 4 (dD); 2 (d18O) |
| McDermitt, OR | BR | 42.0017 | -117.7217 | 1366 | 8.3 | 24.4 | 1.28 | -15.4 | Friedman et al., 2002 | 1991-1997 | 4 (dD); 3 (d18O) |
| Middle Canyon, UT | BR | 40.4617 | -112.1917 | 2134 | 5.2 | 76.7 | 1.71 | -14.9 | Friedman et al., 2002 | 1991-1997 | 6 (dD); 4 (d18O) |
| Mitchell Caverns, CA | BR* | 34.9433 | -115.5117 | 1315 | 17.3 | 24.0 | 1.40 | -11.5 | Friedman et al., 1992 | 1982-1989 | 5 (dD); 1 (d18O) |
| Mount Hamilton, NV | BR | 39.2400 | -115.5400 | 3216 | 6.7 | 53.5 | 1.26 | -14.2 | Friedman et al., 2002 | 1991-1997 | 2 (dD); 1 (d18O) |
| Mount Moriah, NV | BR | 39.3183 | -114.2383 | 2858 | 4.7 | 49.2 | 1.15 | -16.3 | Friedman et al., 2002 | 1991-1997 | 3 (dD); 1 (d18O) |
| Mount Wilson, NV | BR | 38.2400 | -114.3883 | 2804 | 8.0 | 47.6 | 1.22 | -14.7 | Friedman et al., 2002 | 1991-1997 | 3 (dD); 2 (d18O) |
| Needles, CA | BR* | 34.7700 | -114.6200 | 295 | 21.7 | 11.6 | 1.37 | -8.3 | Friedman et al., 1992 | 1982-1989 | 5 (dD); 2 (d18O) |
| Organ Pipe Cactus Nat'l Mon. | BR* | 31.9500 | -112.8000 | 506 | 20.6 | 23.0 | 0.76 | -8.6 | USNIP | 1989-2001 | NR |
| Owyhee, NV | BR | 41.9533 | -116.1867 | 1638 | 7.2 | 30.7 | 1.34 | -13.5 | Friedman et al., 2002 | 1991-1997 | 1 (dD); 1 (d18O) |
| Parker, NV | BR* | 34.1517 | -114.2717 | 135 | 22.8 | 12.1 | 1.46 | -8.3 | Friedman et al., 1992 | 1982-1989 | 6 (dD); 2 (d18O) |
| Pine Mountain, OR | BR | 43.7917 | -120.9400 | 1920 | 6.6 | 54.0 | 2.06 | -15.7 | Friedman et al., 2002 | 1991-1997 | 4 (dD); 3 (d18O) |
| Potosi Peak, NV | BR* | 35.9450 | -115.5000 | 2463 | 11.6 | 38.4 | 1.56 | -12.9 | Friedman et al., 2002 | 1991-1997 | 5 (dD); 3 (d18O) |
| PT1 | BR | 37.2811 | -116.3016 | 2200 | 9.4 | 26.5 | 1.38 | -12.5 | Ingraham et al., 1991 | 1982-1986 | NR |
| PT2 | BR | 37.2854 | -116.3529 | 2060 | 9.4 | 24.9 | 1.35 | -13.2 | Ingraham et al., 1991 | 1982-1986 | NR |
| PT3 | BR | 37.2240 | -116.4576 | 1890 | 10.7 | 22.0 | 1.37 | -12.2 | Ingraham et al., 1991 | 1982-1986 | NR |
| Randsburg, CA | BR* | 35.3533 | -117.6667 | 1340 | 17.2 | 20.2 | 4.43 | -10.6 | Friedman et al., 1992 | 1982-1989 | 6 (dD); 2 (d18O) |
| Red Rock Canyon, NV | BR* | 36.1400 | -115.4300 | 1137 | 15.8 | 16.4 | 1.33 | -9.7 | USNIP | 1989-2001 | NR |
| Rowland Creek | BR | 40.0133 | -120.2933 | 2040 | 6.6 | 60.6 | 2.94 | -14.5 | Friedman and Smith, 1972 | 1970-71 | 2 |
| RT1 | BR | 37.2038 | -116.2054 | 2230 | 10.4 | 28.5 | 1.42 | -12.7 | Ingraham et al., 1991 | 1982-1986 | NR |
| RT2 | BR | 37.1598 | -116.2179 | 1900 | 11.3 | 24.4 | 1.40 | -12.9 | Ingraham et al., 1991 | 1982-1986 | NR |
| RT3 | BR | 37.1316 | -116.2894 | 1590 | 11.4 | 19.3 | 1.41 | -11.0 | Ingraham et al., 1991 | 1982-1986 | NR |
| SB1 | BR | 36.8566 | -115.9508 | 960 | 16.1 | 13.4 | 1.54 | -9.5 | Ingraham et al., 1991 | 1982-1986 | NR |
| Searchlight, NV | BR* | 35.4417 | -114.9000 | 1040 | 18.3 | 18.0 | 1.25 | -10.5 | Friedman et al. 1992, 2002 | 1983-1988; 1991-1997 | 11 (dD); 5 (d18O) |
| Sheep Peak, NV | BR* | 36.5833 | -115.2500 | 2926 | 6.6 | 49.4 | 1.53 | -13.0 | Friedman et al., 2002 | 1991-1997 | 2 (dD); 1 (d18O) |
| Smith Valley, NV | BR | 38.8000 | -119.2600 | 1501 | 9.6 | 18.5 | 1.48 | -16.0 | USNIP | 1989-2001 | NR |
| ST1 | BR | 36.9454 | -116.2591 | 2133 | 12.0 | 24.8 | 1.50 | -12.5 | Ingraham et al., 1991 | 1982-1986 | NR |
| ST2 | BR | 36.9396 | -116.2504 | 1830 | 12.2 | 23.0 | 1.49 | -12.4 | Ingraham et al., 1991 | 1982-1986 | NR |
| ST3 | BR* | 36.1929 | -116.2648 | 1520 | 17.5 | 12.1 | 1.74 | -11.7 | Ingraham et al., 1991 | 1982-1986 | NR |
| ST4 | BR | 36.8501 | -116.2684 | 1225 | 16.0 | 15.0 | 1.61 | -11.6 | Ingraham et al., 1991 | 1982-1986 | NR |
| Susanville, CA | BR | 40.6533 | -120.7683 | 1558 | 7.2 | 47.0 | 2.53 | -13.8 | Friedman et al., 2002 | 1991-1997 | 2 (dD); 2 (d18O) |
| Tonopah, NV | BR | 38.0600 | -117.0867 | 1654 | 10.6 | 13.8 | 0.79 | -13.4 | Friedman et al., 2002 | 1991-1997 | 5 (dD); 4 (d18O) |

## Table A2.1 – Compilation of western US precipitation $\delta^{18}O$ records

| Location | Subregion | LAT (º) | LON (º) | ELEV (m) | MAT (ºC) | MAP (cm) | W:S | Wgt. $\delta^{18}O$ (‰ SMOW) | Reference | Sample Period | Number of seasons |
|---|---|---|---|---|---|---|---|---|---|---|---|
| Tooele, UT | BR | 40.6117 | -112.3500 | 1518 | 10.5 | 35.0 | 1.08 | -14.7 | Friedman et al., 2002 | 1991-1997 | 5 (dD); 4 (d18O) |
| Trona, CA | BR* | 35.8117 | -117.3267 | 525 | 18.7 | 9.1 | 2.62 | -8.9 | Friedman et al., 1992 | 1982-1989 | 6 (dD); 2 (d18O) |
| TT1 | BR | 37.0587 | -116.4445 | 1840 | 12.0 | 22.1 | 1.44 | -10.3 | Ingraham et al., 1991 | 1982-1986 | NR |
| TT2 | BR | 37.0494 | -116.3854 | 1630 | 11.7 | 19.3 | 1.44 | -11.3 | Ingraham et al., 1991 | 1982-1986 | NR |
| TT3 | BR | 37.0465 | -116.3233 | 1400 | 12.2 | 16.7 | 1.49 | -11.4 | Ingraham et al., 1991 | 1982-1986 | NR |
| Twentynine Palms, CA | BR* | 34.1283 | -115.9450 | 570 | 19.9 | 11.3 | 1.09 | -8.7 | Friedman et al., 1992 | 1982-1989 | 6 (dD); 2 (d18O) |
| Wendover, UT | BR | 40.7183 | -114.0300 | 1292 | 10.1 | 14.6 | 0.66 | -12.8 | Friedman et al., 2002 | 1991-1997 | 5 (dD); 3 (d18O) |
| White Mountain, CA | BR* | 37.3517 | -118.1833 | 2697 | 6.7 | 32.3 | 2.23 | -16.0 | Friedman et al., 2002 | 1991-1997 | 4 (dD); 3 (d18O) |
| Winnemucca, NC | BR | 40.8967 | -117.8050 | 1312 | 9.4 | 20.5 | 1.41 | -14.3 | Friedman et al., 2002 | 1991-1997 | 5 (dD); 2 (d18O) |
| Yuma, AZ | BR* | 32.6567 | -114.6067 | 65 | 22.8 | 7.9 | 1.13 | -8.7 | Friedman et al., 1992 | 1982-1989 | 6 (dD); 2 (d18O) |
| Brian Head, UT | RMCP | 37.6800 | -112.8450 | 3002 | 3.6 | 64.1 | 1.24 | -15.5 | Friedman et al., 2002 | 1991-1997 | 4 (dD); 2 (d18O) |
| Brooklyn Lake, WY | RMCP | 41.3600 | -106.2400 | 3212 | -0.5 | 58.1 | 0.91 | -16.3 | USNIP | 1989-2001 | NR |
| Bryce Canyon Nat'l Park, UT | RMCP | 37.6200 | -112.1700 | 2477 | 6.0 | 36.0 | 0.87 | -11.8 | USNIP | 1989-2001 | NR |
| Deer Valley, UT | RMCP | 40.6367 | -111.4950 | 2195 | 4.8 | 67.6 | 1.65 | -15.1 | Friedman et al., 2002 | 1991-1997 | 6 (dD); 4 (d18O) |
| Flagstaff, AZ | RMCP* | 35.1300 | -111.6700 | 2137 | 8.1 | 56.6 | 1.13 | -9.6 | GNIP | 1962-1969 | 8 |
| Gila Cliff Dwellings Nat'l Mon., NM | RMCP | 33.2200 | -108.2300 | 1772 | 11.7 | 41.2 | 0.48 | -8.2 | USNIP | 1989-2001 | NR |
| Glacier Nat'l Park, MT | RMCP | 48.5100 | -113.9900 | 968 | 5.0 | 69.3 | 1.13 | -18.3 | USNIP | 1989-2001 | NR |
| Grand Canyon Nat'l Park | RMCP | 36.0700 | -112.1600 | 2152 | 14.6 | 41.8 | 1.13 | -7.3 | USNIP | 1989-2001 | NR |
| Hanksville, UT | RMCP | 38.4183 | -110.7033 | 1170 | 11.7 | 15.2 | 0.65 | -12.6 | Friedman et al., 2002 | 1991-1997 | 5 (dD); 3 (d18O) |
| Little Bighorn Nat'l Mon, MT | RMCP | 45.5700 | -107.4400 | 957 | 8.3 | 38.3 | 0.59 | -14.5 | USNIP | 1989-2001 | NR |
| Lost Trail Pass, MT | RMCP | 45.6900 | -113.9700 | 2414 | 2.5 | 48.9 | 0.84 | -16.3 | USNIP | 1989-2001 | NR |
| Mayhill, NM | RMCP | 32.9100 | -105.4700 | 2009 | 10.6 | 44.1 | 0.34 | -10.6 | USNIP | 1989-2001 | NR |
| Mesa Verde Nat'l Park, CO | RMCP | 37.2000 | -108.4900 | 2172 | 9.8 | 44.0 | 1.02 | -11.0 | USNIP | 1989-2001 | NR |
| Niwot Saddle, CO | RMCP | 40.0600 | -105.5900 | 3520 | 1.2 | 78.3 | 1.10 | -14.3 | USNIP | 1989-2001 | NR |
| Oliver Knoll, AZ | RMCP* | 33.0700 | -109.9400 | 1173 | 16.9 | 32.0 | 0.73 | -6.8 | USNIP | 1989-2001 | NR |
| Palouse Conservation Farm, WA | RMCP | 46.7600 | -117.1800 | 766 | 8.3 | 54.9 | 1.87 | -12.1 | USNIP | 1989-2001 | NR |
| Pinedale, WY | RMCP | 42.9200 | -109.8000 | 2388 | 1.7 | 30.2 | 0.67 | -14.7 | USNIP | 1989-2001 | NR |
| Price, UT | RMCP | 39.6067 | -110.7483 | 1804 | 9.0 | 26.4 | 0.77 | -15.1 | Friedman et al., 2002 | 1991-1997 | 4 (dD); 2 (d18O) |
| Sand Spring, CO | RMCP | 40.5100 | -107.7000 | 1998 | 6.1 | 42.0 | 0.97 | -12.0 | USNIP | 1989-2001 | NR |
| Smith's Ferry, ID | RMCP | 44.3000 | -116.0600 | 1442 | 5.0 | 60.0 | 2.03 | -15.1 | USNIP | 1989-2001 | NR |
| Starkey Exp. Forest, OR | RMCP | 45.2200 | -118.5100 | 1253 | 6.4 | 62.6 | 2.03 | -13.2 | USNIP | 1989-2001 | NR |
| Wolf Creek Pass, CO | RMCP | 37.4700 | -106.7900 | 3292 | 1.6 | 93.9 | 1.17 | -17.4 | USNIP | 1989-2001 | NR |
| Yellowstone Nat'l Park, WY | RMCP | 44.9200 | -110.4200 | 1912 | 2.3 | 43.8 | 0.67 | -20.9 | USNIP | 1989-2001 | NR |
| Amarillo, TX | GP | 35.2200 | -101.8300 | 1090 | 13.9 | 49.2 | 0.29 | -8.1 | Nativ & Riggio, 1990 | Oct 1984 - Nov 1985 | NR |
| Ames, IA | GP | 42.0272 | -93.6317 | 287 | 9.4 | 83.5 | 0.42 | -8.0 | Simpkins, 1995 | | NR |
| Attwater Prairie Chicken Refuge, TX | GP | 29.6600 | -96.2600 | 54 | 20.6 | 104.3 | 0.74 | -2.8 | USNIP | 1989-2001 | NR |
| Beeville, TX | GP | 28.4700 | -97.7100 | 82 | 21.7 | 78.0 | 0.52 | -4.0 | USNIP | 1989-2001 | NR |
| Caddo Valley, AR | GP | 34.1800 | -93.1000 | 71 | 16.7 | 136.8 | 1.08 | -4.9 | USNIP | 1989-2001 | NR |
| Capulin Volcano Nat'l Mon., NM | GP | 36.7800 | -103.9800 | 2205 | 9.4 | 48.3 | 0.33 | -10.8 | USNIP | 1989-2001 | NR |
| Clovis, NM | GP | 34.4050 | -103.2050 | 1300 | 13.9 | 41.1 | 0.25 | -8.8 | Nativ & Riggio, 1990 | Oct 1984 - Nov 1985 | NR |

**Table A2.1 – Compilation of western US precipitation $\delta^{18}O$ records**

| Location | Subregion | LAT (°) | LON (°) | ELEV (m) | MAT (°C) | MAP (cm) | W:S | Wgt. $\delta^{18}O$ (‰ SMOW) | Reference | Sample Period | Number of seasons |
|---|---|---|---|---|---|---|---|---|---|---|---|
| Cottonwood, SD | GP | 43.9500 | -101.8600 | 733 | 8.3 | 42.3 | 0.37 | -9.7 | USNIP | 1989-2001 | NR |
| Goodwell Research Station, OK | GP | 36.5900 | -101.6200 | 999 | 13.9 | 43.8 | 0.30 | -7.8 | USNIP | 1989-2001 | NR |
| Great Plains Apiaries, OK | GP | 34.9800 | -97.5200 | 331 | 16.1 | 90.6 | 0.60 | -5.8 | USNIP | 1989-2001 | NR |
| Huron Well Field, SD | GP | 44.3600 | -98.2900 | 398 | 7.2 | 51.4 | 0.40 | -7.1 | USNIP | 1989-2001 | NR |
| Icelandic State Park, ND | GP | 48.7800 | -97.7500 | 306 | 3.5 | 47.6 | 0.31 | -9.7 | USNIP | 1989-2001 | NR |
| Konza Prairie, KS | GP | 39.1000 | -96.6100 | 350 | 12.4 | 86.2 | 0.39 | -10.5 | USNIP | 1989-2001 | NR |
| Ladue, MO | GP | 38.6300 | -90.3700 | 187 | 12.8 | 97.4 | 0.86 | -7.7 | Fredrickson & Criss, 1999 | June 1995-May 1998 | NR |
| Lake Geneva, WI | GP | 42.5800 | -88.5000 | 288 | 8.3 | 90.3 | 0.61 | -7.8 | USNIP | 1989-2001 | NR |
| Lake Scott State Park, KS | GP | 38.6700 | -100.9200 | 863 | 11.7 | 48.9 | 0.35 | -10.2 | USNIP | 1989-2001 | NR |
| Lamberton, MN | GP | 44.2400 | -95.3000 | 343 | 7.2 | 65.9 | 0.41 | -8.6 | USNIP | 1989-2001 | NR |
| LBJ National Grasslands, TX | GP | 33.3900 | -97.6400 | 312 | 18.3 | 86.7 | 0.65 | -4.3 | USNIP | 1989-2001 | NR |
| Lubbock, TX | GP | 33.5000 | -101.8730 | 975 | 15.6 | 47.5 | 0.29 | -7.2 | Nativ & Riggio, 1990 | Oct 1984 - Nov 1985 | NR |
| Mead, NE | GP | 41.1520 | -96.4910 | 352 | 10.6 | 78.0 | 0.40 | -7.4 | Harvey, 2001 | | NR |
| Midland, TX | GP | 32.0000 | -102.1000 | 850 | 17.2 | 39.4 | 0.31 | -6.5 | Nativ & Riggio, 1990 | Oct 1984 - Nov 1985 | NR |
| Morcell Experimental Forest | GP | 47.5300 | -93.4700 | 431 | 3.9 | 68.8 | 0.32 | -14.9 | USNIP | 1989-2001 | NR |
| Newcastle, WY | GP | 43.8700 | -104.1900 | 1466 | 7.3 | 42.8 | 0.41 | -17.9 | USNIP | 1989-2001 | NR |
| North Platte Agr. Station, NE | GP | 41.0600 | -100.7500 | 919 | 9.4 | 50.5 | 0.34 | -9.6 | USNIP | 1989-2001 | NR |
| Paducah, TX | GP | 34.0100 | -100.3000 | 560 | 17.2 | 56.5 | 0.39 | -6.5 | Nativ & Riggio, 1990 | Oct 1984 - Nov 1985 | NR |
| Pawnee National Grasslands, CO | GP | 40.8063 | -104.7547 | 1641 | 8.3 | 36.4 | 0.40 | -10.6 | Harvey, 2005 | 1994-1998 | NR |
| Salt Plains Nat'k Wildlfe Refuge, OK | GP | 36.8100 | -98.2000 | 345 | 15.0 | 72.1 | 0.50 | -8.7 | USNIP | 1989-2001 | NR |
| Sparkling Lake, WI | GP | 46.0010 | -89.6990 | 150 | 3.9 | 81.5 | 0.44 | -10.9 | Krabbenhoft, 1990 | Nov 1985 - Aug 1987 | NR |
| Theodore Roosevelt Nat'l Park, ND | GP | 47.6000 | -103.2600 | 611 | 6.0 | 38.8 | 0.31 | -10.1 | USNIP | 1989-2001 | NR |
| Trout Lake, WI | GP | 46.0500 | -89.6500 | 501 | 3.9 | 82.0 | 0.45 | -14.4 | USNIP | 1989-2001 | NR |
| Waco, TX | GP | 31.6200 | -97.2200 | 143 | 19.4 | 82.1 | 0.81 | -4.3 | GNIP | 1962-1965, 1973-1976 | 7 |

**Table A2.1 Notes –** Modern precipitation $\delta^{18}O$ records compiled from various published sources (see 'Reference' column). Reported $\delta^{18}O$ values are annual weighted mean values. In cases where weighted mean annual values were not provided, $\delta^{18}O$ values were calculated as part of this study using reported precipitation amounts (see text for discussion). Latitude (LAT), longitude (LON), and elevation (ELEV) values were extracted using the USGS ETOPO30 digital elevation model (DEM) in cases where geographic coordinates and elevations were not reported in the original reference. MAT and MAP values were obtained from the Matsuura and Wilmott dataset (http://climate.geog.udel.edu/~climate/) for sites with no climate parameters reported. The Matsuura and Wilmott dataset was also used for calculation of W:S values. Subregion abbreviations: BR = Basin and Range; RMCP = Rocky Mountains-Colorado Plateau; GP = Great Plains. Subregion labels with an asterisk (*) indicate sites that were also part of the 'Coast-Gulf of CA' subregion analysis. Sites in the RMCP and BR subregions were included in the 'Continental Interior' analysis. NR = not reported.

## Table A2.2 – Compilation of east Asia meteoric water $\delta^{18}O$ records

| Location | Subregion | LAT (º) | LON (º) | Site ELEV (m) | Ppt ELEV (m) | MAT (ºC) | MAP (cm) | Wgt. $\delta^{18}O$ (‰ SMOW) | Reference | Record length |
|---|---|---|---|---|---|---|---|---|---|---|
| Beijing | eastern Asia | 39.9200 | 116.4600 | 43 | 43 | -3.4 | 59.5 | -8.8 | Liu et al. (2008) | 1979-1980 |
| Changchun | eastern Asia | 43.9000 | 125.2200 | 273 | 273 | -16.2 | 60.2 | -10.1 | Liu et al. (2008) | 2000 |
| Changsha | eastern Asia | 28.1200 | 113.0400 | 37 | 37 | 17.2 | 127.1 | -5.7 | Liu et al. (2008) | 1988-1992 |
| Chengdu | eastern Asia | 30.6700 | 104.0200 | 506 | 506 | 15.7 | 88.8 | -7.5 | Araguás-Araguás et al. (1998) | 45 months |
| Fuzhou | eastern Asia | 26.0500 | 119.1700 | 16 | 16 | 19.6 | 142.3 | -6.9 | Average of Liu et al. (2008) and Johnson and Ingram (2004) | 71 months |
| Gaoling | eastern Asia | 34.5500 | 109.1000 | 378 | 378 | 1.2 | 51.1 | -7.1 | Liu et al. (2008) | 1986-1987 |
| Guangzhou | eastern Asia | 23.1300 | 113.3200 | 7 | 7 | 22.2 | 172.4 | -5.8 | Liu et al. (2008) | 1986-1989 |
| Guilin | eastern Asia | 25.0700 | 110.0800 | 170 | 170 | 19.2 | 148.7 | -6.2 | Liu et al. (2008) | 1983-1990 |
| Guiyang | eastern Asia | 26.3500 | 106.4300 | 1071 | 1071 | 15.2 | 91.0 | -8.3 | Liu et al. (2008) | 1988-1992 |
| Haerbin | eastern Asia | 45.6800 | 126.6200 | 172 | 172 | -18.6 | 57.0 | -10.2 | Liu et al. (2008) | 1986-1989 |
| Haikou | eastern Asia | 20.0200 | 110.2100 | 15 | 15 | 25.3 | 165.8 | -6.1 | Liu et al. (2008) | 1988-1997 |
| Hongkong | eastern Asia | 22.3200 | 114.1700 | 66 | 66 | 22.9 | 189.3 | -6.6 | Liu et al. (2008) | 1973-2001 |
| Jinzhou | eastern Asia | 41.1300 | 121.1000 | 66 | 66 | -9.6 | 56.7 | -8.5 | Liu et al. (2008) | 1987 |
| Kunming | eastern Asia | 23.0200 | 102.6800 | 1841 | 1841 | 15.0 | 94.2 | -10.4 | Araguás-Araguás et al. (1998) | 67 months |
| Liuzhou | eastern Asia | 24.3500 | 109.4000 | 97 | 97 | 20.9 | 104.1 | -6.5 | Liu et al. (2008) | 1988-1992 |
| Luang-Prabang | eastern Asia | 19.8800 | 102.1300 | 305 | 305 | 25.7 | 122.9 | -7.5 | Araguás-Araguás et al. (1998) | 26 months |
| Nanjing | eastern Asia | 32.1800 | 118.1800 | 26 | 26 | 4.6 | 110.8 | -8.4 | Araguás-Araguás et al. (1998) | 58 months |
| Nanzheng | eastern Asia | 33.0000 | 106.9300 | 458 | 458 | -0.4 | 86.9 | -7.1 | Liu et al. (2008) | 1986-1987 |
| Qiqihar | eastern Asia | 47.2300 | 123.5500 | 147 | 147 | 4.3 | 58.1 | -10.6 | Liu et al. (2008) | 1988-1992 |
| Shanghai | eastern Asia | 31.2200 | 121.4800 | 4 | 4 | 6.8 | 107.1 | -7.5 | Liu et al. (2008) | 1979-1980 |
| Shijiazuang | eastern Asia | 38.0200 | 114.2500 | 80 | 80 | 13.1 | 55.1 | -7.8 | Araguás-Araguás et al. (1998) | 76 months |
| Taiyuan | eastern Asia | 37.7800 | 112.5500 | 778 | 778 | 10.3 | 41.5 | -8.5 | Liu et al. (2008) | 1985-1992 |
| Tangchong | eastern Asia | 25.0100 | 98.3000 | 1648 | 1648 | 6.3 | 156.0 | -8.4 | Liu et al. (2008) | 1985 |
| Tianjin | eastern Asia | 39.0600 | 117.1000 | 3 | 3 | -4.0 | 52.3 | -7.7 | Liu et al. (2008) | 1995-1999 |
| Wuhan | eastern Asia | 30.6200 | 114.1300 | 23 | 23 | 16.4 | 105.1 | -6.7 | Liu et al. (2008) | 1996-1998 |
| Xian | eastern Asia | 34.3000 | 108.9300 | 397 | 397 | 13.5 | 51.9 | -7.4 | Liu et al. (2008) | 1985-1992 |
| Yanan | eastern Asia | 36.6000 | 109.4700 | 1020 | 1020 | -3.8 | 54.1 | -7.2 | Liu et al. (2008) | 1986-1987 |
| Yantai | eastern Asia | 37.5300 | 121.4000 | 47 | 47 | 13.1 | 56.8 | -7.2 | Liu et al. (2008) | 1986-1991 |
| Zhengzhou | eastern Asia | 34.7200 | 113.6500 | 110 | 110 | 14.2 | 53.6 | -7.6 | Araguás-Araguás et al. (1998) | 57 months |
| Zunyi | eastern Asia | 27.7000 | 106.8800 | 844 | 844 | 15.4 | 95.8 | -8.3 | Liu et al. (2008) | 1986-1992 |
| 04Tibet66 | Himalaya-S. Tibet | 29.3077 | 94.3473 | 2969 | 2969 | -0.4 | 68.0 | -11.2 | Hren et al. (2009) | Stream/tributary |
| 04Tibet67 | Himalaya-S. Tibet | 29.6162 | 94.9410 | 5037 | 5037 | 0.3 | 95.0 | -14.7 | Hren et al. (2009) | Stream/tributary |
| 04Tibet68 | Himalaya-S. Tibet | 29.6064 | 94.9410 | 5183 | 5183 | 0.2 | 75.0 | -14.8 | Hren et al. (2009) | Stream/tributary |
| 04Tibet72a | Himalaya-S. Tibet | 29.5203 | 94.8817 | 3587 | 3587 | -1.4 | 38.0 | -13.6 | Hren et al. (2009) | Stream/tributary |
| 05Tibet100 | Himalaya-S. Tibet | 29.2193 | 92.0144 | 4717 | 4717 | 3.7 | 42.0 | -17.2 | Hren et al. (2009) | Stream/tributary |
| 05Tibet101 | Himalaya-S. Tibet | 29.2787 | 92.0265 | 4884 | 4884 | 3.8 | 35.0 | -17.2 | Hren et al. (2009) | Stream/tributary |
| 05Tibet103 | Himalaya-S. Tibet | 29.1352 | 91.7949 | 4711 | 4711 | 3.4 | 39.0 | -17.0 | Hren et al. (2009) | Stream/tributary |
| 05Tibet38 | Himalaya-S. Tibet | 30.0089 | 94.9744 | 2705 | 2705 | -1.8 | 53.0 | -13.7 | Hren et al. (2009) | Stream/tributary |
| 05Tibet39 | Himalaya-S. Tibet | 30.0089 | 94.9578 | 3548 | 3548 | -1.8 | 100.0 | -10.5 | Hren et al. (2009) | Stream/tributary |
| 05Tibet40 | Himalaya-S. Tibet | 29.9969 | 94.9239 | 3866 | 3866 | -1.6 | 82.0 | -11.6 | Hren et al. (2009) | Stream/tributary |
| 05Tibet41 | Himalaya-S. Tibet | 30.0034 | 94.8965 | 3657 | 3657 | -1.6 | 87.0 | -11.4 | Hren et al. (2009) | Stream/tributary |
| 05Tibet42 | Himalaya-S. Tibet | 29.9984 | 94.8811 | 4057 | 4057 | -1.6 | 81.0 | -13.1 | Hren et al. (2009) | Stream/tributary |
| 05Tibet43 | Himalaya-S. Tibet | 29.9866 | 94.8726 | 3430 | 3430 | -1.5 | 109.0 | -12.2 | Hren et al. (2009) | Stream/tributary |
| 05Tibet44 | Himalaya-S. Tibet | 29.9617 | 94.8470 | 3897 | 3897 | -1.4 | 110.0 | -12.8 | Hren et al. (2009) | Stream/tributary |
| 05Tibet45 | Himalaya-S. Tibet | 29.9561 | 94.8138 | 3357 | 3357 | -1.4 | 109.0 | -13.0 | Hren et al. (2009) | Stream/tributary |
| 05Tibet46 | Himalaya-S. Tibet | 29.9484 | 94.8026 | 4075 | 4075 | -1.4 | 87.0 | -13.6 | Hren et al. (2009) | Stream/tributary |

## Table A2.2 – Compilation of east Asia meteoric water $\delta^{18}O$ records

| Location | Subregion | LAT (º) | LON (º) | Site ELEV (m) | Ppt ELEV (m) | MAT (ºC) | MAP (cm) | Wgt. $\delta^{18}O$ (‰ SMOW) | Reference | Record length |
|---|---|---|---|---|---|---|---|---|---|---|
| 05Tibet47 | Himalaya-S. Tibet | 29.9491 | 94.8032 | 4278 | 4278 | -1.4 | 48.0 | -14.0 | Hren et al. (2009) | Stream/tributary |
| 05Tibet49 | Himalaya-S. Tibet | 29.7328 | 94.7269 | 4384 | 4384 | -1.4 | 41.0 | -11.9 | Hren et al. (2009) | Stream/tributary |
| 05Tibet50 | Himalaya-S. Tibet | 29.9110 | 94.7973 | 3754 | 3754 | -1.3 | 93.0 | -13.2 | Hren et al. (2009) | Stream/tributary |
| 05Tibet51 | Himalaya-S. Tibet | 29.8999 | 94.7901 | 3950 | 3950 | -1.2 | 104.0 | -13.2 | Hren et al. (2009) | Stream/tributary |
| 05Tibet52 | Himalaya-S. Tibet | 29.8814 | 94.7844 | 4136 | 4136 | -1.2 | 93.0 | -13.8 | Hren et al. (2009) | Stream/tributary |
| 05Tibet53 | Himalaya-S. Tibet | 29.8466 | 94.7557 | 3994 | 3994 | -1.3 | 87.0 | -13.6 | Hren et al. (2009) | Stream/tributary |
| 05Tibet54 | Himalaya-S. Tibet | 29.8287 | 94.7412 | 4057 | 4057 | -1.3 | 79.0 | -13.8 | Hren et al. (2009) | Stream/tributary |
| 05Tibet55 | Himalaya-S. Tibet | 29.8166 | 94.7418 | 3677 | 3677 | -1.3 | 90.0 | -14.0 | Hren et al. (2009) | Stream/tributary |
| 05Tibet56 | Himalaya-S. Tibet | 29.7666 | 94.7394 | 4263 | 4263 | -1.2 | 69.0 | -13.6 | Hren et al. (2009) | Stream/tributary |
| 05Tibet57 | Himalaya-S. Tibet | 29.6686 | 94.7139 | 4346 | 4346 | -2.1 | 39.0 | -11.0 | Hren et al. (2009) | Stream/tributary |
| 05Tibet58 | Himalaya-S. Tibet | 29.6419 | 94.6970 | 4484 | 4484 | -2.3 | 35.0 | -11.0 | Hren et al. (2009) | Stream/tributary |
| 05Tibet63 | Himalaya-S. Tibet | 29.4319 | 94.5379 | 3970 | 3970 | -2.6 | 29.0 | -13.2 | Hren et al. (2009) | Stream/tributary |
| 05Tibet63a | Himalaya-S. Tibet | 29.4378 | 94.5447 | 3704 | 3704 | -2.7 | 33.0 | -12.7 | Hren et al. (2009) | Stream/tributary |
| 05Tibet65 | Himalaya-S. Tibet | 29.3436 | 94.4162 | 4049 | 4049 | -1.4 | 26.0 | -11.6 | Hren et al. (2009) | Stream/tributary |
| 05Tibet69 | Himalaya-S. Tibet | 29.6013 | 94.9374 | 4445 | 4445 | 0.2 | 30.0 | -14.3 | Hren et al. (2009) | Stream/tributary |
| 05Tibet70 | Himalaya-S. Tibet | 29.5449 | 94.8925 | 3173 | 3173 | -1.0 | 142.0 | -13.1 | Hren et al. (2009) | Stream/tributary |
| 05Tibet71 | Himalaya-S. Tibet | 29.5254 | 94.8898 | 3050 | 3050 | -1.2 | 158.0 | -12.3 | Hren et al. (2009) | Stream/tributary |
| 05Tibet72 | Himalaya-S. Tibet | 29.5145 | 94.8810 | 4179 | 4179 | -1.5 | 37.0 | -11.9 | Hren et al. (2009) | Stream/tributary |
| 05Tibet73 | Himalaya-S. Tibet | 29.4611 | 94.8288 | 3965 | 3965 | -3.2 | 36.0 | -12.5 | Hren et al. (2009) | Stream/tributary |
| 05Tibet74 | Himalaya-S. Tibet | 29.4412 | 94.8326 | 4370 | 4370 | -3.2 | 46.0 | -12.6 | Hren et al. (2009) | Stream/tributary |
| 05Tibet75 | Himalaya-S. Tibet | 29.4627 | 94.6502 | 2950 | 2950 | -3.9 | 65.0 | -12.4 | Hren et al. (2009) | Stream/tributary |
| 05Tibet76 | Himalaya-S. Tibet | 29.4573 | 94.8157 | 4142 | 4142 | -3.5 | 35.0 | -13.0 | Hren et al. (2009) | Stream/tributary |
| 05Tibet77 | Himalaya-S. Tibet | 29.2394 | 94.2477 | 3965 | 3965 | 1.1 | 34.0 | -10.4 | Hren et al. (2009) | Stream/tributary |
| 05Tibet78 | Himalaya-S. Tibet | 29.1859 | 94.1913 | 3762 | 3762 | 0.0 | 61.0 | -9.8 | Hren et al. (2009) | Stream/tributary |
| 05Tibet79 | Himalaya-S. Tibet | 29.1908 | 94.1276 | 4127 | 4127 | -1.3 | 23.0 | -12.0 | Hren et al. (2009) | Stream/tributary |
| 05Tibet80 | Himalaya-S. Tibet | 29.1896 | 94.0588 | 4136 | 4136 | -2.7 | 24.0 | -13.4 | Hren et al. (2009) | Stream/tributary |
| 05Tibet81 | Himalaya-S. Tibet | 29.1849 | 93.9523 | 4304 | 4304 | -4.9 | 37.0 | -13.9 | Hren et al. (2009) | Stream/tributary |
| 05Tibet82 | Himalaya-S. Tibet | 29.1185 | 93.8697 | 4349 | 4349 | -6.1 | 25.0 | -12.4 | Hren et al. (2009) | Stream/tributary |
| 05Tibet84 | Himalaya-S. Tibet | 29.1158 | 93.9103 | 4366 | 4366 | -5.3 | 24.0 | -13.6 | Hren et al. (2009) | Stream/tributary |
| 05Tibet85 | Himalaya-S. Tibet | 29.1251 | 93.7403 | 3640 | 3640 | -8.4 | 38.0 | -14.7 | Hren et al. (2009) | Stream/tributary |
| 05Tibet86 | Himalaya-S. Tibet | 29.1483 | 93.6335 | 4503 | 4503 | -8.6 | 22.0 | -15.1 | Hren et al. (2009) | Stream/tributary |
| 05Tibet87 | Himalaya-S. Tibet | 29.1040 | 93.4454 | 4595 | 4595 | -8.3 | 32.0 | -15.4 | Hren et al. (2009) | Stream/tributary |
| 05Tibet89 | Himalaya-S. Tibet | 28.9996 | 93.3206 | 4543 | 4543 | -8.0 | 24.0 | -13.9 | Hren et al. (2009) | Stream/tributary |
| 05Tibet90 | Himalaya-S. Tibet | 28.9987 | 93.2337 | 4693 | 4693 | -8.1 | 29.0 | -15.2 | Hren et al. (2009) | Stream/tributary |
| 05Tibet91 | Himalaya-S. Tibet | 29.0128 | 93.1651 | 4399 | 4399 | -8.1 | 34.0 | -15.6 | Hren et al. (2009) | Stream/tributary |
| 05Tibet92 | Himalaya-S. Tibet | 29.0442 | 93.0764 | 4445 | 4445 | -7.9 | 30.0 | -14.4 | Hren et al. (2009) | Stream/tributary |
| 05Tibet93 | Himalaya-S. Tibet | 29.0448 | 92.9994 | 4229 | 4229 | -7.8 | 42.0 | -15.5 | Hren et al. (2009) | Stream/tributary |
| 05Tibet95 | Himalaya-S. Tibet | 29.0633 | 92.8251 | 4482 | 4482 | -7.4 | 48.0 | -15.7 | Hren et al. (2009) | Stream/tributary |
| 05Tibet96 | Himalaya-S. Tibet | 29.0764 | 92.7221 | 4234 | 4234 | -6.8 | 60.0 | -15.9 | Hren et al. (2009) | Stream/tributary |
| 05Tibet97 | Himalaya-S. Tibet | 29.1406 | 92.5613 | 4367 | 4367 | -3.9 | 68.0 | -16.0 | Hren et al. (2009) | Stream/tributary |
| 05Tibet98 | Himalaya-S. Tibet | 29.1409 | 92.5186 | 4316 | 4316 | -3.2 | 64.0 | -15.9 | Hren et al. (2009) | Stream/tributary |
| 05Tibet99 | Himalaya-S. Tibet | 29.0430 | 92.2632 | 4945 | 4945 | -0.7 | 45.0 | -17.3 | Hren et al. (2009) | Stream/tributary |
| NB-15 | Himalaya-S. Tibet | 29.4427 | 94.7258 | 4092 | 4092 | -5.1 | 33.0 | -11.4 | Hren et al. (2009) | Stream/tributary |
| NB-16 | Himalaya-S. Tibet | 29.4430 | 94.7043 | 3018 | 3018 | -4.8 | 64.0 | -11.6 | Hren et al. (2009) | Stream/tributary |
| NB-17 | Himalaya-S. Tibet | 29.4509 | 94.6936 | 4153 | 4153 | -4.6 | 40.0 | -12.9 | Hren et al. (2009) | Stream/tributary |
| NB-19A | Himalaya-S. Tibet | 29.4648 | 94.6103 | 3208 | 3208 | -3.3 | 79.0 | -13.6 | Hren et al. (2009) | Stream/tributary |
| NB-8A | Himalaya-S. Tibet | 29.5025 | 94.8426 | 3658 | 3658 | -2.4 | 116.0 | -13.5 | Hren et al. (2009) | Stream/tributary |

## Table A2.2 – Compilation of east Asia meteoric water $\delta^{18}O$ records

| Location | Subregion | LAT (º) | LON (º) | Site ELEV (m) | Ppt ELEV (m) | MAT (ºC) | MAP (cm) | Wgt. $\delta^{18}O$ (‰ SMOW) | Reference | Record length |
|---|---|---|---|---|---|---|---|---|---|---|
| SUTLEJ | Himalaya-S. Tibet | 31.4787 | 79.7447 | 4087 | 4087 | -4.7 | 10.3 | -16.3 | Hren et al. (2009) | Stream/tributary |
| W-2-10 | Himalaya-S. Tibet | 30.9577 | 81.2750 | 5537 | 5537 | -6.5 | 49.0 | -16.5 | Hren et al. (2009) | Stream/tributary |
| W-2-11 | Himalaya-S. Tibet | 30.6903 | 81.8298 | 5183 | 5183 | -8.3 | 11.0 | -17.4 | Hren et al. (2009) | Stream/tributary |
| W-2-12 | Himalaya-S. Tibet | 29.7757 | 83.9142 | 4793 | 4793 | -7.1 | 24.0 | -18.4 | Hren et al. (2009) | Stream/tributary |
| W-2-13 | Himalaya-S. Tibet | 29.5433 | 84.6182 | 5288 | 5288 | -8.4 | 21.0 | -19.9 | Hren et al. (2009) | Stream/tributary |
| W-2-14 | Himalaya-S. Tibet | 29.4272 | 85.2341 | 5274 | 5274 | -9.2 | 23.0 | -19.6 | Hren et al. (2009) | Stream/tributary |
| W-2-15 | Himalaya-S. Tibet | 29.3347 | 85.4051 | 5258 | 5258 | -8.0 | 26.0 | -20.5 | Hren et al. (2009) | Stream/tributary |
| W-2-16 | Himalaya-S. Tibet | 29.3782 | 85.4946 | 5297 | 5297 | -8.3 | 26.0 | -20.1 | Hren et al. (2009) | Stream/tributary |
| W-2-17 | Himalaya-S. Tibet | 29.5061 | 86.3408 | 5065 | 5065 | -8.4 | 20.0 | -20.8 | Hren et al. (2009) | Stream/tributary |
| W-2-18 | Himalaya-S. Tibet | 29.3604 | 86.8967 | 4716 | 4716 | -8.2 | 34.0 | -18.9 | Hren et al. (2009) | Stream/tributary |
| W-2-19 | Himalaya-S. Tibet | 29.3126 | 87.0385 | 4702 | 4702 | -8.0 | 29.0 | -19.8 | Hren et al. (2009) | Stream/tributary |
| W-2-2 | Himalaya-S. Tibet | 29.3266 | 88.4075 | 4693 | 4693 | -6.2 | 38.0 | -19.8 | Hren et al. (2009) | Stream/tributary |
| W-2-20 | Himalaya-S. Tibet | 29.1047 | 87.5988 | 4614 | 4614 | -6.2 | 34.0 | -19.7 | Hren et al. (2009) | Stream/tributary |
| W-2-21 | Himalaya-S. Tibet | 29.3429 | 87.9339 | 4654 | 4654 | -5.2 | 47.0 | -19.9 | Hren et al. (2009) | Stream/tributary |
| W-2-22 | Himalaya-S. Tibet | 29.3685 | 88.8227 | 4995 | 4995 | -5.5 | 34.0 | -19.8 | Hren et al. (2009) | Stream/tributary |
| W-2-23C | Himalaya-S. Tibet | 29.3277 | 89.3965 | 3830 | 3830 | -4.0 | 36.0 | -18.5 | Hren et al. (2009) | Stream/tributary |
| W-2-25 | Himalaya-S. Tibet | 29.3344 | 90.2804 | 4995 | 4995 | -3.2 | 31.0 | -19.7 | Hren et al. (2009) | Stream/tributary |
| W-2-3 | Himalaya-S. Tibet | 29.3965 | 88.2570 | 4641 | 4641 | -7.5 | 38.0 | -20.1 | Hren et al. (2009) | Stream/tributary |
| W-2-4 | Himalaya-S. Tibet | 29.1139 | 87.6697 | 4839 | 4839 | -5.8 | 27.0 | -20.4 | Hren et al. (2009) | Stream/tributary |
| W-2-6 | Himalaya-S. Tibet | 31.5342 | 79.9818 | 5164 | 5164 | -4.5 | 10.0 | -16.2 | Hren et al. (2009) | Stream/tributary |
| W-2-7 | Himalaya-S. Tibet | 31.4532 | 80.1417 | 5185 | 5185 | -4.6 | 17.0 | -18.2 | Hren et al. (2009) | Stream/tributary |
| W-2-9 | Himalaya-S. Tibet | 31.0579 | 81.0460 | 5459 | 5459 | -5.8 | 17.0 | -17.1 | Hren et al. (2009) | Stream/tributary |
| 99kg01 | Himalaya-S. Tibet* | 28.8750 | 83.8590 | 3450 | 4450 | -1.1 | 42.5 | -17.7 | Garzione et al. (2000) | Stream/tributary |
| 99kg02 | Himalaya-S. Tibet* | 28.9170 | 83.8520 | 2960 | 3960 | -2.1 | 39.1 | -18.8 | Garzione et al. (2000) | Stream/tributary |
| 99kg03/97kg1 | Himalaya-S. Tibet* | 28.9380 | 83.8300 | 3000 | 4000 | -2.4 | 34.4 | -18.9 | Garzione et al. (2000) | Stream/tributary |
| 99kg04 | Himalaya-S. Tibet* | 28.9370 | 83.8180 | 2960 | 3960 | -2.2 | 36.2 | -17.5 | Garzione et al. (2000) | Stream/tributary |
| 99kg05 | Himalaya-S. Tibet* | 28.9230 | 83.7970 | 3250 | 4250 | -1.5 | 38.6 | -17.5 | Garzione et al. (2000) | Stream/tributary |
| 99kg06 | Himalaya-S. Tibet* | 28.9710 | 83.8160 | 3670 | 4670 | -3.1 | 40.8 | -17.6 | Garzione et al. (2000) | Stream/tributary |
| 99kg08 | Himalaya-S. Tibet* | 29.0020 | 83.8170 | 3800 | 4800 | -4.0 | 44.4 | -18.3 | Garzione et al. (2000) | Stream/tributary |
| 99kg09 | Himalaya-S. Tibet* | 29.0040 | 83.8340 | 3900 | 4900 | -4.3 | 42.2 | -17.5 | Garzione et al. (2000) | Stream/tributary |
| 99kg10 | Himalaya-S. Tibet* | 29.0250 | 83.8530 | 3750 | 4750 | -5.0 | 40.8 | -17.4 | Garzione et al. (2000) | Stream/tributary |
| 99kg11 | Himalaya-S. Tibet* | 29.0660 | 83.8770 | 3700 | 4700 | -6.3 | 38.2 | -20.5 | Garzione et al. (2000) | Stream/tributary |
| 99kg12 | Himalaya-S. Tibet* | 29.0700 | 83.8920 | 3700 | 4700 | -6.5 | 39.0 | -19.3 | Garzione et al. (2000) | Stream/tributary |
| 99kg13 | Himalaya-S. Tibet* | 29.0590 | 83.9560 | 3300 | 4300 | -6.6 | 36.3 | -19.5 | Garzione et al. (2000) | Stream/tributary |
| 99kg14 | Himalaya-S. Tibet* | 29.0590 | 83.9450 | 3300 | 4300 | -6.6 | 35.2 | -21.2 | Garzione et al. (2000) | Stream/tributary |
| 99kg15 | Himalaya-S. Tibet* | 29.0950 | 83.9970 | 3500 | 4500 | -7.6 | 36.1 | -18.5 | Garzione et al. (2000) | Stream/tributary |
| 99kg16 | Himalaya-S. Tibet* | 29.0610 | 84.0190 | 3550 | 4550 | -7.1 | 38.8 | -19.8 | Garzione et al. (2000) | Stream/tributary |
| 99kg17 | Himalaya-S. Tibet* | 29.0080 | 83.9550 | 3280 | 4280 | -5.5 | 35.9 | -19.1 | Garzione et al. (2000) | Stream/tributary |
| 99kg18 | Himalaya-S. Tibet* | 28.9890 | 83.9500 | 3410 | 4410 | -5.1 | 36.4 | -18.8 | Garzione et al. (2000) | Stream/tributary |
| 99kg20 | Himalaya-S. Tibet* | 28.7980 | 83.7660 | 2800 | 3800 | 3.0 | 33.7 | -16.5 | Garzione et al. (2000) | Stream/tributary |
| 99kg21 | Himalaya-S. Tibet* | 28.7940 | 83.7470 | 2700 | 3700 | 3.4 | 34.1 | -13.7 | Garzione et al. (2000) | Stream/tributary |
| 99kg22 | Himalaya-S. Tibet* | 28.7960 | 83.7290 | 2750 | 3750 | 2.8 | 39.7 | -15.7 | Garzione et al. (2000) | Stream/tributary |
| 99kg23 | Himalaya-S. Tibet* | 28.7520 | 83.6830 | 2600 | 3600 | 2.8 | 36.0 | -11.2 | Garzione et al. (2000) | Stream/tributary |
| 99kg24 | Himalaya-S. Tibet* | 28.7280 | 83.6480 | 2500 | 3500 | 2.2 | 44.3 | -13.4 | Garzione et al. (2000) | Stream/tributary |
| 99kg25 | Himalaya-S. Tibet* | 28.7200 | 83.6360 | 2500 | 3500 | 2.1 | 40.7 | -12.8 | Garzione et al. (2000) | Stream/tributary |
| 99kg26 | Himalaya-S. Tibet* | 28.7030 | 83.6160 | 2440 | 3440 | 1.9 | 42.3 | -12.2 | Garzione et al. (2000) | Stream/tributary |
| 99kg27 | Himalaya-S. Tibet* | 28.6390 | 83.6070 | 2300 | 3300 | 3.1 | 72.3 | -13.0 | Garzione et al. (2000) | Stream/tributary |

## Table A2.2 – Compilation of east Asia meteoric water $\delta^{18}O$ records

| Location | Subregion | LAT (º) | LON (º) | Site ELEV (m) | Ppt ELEV (m) | MAT (ºC) | MAP (cm) | Wgt. $\delta^{18}O$ (‰ SMOW) | Reference | Record length |
|---|---|---|---|---|---|---|---|---|---|---|
| 99kg28 | Himalaya-S. Tibet* | 28.6150 | 83.6330 | 2000 | 3000 | 4.3 | 123.0 | -11.9 | Garzione et al. (2000) | Stream/tributary |
| 99kg29 | Himalaya-S. Tibet* | 28.5960 | 83.6410 | 1850 | 2850 | 4.9 | 176.3 | -11.2 | Garzione et al. (2000) | Stream/tributary |
| 99kg30 | Himalaya-S. Tibet* | 28.5830 | 83.6550 | 1800 | 2800 | 5.6 | 120.7 | -12.0 | Garzione et al. (2000) | Stream/tributary |
| 99kg31 | Himalaya-S. Tibet* | 28.5630 | 83.6340 | 1700 | 2700 | 5.5 | 241.8 | -11.4 | Garzione et al. (2000) | Stream/tributary |
| 99kg32 | Himalaya-S. Tibet* | 28.5410 | 83.6360 | 1400 | 2400 | 6.0 | 234.2 | -10.0 | Garzione et al. (2000) | Stream/tributary |
| 99kg33 | Himalaya-S. Tibet* | 28.5280 | 83.6470 | 1350 | 2350 | 6.6 | 261.0 | -10.7 | Garzione et al. (2000) | Stream/tributary |
| 99kg34 | Himalaya-S. Tibet* | 28.4970 | 83.6480 | 1240 | 2240 | 7.3 | 237.6 | -9.6 | Garzione et al. (2000) | Stream/tributary |
| 99kg35 | Himalaya-S. Tibet* | 28.4510 | 83.6300 | 1140 | 2140 | 7.9 | 257.0 | -10.7 | Garzione et al. (2000) | Stream/tributary |
| 99kg36 | Himalaya-S. Tibet* | 28.4490 | 83.6050 | 1040 | 2040 | 7.5 | 249.5 | -9.8 | Garzione et al. (2000) | Stream/tributary |
| 99kg37 | Himalaya-S. Tibet* | 28.3710 | 83.5600 | 870 | 1870 | 8.5 | 174.5 | -9.5 | Garzione et al. (2000) | Stream/tributary |
| 99kg38 | Himalaya-S. Tibet* | 28.2710 | 83.6230 | 760 | 1760 | 11.9 | 174.6 | -9.6 | Garzione et al. (2000) | Stream/tributary |
| 99kg39 | Himalaya-S. Tibet* | 28.2090 | 83.6880 | 680 | 1680 | 13.2 | 213.2 | -9.3 | Garzione et al. (2000) | Stream/tributary |
| 99kg40 | Himalaya-S. Tibet* | 28.1640 | 83.6680 | 800 | 1800 | 12.9 | 201.0 | -9.6 | Garzione et al. (2000) | Stream/tributary |
| 99kg41 | Himalaya-S. Tibet* | 28.1330 | 83.6390 | 720 | 1720 | 12.7 | 199.6 | -9.8 | Garzione et al. (2000) | Stream/tributary |
| 99kg42 | Himalaya-S. Tibet* | 28.1000 | 83.6280 | 790 | 1790 | 12.7 | 249.7 | -9.4 | Garzione et al. (2000) | Stream/tributary |
| 99kg43 | Himalaya-S. Tibet* | 28.0890 | 83.5950 | 720 | 1720 | 12.6 | 190.0 | -9.7 | Garzione et al. (2000) | Stream/tributary |
| 99KG44 | Himalaya-S. Tibet* | 28.0420 | 83.5760 | 620 | 1620 | 12.7 | 183.1 | -8.2 | Garzione et al. (2000) | Stream/tributary |
| 99kg45 | Himalaya-S. Tibet* | 28.0010 | 83.6100 | 720 | 1720 | 12.9 | 188.2 | -8.7 | Garzione et al. (2000) | Stream/tributary |
| 99kg47 | Himalaya-S. Tibet* | 27.9890 | 83.6030 | 620 | 1620 | 12.9 | 188.5 | -8.8 | Garzione et al. (2000) | Stream/tributary |
| 99kg48 | Himalaya-S. Tibet* | 27.8370 | 83.5420 | 855 | 1855 | 13.9 | 173.1 | -9.0 | Garzione et al. (2000) | Stream/tributary |
| 99kg49 | Himalaya-S. Tibet* | 27.8180 | 83.5440 | 820 | 1820 | 14.0 | 177.7 | -9.2 | Garzione et al. (2000) | Stream/tributary |
| 99kg50 | Himalaya-S. Tibet* | 27.7850 | 83.5350 | 660 | 1660 | 14.3 | 174.7 | -8.7 | Garzione et al. (2000) | Stream/tributary |
| 99kg51 | Himalaya-S. Tibet* | 27.7730 | 83.5270 | 480 | 1480 | 14.4 | 170.4 | -8.1 | Garzione et al. (2000) | Stream/tributary |
| Kathmandu | Himalaya-S. Tibet* | 27.7000 | 85.3700 | 1340 | 1340 | 18.6 | 126.0 | -6.2 | Zhang et al. (2002) | 1993; 1995-1996 |
| Kyangjin | Himalaya-S. Tibet* | 28.2000 | 85.5700 | 3880 | 3880 | 1.6 | 64.9 | -14.3 | Zhang et al. (2002) | 1993-1996 |
| New Delhi | Himalaya-S. Tibet* | 28.5800 | 77.2000 | 212 | 212 | 25.0 | 80.6 | -5.9 | Zhang et al. (2002) | 1961-1996 |
| Nyalam | Himalaya-S. Tibet* | 28.1800 | 85.9700 | 3180 | 3180 | -11.7 | 65.0 | -14.2 | Liu et al. (2008) | 1996-1999 |
| Seti 06 | Himalaya-S. Tibet* | 29.4760 | 80.9930 | 910 | 1510 | 9.5 | 158.2 | -8.8 | Garzione et al. (2000) | Stream/tributary |
| Seti 09 | Himalaya-S. Tibet* | 29.4980 | 81.1370 | 1130 | 1730 | 8.4 | 150.4 | -9.3 | Garzione et al. (2000) | Stream/tributary |
| Seti 12 | Himalaya-S. Tibet* | 29.5160 | 81.1660 | 1220 | 1820 | 7.8 | 150.2 | -9.5 | Garzione et al. (2000) | Stream/tributary |
| Seti 14 | Himalaya-S. Tibet* | 29.5440 | 81.2100 | 1310 | 1910 | 6.9 | 146.0 | -9.7 | Garzione et al. (2000) | Stream/tributary |
| Seti 24 | Himalaya-S. Tibet* | 29.6060 | 81.3070 | 1460 | 2060 | 4.6 | 135.9 | -8.4 | Garzione et al. (2000) | Stream/tributary |
| Seti 26 | Himalaya-S. Tibet* | 29.6330 | 81.3210 | 1590 | 2190 | 3.9 | 121.6 | -9.1 | Garzione et al. (2000) | Stream/tributary |
| Seti 27 | Himalaya-S. Tibet* | 29.6660 | 81.3410 | 1710 | 2310 | 3.1 | 115.0 | -9.7 | Garzione et al. (2000) | Stream/tributary |
| Seti 30 | Himalaya-S. Tibet* | 29.6800 | 81.3450 | 1770 | 2370 | 2.7 | 115.9 | -10.2 | Garzione et al. (2000) | Stream/tributary |
| Seti 33 | Himalaya-S. Tibet* | 29.7510 | 81.3020 | 2040 | 2640 | 1.3 | 108.1 | -10.5 | Garzione et al. (2000) | Stream/tributary |
| Seti 42 | Himalaya-S. Tibet* | 29.7820 | 81.2600 | 2350 | 2950 | 0.8 | 105.4 | -10.4 | Garzione et al. (2000) | Stream/tributary |
| Seti 49 | Himalaya-S. Tibet* | 29.4270 | 80.8720 | 820 | 1420 | 10.4 | 158.4 | -7.7 | Garzione et al. (2000) | Stream/tributary |
| Seti 54 | Himalaya-S. Tibet* | 29.3730 | 80.7830 | 720 | 1320 | 10.8 | 162.2 | -7.8 | Garzione et al. (2000) | Stream/tributary |
| Seti 58 | Himalaya-S. Tibet* | 29.2790 | 80.8490 | 610 | 1210 | 11.4 | 160.3 | -7.4 | Garzione et al. (2000) | Stream/tributary |
| Seti 59 | Himalaya-S. Tibet* | 29.2380 | 80.8940 | 570 | 1170 | 12.0 | 159.2 | -7.7 | Garzione et al. (2000) | Stream/tributary |
| Seti 61 | Himalaya-S. Tibet* | 29.2170 | 80.9900 | 530 | 1130 | 12.8 | 153.5 | -7.7 | Garzione et al. (2000) | Stream/tributary |
| Seti 63 | Himalaya-S. Tibet* | 29.2030 | 81.0250 | 490 | 1090 | 13.1 | 151.3 | -7.7 | Garzione et al. (2000) | Stream/tributary |
| Seti 66 | Himalaya-S. Tibet* | 29.1140 | 81.0790 | 430 | 1030 | 14.2 | 152.6 | -7.2 | Garzione et al. (2000) | Stream/tributary |
| Shillong | Himalaya-S. Tibet* | 25.5700 | 91.8800 | 1598 | 1598 | 16.8 | 206.4 | -4.9 | Zhang et al. (2002) | 1969-1978 |
| WA-1 | Himalaya-S. Tibet* | 28.2365 | 94.9515 | 1934 | 1934 | 11.3 | 179.0 | -6.2 | Hren et al. (2009) | Stream/tributary |
| WA-11 | Himalaya-S. Tibet* | 28.3548 | 95.0408 | 1003 | 1003 | 9.6 | 245.0 | -5.8 | Hren et al. (2009) | Stream/tributary |

## Table A2.2 – Compilation of east Asia meteoric water $\delta^{18}O$ records

| Location | Subregion | LAT (º) | LON (º) | Site ELEV (m) | Ppt ELEV (m) | MAT (ºC) | MAP (cm) | Wgt. $\delta^{18}O$ (‰ SMOW) | Reference | Record length |
|---|---|---|---|---|---|---|---|---|---|---|
| WA-12 | Himalaya-S. Tibet* | 28.6730 | 94.9644 | 1505 | 1505 | 8.0 | 308.0 | -6.8 | Hren et al. (2009) | Stream/tributary |
| WA-13 | Himalaya-S. Tibet* | 28.7769 | 94.7682 | 1666 | 1666 | 10.0 | 324.0 | -7.9 | Hren et al. (2009) | Stream/tributary |
| WA-14 | Himalaya-S. Tibet* | 28.7305 | 94.9236 | 1191 | 1191 | 8.3 | 281.0 | -6.0 | Hren et al. (2009) | Stream/tributary |
| WA-15 | Himalaya-S. Tibet* | 28.5260 | 95.0492 | 1622 | 1622 | 7.9 | 204.0 | -7.2 | Hren et al. (2009) | Stream/tributary |
| WA-16 | Himalaya-S. Tibet* | 28.3022 | 95.2020 | 1624 | 1624 | 8.6 | 261.0 | -7.2 | Hren et al. (2009) | Stream/tributary |
| WA-17 | Himalaya-S. Tibet* | 28.1405 | 95.0930 | 960 | 960 | 11.3 | 235.0 | -6.7 | Hren et al. (2009) | Stream/tributary |
| WA-2 | Himalaya-S. Tibet* | 28.2880 | 94.9469 | 866 | 866 | 11.0 | 134.0 | -6.8 | Hren et al. (2009) | Stream/tributary |
| WA-3 | Himalaya-S. Tibet* | 28.3497 | 94.9992 | 1301 | 1301 | 10.0 | 224.0 | -6.6 | Hren et al. (2009) | Stream/tributary |
| WA-4 | Himalaya-S. Tibet* | 28.5952 | 95.0693 | 1110 | 1110 | 7.0 | 215.0 | -5.8 | Hren et al. (2009) | Stream/tributary |
| WA-5 | Himalaya-S. Tibet* | 28.6224 | 95.0359 | 1355 | 1355 | 7.2 | 243.0 | -6.3 | Hren et al. (2009) | Stream/tributary |
| WA-6 | Himalaya-S. Tibet* | 28.5120 | 95.0993 | 935 | 935 | 7.4 | 205.0 | -6.5 | Hren et al. (2009) | Stream/tributary |
| WA-7 | Himalaya-S. Tibet* | 28.4361 | 95.1007 | 1296 | 1296 | 8.1 | 204.0 | -6.7 | Hren et al. (2009) | Stream/tributary |
| WA-8 | Himalaya-S. Tibet* | 28.4030 | 95.0798 | 1242 | 1242 | 8.7 | 206.0 | -6.4 | Hren et al. (2009) | Stream/tributary |
| WA-9 | Himalaya-S. Tibet* | 28.3753 | 95.0743 | 755 | 755 | 9.0 | 212.0 | -6.5 | Hren et al. (2009) | Stream/tributary |
| 05Tibet10 | N-C Tibet | 29.8725 | 92.5229 | 5027 | 5027 | -4.1 | 20.0 | -17.8 | Hren et al. (2009) | Stream/tributary |
| 05Tibet11 | N-C Tibet | 29.8737 | 92.6848 | 5105 | 5105 | -4.9 | 23.0 | -17.6 | Hren et al. (2009) | Stream/tributary |
| 05Tibet12 | N-C Tibet | 29.9443 | 92.8182 | 5081 | 5081 | -5.1 | 27.0 | -17.0 | Hren et al. (2009) | Stream/tributary |
| 05Tibet13 | N-C Tibet | 29.9557 | 92.8580 | 4950 | 4950 | -5.1 | 31.0 | -17.0 | Hren et al. (2009) | Stream/tributary |
| 05Tibet14 | N-C Tibet | 30.0295 | 92.9007 | 4902 | 4902 | -4.9 | 34.0 | -17.1 | Hren et al. (2009) | Stream/tributary |
| 05Tibet15 | N-C Tibet | 30.0052 | 93.0166 | 5026 | 5026 | -5.0 | 30.0 | -17.4 | Hren et al. (2009) | Stream/tributary |
| 05Tibet16 | N-C Tibet | 29.9344 | 93.1498 | 5025 | 5025 | -5.3 | 26.0 | -16.7 | Hren et al. (2009) | Stream/tributary |
| 05Tibet17 | N-C Tibet | 29.9110 | 93.1723 | 4979 | 4979 | -5.4 | 27.0 | -16.9 | Hren et al. (2009) | Stream/tributary |
| 05Tibet18 | N-C Tibet | 30.0130 | 92.9866 | 4728 | 4728 | -5.0 | 44.0 | -17.0 | Hren et al. (2009) | Stream/tributary |
| 05Tibet19 | N-C Tibet | 29.9996 | 93.0386 | 4778 | 4778 | -5.0 | 32.0 | -16.9 | Hren et al. (2009) | Stream/tributary |
| 05Tibet2 | N-C Tibet | 29.8745 | 92.3279 | 5221 | 5221 | -3.1 | 38.0 | -18.9 | Hren et al. (2009) | Stream/tributary |
| 05Tibet20 | N-C Tibet | 29.9758 | 93.1033 | 4617 | 4617 | -5.1 | 29.0 | -16.7 | Hren et al. (2009) | Stream/tributary |
| 05Tibet21 | N-C Tibet | 29.8886 | 93.2547 | 4753 | 4753 | -5.6 | 34.0 | -15.9 | Hren et al. (2009) | Stream/tributary |
| 05Tibet22 | N-C Tibet | 29.8916 | 93.3513 | 4863 | 4863 | -5.5 | 29.0 | -15.7 | Hren et al. (2009) | Stream/tributary |
| 05Tibet23 | N-C Tibet | 29.8889 | 93.4367 | 4586 | 4586 | -5.5 | 35.0 | -16.2 | Hren et al. (2009) | Stream/tributary |
| 05Tibet24 | N-C Tibet | 29.8904 | 93.5251 | 4613 | 4613 | -5.5 | 41.0 | -15.8 | Hren et al. (2009) | Stream/tributary |
| 05Tibet25 | N-C Tibet | 29.8979 | 93.5721 | 4650 | 4650 | -5.4 | 36.0 | -15.7 | Hren et al. (2009) | Stream/tributary |
| 05Tibet26 | N-C Tibet | 29.8645 | 93.6677 | 4694 | 4694 | -5.5 | 45.0 | -16.2 | Hren et al. (2009) | Stream/tributary |
| 05Tibet27 | N-C Tibet | 29.7943 | 93.9051 | 4360 | 4360 | -3.5 | 50.0 | -15.4 | Hren et al. (2009) | Stream/tributary |
| 05Tibet28 | N-C Tibet | 29.7925 | 93.9604 | 4323 | 4323 | -2.6 | 55.0 | -15.5 | Hren et al. (2009) | Stream/tributary |
| 05Tibet29 | N-C Tibet | 29.7337 | 94.0763 | 4314 | 4314 | -0.8 | 49.0 | -15.1 | Hren et al. (2009) | Stream/tributary |
| 05Tibet30 | N-C Tibet | 29.7473 | 94.1678 | 4315 | 4315 | 0.8 | 60.0 | -13.5 | Hren et al. (2009) | Stream/tributary |
| 05Tibet32 | N-C Tibet | 29.7555 | 94.2391 | 4377 | 4377 | 1.9 | 37.0 | -13.7 | Hren et al. (2009) | Stream/tributary |
| 05Tibet33 | N-C Tibet | 29.6776 | 94.3546 | 4371 | 4371 | 1.1 | 42.0 | -14.5 | Hren et al. (2009) | Stream/tributary |
| 05Tibet36 | N-C Tibet | 29.6662 | 94.3102 | 4458 | 4458 | 1.4 | 31.0 | -14.2 | Hren et al. (2009) | Stream/tributary |
| 05Tibet4 | N-C Tibet | 29.9006 | 92.3495 | 5115 | 5115 | -3.3 | 37.0 | -16.5 | Hren et al. (2009) | Stream/tributary |
| 05Tibet5 | N-C Tibet | 29.9135 | 92.3658 | 5139 | 5139 | -3.4 | 34.0 | -18.4 | Hren et al. (2009) | Stream/tributary |
| 05Tibet59 | N-C Tibet | 29.6017 | 94.6068 | 4495 | 4495 | -1.8 | 49.0 | -10.5 | Hren et al. (2009) | Stream/tributary |
| 05Tibet6 | N-C Tibet | 29.9090 | 92.3822 | 4917 | 4917 | -3.4 | 30.0 | -17.3 | Hren et al. (2009) | Stream/tributary |
| 05Tibet60 | N-C Tibet | 29.5679 | 94.5659 | 4333 | 4333 | -1.7 | 59.0 | -10.7 | Hren et al. (2009) | Stream/tributary |
| 05Tibet61 | N-C Tibet | 29.4699 | 94.3984 | 4280 | 4280 | -0.4 | 31.0 | -12.2 | Hren et al. (2009) | Stream/tributary |
| 05Tibet9 | N-C Tibet | 29.8908 | 92.4580 | 4963 | 4963 | -3.8 | 28.0 | -18.0 | Hren et al. (2009) | Stream/tributary |
| Delingha | N-C Tibet | 37.3700 | 97.3700 | 2981 | 2981 | -9.7 | 15.5 | -7.7 | Liu et al. (2008) | 1991-1999 |

## Table A2.2 – Compilation of east Asia meteoric water $\delta^{18}O$ records

| Location | Subregion | LAT (º) | LON (º) | Site ELEV (m) | Ppt ELEV (m) | MAT (ºC) | MAP (cm) | Wgt. $\delta^{18}O$ (‰ SMOW) | Reference | Record length |
|---|---|---|---|---|---|---|---|---|---|---|
| Gaize | N-C Tibet | 32.3000 | 84.0500 | 4416 | 4416 | -4.4 | 17.0 | -11.6 | Liu et al. (2008) | 1998-2003 |
| Hetian | N-C Tibet | 37.0800 | 79.5600 | 1375 | 1375 | 7.9 | 23.8 | -5.7 | Liu et al. (2008) | 1988-1992 |
| Lanzhou | N-C Tibet | 36.0500 | 103.8800 | 1517 | 1517 | 10.0 | 30.4 | -5.7 | Zhang et al. (2002) | 1985-1987; 1996-1997 |
| Lhasa | N-C Tibet | 29.7167 | 91.0330 | 3650 | 3650 | 8.0 | 48.0 | -17.3 | Average of Liu et al. (2008) and Johnson and Ingram (2004) | 1988-1990; 1993-1999 |
| Nagqu | N-C Tibet | 31.4800 | 92.0700 | 4507 | 4507 | -0.7 | 41.6 | -16.6 | Liu et al. (2008) | 2000-2003 |
| Nam Co | N-C Tibet | 30.7700 | 90.9900 | 4730 | 4730 | -1.3 | 31.4 | -18.4 | Liu et al. (2008) | 2005-2006 |
| Shiquanhe | N-C Tibet | 32.5000 | 80.1000 | 4279 | 4279 | -10.2 | 7.1 | -11.3 | Liu et al. (2008) | 1999-2002 |
| T99-1 | N-C Tibet | 34.3235 | 89.9730 | 5303 | 5303 | -12.0 | 13.0 | -13.0 | Hren et al. (2009) | Stream/tributary |
| T99-10 | N-C Tibet | 33.0073 | 88.5518 | 5261 | 5261 | -5.9 | 15.0 | -14.3 | Hren et al. (2009) | Stream/tributary |
| T99-11 | N-C Tibet | 31.8211 | 87.5237 | 4917 | 4917 | -6.2 | 7.0 | -15.5 | Hren et al. (2009) | Stream/tributary |
| T99-12 | N-C Tibet | 31.3704 | 90.5952 | 4859 | 4859 | -1.8 | 13.0 | -15.5 | Hren et al. (2009) | Stream/tributary |
| T99-13 | N-C Tibet | 31.1499 | 90.7560 | 4910 | 4910 | -0.9 | 13.0 | -14.6 | Hren et al. (2009) | Stream/tributary |
| T99-14 | N-C Tibet | 30.8301 | 91.0638 | 5037 | 5037 | -1.3 | 17.0 | -17.2 | Hren et al. (2009) | Stream/tributary |
| T99-15 | N-C Tibet | 30.6712 | 91.0968 | 5514 | 5514 | -1.1 | 16.0 | -16.8 | Hren et al. (2009) | Stream/tributary |
| T99-16 | N-C Tibet | 30.6058 | 91.1098 | 5399 | 5399 | -0.8 | 16.0 | -16.8 | Hren et al. (2009) | Stream/tributary |
| T99-17 | N-C Tibet | 30.2639 | 90.6711 | 4902 | 4902 | -0.4 | 19.0 | -15.7 | Hren et al. (2009) | Stream/tributary |
| T99-18 | N-C Tibet | 29.8339 | 90.7470 | 5252 | 5252 | 1.9 | 18.0 | -16.3 | Hren et al. (2009) | Stream/tributary |
| T99-2 | N-C Tibet | 34.3649 | 88.8754 | 5242 | 5242 | -16.9 | 13.0 | -11.4 | Hren et al. (2009) | Stream/tributary |
| T99-3 | N-C Tibet | 34.2522 | 88.9311 | 5268 | 5268 | -16.5 | 13.0 | -12.3 | Hren et al. (2009) | Stream/tributary |
| T99-4 | N-C Tibet | 34.1595 | 88.9078 | 5312 | 5312 | -15.6 | 12.0 | -11.4 | Hren et al. (2009) | Stream/tributary |
| T99-5 | N-C Tibet | 33.8824 | 88.8676 | 5177 | 5177 | -12.7 | 14.0 | -11.0 | Hren et al. (2009) | Stream/tributary |
| T99-6 | N-C Tibet | 33.6173 | 88.7611 | 5186 | 5186 | -10.2 | 15.0 | -13.3 | Hren et al. (2009) | Stream/tributary |
| T99-7 | N-C Tibet | 33.3770 | 88.0047 | 5296 | 5296 | -9.6 | 12.0 | -11.9 | Hren et al. (2009) | Stream/tributary |
| T99-8 | N-C Tibet | 33.0540 | 88.6908 | 5154 | 5154 | -5.8 | 15.0 | -14.0 | Hren et al. (2009) | Stream/tributary |
| T99-9 | N-C Tibet | 33.0292 | 88.6683 | 5206 | 5206 | -5.7 | 13.0 | -12.2 | Hren et al. (2009) | Stream/tributary |
| TP 1 | N-C Tibet | 33.1909 | 88.8364 | 5298 | 5298 | -5.9 | 13.0 | -11.3 | Hren et al. (2009) | Stream/tributary |
| TS 1 | N-C Tibet | 34.0223 | 88.8810 | 5487 | 5487 | -14.2 | 15.0 | -11.5 | Hren et al. (2009) | Stream/tributary |
| TS 10 | N-C Tibet | 33.3978 | 88.7952 | 5579 | 5579 | -7.9 | 16.0 | -10.5 | Hren et al. (2009) | Stream/tributary |
| TS 11 | N-C Tibet | 33.0567 | 88.6336 | 5356 | 5356 | -6.0 | 15.0 | -12.0 | Hren et al. (2009) | Stream/tributary |
| TS 12 | N-C Tibet | 33.1719 | 88.8114 | 5529 | 5529 | -5.9 | 15.0 | -11.0 | Hren et al. (2009) | Stream/tributary |
| TS 13 | N-C Tibet | 33.1374 | 88.7680 | 5514 | 5514 | -6.0 | 16.0 | -11.1 | Hren et al. (2009) | Stream/tributary |
| TS 14 | N-C Tibet | 33.0918 | 88.7327 | 5037 | 5037 | -5.9 | 15.0 | -10.7 | Hren et al. (2009) | Stream/tributary |
| TS 15 | N-C Tibet | 33.0908 | 88.7316 | 5514 | 5514 | -5.9 | 16.0 | -11.3 | Hren et al. (2009) | Stream/tributary |
| TS 16 | N-C Tibet | 33.0540 | 88.6907 | 5399 | 5399 | -5.8 | 15.0 | -9.5 | Hren et al. (2009) | Stream/tributary |
| TS 17 | N-C Tibet | 33.0292 | 88.6683 | 4902 | 4902 | -5.7 | 9.0 | -12.3 | Hren et al. (2009) | Stream/tributary |
| TS 18 | N-C Tibet | 32.9791 | 88.4575 | 5252 | 5252 | -6.1 | 15.0 | -11.4 | Hren et al. (2009) | Stream/tributary |
| TS 19 | N-C Tibet | 32.6977 | 88.1548 | 5158 | 5158 | -5.5 | 9.0 | -10.0 | Hren et al. (2009) | Stream/tributary |
| TS 20 | N-C Tibet | 32.6765 | 88.1149 | 5125 | 5125 | -5.4 | 13.0 | -11.9 | Hren et al. (2009) | Stream/tributary |
| TS 21 | N-C Tibet | 32.4706 | 88.0690 | 5264 | 5264 | -5.2 | 9.0 | -12.3 | Hren et al. (2009) | Stream/tributary |
| TS 22 | N-C Tibet | 33.5622 | 88.0040 | 5207 | 5207 | -13.2 | 12.0 | -13.2 | Hren et al. (2009) | Stream/tributary |
| TS 24 | N-C Tibet | 32.0191 | 88.4111 | 4759 | 4759 | -4.0 | 8.0 | -13.0 | Hren et al. (2009) | Stream/tributary |
| TS 25 | N-C Tibet | 32.3732 | 87.9984 | 5341 | 5341 | -5.0 | 12.0 | -13.5 | Hren et al. (2009) | Stream/tributary |
| TS 26 | N-C Tibet | 32.3223 | 87.9568 | 5287 | 5287 | -4.9 | 11.0 | -12.8 | Hren et al. (2009) | Stream/tributary |
| TS 27 | N-C Tibet | 32.2825 | 87.9083 | 5421 | 5421 | -4.8 | 10.0 | -12.5 | Hren et al. (2009) | Stream/tributary |
| TS 4 | N-C Tibet | 33.0445 | 88.6387 | 5616 | 5616 | -5.9 | 15.0 | -12.5 | Hren et al. (2009) | Stream/tributary |
| TS 6 | N-C Tibet | 33.2809 | 88.8439 | 4979 | 4979 | -6.4 | 15.0 | -10.3 | Hren et al. (2009) | Stream/tributary |

**Table A2.2 – Compilation of east Asia meteoric water $\delta^{18}O$ records**

| Location | Subregion | LAT (º) | LON (º) | Site ELEV (m) | Ppt ELEV (m) | MAT (ºC) | MAP (cm) | Wgt. $\delta^{18}O$ (‰ SMOW) | Reference | Record length |
|---|---|---|---|---|---|---|---|---|---|---|
| TS 9 | N-C Tibet | 33.3187 | 88.8455 | 5450 | 5450 | -6.8 | 15.0 | -11.0 | Hren et al. (2009) | Stream/tributary |
| Tuotuohe | N-C Tibet | 34.2200 | 92.4300 | 4533 | 4533 | -3.5 | 28.0 | -12.0 | Liu et al. (2008) | 1991-1999 |
| WT06-1 | N-C Tibet | 30.5494 | 91.0652 | 5194 | 5194 | -0.5 | 32.0 | -18.0 | Hren et al. (2009) | Stream/tributary |
| WT06-10 | N-C Tibet | 33.0083 | 91.9730 | 5032 | 5032 | -6.0 | 33.7 | -15.2 | Hren et al. (2009) | Stream/tributary |
| WT06-2 | N-C Tibet | 30.5163 | 91.0168 | 5344 | 5344 | -0.3 | 33.0 | -18.1 | Hren et al. (2009) | Stream/tributary |
| WT06-3 | N-C Tibet | 29.9398 | 90.2656 | 5462 | 5462 | -7.3 | 38.0 | -19.0 | Hren et al. (2009) | Stream/tributary |
| WT06-4 | N-C Tibet | 30.0732 | 90.3286 | 5518 | 5518 | -6.3 | 27.0 | -18.5 | Hren et al. (2009) | Stream/tributary |
| WT06-5 | N-C Tibet | 30.1492 | 90.4898 | 5546 | 5546 | -3.4 | 37.0 | -18.5 | Hren et al. (2009) | Stream/tributary |
| WT06-6 | N-C Tibet | 30.3072 | 90.6340 | 5720 | 5720 | -1.1 | 36.0 | -18.5 | Hren et al. (2009) | Stream/tributary |
| WT06-7 | N-C Tibet | 30.3564 | 90.7233 | 5505 | 5505 | 0.2 | 65.0 | -18.2 | Hren et al. (2009) | Stream/tributary |
| WT06-8 | N-C Tibet | 32.6982 | 91.8773 | 4981 | 4981 | -4.7 | 34.7 | -12.5 | Hren et al. (2009) | Stream/tributary |
| WT06-9 | N-C Tibet | 32.8305 | 91.9153 | 5128 | 5128 | -5.5 | 33.9 | -17.1 | Hren et al. (2009) | Stream/tributary |
| Xining | N-C Tibet | 36.6200 | 101.7700 | 2261 | 2261 | -5.0 | 37.2 | -6.8 | Liu et al. (2008) | 1991-1992 |
| Yushu | N-C Tibet | 33.0167 | 97.0167 | 3682 | 3682 | 3.0 | 48.2 | -12.5 | Liu et al. (2008) | 2000-2002 |
| Zhangye | N-C Tibet | 38.9300 | 100.4300 | 1483 | 1483 | 7.5 | 13.5 | -6.3 | Araguás-Araguás et al. (1998) | 52 months |
| Baotou | NS | 40.6700 | 109.8500 | 1067 | 1067 | 7.5 | 35.4 | -8.0 | Average of Liu et al. (2008) and Johnson and Ingram (2004) | 1986-1992; 1988-1990 |
| Urumqi | NS | 43.7800 | 87.6200 | 918 | 918 | 7.4 | 28.3 | -10.9 | Zhang et al. (2002) | 1986-1992; 1995-1997 |
| Yinchuan | NS | 38.2900 | 106.1300 | 1112 | 1112 | 8.9 | 20.5 | -6.6 | Liu et al. (2008) | 1988-1992 |

**Table A2.2 Notes –** Modern precipitation and stream water $\delta^{18}O$ data for east Asia compiled from various sources (see 'Reference' column). Weighted mean annual $\delta^{18}O$ values were provided in original data sources. For sites with no reported climate values, MAT and MAP were extracted from Matsuura and Wilmott climate datasets (http://climate.geog.udel.edu/~climate/) using reported geographic coordinates. Both sample site elevations (Site ELEV) and precipitation-weighted hypsometric mean basin elevations (Ppt ELEV) for Garzione et al. (2000) stream water datasets are listed. Only precipitation-weighted hypsometric mean basin elevations are listed for Hren et al. (2009) stream and tributary samples. See references cited in the Liu et al. (2008) precipitation dataset for additional information on precipitation $\delta^{18}O$ values and original references. Sites marked with an asterisk (*) in the Himalaya-S. Tibet subregion were also analyzed as part of a Himalaya-only statistical analysis. Subregion designations 'NS' = no subregion. However, NS sites were included in the full regional analysis.

**Table A4.1 –** Detrital zircon U-Pb analyses

| Analysis | U (ppm) | $^{206}Pb/^{204}Pb$ | U/Th | Isotopic Ratio | | | | | | Error | Apparent Age (Ma) | | | | | | Best Age (Ma) | |
|---|---|---|---|---|---|---|---|---|---|---|---|---|---|---|---|---|---|---|
| | | | | $^{206}Pb/^{207}Pb$ | ± (%) | $^{207}Pb/^{235}U$ | ± (%) | $^{206}Pb/^{238}U$ | ± (%) | | $^{206}Pb/^{238}U$ | ± (Ma) | $^{207}Pb/^{235}U$ | ± (Ma) | $^{206}Pb/^{207}Pb$ | ± (Ma) | Age | ± |
| KR-09-01-1 | 448 | 4062 | 2.1 | 20.8408 | 9.4 | 0.0960 | 9.4 | 0.0145 | 1.0 | 0.11 | 92.9 | 0.9 | 93.1 | 8.4 | 98.4 | 222.2 | 92.9 | 0.9 |
| KR-09-01-2 | 229 | 3902 | 0.9 | 20.9816 | 11.3 | 0.1505 | 11.3 | 0.0229 | 1.2 | 0.11 | 146.0 | 1.8 | 142.3 | 15.0 | 82.4 | 268.0 | 146.0 | 1.8 |
| KR-09-01-3 | 318 | 4536 | 1.2 | 20.6465 | 6.9 | 0.1529 | 7.0 | 0.0229 | 1.3 | 0.19 | 145.9 | 1.9 | 144.4 | 9.5 | 120.5 | 162.8 | 145.9 | 1.9 |
| KR-09-01-4 | 238 | 3856 | 0.6 | 21.1475 | 13.2 | 0.1547 | 13.3 | 0.0237 | 1.7 | 0.13 | 151.2 | 2.6 | 146.1 | 18.2 | 63.8 | 316.3 | 151.2 | 2.6 |
| KR-09-01-5 | 238 | 4394 | 1.0 | 22.6628 | 10.1 | 0.1408 | 10.3 | 0.0231 | 2.3 | 0.22 | 147.4 | 3.3 | 133.7 | 13.0 | -103.7 | 248.6 | 147.4 | 3.3 |
| KR-09-01-6 | 68 | 523 | 2.5 | -2091.9308 | 1618.0 | -0.0015 | 1618.0 | 0.0226 | 2.9 | 0.00 | 144.0 | 4.1 | -1.5 | -24.5 | 0.0 | 0.0 | 144.0 | 4.1 |
| KR-09-01-7 | 683 | 7952 | 1.4 | 20.6761 | 4.8 | 0.1807 | 5.1 | 0.0271 | 1.7 | 0.33 | 172.3 | 2.9 | 168.6 | 8.0 | 117.2 | 114.0 | 172.3 | 2.9 |
| KR-09-01-8 | 514 | 4067 | 1.1 | 21.5078 | 4.8 | 0.1452 | 5.2 | 0.0226 | 1.9 | 0.36 | 144.4 | 2.7 | 137.7 | 6.7 | 23.4 | 115.9 | 144.4 | 2.7 |
| KR-09-01-9 | 155 | 1245 | 3.5 | 30.8955 | 17.7 | 0.0987 | 17.9 | 0.0221 | 2.4 | 0.13 | 141.0 | 3.3 | 95.5 | 16.3 | -931.5 | 519.9 | 141.0 | 3.3 |
| KR-09-01-10 | 403 | 2217 | 2.8 | 24.7605 | 14.5 | 0.0887 | 14.7 | 0.0159 | 2.4 | 0.16 | 101.9 | 2.5 | 86.3 | 12.2 | -326.1 | 375.1 | 101.9 | 2.5 |
| KR-09-01-11 | 477 | 6232 | 0.8 | 20.9705 | 8.4 | 0.1500 | 9.1 | 0.0228 | 3.4 | 0.38 | 145.4 | 4.9 | 141.9 | 12.0 | 83.7 | 199.5 | 145.4 | 4.9 |
| KR-09-01-13 | 430 | 6862 | 0.8 | 19.6832 | 6.3 | 0.1821 | 6.4 | 0.0260 | 1.3 | 0.20 | 165.5 | 2.1 | 169.9 | 10.0 | 232.0 | 144.6 | 165.5 | 2.1 |
| KR-09-01-14 | 127 | 2376 | 1.3 | 48.3313 | 167.1 | 0.0389 | 167.2 | 0.0136 | 3.4 | 0.02 | 87.4 | 3.0 | 38.8 | 63.7 | -2489.2 | 0.0 | 87.4 | 3.0 |
| KR-09-01-15 | 314 | 4926 | 1.2 | 20.5639 | 13.0 | 0.1392 | 13.2 | 0.0208 | 2.0 | 0.16 | 132.4 | 2.7 | 132.3 | 16.3 | 130.0 | 306.9 | 132.4 | 2.7 |
| KR-09-01-16 | 287 | 1814 | 1.3 | 25.1508 | 12.3 | 0.0854 | 12.6 | 0.0156 | 2.5 | 0.20 | 99.7 | 2.5 | 83.2 | 10.1 | -366.5 | 320.5 | 99.7 | 2.5 |
| KR-09-01-17 | 1044 | 6457 | 4.1 | 21.3154 | 5.4 | 0.0990 | 5.5 | 0.0153 | 0.8 | 0.15 | 97.9 | 0.8 | 95.9 | 5.0 | 44.9 | 130.1 | 97.9 | 0.8 |
| KR-09-01-18 | 534 | 5492 | 1.1 | 20.6315 | 3.6 | 0.1838 | 3.8 | 0.0275 | 1.3 | 0.34 | 174.9 | 2.2 | 171.3 | 6.0 | 122.3 | 85.1 | 174.9 | 2.2 |
| KR-09-01-19 | 507 | 2514 | 1.5 | 23.3050 | 8.7 | 0.0880 | 8.8 | 0.0149 | 1.6 | 0.18 | 95.2 | 1.5 | 85.6 | 7.2 | -172.8 | 216.4 | 95.2 | 1.5 |
| KR-09-01-20 | 1030 | 8849 | 1.5 | 20.9528 | 2.6 | 0.1760 | 4.3 | 0.0268 | 3.4 | 0.79 | 170.2 | 5.7 | 164.6 | 6.5 | 85.7 | 62.2 | 170.2 | 5.7 |
| KR-09-01-21 | 142 | 2332 | 0.9 | 17.9170 | 17.7 | 0.1666 | 19.5 | 0.0216 | 8.3 | 0.42 | 138.1 | 11.3 | 156.5 | 28.4 | 444.9 | 396.5 | 138.1 | 11.3 |
| KR-09-01-22 | 1171 | 16811 | 0.9 | 20.4113 | 2.3 | 0.1549 | 3.5 | 0.0229 | 2.6 | 0.75 | 146.1 | 3.8 | 146.2 | 4.8 | 147.4 | 54.6 | 146.1 | 3.8 |
| KR-09-01-23 | 173 | 1695 | 1.7 | 23.9785 | 21.2 | 0.0884 | 21.2 | 0.0154 | 2.0 | 0.09 | 98.4 | 1.9 | 86.0 | 17.5 | -244.4 | 539.8 | 98.4 | 1.9 |
| KR-09-01-24 | 384 | 6632 | 1.4 | 23.0059 | 5.5 | 0.1347 | 5.9 | 0.0225 | 2.0 | 0.34 | 143.3 | 2.8 | 128.3 | 7.1 | -140.8 | 137.0 | 143.3 | 2.8 |
| KR-09-01-25 | 413 | 9694 | 0.8 | 22.3382 | 12.1 | 0.1346 | 12.2 | 0.0218 | 1.8 | 0.15 | 139.1 | 2.5 | 128.2 | 14.7 | -68.3 | 296.2 | 139.1 | 2.5 |
| KR-09-01-26 | 575 | 6730 | 1.6 | 20.3621 | 3.5 | 0.1835 | 3.9 | 0.0271 | 1.7 | 0.45 | 172.3 | 3.0 | 171.0 | 6.1 | 153.1 | 81.9 | 172.3 | 3.0 |
| KR-09-01-27 | 453 | 2897 | 0.9 | 23.3920 | 9.2 | 0.0878 | 9.3 | 0.0149 | 1.6 | 0.17 | 95.3 | 1.5 | 85.4 | 7.7 | -182.1 | 230.4 | 95.3 | 1.5 |
| KR-09-01-28 | 210 | 1584 | 2.4 | 25.4763 | 14.5 | 0.0813 | 14.6 | 0.0150 | 1.9 | 0.13 | 96.1 | 1.8 | 79.4 | 11.1 | -399.9 | 378.7 | 96.1 | 1.8 |
| KR-09-01-29 | 33 | 331 | 1.8 | 14.6025 | 114.0 | 0.1784 | 114.1 | 0.0189 | 4.9 | 0.04 | 120.6 | 5.8 | 166.6 | 177.2 | 883.2 | 482.6 | 120.6 | 5.8 |
| KR-09-01-30 | 526 | 3622 | 1.6 | 22.2657 | 10.9 | 0.0861 | 11.0 | 0.0139 | 1.1 | 0.10 | 89.0 | 1.0 | 83.8 | 8.8 | -60.4 | 266.9 | 89.0 | 1.0 |
| KR-09-01-31 | 116 | 1657 | 1.8 | 16.3073 | 52.1 | 0.1190 | 52.1 | 0.0141 | 2.6 | 0.05 | 90.1 | 2.3 | 114.1 | 56.4 | 650.5 | 1200.4 | 90.1 | 2.3 |
| KR-09-01-32 | 341 | 8302 | 0.9 | 21.9373 | 8.6 | 0.1663 | 8.8 | 0.0265 | 2.0 | 0.23 | 168.4 | 3.4 | 156.2 | 12.8 | -24.3 | 208.3 | 168.4 | 3.4 |
| KR-09-01-33 | 218 | 2754 | 1.5 | 29.2562 | 31.5 | 0.0728 | 31.5 | 0.0154 | 2.2 | 0.07 | 98.8 | 2.2 | 71.3 | 21.7 | -775.0 | 905.6 | 98.8 | 2.2 |
| KR-09-01-34 | 186 | 2013 | 1.6 | 29.4060 | 36.8 | 0.0708 | 36.8 | 0.0151 | 2.6 | 0.07 | 96.6 | 2.4 | 69.4 | 24.7 | -789.4 | 1069.7 | 96.6 | 2.4 |
| KR-09-01-35 | 479 | 5531 | 2.0 | 25.0877 | 19.7 | 0.0784 | 20.1 | 0.0143 | 3.7 | 0.19 | 91.3 | 3.4 | 76.7 | 14.8 | -360.0 | 514.8 | 91.3 | 3.4 |
| KR-09-01-36 | 153 | 2072 | 0.9 | 25.0150 | 19.3 | 0.1256 | 19.8 | 0.0228 | 4.7 | 0.24 | 145.2 | 6.8 | 120.1 | 22.5 | -352.5 | 501.9 | 145.2 | 6.8 |
| KR-09-01-37 | 124 | 1796 | 3.5 | 47.6463 | 78.1 | 0.0622 | 78.1 | 0.0215 | 2.9 | 0.04 | 137.2 | 4.0 | 61.3 | 46.5 | -2429.3 | 771.2 | 137.2 | 4.0 |
| KR-09-01-38 | 370 | 3268 | 1.5 | 21.9051 | 6.8 | 0.0978 | 7.0 | 0.0155 | 1.4 | 0.20 | 99.4 | 1.4 | 94.7 | 6.3 | -20.7 | 164.9 | 99.4 | 1.4 |
| KR-09-01-39 | 901 | 5564 | 4.8 | 21.7064 | 5.7 | 0.0989 | 6.0 | 0.0156 | 1.7 | 0.29 | 99.5 | 1.7 | 95.7 | 5.5 | 1.2 | 137.8 | 99.5 | 1.7 |
| KR-09-01-40 | 197 | 1912 | 1.5 | 24.4325 | 13.6 | 0.1315 | 14.1 | 0.0233 | 3.4 | 0.24 | 148.5 | 5.0 | 125.5 | 16.6 | -292.0 | 349.4 | 148.5 | 5.0 |
| KR-09-01-41 | 1295 | 20633 | 0.9 | 20.3709 | 1.8 | 0.1787 | 2.5 | 0.0264 | 1.7 | 0.68 | 168.0 | 2.8 | 167.0 | 3.9 | 152.1 | 43.3 | 168.0 | 2.8 |
| KR-09-01-42 | 383 | 6014 | 1.1 | 19.8980 | 6.4 | 0.1593 | 6.7 | 0.0230 | 2.2 | 0.32 | 146.5 | 3.1 | 150.1 | 9.4 | 206.9 | 148.5 | 146.5 | 3.1 |
| KR-09-01-43 | 238 | 3206 | 1.8 | 22.9789 | 11.1 | 0.1386 | 11.2 | 0.0231 | 1.6 | 0.14 | 147.2 | 2.3 | 131.8 | 13.9 | -137.8 | 276.2 | 147.2 | 2.3 |

**Table A4.1 –** Detrital zircon U-Pb analyses

| Analysis | U (ppm) | $^{206}Pb/^{204}Pb$ | U/Th | Isotopic Ratio | | | | | | Error | Apparent Age (Ma) | | | | | | Best Age (Ma) | |
|---|---|---|---|---|---|---|---|---|---|---|---|---|---|---|---|---|---|---|
| | | | | $^{206}Pb/^{207}Pb$ | ± (%) | $^{207}Pb/^{235}U$ | ± (%) | $^{206}Pb/^{238}U$ | ± (%) | | $^{206}Pb/^{238}U$ | ± (Ma) | $^{207}Pb/^{235}U$ | ± (Ma) | $^{206}Pb/^{207}Pb$ | ± (Ma) | Age | ± |
| KR-09-01-44 | 355 | 5921 | 1.4 | 20.0465 | 6.0 | 0.1888 | 6.1 | 0.0274 | 1.3 | 0.20 | 174.5 | 2.2 | 175.6 | 9.9 | 189.6 | 139.5 | 174.5 | 2.2 |
| KR-09-01-45 | 1347 | 22474 | 1.1 | 20.1138 | 1.9 | 0.1619 | 2.4 | 0.0236 | 1.5 | 0.61 | 150.5 | 2.2 | 152.4 | 3.5 | 181.8 | 45.4 | 150.5 | 2.2 |
| KR-09-01-46 | 267 | 3102 | 1.5 | 25.2640 | 16.4 | 0.0871 | 16.6 | 0.0160 | 2.7 | 0.16 | 102.0 | 2.7 | 84.8 | 13.5 | -378.1 | 427.3 | 102.0 | 2.7 |
| KR-09-01-47 | 2110 | 18777 | 1.5 | 20.5328 | 3.7 | 0.1045 | 4.3 | 0.0156 | 2.1 | 0.49 | 99.5 | 2.1 | 100.9 | 4.1 | 133.5 | 87.6 | 99.5 | 2.1 |
| KR-09-01-48 | 291 | 34743 | 1.2 | 13.2325 | 1.3 | 1.9405 | 2.4 | 0.1862 | 2.1 | 0.85 | 1101.0 | 20.9 | 1095.2 | 16.2 | 1083.7 | 25.5 | 1083.7 | 25.5 |
| KR-09-01-49 | 759 | 7861 | 3.2 | 22.5886 | 8.3 | 0.0947 | 8.4 | 0.0155 | 1.4 | 0.16 | 99.3 | 1.4 | 91.9 | 7.4 | -95.6 | 204.4 | 99.3 | 1.4 |
| KR-09-01-50 | 1011 | 11338 | 1.0 | 20.6929 | 2.5 | 0.1578 | 2.7 | 0.0237 | 1.2 | 0.44 | 150.9 | 1.8 | 148.8 | 3.8 | 115.3 | 58.0 | 150.9 | 1.8 |
| KR-09-01-52 | 175 | 2105 | 0.7 | 19.9072 | 21.7 | 0.1648 | 21.8 | 0.0238 | 1.5 | 0.07 | 151.6 | 2.2 | 154.9 | 31.3 | 205.8 | 508.9 | 151.6 | 2.2 |
| KR-09-01-53 | 64 | 1192 | 2.3 | 19.0168 | 99.9 | 0.1603 | 100.1 | 0.0221 | 5.4 | 0.05 | 141.0 | 7.5 | 151.0 | 141.3 | 310.9 | N/A | 141.0 | 7.5 |
| KR-09-01-54 | 38 | 807 | 1.3 | 19.2768 | 62.4 | 0.1143 | 62.9 | 0.0160 | 7.2 | 0.11 | 102.2 | 7.3 | 109.9 | 65.6 | 280.0 | 1587.5 | 102.2 | 7.3 |
| KR-09-01-55 | 64 | 1025 | 2.7 | 5.9424 | 177.4 | 0.3469 | 177.5 | 0.0150 | 5.9 | 0.03 | 95.7 | 5.6 | 302.4 | 501.2 | 2540.6 | 313.8 | 2540.6 | 313.8 |
| KR-09-01-56 | 108 | 959 | 1.8 | 28.9963 | 40.3 | 0.0716 | 40.6 | 0.0151 | 4.8 | 0.12 | 96.3 | 4.6 | 70.2 | 27.5 | -749.9 | 1169.3 | 96.3 | 4.6 |
| KR-09-01-57 | 56 | 628 | 1.3 | 16.5658 | 118.4 | 0.1238 | 118.5 | 0.0149 | 4.0 | 0.03 | 95.1 | 3.8 | 118.5 | 133.2 | 616.7 | 709.0 | 95.1 | 3.8 |
| KR-09-01-58 | 658 | 8742 | 1.9 | 20.1835 | 6.2 | 0.1600 | 6.5 | 0.0234 | 1.8 | 0.27 | 149.3 | 2.6 | 150.7 | 9.1 | 173.7 | 145.6 | 149.3 | 2.6 |
| KR-09-01-59 | 88 | 1822 | 1.5 | 22.8210 | 42.5 | 0.1366 | 42.6 | 0.0226 | 2.7 | 0.06 | 144.1 | 3.8 | 130.0 | 52.0 | -120.8 | 1092.8 | 144.1 | 3.8 |
| KR-09-01-60 | 437 | 9184 | 0.8 | 22.0128 | 10.4 | 0.1609 | 10.6 | 0.0257 | 1.8 | 0.17 | 163.5 | 3.0 | 151.5 | 14.9 | -32.6 | 253.1 | 163.5 | 3.0 |
| KR-09-01-61 | 122 | 1804 | 1.8 | 24.4634 | 26.3 | 0.0847 | 26.7 | 0.0150 | 4.2 | 0.16 | 96.2 | 4.0 | 82.6 | 21.2 | -295.2 | 682.3 | 96.2 | 4.0 |
| KR-09-01-62 | 228 | 3687 | 1.7 | 26.9524 | 35.8 | 0.0748 | 35.8 | 0.0146 | 1.7 | 0.05 | 93.5 | 1.6 | 73.2 | 25.3 | -549.1 | 988.1 | 93.5 | 1.6 |
| KR-09-01-63 | 180 | 3799 | 2.3 | 21.8743 | 19.8 | 0.1420 | 19.9 | 0.0225 | 2.0 | 0.10 | 143.6 | 2.8 | 134.8 | 25.1 | -17.3 | 483.3 | 143.6 | 2.8 |
| KR-09-01-64 | 248 | 3377 | 1.9 | 23.4301 | 21.5 | 0.1399 | 21.6 | 0.0238 | 1.7 | 0.08 | 151.5 | 2.6 | 133.0 | 26.9 | -186.2 | 543.3 | 151.5 | 2.6 |
| KR-09-01-65 | 312 | 6264 | 0.9 | 21.5467 | 11.2 | 0.1515 | 11.2 | 0.0237 | 0.5 | 0.04 | 150.9 | 0.7 | 143.3 | 15.0 | 19.0 | 270.1 | 150.9 | 0.7 |
| KR-09-01-66 | 541 | 10126 | 5.2 | 20.3626 | 6.8 | 0.1636 | 7.2 | 0.0242 | 2.3 | 0.32 | 153.9 | 3.5 | 153.9 | 10.2 | 153.1 | 158.9 | 153.9 | 3.5 |
| KR-09-01-67 | 128 | 3078 | 1.3 | 24.1434 | 17.2 | 0.1303 | 17.3 | 0.0228 | 1.5 | 0.09 | 145.5 | 2.2 | 124.4 | 20.2 | -261.7 | 439.1 | 145.5 | 2.2 |
| KR-09-01-68 | 280 | 6080 | 1.5 | 21.0072 | 12.1 | 0.1514 | 12.5 | 0.0231 | 2.9 | 0.24 | 147.0 | 4.3 | 143.1 | 16.7 | 79.6 | 288.9 | 147.0 | 4.3 |
| KR-09-01-69 | 315 | 3937 | 2.4 | 20.4940 | 18.1 | 0.1022 | 18.1 | 0.0152 | 0.5 | 0.03 | 97.2 | 0.4 | 98.8 | 17.0 | 138.0 | 428.1 | 97.2 | 0.4 |
| KR-09-01-70 | 247 | 4716 | 1.2 | 22.1402 | 11.6 | 0.1504 | 11.8 | 0.0241 | 1.7 | 0.15 | 153.8 | 2.6 | 142.2 | 15.6 | -46.6 | 283.5 | 153.8 | 2.6 |
| KR-09-01-71 | 1385 | 16514 | 2.4 | 20.9909 | 3.7 | 0.0979 | 3.9 | 0.0149 | 1.2 | 0.32 | 95.4 | 1.2 | 94.8 | 3.6 | 81.4 | 88.4 | 95.4 | 1.2 |
| KR-09-01-72 | 104 | 1919 | 1.1 | 20.6582 | 21.6 | 0.1425 | 21.7 | 0.0213 | 1.8 | 0.09 | 136.2 | 2.5 | 135.2 | 27.4 | 119.2 | 514.2 | 136.2 | 2.5 |
| KR-09-01-73 | 112 | 2900 | 1.1 | 23.6339 | 16.0 | 0.1240 | 16.1 | 0.0213 | 2.0 | 0.12 | 135.6 | 2.7 | 118.7 | 18.1 | -207.9 | 404.0 | 135.6 | 2.7 |
| KR-09-01-74 | 161 | 2533 | 2.4 | 23.2265 | 26.1 | 0.0898 | 26.1 | 0.0151 | 2.0 | 0.08 | 96.8 | 1.9 | 87.4 | 21.9 | -164.5 | 658.0 | 96.8 | 1.9 |
| KR-09-01-75 | 666 | 9966 | 1.5 | 21.4448 | 4.5 | 0.1450 | 4.9 | 0.0226 | 2.0 | 0.40 | 143.8 | 2.8 | 137.5 | 6.3 | 30.4 | 107.7 | 143.8 | 2.8 |
| KR-09-01-76 | 165 | 488 | 2.4 | 15.0457 | 35.3 | 0.1380 | 35.7 | 0.0151 | 5.6 | 0.16 | 96.3 | 5.3 | 131.2 | 44.0 | 821.1 | 759.7 | 96.3 | 5.3 |
| KR-09-01-77 | 312 | 4149 | 2.0 | 23.6322 | 20.1 | 0.0856 | 20.3 | 0.0147 | 2.7 | 0.14 | 93.9 | 2.6 | 83.4 | 16.2 | -207.7 | 507.9 | 93.9 | 2.6 |
| KR-09-01-78 | 204 | 2561 | 1.8 | 29.7899 | 27.3 | 0.0698 | 27.4 | 0.0151 | 2.4 | 0.09 | 96.5 | 2.3 | 68.5 | 18.1 | -826.3 | 789.2 | 96.5 | 2.3 |
| KR-09-01-79 | 151 | 1839 | 1.6 | 37.5667 | 41.4 | 0.0501 | 41.4 | 0.0137 | 1.7 | 0.04 | 87.4 | 1.4 | 49.7 | 20.1 | -1542.7 | 1437.8 | 87.4 | 1.4 |
| KR-09-01-80 | 106 | 3233 | 1.7 | 13.5129 | 121.0 | 0.2376 | 121.1 | 0.0233 | 2.5 | 0.02 | 148.4 | 3.7 | 216.5 | 240.4 | 1041.5 | 416.9 | 148.4 | 3.7 |
| KR-09-01-81 | 789 | 5793 | 1.5 | 20.6433 | 9.5 | 0.0902 | 9.9 | 0.0135 | 2.9 | 0.29 | 86.5 | 2.5 | 87.7 | 8.3 | 120.9 | 223.8 | 86.5 | 2.5 |
| KR-09-01-82 | 228 | 3014 | 1.7 | 24.4636 | 19.4 | 0.0831 | 19.6 | 0.0147 | 2.6 | 0.13 | 94.3 | 2.4 | 81.0 | 15.2 | -295.2 | 499.2 | 94.3 | 2.4 |
| KR-09-01-83 | 106 | 2458 | 1.4 | 15.9685 | 79.3 | 0.2094 | 79.5 | 0.0242 | 6.3 | 0.08 | 154.4 | 9.6 | 193.0 | 140.7 | 695.5 | 2098.1 | 154.4 | 9.6 |
| KR-09-01-85 | 438 | 7785 | 1.7 | 20.8523 | 5.4 | 0.1707 | 5.6 | 0.0258 | 1.6 | 0.28 | 164.3 | 2.6 | 160.1 | 8.3 | 97.1 | 127.1 | 164.3 | 2.6 |
| KR-09-01-86 | 191 | 1138 | 2.6 | 20.8044 | 15.8 | 0.0966 | 16.1 | 0.0146 | 2.9 | 0.18 | 93.3 | 2.7 | 93.7 | 14.4 | 102.6 | 376.6 | 93.3 | 2.7 |
| KR-09-01-87 | 734 | 13741 | 1.3 | 20.9161 | 4.1 | 0.1741 | 5.8 | 0.0264 | 4.1 | 0.71 | 168.1 | 6.8 | 163.0 | 8.7 | 89.9 | 96.0 | 168.1 | 6.8 |

**Table A4.1 –** Detrital zircon U-Pb analyses

| Analysis | U (ppm) | $^{206}Pb/^{204}Pb$ | U/Th | Isotopic Ratio | | | | | | Error | Apparent Age (Ma) | | | | | | Best Age (Ma) | |
|---|---|---|---|---|---|---|---|---|---|---|---|---|---|---|---|---|---|---|
| | | | | $^{206}Pb/^{207}Pb$ | ± (%) | $^{207}Pb/^{235}U$ | ± (%) | $^{206}Pb/^{238}U$ | ± (%) | | $^{206}Pb/^{238}U$ | ± (Ma) | $^{207}Pb/^{235}U$ | ± (Ma) | $^{206}Pb/^{207}Pb$ | ± (Ma) | Age | ± |
| KR-09-01-88 | 1067 | 15311 | 1.2 | 18.9667 | 9.9 | 0.1926 | 11.5 | 0.0265 | 5.8 | 0.50 | 168.6 | 9.6 | 178.9 | 18.8 | 316.9 | 225.4 | 168.6 | 9.6 |
| KR-09-01-89 | 126 | 2271 | 2.0 | 24.2429 | 13.2 | 0.1256 | 13.2 | 0.0221 | 1.1 | 0.08 | 140.8 | 1.5 | 120.2 | 15.0 | -272.2 | 336.8 | 140.8 | 1.5 |
| KR-09-01-90 | 487 | 4213 | 1.7 | 21.4728 | 6.4 | 0.0915 | 6.6 | 0.0142 | 1.7 | 0.26 | 91.2 | 1.6 | 88.9 | 5.6 | 27.3 | 152.8 | 91.2 | 1.6 |
| KR-09-01-91 | 102 | 1661 | 2.5 | 28.4256 | 34.1 | 0.1043 | 34.2 | 0.0215 | 3.1 | 0.09 | 137.2 | 4.2 | 100.8 | 32.8 | -694.4 | 968.2 | 137.2 | 4.2 |
| KR-09-01-92 | 288 | 4476 | 1.5 | 20.3273 | 12.8 | 0.1029 | 12.9 | 0.0152 | 1.2 | 0.09 | 97.0 | 1.1 | 99.4 | 12.2 | 157.1 | 301.1 | 97.0 | 1.1 |
| KR-09-01-94 | 544 | 14648 | 1.5 | 19.7198 | 7.7 | 0.1866 | 8.3 | 0.0267 | 3.1 | 0.37 | 169.8 | 5.1 | 173.8 | 13.3 | 227.7 | 178.4 | 169.8 | 5.1 |
| KR-09-01-95 | 336 | 5213 | 2.2 | 21.1394 | 11.3 | 0.1504 | 11.7 | 0.0231 | 3.1 | 0.26 | 147.0 | 4.5 | 142.3 | 15.6 | 64.7 | 270.5 | 147.0 | 4.5 |
| KR-09-01-96 | 834 | 7784 | 1.8 | 21.6421 | 5.5 | 0.0890 | 5.8 | 0.0140 | 1.9 | 0.32 | 89.4 | 1.7 | 86.6 | 4.8 | 8.4 | 133.0 | 89.4 | 1.7 |
| KR-09-01-97 | 162 | 3681 | 2.3 | 21.2764 | 16.0 | 0.1403 | 16.3 | 0.0216 | 2.6 | 0.16 | 138.0 | 3.5 | 133.3 | 20.3 | 49.2 | 385.3 | 138.0 | 3.5 |
| KR-09-01-98 | 241 | 4007 | 1.7 | 20.8429 | 15.1 | 0.1383 | 15.2 | 0.0209 | 1.8 | 0.12 | 133.4 | 2.4 | 131.5 | 18.7 | 98.2 | 358.8 | 133.4 | 2.4 |
| KR-09-01-99 | 390 | 3544 | 1.8 | 21.9348 | 11.6 | 0.0932 | 11.8 | 0.0148 | 2.0 | 0.17 | 94.9 | 1.9 | 90.5 | 10.2 | -24.0 | 281.3 | 94.9 | 1.9 |
| KR-09-01-100 | 835 | 17251 | 1.5 | 19.3443 | 2.6 | 0.2900 | 4.0 | 0.0407 | 3.1 | 0.77 | 257.1 | 7.7 | 258.6 | 9.1 | 271.9 | 58.5 | 257.1 | 7.7 |
| KR-09-02-2 | 283 | 5599 | 1.6 | 19.6133 | 6.3 | 0.1900 | 6.5 | 0.0270 | 1.6 | 0.25 | 171.9 | 2.8 | 176.6 | 10.5 | 240.2 | 144.4 | 171.9 | 2.8 |
| KR-09-02-3 | 443 | 7607 | 0.9 | 21.5372 | 5.4 | 0.1443 | 5.7 | 0.0225 | 1.7 | 0.30 | 143.7 | 2.4 | 136.9 | 7.3 | 20.1 | 130.3 | 143.7 | 2.4 |
| KR-09-02-4 | 170 | 2249 | 2.1 | 22.1373 | 19.5 | 0.1003 | 19.6 | 0.0161 | 2.1 | 0.11 | 103.0 | 2.2 | 97.1 | 18.1 | -46.3 | 477.3 | 103.0 | 2.2 |
| KR-09-02-5 | 521 | 3775 | 3.3 | 17.5064 | 19.5 | 0.1783 | 20.3 | 0.0226 | 5.8 | 0.28 | 144.3 | 8.2 | 166.6 | 31.2 | 496.2 | 433.2 | 144.3 | 8.2 |
| KR-09-02-6 | 208 | 4370 | 1.4 | 21.4934 | 11.3 | 0.1614 | 11.3 | 0.0252 | 1.3 | 0.12 | 160.2 | 2.1 | 151.9 | 16.0 | 25.0 | 270.7 | 160.2 | 2.1 |
| KR-09-02-7 | 182 | 7730 | 1.4 | 19.7745 | 12.2 | 0.1980 | 12.3 | 0.0284 | 1.4 | 0.12 | 180.5 | 2.5 | 183.4 | 20.7 | 221.3 | 283.6 | 180.5 | 2.5 |
| KR-09-02-8 | 241 | 4112 | 1.3 | 23.7099 | 10.6 | 0.1476 | 10.9 | 0.0254 | 2.3 | 0.21 | 161.6 | 3.6 | 139.8 | 14.2 | -216.0 | 267.4 | 161.6 | 3.6 |
| KR-09-02-9 | 81 | 2064 | 1.4 | 21.3135 | 23.3 | 0.1565 | 23.4 | 0.0242 | 2.1 | 0.09 | 154.1 | 3.2 | 147.6 | 32.1 | 45.1 | 562.9 | 154.1 | 3.2 |
| KR-09-02-10 | 171 | 2884 | 1.2 | 20.4510 | 16.0 | 0.1510 | 16.1 | 0.0224 | 1.3 | 0.08 | 142.8 | 1.8 | 142.8 | 21.4 | 142.9 | 377.8 | 142.8 | 1.8 |
| KR-09-02-11 | 77 | 2000 | 1.0 | 14.2221 | 87.7 | 0.2086 | 88.0 | 0.0215 | 6.6 | 0.08 | 137.2 | 9.0 | 192.4 | 155.4 | 937.5 | 261.9 | 137.2 | 9.0 |
| KR-09-02-12 | 133 | 1249 | 1.4 | 19.6718 | 36.9 | 0.1479 | 37.6 | 0.0211 | 7.2 | 0.19 | 134.7 | 9.6 | 140.1 | 49.2 | 233.3 | 879.0 | 134.7 | 9.6 |
| KR-09-02-13 | 400 | 4651 | 1.4 | 20.9722 | 8.7 | 0.1046 | 9.0 | 0.0159 | 2.2 | 0.25 | 101.7 | 2.2 | 101.0 | 8.7 | 83.5 | 207.8 | 101.7 | 2.2 |
| KR-09-02-14 | 261 | 5177 | 1.6 | 23.8019 | 11.7 | 0.1337 | 11.7 | 0.0231 | 1.1 | 0.09 | 147.1 | 1.6 | 127.4 | 14.1 | -225.7 | 295.3 | 147.1 | 1.6 |
| KR-09-02-15 | 68 | 2147 | 3.3 | 22.2789 | 37.8 | 0.2255 | 37.9 | 0.0364 | 2.2 | 0.06 | 230.7 | 4.9 | 206.5 | 70.9 | -61.8 | 952.7 | 230.7 | 4.9 |
| KR-09-02-16 | 496 | 7616 | 2.5 | 21.7803 | 7.7 | 0.0993 | 7.9 | 0.0157 | 1.7 | 0.21 | 100.3 | 1.6 | 96.1 | 7.2 | -6.9 | 186.3 | 100.3 | 1.6 |
| KR-09-02-17 | 92 | 3165 | 2.2 | 19.8133 | 13.0 | 0.2739 | 13.3 | 0.0394 | 2.9 | 0.22 | 248.9 | 7.1 | 245.8 | 29.1 | 216.8 | 301.8 | 248.9 | 7.1 |
| KR-09-02-18 | 171 | 3854 | 2.0 | 20.3866 | 9.8 | 0.1510 | 10.0 | 0.0223 | 2.3 | 0.23 | 142.4 | 3.2 | 142.8 | 13.4 | 150.3 | 229.8 | 142.4 | 3.2 |
| KR-09-02-19 | 36 | 1287 | 2.5 | 1.5319 | 1921.3 | 3.1004 | 1921.3 | 0.0344 | 4.0 | 0.00 | 218.3 | 8.6 | 1432.8 | N/A | 0.0 | 469.0 | 218.3 | 8.6 |
| KR-09-02-21 | 236 | 7942 | 2.9 | 13.6591 | 7.4 | 0.6099 | 10.6 | 0.0604 | 7.6 | 0.72 | 378.2 | 28.0 | 483.5 | 40.8 | 1019.8 | 149.1 | 378.2 | 28.0 |
| KR-09-02-22 | 38 | 351 | 2.0 | 2.6335 | 1033.2 | 0.6136 | 1033.2 | 0.0117 | 4.4 | 0.00 | 75.1 | 3.3 | 485.8 | N/A | 3830.6 | 415.6 | 3830.6 | 415.6 |
| KR-09-02-22 | 77 | 1306 | 2.5 | 23.7968 | 37.2 | 0.0887 | 37.3 | 0.0153 | 2.1 | 0.06 | 97.9 | 2.0 | 86.3 | 30.9 | -225.2 | 966.6 | 97.9 | 2.0 |
| KR-09-02-24 | 134 | 3174 | 1.3 | 23.8196 | 21.4 | 0.1610 | 21.5 | 0.0278 | 1.4 | 0.06 | 176.8 | 2.4 | 151.5 | 30.3 | -227.6 | 545.5 | 176.8 | 2.4 |
| KR-09-02-25 | 374 | 4544 | 1.7 | 24.6218 | 10.1 | 0.0783 | 10.3 | 0.0140 | 1.7 | 0.16 | 89.5 | 1.5 | 76.5 | 7.6 | -311.7 | 260.5 | 89.5 | 1.5 |
| KR-09-02-27 | 105 | 3003 | 1.9 | 21.9792 | 20.5 | 0.1424 | 20.6 | 0.0227 | 2.1 | 0.10 | 144.7 | 3.0 | 135.2 | 26.1 | -28.9 | 501.8 | 144.7 | 3.0 |
| KR-09-02-28 | 163 | 3706 | 0.7 | 20.8143 | 12.9 | 0.1697 | 12.9 | 0.0256 | 1.0 | 0.07 | 163.1 | 1.5 | 159.2 | 19.0 | 101.4 | 305.0 | 163.1 | 1.5 |
| KR-09-02-29 | 133 | 2894 | 2.1 | 23.4212 | 11.6 | 0.1345 | 11.8 | 0.0228 | 1.9 | 0.16 | 145.6 | 2.7 | 128.1 | 14.2 | -185.3 | 291.6 | 145.6 | 2.7 |
| KR-09-02-30 | 200 | 6250 | 3.1 | 20.9775 | 8.9 | 0.2303 | 10.9 | 0.0350 | 6.4 | 0.59 | 222.0 | 14.1 | 210.4 | 20.8 | 82.9 | 210.4 | 222.0 | 14.1 |
| KR-09-02-31 | 239 | 10837 | 1.6 | 21.5943 | 7.1 | 0.1657 | 7.6 | 0.0259 | 2.8 | 0.37 | 165.1 | 4.6 | 155.7 | 11.0 | 13.7 | 170.0 | 165.1 | 4.6 |
| KR-09-02-32 | 78 | 2634 | 1.0 | 20.8494 | 33.2 | 0.1370 | 34.2 | 0.0207 | 8.5 | 0.25 | 132.2 | 11.1 | 130.4 | 41.9 | 97.4 | 804.7 | 132.2 | 11.1 |
| KR-09-02-33 | 179 | 3613 | 1.2 | 23.1989 | 17.7 | 0.1346 | 17.7 | 0.0226 | 0.9 | 0.05 | 144.3 | 1.3 | 128.2 | 21.4 | -161.5 | 443.5 | 144.3 | 1.3 |

**Table A4.1 –** Detrital zircon U-Pb analyses

| Analysis | U (ppm) | $^{206}Pb/^{204}Pb$ | U/Th | Isotopic Ratio | | | | | | Error | Apparent Age (Ma) | | | | | | Best Age (Ma) | |
|---|---|---|---|---|---|---|---|---|---|---|---|---|---|---|---|---|---|---|
| | | | | $^{206}Pb/^{207}Pb$ | ± (%) | $^{207}Pb/^{235}U$ | ± (%) | $^{206}Pb/^{238}U$ | ± (%) | | $^{206}Pb/^{238}U$ | ± (Ma) | $^{207}Pb/^{235}U$ | ± (Ma) | $^{206}Pb/^{207}Pb$ | ± (Ma) | Age | ± |
| KR-09-02-34 | 80 | 1687 | 1.2 | 26.1176 | 46.3 | 0.1135 | 46.4 | 0.0215 | 3.0 | 0.07 | 137.2 | 4.1 | 109.2 | 48.1 | -465.2 | 1283.6 | 137.2 | 4.1 |
| KR-09-02-35 | 125 | 3648 | 1.4 | 24.4171 | 19.8 | 0.1680 | 19.8 | 0.0298 | 0.9 | 0.04 | 189.0 | 1.6 | 157.7 | 29.0 | -290.4 | 509.6 | 189.0 | 1.6 |
| KR-09-02-37 | 93 | 2068 | 1.5 | 26.5533 | 26.0 | 0.1107 | 26.1 | 0.0213 | 2.8 | 0.11 | 136.0 | 3.8 | 106.6 | 26.4 | -509.1 | 701.8 | 136.0 | 3.8 |
| KR-09-02-38 | 214 | 6801 | 1.0 | 21.4475 | 7.4 | 0.1808 | 8.6 | 0.0281 | 4.5 | 0.52 | 178.8 | 7.9 | 168.8 | 13.4 | 30.1 | 176.7 | 178.8 | 7.9 |
| KR-09-02-39 | 110 | 2403 | 0.8 | 33.2832 | 56.3 | 0.0942 | 56.3 | 0.0227 | 1.8 | 0.03 | 144.9 | 2.6 | 91.4 | 49.3 | -1154.3 | 1852.3 | 144.9 | 2.6 |
| KR-09-02-40 | 525 | 10729 | 1.4 | 20.6909 | 7.6 | 0.1385 | 8.7 | 0.0208 | 4.4 | 0.50 | 132.6 | 5.8 | 131.7 | 10.8 | 115.5 | 178.5 | 132.6 | 5.8 |
| KR-09-02-41 | 68 | 2726 | 1.8 | 26.1099 | 24.2 | 0.1962 | 24.4 | 0.0372 | 3.2 | 0.13 | 235.2 | 7.4 | 181.9 | 40.7 | -464.4 | 648.2 | 235.2 | 7.4 |
| KR-09-02-42 | 191 | 6121 | 1.1 | 19.3168 | 12.0 | 0.1928 | 12.2 | 0.0270 | 1.7 | 0.14 | 171.8 | 2.8 | 179.0 | 20.0 | 275.2 | 276.8 | 171.8 | 2.8 |
| KR-09-02-43 | 138 | 2650 | 2.0 | 21.3722 | 18.4 | 0.1441 | 18.5 | 0.0223 | 1.7 | 0.09 | 142.4 | 2.5 | 136.7 | 23.6 | 38.5 | 443.6 | 142.4 | 2.5 |
| KR-09-02-44 | 325 | 6741 | 2.4 | 24.3752 | 8.7 | 0.1283 | 9.0 | 0.0227 | 2.3 | 0.26 | 144.6 | 3.3 | 122.6 | 10.4 | -286.0 | 222.6 | 144.6 | 3.3 |
| KR-09-02-45 | 95 | 2284 | 2.0 | 20.3678 | 37.3 | 0.1522 | 37.4 | 0.0225 | 2.8 | 0.07 | 143.3 | 4.0 | 143.8 | 50.2 | 152.5 | 901.8 | 143.3 | 4.0 |
| KR-09-02-46 | 92 | 812 | 1.4 | 26.0670 | 21.5 | 0.1163 | 21.7 | 0.0220 | 2.9 | 0.14 | 140.2 | 4.1 | 111.7 | 23.0 | -460.1 | 572.7 | 140.2 | 4.1 |
| KR-09-02-47 | 413 | 4337 | 1.4 | 21.0075 | 12.6 | 0.0846 | 13.1 | 0.0129 | 3.5 | 0.27 | 82.6 | 2.9 | 82.5 | 10.4 | 79.5 | 301.2 | 82.6 | 2.9 |
| KR-09-02-48 | 461 | 6246 | 1.5 | 19.7370 | 4.7 | 0.1066 | 4.9 | 0.0153 | 1.4 | 0.29 | 97.6 | 1.4 | 102.8 | 4.8 | 225.7 | 108.3 | 97.6 | 1.4 |
| KR-09-02-49 | 65 | 1277 | 1.4 | 14.2406 | 86.2 | 0.2095 | 86.3 | 0.0216 | 2.2 | 0.03 | 138.0 | 3.0 | 193.1 | 152.8 | 934.8 | 2388.5 | 138.0 | 3.0 |
| KR-09-02-50 | 651 | 7798 | 1.9 | 20.5619 | 5.3 | 0.0950 | 5.5 | 0.0142 | 1.7 | 0.31 | 90.6 | 1.5 | 92.1 | 4.9 | 130.2 | 123.7 | 90.6 | 1.5 |
| KR-09-02-51 | 53 | 1017 | 0.9 | 26.3184 | 27.9 | 0.1266 | 28.0 | 0.0242 | 3.0 | 0.11 | 154.0 | 4.5 | 121.1 | 32.0 | -485.5 | 751.7 | 154.0 | 4.5 |
| KR-09-02-52 | 351 | 10132 | 1.6 | 20.2213 | 4.8 | 0.1585 | 5.1 | 0.0232 | 1.5 | 0.31 | 148.1 | 2.3 | 149.4 | 7.0 | 169.3 | 112.5 | 148.1 | 2.3 |
| KR-09-02-53 | 346 | 5097 | 0.5 | 19.7332 | 13.5 | 0.1078 | 13.7 | 0.0154 | 2.2 | 0.16 | 98.7 | 2.2 | 103.9 | 13.5 | 226.1 | 313.3 | 98.7 | 2.2 |
| KR-09-02-55 | 86 | 2971 | 2.8 | 19.8212 | 13.6 | 0.2618 | 13.8 | 0.0376 | 2.6 | 0.19 | 238.1 | 6.0 | 236.1 | 29.2 | 215.8 | 316.3 | 238.1 | 6.0 |
| KR-09-02-56 | 335 | 3992 | 1.3 | 24.2634 | 16.7 | 0.0789 | 17.7 | 0.0139 | 5.9 | 0.33 | 88.8 | 5.2 | 77.1 | 13.1 | -274.3 | 426.3 | 88.8 | 5.2 |
| KR-09-02-57 | 116 | 2601 | 0.9 | 24.6179 | 28.2 | 0.1163 | 28.3 | 0.0208 | 2.1 | 0.07 | 132.5 | 2.7 | 111.7 | 30.0 | -311.3 | 735.7 | 132.5 | 2.7 |
| KR-09-02-58 | 530 | 6438 | 2.5 | 20.4844 | 7.3 | 0.0947 | 8.3 | 0.0141 | 4.0 | 0.48 | 90.1 | 3.6 | 91.9 | 7.3 | 139.1 | 170.5 | 90.1 | 3.6 |
| KR-09-02-59 | 947 | 9529 | 3.9 | 21.1221 | 5.7 | 0.0977 | 5.9 | 0.0150 | 1.4 | 0.23 | 95.8 | 1.3 | 94.7 | 5.3 | 66.6 | 136.3 | 95.8 | 1.3 |
| KR-09-02-61 | 409 | 5153 | 1.7 | 21.5665 | 12.8 | 0.1002 | 12.9 | 0.0157 | 1.1 | 0.08 | 100.3 | 1.0 | 97.0 | 11.9 | 16.8 | 309.8 | 100.3 | 1.0 |
| KR-09-02-62 | 166 | 1869 | 2.3 | 22.9422 | 58.0 | 0.0819 | 58.4 | 0.0136 | 6.1 | 0.10 | 87.2 | 5.3 | 79.9 | 44.9 | -133.9 | 1559.8 | 87.2 | 5.3 |
| KR-09-02-63 | 73 | 961 | 2.8 | 14.8629 | 31.1 | 0.1412 | 31.3 | 0.0152 | 3.5 | 0.11 | 97.4 | 3.4 | 134.1 | 39.4 | 846.5 | 662.7 | 97.4 | 3.4 |
| KR-09-02-64 | 252 | 5330 | 1.6 | 22.0472 | 10.2 | 0.1398 | 10.4 | 0.0224 | 2.2 | 0.21 | 142.5 | 3.1 | 132.9 | 13.0 | -36.4 | 248.2 | 142.5 | 3.1 |
| KR-09-02-65 | 246 | 6296 | 1.7 | 21.1249 | 6.6 | 0.2022 | 6.7 | 0.0310 | 1.2 | 0.17 | 196.7 | 2.3 | 187.0 | 11.5 | 66.3 | 158.3 | 196.7 | 2.3 |
| KR-09-02-66 | 251 | 4999 | 1.1 | 21.1906 | 11.5 | 0.1702 | 11.9 | 0.0262 | 3.0 | 0.25 | 166.5 | 4.9 | 159.6 | 17.5 | 58.9 | 274.6 | 166.5 | 4.9 |
| KR-09-02-67 | 199 | 5225 | 0.7 | 20.6045 | 10.9 | 0.1534 | 11.2 | 0.0229 | 2.8 | 0.25 | 146.1 | 4.0 | 144.9 | 15.1 | 125.3 | 256.6 | 146.1 | 4.0 |
| KR-09-02-68 | 729 | 17740 | 1.4 | 19.8990 | 2.5 | 0.2021 | 3.3 | 0.0292 | 2.2 | 0.66 | 185.4 | 4.0 | 186.9 | 5.7 | 206.8 | 58.3 | 185.4 | 4.0 |
| KR-09-02-69 | 104 | 1826 | 0.8 | 45.9817 | 35.2 | 0.0663 | 35.2 | 0.0221 | 1.2 | 0.03 | 141.0 | 1.6 | 65.2 | 22.3 | -2283.7 | 412.8 | 141.0 | 1.6 |
| KR-09-02-71 | 252 | 4267 | 1.4 | 21.7686 | 10.7 | 0.1435 | 10.8 | 0.0227 | 1.6 | 0.15 | 144.4 | 2.3 | 136.1 | 13.7 | -5.6 | 257.9 | 144.4 | 2.3 |
| KR-09-02-72 | 167 | 5551 | 1.8 | 20.2358 | 9.5 | 0.2790 | 9.5 | 0.0409 | 1.1 | 0.11 | 258.7 | 2.7 | 249.9 | 21.1 | 167.7 | 221.8 | 258.7 | 2.7 |
| KR-09-02-73 | 96 | 3690 | 4.1 | 22.8385 | 28.2 | 0.2243 | 28.3 | 0.0371 | 2.4 | 0.08 | 235.1 | 5.4 | 205.4 | 52.7 | -122.7 | 708.4 | 235.1 | 5.4 |
| KR-09-02-75 | 260 | 3452 | 2.0 | 29.1078 | 28.5 | 0.0735 | 28.5 | 0.0155 | 1.2 | 0.04 | 99.2 | 1.2 | 72.0 | 19.8 | -760.7 | 814.6 | 99.2 | 1.2 |
| KR-09-02-76 | 170 | 4232 | 1.8 | 21.1751 | 13.8 | 0.1670 | 14.5 | 0.0256 | 4.4 | 0.30 | 163.3 | 7.1 | 156.8 | 21.1 | 60.7 | 330.4 | 163.3 | 7.1 |
| KR-09-02-77 | 103 | 1743 | 1.1 | 21.4008 | 24.0 | 0.1456 | 24.1 | 0.0226 | 1.6 | 0.07 | 144.0 | 2.3 | 138.0 | 31.1 | 35.3 | 582.7 | 144.0 | 2.3 |
| KR-09-02-78 | 329 | 7392 | 1.6 | 21.2013 | 4.3 | 0.1773 | 4.6 | 0.0273 | 1.6 | 0.35 | 173.4 | 2.8 | 165.8 | 7.1 | 57.7 | 103.2 | 173.4 | 2.8 |
| KR-09-02-79 | 141 | 3613 | 1.6 | 22.3301 | 10.3 | 0.1885 | 10.5 | 0.0305 | 2.1 | 0.20 | 193.9 | 4.0 | 175.4 | 17.0 | -67.4 | 253.0 | 193.9 | 4.0 |
| KR-09-02-80 | 77 | 1648 | 1.3 | 31.6517 | 30.8 | 0.1129 | 30.9 | 0.0259 | 2.4 | 0.08 | 165.0 | 3.9 | 108.6 | 31.9 | -1002.6 | 931.7 | 165.0 | 3.9 |

**Table A4.1 –** Detrital zircon U-Pb analyses

| Analysis | U (ppm) | $^{206}Pb/^{204}Pb$ | U/Th | Isotopic Ratio | | | | | | Error | Apparent Age (Ma) | | | | | | Best Age (Ma) | |
|---|---|---|---|---|---|---|---|---|---|---|---|---|---|---|---|---|---|---|
| | | | | $^{206}Pb/^{207}Pb$ | ± (%) | $^{207}Pb/^{235}U$ | ± (%) | $^{206}Pb/^{238}U$ | ± (%) | | $^{206}Pb/^{238}U$ | ± (Ma) | $^{207}Pb/^{235}U$ | ± (Ma) | $^{206}Pb/^{207}Pb$ | ± (Ma) | Age | ± |
| KR-09-02-81 | 165 | 2101 | 1.3 | 24.0716 | 11.4 | 0.1565 | 11.5 | 0.0273 | 1.3 | 0.12 | 173.8 | 2.3 | 147.6 | 15.8 | -254.2 | 289.2 | 173.8 | 2.3 |
| KR-09-02-82 | 175 | 3246 | 0.9 | 23.6284 | 16.4 | 0.1494 | 16.8 | 0.0256 | 3.6 | 0.21 | 162.9 | 5.7 | 141.4 | 22.2 | -207.3 | 415.0 | 162.9 | 5.7 |
| KR-09-02-83 | 746 | 9343 | 2.1 | 20.6470 | 3.0 | 0.0923 | 5.0 | 0.0138 | 4.0 | 0.80 | 88.5 | 3.5 | 89.7 | 4.3 | 120.5 | 70.5 | 88.5 | 3.5 |
| KR-09-02-84 | 263 | 8724 | 2.5 | 19.9633 | 6.4 | 0.2744 | 6.6 | 0.0397 | 1.4 | 0.21 | 251.1 | 3.4 | 246.2 | 14.3 | 199.3 | 149.1 | 251.1 | 3.4 |
| KR-09-02-85 | 161 | 3353 | 2.3 | 23.2076 | 15.6 | 0.1391 | 15.7 | 0.0234 | 2.0 | 0.13 | 149.2 | 2.9 | 132.2 | 19.5 | -162.4 | 390.4 | 149.2 | 2.9 |
| KR-09-02-86 | 177 | 6612 | 1.0 | 21.3750 | 15.8 | 0.1503 | 15.9 | 0.0233 | 2.0 | 0.12 | 148.4 | 2.9 | 142.1 | 21.1 | 38.2 | 379.4 | 148.4 | 2.9 |
| KR-09-02-87 | 44 | 1191 | 3.0 | 55.7825 | 94.2 | 0.0913 | 94.2 | 0.0369 | 1.6 | 0.02 | 233.8 | 3.7 | 88.7 | 80.1 | -3148.0 | 1752.8 | 233.8 | 3.7 |
| KR-09-02-88 | 541 | 10715 | 2.4 | 21.2776 | 5.2 | 0.1955 | 5.9 | 0.0302 | 2.8 | 0.47 | 191.6 | 5.2 | 181.3 | 9.8 | 49.1 | 123.8 | 191.6 | 5.2 |
| KR-09-02-89 | 373 | 7646 | 1.2 | 20.4399 | 9.7 | 0.1557 | 10.0 | 0.0231 | 2.6 | 0.26 | 147.1 | 3.8 | 147.0 | 13.7 | 144.2 | 227.4 | 147.1 | 3.8 |
| KR-09-02-90 | 348 | 6864 | 0.6 | 21.2733 | 11.7 | 0.1468 | 11.8 | 0.0227 | 1.3 | 0.11 | 144.4 | 1.8 | 139.1 | 15.3 | 49.6 | 280.0 | 144.4 | 1.8 |
| KR-09-02-91 | 809 | 11127 | 2.3 | 20.3304 | 3.5 | 0.1876 | 3.9 | 0.0277 | 1.7 | 0.44 | 175.9 | 3.0 | 174.6 | 6.3 | 156.8 | 83.0 | 175.9 | 3.0 |
| KR-09-02-92 | 48 | 1238 | 4.0 | 29.9541 | 31.0 | 0.1592 | 31.2 | 0.0346 | 2.9 | 0.09 | 219.2 | 6.2 | 150.0 | 43.5 | -842.0 | 906.2 | 219.2 | 6.2 |
| KR-09-02-93 | 172 | 3368 | 1.9 | 19.9447 | 11.1 | 0.1600 | 11.2 | 0.0231 | 1.7 | 0.15 | 147.5 | 2.5 | 150.7 | 15.7 | 201.4 | 257.7 | 147.5 | 2.5 |
| KR-09-02-94 | 418 | 5027 | 3.0 | 20.5677 | 5.8 | 0.2079 | 6.2 | 0.0310 | 2.2 | 0.36 | 196.9 | 4.3 | 191.8 | 10.9 | 129.5 | 136.8 | 196.9 | 4.3 |
| KR-09-02-95 | 135 | 2872 | 1.5 | 22.5983 | 17.1 | 0.1338 | 17.2 | 0.0219 | 1.5 | 0.09 | 139.9 | 2.1 | 127.5 | 20.6 | -96.7 | 422.6 | 139.9 | 2.1 |
| KR-09-02-96 | 240 | 9634 | 1.6 | 19.7066 | 5.7 | 0.2745 | 6.4 | 0.0392 | 2.9 | 0.45 | 248.0 | 7.0 | 246.2 | 13.9 | 229.2 | 131.2 | 248.0 | 7.0 |
| KR-09-02-97 | 105 | 2120 | 0.8 | 24.4009 | 35.2 | 0.1247 | 35.8 | 0.0221 | 6.1 | 0.17 | 140.7 | 8.5 | 119.3 | 40.3 | -288.7 | 923.0 | 140.7 | 8.5 |
| KR-09-02-98 | 97 | 2629 | 1.3 | 28.5473 | 27.9 | 0.1066 | 27.9 | 0.0221 | 1.8 | 0.06 | 140.8 | 2.5 | 102.9 | 27.3 | -706.3 | 787.7 | 140.8 | 2.5 |
| KR-09-02-99 | 237 | 6864 | 0.6 | 21.1984 | 10.7 | 0.1709 | 10.8 | 0.0263 | 1.8 | 0.17 | 167.2 | 3.0 | 160.2 | 16.0 | 58.0 | 255.0 | 167.2 | 3.0 |
| KR-09-02-100 | 306 | 6530 | 2.0 | 21.6383 | 8.5 | 0.1391 | 9.1 | 0.0218 | 3.1 | 0.35 | 139.2 | 4.3 | 132.3 | 11.3 | 8.8 | 205.5 | 139.2 | 4.3 |
| SE-09-02-1 | 91 | 7937 | 2.6 | 13.7617 | 2.7 | 1.7544 | 3.4 | 0.1751 | 2.0 | 0.60 | 1040.2 | 19.6 | 1028.8 | 22.0 | 1004.6 | 55.4 | 1004.6 | 55.4 |
| SE-09-02-2 | 136 | 1428 | 3.6 | 37.4849 | 27.8 | 0.0673 | 27.8 | 0.0183 | 1.6 | 0.06 | 116.8 | 1.8 | 66.1 | 17.8 | -1535.3 | 944.8 | 116.8 | 1.8 |
| SE-09-02-4 | 59 | 475 | 3.6 | 30.3045 | 66.1 | 0.0683 | 66.2 | 0.0150 | 3.8 | 0.06 | 96.0 | 3.6 | 67.1 | 43.0 | -875.4 | 2120.3 | 96.0 | 3.6 |
| SE-09-02-4 | 984 | 6525 | 3.6 | 21.2093 | 3.7 | 0.1044 | 3.8 | 0.0161 | 0.9 | 0.24 | 102.7 | 0.9 | 100.8 | 3.6 | 56.8 | 87.2 | 102.7 | 0.9 |
| SE-09-02-5 | 636 | 5274 | 2.4 | 21.7140 | 5.9 | 0.0990 | 6.2 | 0.0156 | 1.8 | 0.29 | 99.7 | 1.8 | 95.8 | 5.7 | 0.4 | 142.5 | 99.7 | 1.8 |
| SE-09-02-6 | 78 | 527 | 2.8 | 120.6815 | 115.5 | 0.0176 | 115.8 | 0.0154 | 7.6 | 0.07 | 98.6 | 7.4 | 17.7 | 20.3 | 0.0 | 0.0 | 98.6 | 7.4 |
| SE-09-02-7 | 210 | 1336 | 1.9 | 23.8028 | 14.1 | 0.0930 | 14.4 | 0.0161 | 2.6 | 0.18 | 102.7 | 2.7 | 90.3 | 12.4 | -225.8 | 357.1 | 102.7 | 2.7 |
| SE-09-02-8 | 93 | 734 | 3.1 | 40.9299 | 27.7 | 0.0640 | 27.7 | 0.0190 | 1.0 | 0.04 | 121.2 | 1.2 | 63.0 | 16.9 | -1840.9 | 1014.2 | 121.2 | 1.2 |
| SE-09-02-9 | 48 | 417 | 3.4 | 50.9558 | 45.6 | 0.0595 | 45.9 | 0.0220 | 5.1 | 0.11 | 140.3 | 7.0 | 58.7 | 26.2 | -2719.6 | 312.4 | 140.3 | 7.0 |
| SE-09-02-10 | 235 | 2127 | 6.2 | 22.9545 | 9.7 | 0.1096 | 9.8 | 0.0182 | 1.4 | 0.14 | 116.6 | 1.6 | 105.6 | 9.8 | -135.2 | 239.5 | 116.6 | 1.6 |
| SE-09-02-11 | 286 | 2664 | 3.8 | 24.7368 | 12.4 | 0.1047 | 12.5 | 0.0188 | 1.1 | 0.09 | 119.9 | 1.3 | 101.1 | 12.0 | -323.7 | 319.8 | 119.9 | 1.3 |
| SE-09-02-12 | 48 | 442 | 4.9 | 11.6092 | 199.0 | 0.2136 | 199.0 | 0.0180 | 2.2 | 0.01 | 114.9 | 2.5 | 196.5 | 371.4 | 1341.3 | 642.7 | 114.9 | 2.5 |
| SE-09-02-13 | 660 | 5002 | 2.2 | 22.1154 | 9.6 | 0.0934 | 9.7 | 0.0150 | 1.0 | 0.10 | 95.8 | 0.9 | 90.6 | 8.4 | -43.9 | 234.6 | 95.8 | 0.9 |
| SE-09-02-14 | 433 | 4235 | 7.8 | 22.9183 | 6.1 | 0.1123 | 6.2 | 0.0187 | 0.7 | 0.12 | 119.2 | 0.9 | 108.0 | 6.3 | -131.3 | 152.0 | 119.2 | 0.9 |
| SE-09-02-15 | 249 | 2351 | 3.7 | 25.7355 | 14.3 | 0.0976 | 14.4 | 0.0182 | 1.9 | 0.13 | 116.4 | 2.2 | 94.6 | 13.0 | -426.4 | 376.4 | 116.4 | 2.2 |
| SE-09-02-16 | 1016 | 7928 | 4.7 | 20.2817 | 4.4 | 0.1073 | 4.5 | 0.0158 | 0.9 | 0.21 | 101.0 | 0.9 | 103.5 | 4.4 | 162.4 | 102.1 | 101.0 | 0.9 |
| SE-09-02-17 | 388 | 3593 | 2.5 | 22.6369 | 8.3 | 0.1016 | 8.4 | 0.0167 | 1.1 | 0.13 | 106.6 | 1.2 | 98.2 | 7.9 | -100.9 | 204.7 | 106.6 | 1.2 |
| SE-09-02-18 | 96 | 1031 | 2.5 | 21.8977 | 27.9 | 0.1165 | 28.0 | 0.0185 | 3.2 | 0.11 | 118.2 | 3.7 | 111.9 | 29.7 | -19.9 | 685.3 | 118.2 | 3.7 |
| SE-09-02-19 | 86 | 735 | 3.3 | 50.1635 | 52.0 | 0.0420 | 52.0 | 0.0153 | 2.2 | 0.04 | 97.8 | 2.1 | 41.8 | 21.3 | -2649.9 | 128.6 | 97.8 | 2.1 |
| SE-09-02-20 | 158 | 1676 | 4.8 | 24.4678 | 11.7 | 0.1041 | 11.9 | 0.0185 | 2.2 | 0.19 | 118.0 | 2.6 | 100.6 | 11.4 | -295.7 | 299.4 | 118.0 | 2.6 |
| SE-09-02-21 | 382 | 2774 | 2.7 | 22.4132 | 13.9 | 0.0960 | 13.9 | 0.0156 | 0.7 | 0.05 | 99.9 | 0.7 | 93.1 | 12.4 | -76.5 | 341.0 | 99.9 | 0.7 |
| SE-09-02-22 | 71 | 424 | 4.8 | 25.2630 | 104.0 | 0.0879 | 104.1 | 0.0161 | 4.0 | 0.04 | 102.9 | 4.1 | 85.5 | 85.5 | -378.0 | 1385.1 | 102.9 | 4.1 |

**Table A4.1 –** Detrital zircon U-Pb analyses

| Analysis | U (ppm) | $^{206}Pb/^{204}Pb$ | U/Th | Isotopic Ratio | | | | | | Error | Apparent Age (Ma) | | | | | | Best Age (Ma) | |
|---|---|---|---|---|---|---|---|---|---|---|---|---|---|---|---|---|---|---|
| | | | | $^{206}Pb/^{207}Pb$ | ± (%) | $^{207}Pb/^{235}U$ | ± (%) | $^{206}Pb/^{238}U$ | ± (%) | | $^{206}Pb/^{238}U$ | ± (Ma) | $^{207}Pb/^{235}U$ | ± (Ma) | $^{206}Pb/^{207}Pb$ | ± (Ma) | Age | ± |
| SE-09-02-23 | 209 | 2030 | 2.1 | 25.8004 | 19.0 | 0.1226 | 19.1 | 0.0229 | 2.0 | 0.10 | 146.3 | 2.9 | 117.5 | 21.2 | -433.0 | 502.6 | 146.3 | 2.9 |
| SE-09-02-24 | 274 | 2055 | 1.8 | 25.1523 | 12.1 | 0.0907 | 12.2 | 0.0166 | 1.6 | 0.13 | 105.8 | 1.6 | 88.2 | 10.3 | -366.6 | 314.5 | 105.8 | 1.6 |
| SE-09-02-25 | 208 | 2338 | 1.5 | 23.2980 | 14.5 | 0.1350 | 14.7 | 0.0228 | 2.2 | 0.15 | 145.4 | 3.2 | 128.6 | 17.8 | -172.1 | 364.0 | 145.4 | 3.2 |
| SE-09-02-27 | 362 | 2934 | 5.8 | 21.0712 | 11.2 | 0.1076 | 12.5 | 0.0164 | 5.5 | 0.44 | 105.2 | 5.8 | 103.8 | 12.3 | 72.4 | 267.0 | 105.2 | 5.8 |
| SE-09-02-28 | 78 | 835 | 3.5 | 40.9147 | 41.6 | 0.0619 | 41.6 | 0.0184 | 0.7 | 0.02 | 117.3 | 0.8 | 61.0 | 24.6 | -1839.6 | 118.5 | 117.3 | 0.8 |
| SE-09-02-29 | 424 | 4190 | 3.5 | 22.8890 | 9.9 | 0.0960 | 10.1 | 0.0159 | 1.7 | 0.17 | 101.9 | 1.7 | 93.1 | 9.0 | -128.2 | 246.3 | 101.9 | 1.7 |
| SE-09-02-30 | 161 | 1636 | 1.5 | 24.2512 | 21.5 | 0.0945 | 21.5 | 0.0166 | 0.9 | 0.04 | 106.3 | 0.9 | 91.7 | 18.8 | -273.0 | 551.3 | 106.3 | 0.9 |
| SE-09-02-31 | 105 | 996 | 4.0 | 29.6617 | 31.8 | 0.0726 | 32.1 | 0.0156 | 3.9 | 0.12 | 100.0 | 3.8 | 71.2 | 22.1 | -814.0 | 925.0 | 100.0 | 3.8 |
| SE-09-02-32 | 126 | 1441 | 5.3 | 28.7433 | 23.4 | 0.0879 | 23.5 | 0.0183 | 2.8 | 0.12 | 117.1 | 3.3 | 85.6 | 19.3 | -725.3 | 659.2 | 117.1 | 3.3 |
| SE-09-02-33 | 122 | 1110 | 4.1 | 26.8876 | 23.9 | 0.0833 | 24.0 | 0.0162 | 1.5 | 0.06 | 103.9 | 1.6 | 81.2 | 18.7 | -542.6 | 650.6 | 103.9 | 1.6 |
| SE-09-02-34 | 262 | 2432 | 3.6 | 25.1556 | 10.3 | 0.0864 | 10.4 | 0.0158 | 1.1 | 0.11 | 100.9 | 1.1 | 84.2 | 8.4 | -367.0 | 267.7 | 100.9 | 1.1 |
| SE-09-02-35 | 384 | 3423 | 3.0 | 23.1281 | 9.9 | 0.0916 | 10.1 | 0.0154 | 2.1 | 0.21 | 98.3 | 2.1 | 89.0 | 8.6 | -153.9 | 246.2 | 98.3 | 2.1 |
| SE-09-02-36 | 139 | 1253 | 2.4 | 18.8012 | 11.5 | 0.1217 | 12.9 | 0.0166 | 5.9 | 0.46 | 106.1 | 6.2 | 116.6 | 14.2 | 336.8 | 260.8 | 106.1 | 6.2 |
| SE-09-02-37 | 264 | 2450 | 4.2 | 24.7154 | 13.9 | 0.0916 | 14.1 | 0.0164 | 2.3 | 0.16 | 105.0 | 2.4 | 89.0 | 12.0 | -321.5 | 357.7 | 105.0 | 2.4 |
| SE-09-02-38 | 52 | 773 | 3.5 | 43.8734 | 50.1 | 0.0782 | 50.2 | 0.0249 | 3.0 | 0.06 | 158.5 | 4.7 | 76.5 | 37.0 | -2099.3 | 9.5 | 158.5 | 4.7 |
| SE-09-02-39 | 345 | 3206 | 1.7 | 22.3886 | 7.4 | 0.1029 | 7.6 | 0.0167 | 1.8 | 0.23 | 106.9 | 1.9 | 99.5 | 7.2 | -73.8 | 180.9 | 106.9 | 1.9 |
| SE-09-02-40 | 186 | 2146 | 2.8 | 25.4495 | 15.9 | 0.1027 | 16.0 | 0.0190 | 1.7 | 0.11 | 121.0 | 2.1 | 99.3 | 15.2 | -397.2 | 417.3 | 121.0 | 2.1 |
| SE-09-02-41 | 104 | 1126 | 3.2 | 29.5778 | 21.4 | 0.0736 | 21.5 | 0.0158 | 2.7 | 0.13 | 101.0 | 2.7 | 72.1 | 15.0 | -805.9 | 612.4 | 101.0 | 2.7 |
| SE-09-02-42 | 150 | 2473 | 2.1 | 22.0478 | 6.2 | 0.1560 | 6.5 | 0.0249 | 1.9 | 0.30 | 158.8 | 3.1 | 147.2 | 8.9 | -36.5 | 150.8 | 158.8 | 3.1 |
| SE-09-02-43 | 226 | 2448 | 4.5 | 22.2025 | 14.6 | 0.0964 | 14.7 | 0.0155 | 1.7 | 0.11 | 99.3 | 1.7 | 93.4 | 13.1 | -53.5 | 357.4 | 99.3 | 1.7 |
| SE-09-02-44 | 576 | 6586 | 4.8 | 22.2709 | 8.3 | 0.0926 | 8.8 | 0.0150 | 3.0 | 0.34 | 95.7 | 2.8 | 89.9 | 7.6 | -61.0 | 202.6 | 95.7 | 2.8 |
| SE-09-02-45 | 82 | 1057 | 3.4 | 24.0306 | 30.4 | 0.1005 | 30.5 | 0.0175 | 2.4 | 0.08 | 111.9 | 2.6 | 97.2 | 28.3 | -249.8 | 784.0 | 111.9 | 2.6 |
| SE-09-02-46 | 330 | 2686 | 3.3 | 23.1932 | 12.4 | 0.0946 | 12.4 | 0.0159 | 1.0 | 0.08 | 101.8 | 1.0 | 91.8 | 10.9 | -160.9 | 308.8 | 101.8 | 1.0 |
| SE-09-02-47 | 470 | 3675 | 3.6 | 22.2392 | 8.7 | 0.0983 | 8.8 | 0.0159 | 1.0 | 0.11 | 101.4 | 1.0 | 95.2 | 8.0 | -57.5 | 212.6 | 101.4 | 1.0 |
| SE-09-02-48 | 51 | 502 | 2.2 | 97.3151 | 116.2 | 0.0203 | 116.5 | 0.0143 | 8.4 | 0.07 | 91.5 | 7.6 | 20.4 | 23.5 | 0.0 | 0.0 | 91.5 | 7.6 |
| SE-09-02-49 | 222 | 2359 | 3.2 | 20.9658 | 17.4 | 0.1304 | 17.5 | 0.0198 | 2.1 | 0.12 | 126.6 | 2.7 | 124.4 | 20.6 | 84.2 | 415.9 | 126.6 | 2.7 |
| SE-09-02-50 | 175 | 1920 | 3.1 | 27.1588 | 20.3 | 0.0894 | 20.3 | 0.0176 | 0.9 | 0.04 | 112.6 | 1.0 | 87.0 | 16.9 | -569.6 | 551.9 | 112.6 | 1.0 |
| SE-09-02-52 | 614 | 5310 | 2.6 | 22.4968 | 5.5 | 0.0970 | 5.5 | 0.0158 | 0.8 | 0.14 | 101.2 | 0.8 | 94.0 | 5.0 | -85.6 | 134.6 | 101.2 | 0.8 |
| SE-09-02-54 | 230 | 3771 | 0.9 | 20.6374 | 8.7 | 0.1723 | 8.8 | 0.0258 | 1.4 | 0.16 | 164.1 | 2.3 | 161.4 | 13.1 | 121.6 | 204.6 | 164.1 | 2.3 |
| SE-09-02-55 | 141 | 1550 | 3.4 | 32.0261 | 43.3 | 0.0715 | 43.3 | 0.0166 | 1.6 | 0.04 | 106.2 | 1.7 | 70.2 | 29.4 | -1037.6 | 1344.2 | 106.2 | 1.7 |
| SE-09-02-56 | 587 | 3442 | 1.7 | 19.9672 | 5.1 | 0.1118 | 5.2 | 0.0162 | 0.9 | 0.18 | 103.6 | 0.9 | 107.6 | 5.3 | 198.8 | 118.1 | 103.6 | 0.9 |
| SE-09-02-57 | 60 | 759 | 2.3 | 32.4889 | 47.5 | 0.0781 | 47.5 | 0.0184 | 2.3 | 0.05 | 117.6 | 2.7 | 76.4 | 35.0 | -1080.7 | 1502.0 | 117.6 | 2.7 |
| SE-09-02-58 | 752 | 9110 | 3.9 | 21.6312 | 3.7 | 0.1242 | 4.2 | 0.0195 | 1.8 | 0.43 | 124.4 | 2.2 | 118.9 | 4.7 | 9.6 | 90.0 | 124.4 | 2.2 |
| SE-09-02-59 | 103 | 1272 | 1.2 | 31.4597 | 24.2 | 0.0799 | 24.3 | 0.0182 | 1.8 | 0.08 | 116.5 | 2.1 | 78.1 | 18.3 | -984.6 | 724.4 | 116.5 | 2.1 |
| SE-09-02-60 | 245 | 2152 | 2.4 | 23.2008 | 13.0 | 0.1046 | 13.5 | 0.0176 | 3.6 | 0.27 | 112.5 | 4.1 | 101.0 | 13.0 | -161.7 | 323.5 | 112.5 | 4.1 |
| SE-09-02-61 | 452 | 5469 | 3.9 | 21.6931 | 5.4 | 0.1146 | 5.7 | 0.0180 | 1.8 | 0.31 | 115.2 | 2.0 | 110.2 | 5.9 | 2.7 | 129.7 | 115.2 | 2.0 |
| SE-09-02-62 | 25 | 385 | 2.9 | 23.6685 | 146.2 | 0.1435 | 146.2 | 0.0246 | 4.3 | 0.03 | 156.9 | 6.7 | 136.2 | 188.5 | -211.6 | 0.0 | 156.9 | 6.7 |
| SE-09-02-63 | 397 | 3587 | 3.8 | 23.2896 | 11.2 | 0.0927 | 11.2 | 0.0157 | 0.8 | 0.08 | 100.2 | 0.8 | 90.0 | 9.6 | -171.2 | 278.5 | 100.2 | 0.8 |
| SE-09-02-64 | 86 | 676 | 5.1 | 40.8855 | 30.9 | 0.0605 | 31.0 | 0.0179 | 3.3 | 0.11 | 114.5 | 3.8 | 59.6 | 18.0 | -1837.0 | 1132.7 | 114.5 | 3.8 |
| SE-09-02-65 | 213 | 2207 | 3.1 | 23.6800 | 15.4 | 0.1060 | 15.4 | 0.0182 | 0.9 | 0.06 | 116.3 | 1.0 | 102.3 | 15.0 | -212.8 | 387.7 | 116.3 | 1.0 |
| SE-09-02-66 | 48 | 750 | 4.8 | 78.4592 | 75.9 | 0.0360 | 76.3 | 0.0205 | 8.2 | 0.11 | 130.8 | 10.6 | 35.9 | 27.0 | 0.0 | 162.1 | 130.8 | 10.6 |
| SE-09-02-67 | 108 | 1315 | 2.6 | 11.2771 | 416.3 | 0.2009 | 416.3 | 0.0164 | 1.5 | 0.00 | 105.1 | 1.6 | 185.9 | 873.7 | 1397.1 | 0.0 | 105.1 | 1.6 |

**Table A4.1 –** Detrital zircon U-Pb analyses

| Analysis | U (ppm) | $^{206}Pb/^{204}Pb$ | U/Th | Isotopic Ratio | | | | | | Error | Apparent Age (Ma) | | | | | | Best Age (Ma) | |
|---|---|---|---|---|---|---|---|---|---|---|---|---|---|---|---|---|---|---|
| | | | | $^{206}Pb/^{207}Pb$ | ± (%) | $^{207}Pb/^{235}U$ | ± (%) | $^{206}Pb/^{238}U$ | ± (%) | | $^{206}Pb/^{238}U$ | ± (Ma) | $^{207}Pb/^{235}U$ | ± (Ma) | $^{206}Pb/^{207}Pb$ | ± (Ma) | Age | ± |
| SE-09-02-68 | 281 | 1429 | 2.5 | 26.4561 | 13.5 | 0.0894 | 13.5 | 0.0172 | 1.1 | 0.08 | 109.7 | 1.2 | 87.0 | 11.3 | -499.3 | 360.0 | 109.7 | 1.2 |
| SE-09-02-69 | 750 | 6049 | 5.3 | 21.8655 | 4.8 | 0.0979 | 5.0 | 0.0155 | 1.1 | 0.22 | 99.3 | 1.1 | 94.8 | 4.5 | -16.4 | 116.8 | 99.3 | 1.1 |
| SE-09-02-70 | 49 | 616 | 3.2 | 12.5365 | 119.3 | 0.1797 | 119.4 | 0.0163 | 4.0 | 0.03 | 104.5 | 4.1 | 167.8 | 186.7 | 1191.2 | 301.5 | 104.5 | 4.1 |
| SE-09-02-71 | 240 | 3636 | 2.1 | 21.7302 | 9.1 | 0.1776 | 9.4 | 0.0280 | 2.4 | 0.26 | 177.9 | 4.2 | 166.0 | 14.4 | -1.4 | 219.0 | 177.9 | 4.2 |
| SE-09-02-73 | 258 | 3014 | 3.6 | 24.5908 | 11.0 | 0.0936 | 11.0 | 0.0167 | 0.9 | 0.08 | 106.7 | 0.9 | 90.8 | 9.6 | -308.5 | 282.2 | 106.7 | 0.9 |
| SE-09-02-74 | 241 | 2608 | 3.2 | 22.6374 | 15.0 | 0.0986 | 15.1 | 0.0162 | 0.8 | 0.06 | 103.5 | 0.9 | 95.5 | 13.7 | -100.9 | 371.5 | 103.5 | 0.9 |
| SE-09-02-74B | 529 | 6724 | 2.3 | 20.7214 | 6.7 | 0.1075 | 7.4 | 0.0162 | 2.9 | 0.40 | 103.3 | 3.0 | 103.7 | 7.2 | 112.0 | 159.2 | 103.3 | 3.0 |
| SE-09-02-75 | 620 | 5542 | 2.2 | 22.5761 | 5.7 | 0.0908 | 5.9 | 0.0149 | 1.4 | 0.25 | 95.2 | 1.4 | 88.3 | 5.0 | -94.3 | 139.7 | 95.2 | 1.4 |
| SE-09-02-76 | 81 | 1224 | 4.0 | 19.6992 | 27.0 | 0.1261 | 27.2 | 0.0180 | 2.9 | 0.11 | 115.1 | 3.3 | 120.6 | 30.9 | 230.1 | 634.1 | 115.1 | 3.3 |
| SE-09-02-77 | 157 | 2447 | 3.5 | 22.1068 | 18.6 | 0.1006 | 18.8 | 0.0161 | 2.6 | 0.14 | 103.2 | 2.6 | 97.4 | 17.4 | -43.0 | 455.1 | 103.2 | 2.6 |
| SE-09-02-78 | 649 | 8689 | 2.7 | 21.2842 | 3.2 | 0.1027 | 3.7 | 0.0159 | 1.8 | 0.49 | 101.4 | 1.8 | 99.3 | 3.5 | 48.4 | 76.3 | 101.4 | 1.8 |
| SE-09-02-79 | 194 | 2657 | 3.5 | 21.7827 | 13.0 | 0.1386 | 13.2 | 0.0219 | 1.9 | 0.14 | 139.6 | 2.6 | 131.8 | 16.3 | -7.2 | 315.4 | 139.6 | 2.6 |
| SE-09-02-80 | 245 | 2989 | 2.7 | 20.7992 | 11.4 | 0.1090 | 11.5 | 0.0164 | 1.2 | 0.11 | 105.2 | 1.3 | 105.1 | 11.5 | 103.1 | 270.4 | 105.2 | 1.3 |
| SE-09-02-81 | 69 | 1088 | 3.1 | 31.7129 | 34.5 | 0.0781 | 34.5 | 0.0180 | 1.9 | 0.05 | 114.8 | 2.1 | 76.3 | 25.4 | -1008.4 | 1048.0 | 114.8 | 2.1 |
| SE-09-02-83 | 596 | 8796 | 2.4 | 22.2073 | 7.0 | 0.1041 | 7.4 | 0.0168 | 2.4 | 0.33 | 107.2 | 2.6 | 100.6 | 7.1 | -54.0 | 170.3 | 107.2 | 2.6 |
| SE-09-02-84 | 82 | 1287 | 2.0 | 20.8497 | 24.5 | 0.1182 | 24.7 | 0.0179 | 2.9 | 0.12 | 114.3 | 3.3 | 113.5 | 26.5 | 97.4 | 587.6 | 114.3 | 3.3 |
| SE-09-02-85 | 75 | 1191 | 2.1 | 39.1365 | 46.5 | 0.0649 | 46.6 | 0.0184 | 1.4 | 0.03 | 117.7 | 1.6 | 63.9 | 28.8 | -1682.4 | 44.5 | 117.7 | 1.6 |
| SE-09-02-86 | 110 | 1215 | 2.8 | 30.6574 | 23.2 | 0.0709 | 23.2 | 0.0158 | 1.1 | 0.05 | 100.9 | 1.1 | 69.6 | 15.6 | -908.9 | 679.9 | 100.9 | 1.1 |
| SE-09-02-87 | 535 | 5158 | 2.9 | 20.9254 | 6.6 | 0.1103 | 6.6 | 0.0167 | 0.8 | 0.11 | 107.0 | 0.8 | 106.2 | 6.7 | 88.8 | 156.2 | 107.0 | 0.8 |
| SE-09-02-88 | 290 | 3349 | 2.5 | 21.6067 | 10.9 | 0.1057 | 10.9 | 0.0166 | 0.6 | 0.05 | 105.9 | 0.6 | 102.0 | 10.6 | 12.3 | 263.6 | 105.9 | 0.6 |
| SE-09-02-89 | 185 | 4220 | 2.5 | 21.3084 | 12.8 | 0.1584 | 13.0 | 0.0245 | 2.6 | 0.20 | 155.9 | 4.0 | 149.3 | 18.1 | 45.7 | 305.8 | 155.9 | 4.0 |
| SE-09-02-90 | 197 | 3168 | 2.8 | 22.2395 | 13.5 | 0.1021 | 13.7 | 0.0165 | 2.4 | 0.18 | 105.3 | 2.6 | 98.7 | 12.9 | -57.5 | 329.9 | 105.3 | 2.6 |
| SE-09-02-91 | 423 | 6681 | 2.3 | 21.3535 | 8.5 | 0.1058 | 8.6 | 0.0164 | 1.7 | 0.19 | 104.8 | 1.7 | 102.1 | 8.4 | 40.6 | 203.0 | 104.8 | 1.7 |
| SE-09-02-92 | 560 | 8437 | 2.2 | 22.4571 | 10.5 | 0.1112 | 11.6 | 0.0181 | 5.0 | 0.43 | 115.7 | 5.7 | 107.0 | 11.8 | -81.3 | 256.5 | 115.7 | 5.7 |
| SE-09-02-93 | 863 | 8418 | 2.5 | 20.0545 | 6.1 | 0.1033 | 6.3 | 0.0150 | 1.6 | 0.26 | 96.2 | 1.6 | 99.8 | 6.0 | 188.6 | 142.6 | 96.2 | 1.6 |
| SE-09-02-94 | 373 | 5236 | 1.5 | 21.6002 | 9.1 | 0.1031 | 9.2 | 0.0161 | 0.8 | 0.08 | 103.3 | 0.8 | 99.6 | 8.7 | 13.1 | 219.7 | 103.3 | 0.8 |
| SE-09-02-95 | 282 | 4215 | 3.0 | 22.4768 | 9.4 | 0.1194 | 9.5 | 0.0195 | 1.5 | 0.15 | 124.3 | 1.8 | 114.5 | 10.3 | -83.5 | 229.8 | 124.3 | 1.8 |
| SE-09-02-96 | 146 | 2068 | 1.7 | 17.9989 | 20.2 | 0.1270 | 20.2 | 0.0166 | 1.4 | 0.07 | 106.0 | 1.5 | 121.4 | 23.2 | 434.8 | 453.8 | 106.0 | 1.5 |
| SE-09-02-97 | 112 | 1230 | 2.4 | 26.3908 | 32.8 | 0.0922 | 32.9 | 0.0176 | 1.3 | 0.04 | 112.7 | 1.4 | 89.5 | 28.2 | -492.8 | 893.0 | 112.7 | 1.4 |
| SE-09-02-98 | 1560 | 30397 | 1.4 | 20.4448 | 2.0 | 0.1728 | 3.2 | 0.0256 | 2.5 | 0.78 | 163.1 | 4.0 | 161.8 | 4.8 | 143.6 | 46.3 | 163.1 | 4.0 |
| SE-09-02-99 | 110 | 14762 | 4.0 | 12.3408 | 2.4 | 1.9169 | 2.4 | 0.1716 | 0.6 | 0.25 | 1020.7 | 5.7 | 1087.0 | 16.3 | 1222.2 | 46.5 | 1222.2 | 46.5 |
| SE-09-02-100 | 64 | 1674 | 2.6 | 20.2040 | 33.7 | 0.1707 | 33.9 | 0.0250 | 3.8 | 0.11 | 159.2 | 6.0 | 160.0 | 50.3 | 171.3 | 807.9 | 159.2 | 6.0 |
| SE-09-02-103 | 530 | 1587 | 3.2 | 24.5354 | 7.0 | 0.0852 | 7.2 | 0.0152 | 1.7 | 0.24 | 97.0 | 1.6 | 83.0 | 5.8 | -302.7 | 179.6 | 97.0 | 1.6 |
| SE-09-02-104 | 244 | 1105 | 2.6 | 32.4871 | 19.4 | 0.0640 | 19.4 | 0.0151 | 0.8 | 0.04 | 96.6 | 0.8 | 63.0 | 11.9 | -1080.6 | 589.2 | 96.6 | 0.8 |
| SE-09-02-105 | 544 | 1684 | 1.5 | 23.5313 | 7.6 | 0.0887 | 7.7 | 0.0151 | 1.3 | 0.17 | 96.9 | 1.2 | 86.3 | 6.4 | -197.0 | 190.7 | 96.9 | 1.2 |
| SE-09-02-106 | 286 | 3747 | 4.3 | 21.4456 | 8.2 | 0.1160 | 8.9 | 0.0180 | 3.5 | 0.40 | 115.3 | 4.0 | 111.5 | 9.4 | 30.3 | 196.2 | 115.3 | 4.0 |
| SE-09-02-107 | 211 | 3840 | 1.9 | 23.4491 | 12.1 | 0.1106 | 12.2 | 0.0188 | 1.3 | 0.11 | 120.1 | 1.6 | 106.5 | 12.3 | -188.2 | 304.2 | 120.1 | 1.6 |
| SE-09-02-108 | 173 | 2009 | 1.8 | 18.7068 | 16.3 | 0.1251 | 16.5 | 0.0170 | 2.4 | 0.14 | 108.5 | 2.5 | 119.7 | 18.6 | 348.2 | 370.4 | 108.5 | 2.5 |
| SE-09-02-109 | 224 | 928 | 2.3 | 13.8450 | 43.4 | 0.1623 | 43.6 | 0.0163 | 4.1 | 0.09 | 104.2 | 4.3 | 152.7 | 61.9 | 992.4 | 926.2 | 104.2 | 4.3 |
| SE-09-02-110 | 78 | 1443 | 3.3 | 27.5488 | 35.6 | 0.0925 | 35.9 | 0.0185 | 4.3 | 0.12 | 118.1 | 5.0 | 89.9 | 30.8 | -608.3 | 995.4 | 118.1 | 5.0 |
| TM-09-02A-1 | 51 | 1222 | 2.5 | 11.9345 | 190.3 | 0.4027 | 190.4 | 0.0349 | 5.8 | 0.03 | 220.9 | 12.6 | 343.6 | 622.8 | 1287.7 | 639.4 | 220.9 | 12.6 |
| TM-09-02A-2 | 549 | 7070 | 1.6 | 21.4831 | 8.5 | 0.0956 | 8.7 | 0.0149 | 2.0 | 0.23 | 95.3 | 1.9 | 92.7 | 7.7 | 26.1 | 203.8 | 95.3 | 1.9 |

**Table A4.1 –** Detrital zircon U-Pb analyses

| Analysis | U (ppm) | $^{206}Pb/^{204}Pb$ | U/Th | Isotopic Ratio $^{206}Pb/^{207}Pb$ | ± (%) | $^{207}Pb/^{235}U$ | ± (%) | $^{206}Pb/^{238}U$ | ± (%) | Error | Apparent Age (Ma) $^{206}Pb/^{238}U$ | ± (Ma) | $^{207}Pb/^{235}U$ | ± (Ma) | $^{206}Pb/^{207}Pb$ | ± (Ma) | Best Age (Ma) Age | ± |
|---|---|---|---|---|---|---|---|---|---|---|---|---|---|---|---|---|---|---|
| TM-09-02A-3 | 82 | 1714 | 1.8 | 28.5181 | 42.8 | 0.1083 | 42.8 | 0.0224 | 2.8 | 0.07 | 142.9 | 4.0 | 104.4 | 42.6 | -703.4 | 1234.9 | 142.9 | 4.0 |
| TM-09-02A-4 | 289 | 3096 | 2.2 | 22.8869 | 22.4 | 0.0884 | 22.7 | 0.0147 | 3.8 | 0.17 | 93.9 | 3.6 | 86.0 | 18.8 | -127.9 | 559.8 | 93.9 | 3.6 |
| TM-09-02A-5 | 336 | 4408 | 2.5 | 23.0752 | 12.2 | 0.1411 | 12.6 | 0.0236 | 2.9 | 0.23 | 150.4 | 4.3 | 134.0 | 15.8 | -148.2 | 304.2 | 150.4 | 4.3 |
| TM-09-02A-6 | 48 | 1356 | 2.4 | 22.3469 | 40.3 | 0.2158 | 40.3 | 0.0350 | 1.4 | 0.04 | 221.7 | 3.2 | 198.4 | 72.8 | -69.3 | 1020.5 | 221.7 | 3.2 |
| TM-09-02A-7 | 290 | 6355 | 1.8 | 19.5805 | 9.5 | 0.2759 | 9.6 | 0.0392 | 1.0 | 0.10 | 247.8 | 2.4 | 247.4 | 21.0 | 244.0 | 219.4 | 247.8 | 2.4 |
| TM-09-02A-8 | 160 | 2889 | 1.0 | 21.3349 | 10.8 | 0.1585 | 11.4 | 0.0245 | 3.5 | 0.31 | 156.2 | 5.4 | 149.4 | 15.8 | 42.7 | 259.8 | 156.2 | 5.4 |
| TM-09-02A-9 | 287 | 2270 | 2.1 | 22.3814 | 18.6 | 0.0963 | 18.7 | 0.0156 | 1.3 | 0.07 | 100.0 | 1.3 | 93.4 | 16.6 | -73.0 | 458.5 | 100.0 | 1.3 |
| TM-09-02A-10 | 221 | 7848 | 3.1 | 21.6029 | 12.2 | 0.2428 | 12.3 | 0.0380 | 1.8 | 0.15 | 240.7 | 4.2 | 220.7 | 24.4 | 12.8 | 293.5 | 240.7 | 4.2 |
| TM-09-02A-11 | 62 | 1274 | 2.2 | 17.8156 | 30.0 | 0.2643 | 30.8 | 0.0341 | 7.1 | 0.23 | 216.5 | 15.0 | 238.1 | 65.4 | 457.6 | 678.5 | 216.5 | 15.0 |
| TM-09-02A-13 | 560 | 9924 | 2.8 | 21.4422 | 10.1 | 0.1451 | 10.2 | 0.0226 | 1.6 | 0.15 | 143.8 | 2.2 | 137.5 | 13.2 | 30.7 | 243.2 | 143.8 | 2.2 |
| TM-09-02A-14 | 68 | 3444 | 2.9 | 22.3134 | 29.3 | 0.2342 | 29.5 | 0.0379 | 3.2 | 0.11 | 239.8 | 7.5 | 213.7 | 56.9 | -65.6 | 729.7 | 239.8 | 7.5 |
| TM-09-02A-15 | 224 | 6177 | 4.6 | 20.3239 | 18.1 | 0.2438 | 18.2 | 0.0359 | 1.7 | 0.09 | 227.6 | 3.7 | 221.6 | 36.1 | 157.5 | 426.0 | 227.6 | 3.7 |
| TM-09-02A-16 | 544 | 5350 | 4.6 | 22.7797 | 17.9 | 0.0882 | 18.0 | 0.0146 | 1.9 | 0.11 | 93.3 | 1.8 | 85.8 | 14.8 | -116.3 | 445.1 | 93.3 | 1.8 |
| TM-09-02A-17 | 61 | 2209 | 3.8 | 6.8421 | 371.8 | 0.7279 | 371.9 | 0.0361 | 3.6 | 0.01 | 228.7 | 8.0 | 555.3 | N/A | 2301.4 | 530.8 | 2301.4 | 530.8 |
| TM-09-02A-18 | 103 | 992 | 2.0 | 31.4551 | 80.8 | 0.0570 | 81.0 | 0.0130 | 5.7 | 0.07 | 83.2 | 4.7 | 56.2 | 44.4 | -984.2 | 2881.5 | 83.2 | 4.7 |
| TM-09-02A-19 | 46 | 1622 | 4.0 | 49.1147 | 88.0 | 0.0954 | 88.5 | 0.0340 | 9.7 | 0.11 | 215.4 | 20.5 | 92.5 | 78.4 | -2557.9 | 1277.8 | 215.4 | 20.5 |
| TM-09-02A-20 | 213 | 2575 | 3.6 | 23.0672 | 17.6 | 0.0915 | 17.6 | 0.0153 | 1.5 | 0.08 | 97.9 | 1.4 | 88.9 | 15.0 | -147.4 | 438.2 | 97.9 | 1.4 |
| TM-09-02A-21 | 162 | 5559 | 3.2 | 25.9735 | 29.9 | 0.2060 | 30.0 | 0.0388 | 1.9 | 0.06 | 245.4 | 4.5 | 190.2 | 52.0 | -450.6 | 803.0 | 245.4 | 4.5 |
| TM-09-02A-22 | 635 | 7236 | 2.8 | 21.3682 | 9.7 | 0.0943 | 9.8 | 0.0146 | 1.0 | 0.10 | 93.5 | 0.9 | 91.5 | 8.6 | 38.9 | 233.4 | 93.5 | 0.9 |
| TM-09-02A-23 | 179 | 5474 | 2.2 | 20.1096 | 12.4 | 0.2630 | 12.5 | 0.0384 | 1.8 | 0.15 | 242.6 | 4.4 | 237.1 | 26.5 | 182.2 | 289.4 | 242.6 | 4.4 |
| TM-09-02A-24 | 134 | 1704 | 2.1 | 26.3791 | 36.1 | 0.0768 | 37.0 | 0.0147 | 7.9 | 0.21 | 94.1 | 7.4 | 75.2 | 26.8 | -491.6 | 986.7 | 94.1 | 7.4 |
| TM-09-02A-25 | 111 | 3090 | 2.7 | 25.8238 | 20.3 | 0.2031 | 20.3 | 0.0380 | 1.0 | 0.05 | 240.6 | 2.3 | 187.7 | 34.8 | -435.4 | 537.0 | 240.6 | 2.3 |
| TM-09-02A-27 | 100 | 5824 | 1.7 | 24.3962 | 38.9 | 0.2049 | 39.0 | 0.0363 | 3.6 | 0.09 | 229.6 | 8.2 | 189.3 | 67.5 | -288.2 | 1024.1 | 229.6 | 8.2 |
| TM-09-02A-28 | 129 | 1669 | 1.9 | 42.4574 | 131.9 | 0.0428 | 132.1 | 0.0132 | 6.5 | 0.05 | 84.4 | 5.5 | 42.6 | 55.1 | -1975.2 | 0.0 | 84.4 | 5.5 |
| TM-09-02A-29 | 235 | 2643 | 1.9 | 20.7456 | 23.1 | 0.0844 | 23.5 | 0.0127 | 4.2 | 0.18 | 81.3 | 3.4 | 82.2 | 18.5 | 109.2 | 551.6 | 81.3 | 3.4 |
| TM-09-02A-30 | 81 | 4266 | 3.6 | 15.9215 | 29.0 | 0.3284 | 29.0 | 0.0379 | 1.1 | 0.04 | 240.0 | 2.6 | 288.4 | 72.9 | 701.8 | 629.3 | 240.0 | 2.6 |
| TM-09-02A-31 | 161 | 3404 | 2.1 | 22.3529 | 13.7 | 0.2323 | 14.0 | 0.0377 | 2.7 | 0.20 | 238.3 | 6.4 | 212.1 | 26.8 | -69.9 | 336.3 | 238.3 | 6.4 |
| TM-09-02A-32 | 81 | 1878 | 1.2 | 21.4974 | 42.7 | 0.1528 | 42.9 | 0.0238 | 4.3 | 0.10 | 151.7 | 6.4 | 144.3 | 57.8 | 24.5 | 1067.4 | 151.7 | 6.4 |
| TM-09-02A-33 | 99 | 1788 | 1.6 | 34.0463 | 79.2 | 0.0928 | 79.2 | 0.0229 | 2.4 | 0.03 | 146.1 | 3.5 | 90.1 | 68.4 | -1224.4 | 1119.3 | 146.1 | 3.5 |
| TM-09-02A-34 | 218 | 6639 | 2.0 | 19.5392 | 13.0 | 0.2709 | 13.1 | 0.0384 | 1.5 | 0.12 | 242.9 | 3.7 | 243.4 | 28.3 | 248.9 | 300.3 | 242.9 | 3.7 |
| TM-09-02A-35 | 85 | 4602 | 4.0 | 20.5921 | 19.8 | 0.2430 | 20.7 | 0.0363 | 6.1 | 0.29 | 229.9 | 13.8 | 220.9 | 41.1 | 126.8 | 469.4 | 229.9 | 13.8 |
| TM-09-02A-36 | 88 | 3245 | 3.5 | 22.2836 | 26.3 | 0.2263 | 26.3 | 0.0366 | 1.7 | 0.07 | 231.6 | 3.9 | 207.1 | 49.4 | -62.4 | 650.7 | 231.6 | 3.9 |
| TM-09-02A-37 | 79 | 4718 | 2.4 | 21.3663 | 24.2 | 0.2399 | 24.4 | 0.0372 | 2.8 | 0.12 | 235.3 | 6.5 | 218.4 | 48.0 | 39.2 | 587.0 | 235.3 | 6.5 |
| TM-09-02A-38 | 58 | 1927 | 3.0 | 23.6722 | 47.3 | 0.2124 | 47.3 | 0.0365 | 1.8 | 0.04 | 230.8 | 4.1 | 195.5 | 84.3 | -212.0 | 1249.3 | 230.8 | 4.1 |
| TM-09-02A-39 | 115 | 3945 | 1.8 | 21.0441 | 21.0 | 0.2502 | 21.0 | 0.0382 | 0.6 | 0.03 | 241.6 | 1.5 | 226.7 | 42.8 | 75.4 | 504.4 | 241.6 | 1.5 |
| TM-09-02A-40 | 108 | 1894 | 1.6 | 18.3543 | 42.3 | 0.1106 | 42.9 | 0.0147 | 6.8 | 0.16 | 94.2 | 6.4 | 106.5 | 43.4 | 391.1 | 991.8 | 94.2 | 6.4 |
| TM-09-02A-41 | 252 | 2306 | 2.8 | 18.3833 | 12.2 | 0.2880 | 12.2 | 0.0384 | 1.1 | 0.09 | 242.9 | 2.7 | 257.0 | 27.8 | 387.5 | 274.4 | 242.9 | 2.7 |
| TM-09-02A-42 | 204 | 4873 | 1.6 | 17.2937 | 29.4 | 0.1190 | 29.5 | 0.0149 | 3.0 | 0.10 | 95.5 | 2.9 | 114.2 | 31.9 | 523.1 | 657.2 | 95.5 | 2.9 |
| TM-09-02A-43 | 65 | 2099 | 3.6 | 25.5000 | 56.9 | 0.1915 | 57.1 | 0.0354 | 3.8 | 0.07 | 224.4 | 8.3 | 177.9 | 93.4 | -402.3 | 1604.4 | 224.4 | 8.3 |
| TM-09-02A-44 | 476 | 18888 | 1.4 | 20.1652 | 6.2 | 0.1694 | 6.3 | 0.0248 | 1.2 | 0.19 | 157.7 | 1.9 | 158.9 | 9.3 | 175.8 | 144.8 | 157.7 | 1.9 |
| TM-09-02A-45 | 463 | 13769 | 2.3 | 19.1136 | 4.0 | 0.2769 | 4.3 | 0.0384 | 1.5 | 0.36 | 242.8 | 3.7 | 248.2 | 9.5 | 299.3 | 92.0 | 242.8 | 3.7 |
| TM-09-02A-46 | 70 | 1237 | 2.4 | 19.4983 | 92.4 | 0.0937 | 92.5 | 0.0133 | 2.9 | 0.03 | 84.9 | 2.5 | 91.0 | 80.6 | 253.7 | 769.4 | 84.9 | 2.5 |

**Table A4.1 –** Detrital zircon U-Pb analyses

| Analysis | U (ppm) | $^{206}Pb/^{204}Pb$ | U/Th | Isotopic Ratio | | | | | | Error | Apparent Age (Ma) | | | | | | Best Age (Ma) | |
|---|---|---|---|---|---|---|---|---|---|---|---|---|---|---|---|---|---|---|
| | | | | $^{206}Pb/^{207}Pb$ | ± (%) | $^{207}Pb/^{235}U$ | ± (%) | $^{206}Pb/^{238}U$ | ± (%) | | $^{206}Pb/^{238}U$ | ± (Ma) | $^{207}Pb/^{235}U$ | ± (Ma) | $^{206}Pb/^{207}Pb$ | ± (Ma) | Age | ± |
| TM-09-02A-47 | 105 | 2992 | 2.8 | 22.3736 | 31.3 | 0.2216 | 31.4 | 0.0360 | 2.8 | 0.09 | 227.8 | 6.3 | 203.3 | 57.9 | -72.2 | 780.5 | 227.8 | 6.3 |
| TM-09-02A-48 | 263 | 11813 | 1.8 | 20.4986 | 7.5 | 0.2599 | 7.7 | 0.0386 | 1.5 | 0.20 | 244.4 | 3.6 | 234.6 | 16.1 | 137.5 | 177.1 | 244.4 | 3.6 |
| TM-09-02A-49 | 95 | 2739 | 2.9 | 22.2454 | 25.6 | 0.2322 | 25.7 | 0.0375 | 2.1 | 0.08 | 237.0 | 4.8 | 212.0 | 49.2 | -58.2 | 632.8 | 237.0 | 4.8 |
| TM-09-02A-50 | 125 | 3067 | 2.8 | 21.4376 | 20.0 | 0.2467 | 20.1 | 0.0384 | 1.7 | 0.08 | 242.7 | 4.0 | 223.9 | 40.3 | 31.2 | 483.1 | 242.7 | 4.0 |
| TM-09-02A-51 | 185 | 3839 | 1.2 | 23.4455 | 19.0 | 0.1567 | 19.1 | 0.0266 | 1.5 | 0.08 | 169.5 | 2.6 | 147.8 | 26.3 | -187.9 | 479.7 | 169.5 | 2.6 |
| TM-09-02A-52 | 243 | 2472 | 4.3 | 27.2637 | 24.7 | 0.0692 | 24.8 | 0.0137 | 2.3 | 0.09 | 87.6 | 2.0 | 68.0 | 16.3 | -580.1 | 676.0 | 87.6 | 2.0 |
| TM-09-02A-54 | 502 | 9969 | 4.1 | 18.7112 | 19.1 | 0.1099 | 19.1 | 0.0149 | 1.0 | 0.05 | 95.5 | 1.0 | 105.9 | 19.3 | 347.7 | 435.8 | 95.5 | 1.0 |
| TM-09-02A-55 | 168 | 6663 | 3.3 | 21.4419 | 15.5 | 0.2399 | 15.6 | 0.0373 | 1.1 | 0.07 | 236.1 | 2.6 | 218.3 | 30.6 | 30.7 | 374.4 | 236.1 | 2.6 |
| TM-09-02A-56 | 453 | 16175 | 4.7 | 19.6227 | 3.6 | 0.2661 | 4.1 | 0.0379 | 2.0 | 0.49 | 239.7 | 4.7 | 239.6 | 8.7 | 239.1 | 82.0 | 239.7 | 4.7 |
| TM-09-02A-57 | 48 | 2120 | 2.9 | 20.3696 | 106.4 | 0.2546 | 106.5 | 0.0376 | 4.7 | 0.04 | 238.0 | 10.9 | 230.3 | 223.0 | 152.3 | 969.5 | 238.0 | 10.9 |
| TM-09-02A-58 | 95 | 2817 | 1.0 | 38.4981 | 101.5 | 0.0821 | 101.9 | 0.0229 | 9.0 | 0.09 | 146.2 | 13.0 | 80.1 | 78.7 | -1625.7 | 0.0 | 146.2 | 13.0 |
| TM-09-02A-59 | 62 | 20905 | 1.5 | 5.3562 | 0.7 | 13.6013 | 1.8 | 0.5284 | 1.6 | 0.92 | 2734.6 | 36.0 | 2722.4 | 16.6 | 2713.3 | 11.4 | 2713.3 | 11.4 |
| TM-09-02A-60 | 103 | 3303 | 2.0 | 29.4147 | 29.0 | 0.1683 | 29.2 | 0.0359 | 2.7 | 0.09 | 227.4 | 6.0 | 158.0 | 42.7 | -790.3 | 836.2 | 227.4 | 6.0 |
| TM-09-02A-61 | 314 | 3253 | 2.0 | 23.8837 | 23.6 | 0.0850 | 23.7 | 0.0147 | 2.8 | 0.12 | 94.2 | 2.6 | 82.8 | 18.9 | -234.4 | 601.8 | 94.2 | 2.6 |
| TM-09-02A-62 | 153 | 4573 | 2.6 | 22.9578 | 19.7 | 0.2354 | 19.7 | 0.0392 | 1.4 | 0.07 | 247.9 | 3.4 | 214.7 | 38.2 | -135.6 | 491.0 | 247.9 | 3.4 |
| TM-09-02A-63 | 40 | 1909 | 3.5 | 26.4393 | 78.7 | 0.1932 | 78.8 | 0.0370 | 3.2 | 0.04 | 234.5 | 7.5 | 179.3 | 130.2 | -497.6 | 2512.8 | 234.5 | 7.5 |
| TM-09-02A-64 | 219 | 5556 | 3.1 | 21.3880 | 15.7 | 0.0928 | 16.0 | 0.0144 | 2.9 | 0.18 | 92.1 | 2.6 | 90.1 | 13.8 | 36.7 | 378.4 | 92.1 | 2.6 |
| TM-09-02A-65 | 160 | 8119 | 1.6 | 22.1099 | 15.5 | 0.2435 | 15.6 | 0.0390 | 1.5 | 0.10 | 246.9 | 3.8 | 221.3 | 31.0 | -43.3 | 378.4 | 246.9 | 3.8 |
| TM-09-02A-66 | 74 | 2381 | 3.6 | 24.0279 | 18.5 | 0.2101 | 19.0 | 0.0366 | 4.5 | 0.24 | 231.8 | 10.3 | 193.6 | 33.5 | -249.6 | 470.2 | 231.8 | 10.3 |
| TM-09-02A-67 | 123 | 18562 | 2.7 | 22.3032 | 24.6 | 0.2369 | 24.6 | 0.0383 | 1.1 | 0.04 | 242.4 | 2.6 | 215.9 | 47.9 | -64.5 | 607.9 | 242.4 | 2.6 |
| TM-09-02A-68 | 250 | 7549 | 2.6 | 22.2120 | 9.7 | 0.2394 | 9.7 | 0.0386 | 1.1 | 0.12 | 243.9 | 2.7 | 217.9 | 19.1 | -54.5 | 236.0 | 243.9 | 2.7 |
| TM-09-02A-69 | 198 | 8927 | 2.5 | 20.2588 | 9.5 | 0.2655 | 9.6 | 0.0390 | 1.2 | 0.13 | 246.7 | 3.0 | 239.1 | 20.5 | 165.0 | 223.4 | 246.7 | 3.0 |
| TM-09-02A-70 | 48 | 1021 | 1.2 | 18.0508 | 128.3 | 0.1086 | 128.4 | 0.0142 | 4.5 | 0.04 | 91.0 | 4.1 | 104.7 | 128.4 | 428.3 | 932.9 | 91.0 | 4.1 |
| TM-09-02A-71 | 153 | 2970 | 1.0 | 25.4061 | 25.4 | 0.1301 | 25.4 | 0.0240 | 1.0 | 0.04 | 152.8 | 1.5 | 124.2 | 29.8 | -392.7 | 670.8 | 152.8 | 1.5 |
| TM-09-02A-72 | 159 | 10330 | 2.5 | 19.4523 | 18.3 | 0.2767 | 18.6 | 0.0390 | 3.2 | 0.17 | 246.9 | 7.7 | 248.1 | 41.0 | 259.2 | 424.7 | 246.9 | 7.7 |
| TM-09-02A-73 | 57 | 1977 | 2.7 | 21.7004 | 29.5 | 0.2172 | 29.8 | 0.0342 | 4.1 | 0.14 | 216.7 | 8.8 | 199.6 | 54.1 | 1.9 | 725.0 | 216.7 | 8.8 |
| TM-09-02A-74 | 165 | 10088 | 3.1 | 19.7969 | 13.2 | 0.2650 | 13.3 | 0.0380 | 2.2 | 0.16 | 240.7 | 5.1 | 238.7 | 28.4 | 218.7 | 305.7 | 240.7 | 5.1 |
| TM-09-02A-75 | 92 | 2519 | 3.5 | 24.7202 | 35.3 | 0.2117 | 35.5 | 0.0380 | 4.0 | 0.11 | 240.2 | 9.4 | 195.0 | 63.1 | -322.0 | 930.0 | 240.2 | 9.4 |
| TM-09-02A-76 | 928 | 25020 | 1.2 | 20.4770 | 4.4 | 0.1177 | 5.0 | 0.0175 | 2.4 | 0.48 | 111.7 | 2.7 | 113.0 | 5.4 | 139.9 | 103.6 | 111.7 | 2.7 |
| TM-09-02A-77 | 88 | 1630 | 3.7 | 21.4748 | 23.5 | 0.2400 | 23.8 | 0.0374 | 3.9 | 0.17 | 236.6 | 9.2 | 218.4 | 46.8 | 27.0 | 569.6 | 236.6 | 9.2 |
| TM-09-02A-78 | 242 | 17283 | 2.8 | 19.4510 | 9.7 | 0.2808 | 9.9 | 0.0396 | 2.0 | 0.21 | 250.4 | 5.0 | 251.3 | 22.0 | 259.3 | 222.6 | 250.4 | 5.0 |
| TM-09-02A-79 | 60 | 2132 | 3.1 | 19.1976 | 21.4 | 0.2701 | 21.5 | 0.0376 | 1.8 | 0.08 | 238.0 | 4.2 | 242.8 | 46.4 | 289.4 | 493.9 | 238.0 | 4.2 |
| TM-09-02A-80 | 109 | 8480 | 3.8 | 19.7528 | 24.1 | 0.2672 | 24.2 | 0.0383 | 1.0 | 0.04 | 242.1 | 2.5 | 240.4 | 51.7 | 223.8 | 565.1 | 242.1 | 2.5 |
| TM-09-02A-81 | 248 | 6910 | 1.9 | 19.6984 | 8.2 | 0.2712 | 8.4 | 0.0387 | 1.4 | 0.17 | 245.1 | 3.4 | 243.7 | 18.1 | 230.2 | 190.3 | 245.1 | 3.4 |
| TM-09-02A-82 | 165 | 2645 | 2.2 | 23.7067 | 13.4 | 0.1364 | 13.4 | 0.0235 | 1.0 | 0.08 | 149.4 | 1.5 | 129.8 | 16.4 | -215.6 | 337.9 | 149.4 | 1.5 |
| TM-09-02A-83 | 146 | 2144 | 1.1 | 30.0438 | 53.4 | 0.1063 | 53.5 | 0.0232 | 2.2 | 0.04 | 147.6 | 3.2 | 102.6 | 52.2 | -850.6 | 1632.5 | 147.6 | 3.2 |
| TM-09-02A-84 | 53 | 1547 | 2.5 | 18.4481 | 24.2 | 0.2741 | 24.3 | 0.0367 | 2.6 | 0.11 | 232.2 | 5.9 | 245.9 | 53.2 | 379.6 | 551.1 | 232.2 | 5.9 |
| TM-09-02A-85 | 121 | 4854 | 3.2 | 26.4947 | 29.0 | 0.1932 | 29.1 | 0.0371 | 2.9 | 0.10 | 235.0 | 6.8 | 179.4 | 47.9 | -503.2 | 785.4 | 235.0 | 6.8 |
| TM-09-02A-86 | 78 | 1058 | 1.3 | 37.4264 | 66.4 | 0.0606 | 66.7 | 0.0164 | 7.0 | 0.10 | 105.1 | 7.3 | 59.7 | 38.7 | -1530.1 | 591.2 | 105.1 | 7.3 |
| TM-09-02A-87 | 155 | 4920 | 2.3 | 20.9027 | 21.1 | 0.2484 | 21.2 | 0.0377 | 2.6 | 0.12 | 238.3 | 6.1 | 225.2 | 42.9 | 91.4 | 503.7 | 238.3 | 6.1 |
| TM-09-02A-88 | 175 | 6070 | 1.7 | 21.5782 | 9.4 | 0.2440 | 9.6 | 0.0382 | 2.1 | 0.21 | 241.5 | 4.9 | 221.7 | 19.1 | 15.5 | 226.0 | 241.5 | 4.9 |
| TM-09-02A-89 | 34 | 863 | 1.1 | 15.4383 | 49.2 | 0.2213 | 49.4 | 0.0248 | 3.9 | 0.08 | 157.8 | 6.1 | 203.0 | 91.1 | 767.0 | 1104.4 | 157.8 | 6.1 |

**Table A4.1 –** Detrital zircon U-Pb analyses

| Analysis | U (ppm) | $^{206}Pb/^{204}Pb$ | U/Th | Isotopic Ratio | | | | | | Error | Apparent Age (Ma) | | | | | | Best Age (Ma) | |
|---|---|---|---|---|---|---|---|---|---|---|---|---|---|---|---|---|---|---|
| | | | | $^{206}Pb/^{207}Pb$ | ± (%) | $^{207}Pb/^{235}U$ | ± (%) | $^{206}Pb/^{238}U$ | ± (%) | | $^{206}Pb/^{238}U$ | ± (Ma) | $^{207}Pb/^{235}U$ | ± (Ma) | $^{206}Pb/^{207}Pb$ | ± (Ma) | Age | ± |
| TM-09-02A-90 | 84 | 2432 | 2.4 | 24.7220 | 39.5 | 0.1977 | 39.6 | 0.0354 | 2.6 | 0.06 | 224.5 | 5.6 | 183.1 | 66.5 | -322.1 | 1050.1 | 224.5 | 5.6 |
| TM-09-02A-91 | 198 | 6260 | 2.4 | 19.4740 | 8.9 | 0.2817 | 9.0 | 0.0398 | 1.1 | 0.13 | 251.5 | 2.8 | 252.0 | 20.0 | 256.6 | 205.2 | 251.5 | 2.8 |
| TM-09-02A-93 | 717 | 9735 | 3.2 | 20.9566 | 11.5 | 0.1081 | 12.0 | 0.0164 | 3.3 | 0.28 | 105.1 | 3.5 | 104.3 | 11.9 | 85.3 | 274.2 | 105.1 | 3.5 |
| TM-09-02A-94 | 709 | 10569 | 3.1 | 18.3593 | 6.8 | 0.1359 | 6.8 | 0.0181 | 0.7 | 0.11 | 115.6 | 0.8 | 129.4 | 8.3 | 390.4 | 152.1 | 115.6 | 0.8 |
| TM-09-02A-95 | 58 | 779 | 5.8 | 22.0596 | 46.4 | 0.2303 | 46.6 | 0.0369 | 3.1 | 0.07 | 233.3 | 7.0 | 210.5 | 88.7 | -37.8 | 1185.6 | 233.3 | 7.0 |
| TM-09-02A-96 | 680 | 6823 | 1.4 | 20.6071 | 8.3 | 0.1742 | 8.5 | 0.0260 | 1.8 | 0.21 | 165.7 | 2.9 | 163.1 | 12.8 | 125.0 | 195.8 | 165.7 | 2.9 |
| TM-09-02A-97 | 99 | 3041 | 1.1 | 17.1708 | 22.7 | 0.2052 | 22.8 | 0.0256 | 2.2 | 0.10 | 162.7 | 3.6 | 189.5 | 39.4 | 538.7 | 501.9 | 162.7 | 3.6 |
| TM-09-02A-98 | 160 | 4178 | 1.4 | 24.5261 | 21.7 | 0.1401 | 21.8 | 0.0249 | 2.3 | 0.11 | 158.7 | 3.6 | 133.2 | 27.2 | -301.8 | 560.3 | 158.7 | 3.6 |
| TM-09-02A-99 | 488 | 1854 | 2.4 | 20.7804 | 16.8 | 0.0945 | 16.9 | 0.0142 | 1.6 | 0.10 | 91.1 | 1.5 | 91.7 | 14.8 | 105.3 | 399.0 | 91.1 | 1.5 |
| TM-09-02A-100 | 466 | 5284 | 1.6 | 22.0417 | 8.6 | 0.0914 | 8.8 | 0.0146 | 1.5 | 0.17 | 93.5 | 1.4 | 88.8 | 7.4 | -35.8 | 209.9 | 93.5 | 1.4 |
| EP-09-01A-2 | 84 | 1583 | 1.1 | 30.1095 | 59.5 | 0.0680 | 59.5 | 0.0148 | 2.3 | 0.04 | 95.0 | 2.2 | 66.8 | 38.5 | -856.8 | 1852.4 | 95.0 | 2.2 |
| EP-09-01A-3 | 218 | 2613 | 1.6 | 23.1260 | 34.0 | 0.0851 | 34.0 | 0.0143 | 2.1 | 0.06 | 91.3 | 1.9 | 82.9 | 27.1 | -153.7 | 864.4 | 91.3 | 1.9 |
| EP-09-01A-4 | 103 | 3687 | 1.1 | 20.3728 | 24.8 | 0.2056 | 24.8 | 0.0304 | 1.5 | 0.06 | 192.9 | 2.8 | 189.9 | 43.0 | 151.9 | 588.8 | 192.9 | 2.8 |
| EP-09-01A-5 | 43 | 833 | 0.9 | 48.8315 | 76.5 | 0.0605 | 76.7 | 0.0214 | 4.3 | 0.06 | 136.8 | 5.8 | 59.7 | 44.5 | -2533.0 | 683.3 | 136.8 | 5.8 |
| EP-09-01A-6 | 144 | 4130 | 1.0 | 20.5011 | 11.7 | 0.2077 | 11.7 | 0.0309 | 0.7 | 0.06 | 196.1 | 1.4 | 191.6 | 20.5 | 137.2 | 275.4 | 196.1 | 1.4 |
| EP-09-01A-7 | 65 | 967 | 0.9 | 25.6088 | 35.4 | 0.1293 | 35.5 | 0.0240 | 2.2 | 0.06 | 153.0 | 3.3 | 123.5 | 41.3 | -413.5 | 952.0 | 153.0 | 3.3 |
| EP-09-01A-8 | 203 | 4311 | 0.8 | 19.5246 | 12.9 | 0.1693 | 13.2 | 0.0240 | 2.8 | 0.21 | 152.7 | 4.2 | 158.8 | 19.4 | 250.6 | 297.2 | 152.7 | 4.2 |
| EP-09-01A-9 | 117 | 33264 | 2.4 | 9.4466 | 0.6 | 4.5543 | 1.5 | 0.3120 | 1.3 | 0.91 | 1750.7 | 20.2 | 1741.0 | 12.1 | 1729.2 | 11.2 | 1729.2 | 11.2 |
| EP-09-01A-10 | 576 | 3663 | 0.9 | 18.9059 | 10.2 | 0.1668 | 10.6 | 0.0229 | 2.8 | 0.26 | 145.8 | 4.0 | 156.7 | 15.4 | 324.2 | 233.1 | 145.8 | 4.0 |
| EP-09-01A-11 | 120 | 3042 | 0.9 | 25.2898 | 28.7 | 0.1280 | 28.8 | 0.0235 | 2.5 | 0.09 | 149.6 | 3.8 | 122.3 | 33.2 | -380.8 | 758.0 | 149.6 | 3.8 |
| EP-09-01A-12 | 190 | 3511 | 0.9 | 24.4375 | 22.3 | 0.1344 | 22.3 | 0.0238 | 1.8 | 0.08 | 151.7 | 2.7 | 128.0 | 26.9 | -292.5 | 574.3 | 151.7 | 2.7 |
| EP-09-01A-13 | 182 | 4278 | 4.6 | 19.6852 | 21.6 | 0.1770 | 21.6 | 0.0253 | 0.9 | 0.04 | 160.9 | 1.5 | 165.5 | 33.0 | 231.7 | 504.2 | 160.9 | 1.5 |
| EP-09-01A-14 | 64 | 1123 | 1.3 | 10.5039 | 119.5 | 0.1965 | 119.6 | 0.0150 | 5.2 | 0.04 | 95.8 | 4.9 | 182.2 | 202.2 | 1532.1 | 73.3 | 95.8 | 4.9 |
| EP-09-01A-15 | 318 | 7588 | 1.7 | 21.3329 | 5.7 | 0.1779 | 5.7 | 0.0275 | 0.6 | 0.11 | 175.1 | 1.1 | 166.3 | 8.8 | 42.9 | 136.3 | 175.1 | 1.1 |
| EP-09-01A-16 | 84 | 1477 | 0.9 | 17.4639 | 56.1 | 0.1081 | 56.2 | 0.0137 | 4.1 | 0.07 | 87.6 | 3.6 | 104.2 | 55.8 | 501.6 | 1341.7 | 87.6 | 3.6 |
| EP-09-01A-17 | 145 | 5212 | 0.9 | 22.7115 | 13.2 | 0.1850 | 13.5 | 0.0305 | 2.9 | 0.21 | 193.5 | 5.4 | 172.3 | 21.4 | -109.0 | 325.2 | 193.5 | 5.4 |
| EP-09-01A-18 | 189 | 5840 | 1.4 | 22.7044 | 11.0 | 0.1413 | 11.0 | 0.0233 | 1.2 | 0.11 | 148.3 | 1.8 | 134.2 | 13.9 | -108.2 | 270.6 | 148.3 | 1.8 |
| EP-09-01A-19 | 79 | 1460 | 0.6 | 25.6546 | 84.5 | 0.0747 | 84.5 | 0.0139 | 2.6 | 0.03 | 89.0 | 2.3 | 73.2 | 59.7 | -418.1 | 2797.1 | 89.0 | 2.3 |
| EP-09-01A-20 | 87 | 20615 | 0.9 | 9.2566 | 1.2 | 4.6512 | 2.9 | 0.3123 | 2.6 | 0.90 | 1751.8 | 39.9 | 1758.5 | 24.1 | 1766.5 | 22.7 | 1766.5 | 22.7 |
| EP-09-01A-21 | 47 | 858 | 0.8 | 14.9366 | 40.9 | 0.2066 | 41.0 | 0.0224 | 3.3 | 0.08 | 142.7 | 4.7 | 190.7 | 71.5 | 836.2 | 889.0 | 142.7 | 4.7 |
| EP-09-01A-22 | 18 | 540 | 1.2 | 20.3745 | 98.2 | 0.1421 | 98.4 | 0.0210 | 6.5 | 0.07 | 134.0 | 8.6 | 134.9 | 124.9 | 151.7 | N/A | 134.0 | 8.6 |
| EP-09-01A-23 | 114 | 3117 | 0.9 | 21.4544 | 13.5 | 0.1606 | 13.5 | 0.0250 | 1.0 | 0.08 | 159.2 | 1.6 | 151.3 | 19.0 | 29.3 | 324.9 | 159.2 | 1.6 |
| EP-09-01A-24 | 158 | 47427 | 1.5 | 9.4857 | 0.7 | 4.4477 | 1.6 | 0.3060 | 1.4 | 0.91 | 1720.9 | 21.8 | 1721.3 | 13.2 | 1721.7 | 12.2 | 1721.7 | 12.2 |
| EP-09-01A-25 | 143 | 4056 | 1.8 | 25.4983 | 17.5 | 0.1584 | 17.7 | 0.0293 | 2.4 | 0.13 | 186.1 | 4.4 | 149.3 | 24.6 | -402.2 | 460.8 | 186.1 | 4.4 |
| EP-09-01A-26 | 367 | 10783 | 1.4 | 19.4826 | 5.3 | 0.1703 | 5.5 | 0.0241 | 1.4 | 0.25 | 153.3 | 2.1 | 159.7 | 8.1 | 255.6 | 122.2 | 153.3 | 2.1 |
| EP-09-01A-27 | 56 | 1426 | 0.7 | 25.0443 | 47.2 | 0.1292 | 47.3 | 0.0235 | 2.7 | 0.06 | 149.5 | 4.0 | 123.3 | 55.0 | -355.5 | 1282.4 | 149.5 | 4.0 |
| EP-09-01A-28 | 375 | 3287 | 1.5 | 19.2931 | 8.8 | 0.2252 | 8.9 | 0.0315 | 1.1 | 0.12 | 200.0 | 2.1 | 206.3 | 16.6 | 278.0 | 202.1 | 200.0 | 2.1 |
| EP-09-01A-29 | 415 | 124955 | 5.1 | 9.5865 | 0.3 | 4.2273 | 1.0 | 0.2939 | 1.0 | 0.97 | 1661.0 | 14.6 | 1679.3 | 8.4 | 1702.2 | 4.8 | 1702.2 | 4.8 |
| EP-09-01A-30 | 258 | 5602 | 0.8 | 23.2666 | 10.1 | 0.1546 | 10.1 | 0.0261 | 0.6 | 0.06 | 166.0 | 1.1 | 145.9 | 13.7 | -168.7 | 251.9 | 166.0 | 1.1 |
| EP-09-01A-31 | 58 | 1303 | 0.8 | 26.8242 | 36.5 | 0.1257 | 36.6 | 0.0244 | 3.0 | 0.08 | 155.7 | 4.7 | 120.2 | 41.5 | -536.3 | 1005.4 | 155.7 | 4.7 |
| EP-09-01A-32 | 175 | 2661 | 1.2 | 20.9432 | 12.7 | 0.1518 | 12.9 | 0.0231 | 2.0 | 0.16 | 147.0 | 2.9 | 143.5 | 17.2 | 86.8 | 302.5 | 147.0 | 2.9 |
| EP-09-01A-33 | 139 | 3702 | 1.1 | 24.4233 | 17.2 | 0.1737 | 17.4 | 0.0308 | 2.4 | 0.14 | 195.3 | 4.7 | 162.6 | 26.1 | -291.0 | 441.9 | 195.3 | 4.7 |

**Table A4.1 –** Detrital zircon U-Pb analyses

| Analysis | U (ppm) | $^{206}Pb/^{204}Pb$ | U/Th | Isotopic Ratio | | | | | | Error | Apparent Age (Ma) | | | | | | Best Age (Ma) | |
|---|---|---|---|---|---|---|---|---|---|---|---|---|---|---|---|---|---|---|
| | | | | $^{206}Pb/^{207}Pb$ | ± (%) | $^{207}Pb/^{235}U$ | ± (%) | $^{206}Pb/^{238}U$ | ± (%) | | $^{206}Pb/^{238}U$ | ± (Ma) | $^{207}Pb/^{235}U$ | ± (Ma) | $^{206}Pb/^{207}Pb$ | ± (Ma) | Age | ± |
| EP-09-01A-34 | 72 | 2025 | 0.9 | 32.3922 | 49.6 | 0.1078 | 49.6 | 0.0253 | 1.0 | 0.02 | 161.2 | 1.6 | 103.9 | 49.1 | -1071.7 | 1574.9 | 161.2 | 1.6 |
| EP-09-01A-35 | 137 | 4570 | 1.0 | 20.4452 | 7.3 | 0.2051 | 7.5 | 0.0304 | 1.5 | 0.21 | 193.1 | 2.9 | 189.4 | 12.9 | 143.6 | 171.9 | 193.1 | 2.9 |
| EP-09-01A-36 | 170 | 2509 | 0.5 | 20.3824 | 10.9 | 0.1583 | 11.0 | 0.0234 | 1.9 | 0.17 | 149.1 | 2.8 | 149.2 | 15.3 | 150.8 | 254.9 | 149.1 | 2.8 |
| EP-09-01A-37 | 287 | 81821 | 1.1 | 9.2122 | 0.4 | 4.7018 | 2.0 | 0.3141 | 2.0 | 0.98 | 1761.0 | 30.2 | 1767.6 | 16.8 | 1775.2 | 7.8 | 1775.2 | 7.8 |
| EP-09-01A-39 | 123 | 1270 | 1.0 | 23.7385 | 41.7 | 0.0775 | 42.0 | 0.0133 | 4.8 | 0.12 | 85.4 | 4.1 | 75.8 | 30.7 | -219.0 | 1090.8 | 85.4 | 4.1 |
| EP-09-01A-40 | 47 | 1308 | 1.3 | 27.5050 | 50.2 | 0.1080 | 50.4 | 0.0216 | 3.9 | 0.08 | 137.4 | 5.4 | 104.2 | 49.9 | -604.0 | 1445.2 | 137.4 | 5.4 |
| EP-09-01A-41 | 67 | 1631 | 0.9 | 25.7500 | 60.1 | 0.1175 | 60.1 | 0.0219 | 1.6 | 0.03 | 139.9 | 2.3 | 112.8 | 64.3 | -427.9 | 1720.3 | 139.9 | 2.3 |
| EP-09-01A-42 | 279 | 9048 | 0.4 | 21.9193 | 6.0 | 0.1430 | 6.9 | 0.0227 | 3.4 | 0.49 | 144.9 | 4.9 | 135.7 | 8.8 | -22.3 | 146.1 | 144.9 | 4.9 |
| EP-09-01A-43 | 52 | 1515 | 1.1 | 11.7677 | 40.4 | 0.2914 | 40.4 | 0.0249 | 2.4 | 0.06 | 158.4 | 3.8 | 259.7 | 92.9 | 1315.0 | 817.7 | 158.4 | 3.8 |
| EP-09-01A-44 | 122 | 3039 | 1.5 | 21.3696 | 16.6 | 0.1685 | 16.6 | 0.0261 | 1.1 | 0.07 | 166.2 | 1.9 | 158.1 | 24.4 | 38.8 | 399.7 | 166.2 | 1.9 |
| EP-09-01A-45 | 82 | 1209 | 0.8 | 17.1847 | 29.3 | 0.1227 | 29.3 | 0.0153 | 1.3 | 0.04 | 97.9 | 1.3 | 117.5 | 32.6 | 537.0 | 653.9 | 97.9 | 1.3 |
| EP-09-01A-46 | 496 | 10645 | 1.0 | 21.1018 | 4.6 | 0.1562 | 4.9 | 0.0239 | 1.5 | 0.31 | 152.3 | 2.2 | 147.4 | 6.7 | 68.9 | 110.2 | 152.3 | 2.2 |
| EP-09-01A-47 | 159 | 4306 | 1.3 | 21.7720 | 16.3 | 0.1418 | 16.4 | 0.0224 | 1.3 | 0.08 | 142.7 | 1.9 | 134.6 | 20.6 | -6.0 | 395.8 | 142.7 | 1.9 |
| EP-09-01A-48 | 490 | 13133 | 1.1 | 19.7691 | 5.4 | 0.1861 | 6.3 | 0.0267 | 3.4 | 0.54 | 169.7 | 5.7 | 173.3 | 10.1 | 221.9 | 123.9 | 169.7 | 5.7 |
| EP-09-01A-49 | 146 | 2162 | 0.9 | 20.2019 | 21.9 | 0.0993 | 22.1 | 0.0146 | 2.6 | 0.12 | 93.2 | 2.4 | 96.2 | 20.3 | 171.6 | 517.7 | 93.2 | 2.4 |
| EP-09-01A-50 | 102 | 1546 | 1.2 | 23.3532 | 51.6 | 0.0880 | 51.8 | 0.0149 | 3.9 | 0.07 | 95.4 | 3.6 | 85.7 | 42.6 | -178.0 | 1371.1 | 95.4 | 3.6 |
| EP-09-01A-51 | 177 | 3821 | 0.9 | 20.5146 | 18.2 | 0.1527 | 18.2 | 0.0227 | 0.8 | 0.04 | 144.8 | 1.2 | 144.3 | 24.5 | 135.6 | 431.1 | 144.8 | 1.2 |
| EP-09-01A-52 | 184 | 2153 | 0.9 | 21.6003 | 23.8 | 0.0933 | 23.9 | 0.0146 | 2.0 | 0.08 | 93.5 | 1.9 | 90.6 | 20.7 | 13.1 | 580.0 | 93.5 | 1.9 |
| EP-09-01A-53 | 1065 | 28808 | 1.1 | 20.1120 | 2.2 | 0.1670 | 2.5 | 0.0244 | 1.1 | 0.45 | 155.2 | 1.7 | 156.8 | 3.6 | 182.0 | 51.9 | 155.2 | 1.7 |
| EP-09-01A-54 | 168 | 2684 | 1.5 | 20.9985 | 21.7 | 0.1045 | 22.0 | 0.0159 | 3.6 | 0.16 | 101.8 | 3.6 | 101.0 | 21.1 | 80.5 | 519.5 | 101.8 | 3.6 |
| EP-09-01A-55 | 348 | 9081 | 0.9 | 19.8799 | 5.0 | 0.1682 | 5.3 | 0.0243 | 1.6 | 0.31 | 154.5 | 2.5 | 157.9 | 7.7 | 209.0 | 116.6 | 154.5 | 2.5 |
| EP-09-01A-56 | 124 | 1944 | 1.0 | 27.5229 | 28.7 | 0.0758 | 28.8 | 0.0151 | 2.0 | 0.07 | 96.8 | 1.9 | 74.2 | 20.6 | -605.7 | 795.6 | 96.8 | 1.9 |
| EP-09-01A-57 | 1673 | 152232 | 73.2 | 9.5212 | 0.6 | 4.2944 | 5.6 | 0.2965 | 5.6 | 1.00 | 1674.2 | 82.9 | 1692.3 | 46.6 | 1714.8 | 10.1 | 1714.8 | 10.1 |
| EP-09-01A-59 | 182 | 2626 | 0.7 | 25.0173 | 17.2 | 0.0778 | 18.0 | 0.0141 | 5.4 | 0.30 | 90.3 | 4.9 | 76.0 | 13.2 | -352.7 | 446.8 | 90.3 | 4.9 |
| EP-09-01A-60 | 166 | 2971 | 1.2 | 21.3463 | 21.7 | 0.1016 | 21.8 | 0.0157 | 2.1 | 0.10 | 100.6 | 2.1 | 98.2 | 20.4 | 41.4 | 525.1 | 100.6 | 2.1 |
| EP-09-01A-61 | 481 | 10922 | 1.7 | 20.6194 | 5.5 | 0.1560 | 5.6 | 0.0233 | 0.8 | 0.15 | 148.6 | 1.2 | 147.2 | 7.6 | 123.6 | 130.0 | 148.6 | 1.2 |
| EP-09-01A-63 | 29 | 849 | 1.0 | 11.5762 | 68.1 | 0.2781 | 68.3 | 0.0233 | 4.5 | 0.07 | 148.8 | 6.6 | 249.1 | 152.0 | 1346.8 | 1527.2 | 148.8 | 6.6 |
| EP-09-01A-64 | 45 | 950 | 0.6 | 8.6676 | 264.0 | 0.3663 | 264.1 | 0.0230 | 2.7 | 0.01 | 146.8 | 4.0 | 316.9 | 896.7 | 1885.7 | 496.7 | 1885.7 | 496.7 |
| EP-09-01A-65 | 58 | 781 | 1.0 | 16.3286 | 34.4 | 0.2005 | 34.8 | 0.0237 | 5.5 | 0.16 | 151.3 | 8.2 | 185.6 | 59.1 | 647.8 | 760.0 | 151.3 | 8.2 |
| EP-09-01A-66 | 111 | 2427 | 0.8 | 22.9452 | 19.8 | 0.1532 | 19.9 | 0.0255 | 1.2 | 0.06 | 162.3 | 2.0 | 144.7 | 26.8 | -134.2 | 494.5 | 162.3 | 2.0 |
| EP-09-01A-67 | 530 | 17359 | 0.7 | 19.9999 | 6.7 | 0.1829 | 7.0 | 0.0265 | 2.0 | 0.28 | 168.8 | 3.3 | 170.5 | 11.0 | 195.0 | 155.6 | 168.8 | 3.3 |
| EP-09-01A-68 | 522 | 12587 | 1.4 | 20.7207 | 2.6 | 0.1838 | 3.4 | 0.0276 | 2.2 | 0.64 | 175.6 | 3.8 | 171.3 | 5.4 | 112.1 | 61.5 | 175.6 | 3.8 |
| EP-09-01A-69 | 74 | 1930 | 1.1 | 23.3304 | 83.1 | 0.1312 | 83.1 | 0.0222 | 2.3 | 0.03 | 141.5 | 3.3 | 125.2 | 98.2 | -175.6 | 2601.7 | 141.5 | 3.3 |
| EP-09-01A-70 | 175 | 3428 | 1.3 | 19.2143 | 10.8 | 0.1092 | 10.8 | 0.0152 | 1.2 | 0.11 | 97.3 | 1.1 | 105.2 | 10.8 | 287.4 | 246.6 | 97.3 | 1.1 |
| EP-09-01A-71 | 266 | 7987 | 1.0 | 20.6622 | 4.2 | 0.2006 | 4.3 | 0.0301 | 0.8 | 0.18 | 190.9 | 1.5 | 185.6 | 7.3 | 118.7 | 99.5 | 190.9 | 1.5 |
| EP-09-01A-72 | 135 | 16940 | 2.0 | 13.2959 | 1.7 | 1.8784 | 1.8 | 0.1811 | 0.7 | 0.36 | 1073.2 | 6.6 | 1073.5 | 12.2 | 1074.2 | 34.3 | 1074.2 | 34.3 |
| EP-09-01A-73 | 220 | 4607 | 2.0 | 20.3794 | 10.7 | 0.1569 | 10.8 | 0.0232 | 0.9 | 0.08 | 147.8 | 1.3 | 148.0 | 14.9 | 151.1 | 252.4 | 147.8 | 1.3 |
| EP-09-01A-74 | 274 | 4501 | 0.7 | 20.9934 | 12.9 | 0.1611 | 13.1 | 0.0245 | 2.1 | 0.16 | 156.2 | 3.3 | 151.7 | 18.5 | 81.1 | 307.7 | 156.2 | 3.3 |
| EP-09-01A-75 | 149 | 1910 | 1.0 | 19.4011 | 18.7 | 0.1073 | 18.7 | 0.0151 | 1.1 | 0.06 | 96.6 | 1.0 | 103.5 | 18.4 | 265.2 | 432.5 | 96.6 | 1.0 |
| EP-09-01A-76 | 103 | 1974 | 0.8 | 20.1977 | 14.4 | 0.1586 | 14.4 | 0.0232 | 1.1 | 0.07 | 148.1 | 1.5 | 149.5 | 20.1 | 172.1 | 337.8 | 148.1 | 1.5 |
| EP-09-01A-77 | 67 | 944 | 0.9 | 29.3321 | 28.1 | 0.0692 | 28.2 | 0.0147 | 2.7 | 0.09 | 94.3 | 2.5 | 68.0 | 18.5 | -782.3 | 805.4 | 94.3 | 2.5 |
| EP-09-01A-78 | 53 | 1216 | 0.9 | 34.1070 | 67.9 | 0.0884 | 67.9 | 0.0219 | 1.7 | 0.02 | 139.4 | 2.3 | 86.0 | 56.1 | -1229.9 | 727.5 | 139.4 | 2.3 |

**Table A4.1 –** Detrital zircon U-Pb analyses

| Analysis | U (ppm) | $^{206}Pb/^{204}Pb$ | U/Th | Isotopic Ratio | | | | | | Error | Apparent Age (Ma) | | | | | | Best Age (Ma) | |
|---|---|---|---|---|---|---|---|---|---|---|---|---|---|---|---|---|---|---|
| | | | | $^{206}Pb/^{207}Pb$ | ± (%) | $^{207}Pb/^{235}U$ | ± (%) | $^{206}Pb/^{238}U$ | ± (%) | | $^{206}Pb/^{238}U$ | ± (Ma) | $^{207}Pb/^{235}U$ | ± (Ma) | $^{206}Pb/^{207}Pb$ | ± (Ma) | Age | ± |
| EP-09-01A-79 | 80 | 1901 | 0.6 | 40.4844 | 28.7 | 0.0863 | 29.3 | 0.0253 | 6.0 | 0.21 | 161.3 | 9.6 | 84.1 | 23.7 | -1801.6 | 1042.1 | 161.3 | 9.6 |
| EP-09-01A-80 | 324 | 8199 | 1.0 | 20.1281 | 7.9 | 0.1796 | 8.0 | 0.0262 | 0.6 | 0.07 | 166.8 | 0.9 | 167.7 | 12.3 | 180.1 | 185.1 | 166.8 | 0.9 |
| EP-09-01A-81 | 243 | 7641 | 4.6 | 20.1279 | 14.1 | 0.1670 | 14.3 | 0.0244 | 2.5 | 0.18 | 155.3 | 3.8 | 156.8 | 20.8 | 180.1 | 329.2 | 155.3 | 3.8 |
| EP-09-01A-82 | 445 | 14682 | 0.9 | 20.5149 | 7.6 | 0.1819 | 7.9 | 0.0271 | 2.4 | 0.30 | 172.1 | 4.1 | 169.7 | 12.4 | 135.6 | 178.1 | 172.1 | 4.1 |
| EP-09-01A-83 | 669 | 8019 | 1.0 | 21.5600 | 5.0 | 0.0993 | 5.5 | 0.0155 | 2.5 | 0.44 | 99.3 | 2.4 | 96.1 | 5.1 | 17.5 | 119.4 | 99.3 | 2.4 |
| EP-09-01A-85 | 59 | 1767 | 1.1 | 22.7628 | 52.0 | 0.1470 | 52.0 | 0.0243 | 1.4 | 0.03 | 154.6 | 2.1 | 139.3 | 67.8 | -114.5 | 1366.3 | 154.6 | 2.1 |
| EP-09-01A-86 | 192 | 4926 | 1.0 | 19.3437 | 8.3 | 0.1668 | 8.7 | 0.0234 | 2.5 | 0.29 | 149.1 | 3.7 | 156.6 | 12.7 | 272.0 | 191.5 | 149.1 | 3.7 |
| EP-09-01A-87 | 263 | 5689 | 1.1 | 22.9816 | 13.0 | 0.1430 | 13.8 | 0.0238 | 4.8 | 0.34 | 151.8 | 7.1 | 135.7 | 17.5 | -138.1 | 321.9 | 151.8 | 7.1 |
| EP-09-01A-88 | 248 | 5258 | 0.7 | 22.4005 | 13.3 | 0.1414 | 13.4 | 0.0230 | 1.8 | 0.13 | 146.4 | 2.6 | 134.3 | 16.9 | -75.1 | 326.0 | 146.4 | 2.6 |
| EP-09-01A-89 | 518 | 11245 | 1.4 | 20.6294 | 5.4 | 0.1754 | 5.7 | 0.0262 | 1.8 | 0.32 | 167.0 | 3.0 | 164.1 | 8.7 | 122.5 | 128.0 | 167.0 | 3.0 |
| EP-09-01A-90 | 136 | 3185 | 1.7 | 24.3380 | 23.0 | 0.1419 | 23.1 | 0.0251 | 1.0 | 0.04 | 159.5 | 1.5 | 134.8 | 29.1 | -282.1 | 593.3 | 159.5 | 1.5 |
| EP-09-01A-91 | 70 | 1008 | 1.0 | 38.3421 | 88.0 | 0.0498 | 88.0 | 0.0139 | 2.0 | 0.02 | 88.7 | 1.8 | 49.4 | 42.4 | -1611.8 | 1479.1 | 88.7 | 1.8 |
| EP-09-01A-92 | 117 | 1849 | 0.7 | 27.4657 | 52.8 | 0.0721 | 52.8 | 0.0144 | 1.9 | 0.04 | 91.9 | 1.8 | 70.7 | 36.1 | -600.1 | 1528.1 | 91.9 | 1.8 |
| EP-09-01A-93 | 134 | 1694 | 0.6 | 38.0164 | 59.5 | 0.0494 | 59.6 | 0.0136 | 3.8 | 0.06 | 87.2 | 3.3 | 48.9 | 28.5 | -1582.8 | 386.0 | 87.2 | 3.3 |
| EP-09-01A-94 | 245 | 5539 | 0.9 | 21.6330 | 13.4 | 0.1585 | 14.1 | 0.0249 | 4.5 | 0.32 | 158.4 | 7.1 | 149.4 | 19.6 | 9.4 | 323.1 | 158.4 | 7.1 |
| EP-09-01A-95 | 143 | 4515 | 1.1 | 20.8779 | 9.0 | 0.1953 | 9.4 | 0.0296 | 2.6 | 0.28 | 187.9 | 4.9 | 181.2 | 15.5 | 94.2 | 213.2 | 187.9 | 4.9 |
| EP-09-01A-96 | 235 | 6133 | 0.8 | 22.3019 | 10.8 | 0.1559 | 11.1 | 0.0252 | 2.4 | 0.22 | 160.5 | 3.8 | 147.1 | 15.1 | -64.4 | 263.8 | 160.5 | 3.8 |
| EP-09-01A-97 | 432 | 5295 | 0.7 | 21.5285 | 8.7 | 0.1059 | 8.7 | 0.0165 | 0.9 | 0.10 | 105.7 | 1.0 | 102.2 | 8.5 | 21.0 | 208.2 | 105.7 | 1.0 |
| EP-09-01A-98 | 219 | 88156 | 1.6 | 9.1577 | 0.5 | 4.8829 | 2.7 | 0.3243 | 2.6 | 0.98 | 1810.8 | 41.8 | 1799.3 | 22.7 | 1786.1 | 8.6 | 1786.1 | 8.6 |
| EP-09-01A-99 | 199 | 3324 | 0.8 | 24.1380 | 25.1 | 0.0845 | 25.2 | 0.0148 | 1.2 | 0.05 | 94.7 | 1.2 | 82.4 | 19.9 | -261.1 | 646.1 | 94.7 | 1.2 |
| EP-09-04B-1 | 44 | 1030 | 1.5 | 11.6507 | 216.8 | 0.2477 | 216.8 | 0.0209 | 4.3 | 0.02 | 133.5 | 5.7 | 224.7 | 467.5 | 1334.4 | 741.8 | 133.5 | 5.7 |
| EP-09-04B-2 | 53 | 1241 | 1.0 | 33.6540 | 79.5 | 0.0882 | 79.6 | 0.0215 | 2.9 | 0.04 | 137.3 | 4.0 | 85.8 | 65.6 | -1188.4 | 1143.9 | 137.3 | 4.0 |
| EP-09-04B-3 | 400 | 5494 | 0.6 | 21.2287 | 8.6 | 0.1391 | 9.3 | 0.0214 | 3.4 | 0.37 | 136.6 | 4.6 | 132.3 | 11.5 | 54.6 | 206.6 | 136.6 | 4.6 |
| EP-09-04B-4 | 73 | 1445 | 0.7 | 30.3912 | 39.7 | 0.1084 | 40.4 | 0.0239 | 7.3 | 0.18 | 152.2 | 11.0 | 104.5 | 40.1 | -883.7 | 1186.1 | 152.2 | 11.0 |
| EP-09-04B-5 | 108 | 2975 | 1.2 | 18.3285 | 16.1 | 0.2212 | 16.4 | 0.0294 | 2.6 | 0.16 | 186.9 | 4.8 | 202.9 | 30.1 | 394.2 | 364.1 | 186.9 | 4.8 |
| EP-09-04B-6 | 906 | 16810 | 2.1 | 20.5773 | 3.6 | 0.1528 | 3.7 | 0.0228 | 0.7 | 0.20 | 145.3 | 1.0 | 144.4 | 4.9 | 128.5 | 84.3 | 145.3 | 1.0 |
| EP-09-04B-7 | 320 | 2532 | 1.0 | 19.2156 | 7.5 | 0.1636 | 8.0 | 0.0228 | 2.8 | 0.35 | 145.3 | 4.0 | 153.8 | 11.4 | 287.2 | 171.6 | 145.3 | 4.0 |
| EP-09-04B-8 | 219 | 5104 | 1.5 | 21.5899 | 7.3 | 0.2001 | 7.4 | 0.0313 | 1.2 | 0.17 | 198.9 | 2.4 | 185.2 | 12.5 | 14.2 | 175.2 | 198.9 | 2.4 |
| EP-09-04B-9 | 1129 | 28267 | 15.2 | 20.4447 | 2.0 | 0.1675 | 2.7 | 0.0248 | 1.8 | 0.68 | 158.1 | 2.9 | 157.2 | 3.9 | 143.6 | 46.8 | 158.1 | 2.9 |
| EP-09-04B-10 | 269 | 3845 | 1.0 | 23.3032 | 18.0 | 0.0791 | 18.0 | 0.0134 | 0.7 | 0.04 | 85.6 | 0.6 | 77.3 | 13.4 | -172.7 | 450.7 | 85.6 | 0.6 |
| EP-09-04B-11 | 119 | 2924 | 1.2 | 19.3223 | 17.8 | 0.1988 | 17.9 | 0.0279 | 2.1 | 0.12 | 177.1 | 3.7 | 184.1 | 30.2 | 274.5 | 410.1 | 177.1 | 3.7 |
| EP-09-04B-12 | 171 | 3073 | 0.6 | 22.2312 | 10.6 | 0.1534 | 13.1 | 0.0247 | 7.7 | 0.59 | 157.5 | 11.9 | 144.9 | 17.7 | -56.6 | 258.8 | 157.5 | 11.9 |
| EP-09-04B-13 | 238 | 5024 | 1.2 | 19.6049 | 7.7 | 0.1685 | 7.8 | 0.0240 | 1.4 | 0.18 | 152.6 | 2.1 | 158.1 | 11.4 | 241.2 | 177.1 | 152.6 | 2.1 |
| EP-09-04B-14 | 869 | 11370 | 0.6 | 21.1853 | 3.5 | 0.0987 | 3.6 | 0.0152 | 0.6 | 0.16 | 97.1 | 0.5 | 95.6 | 3.2 | 59.5 | 83.8 | 97.1 | 0.5 |
| EP-09-04B-15 | 389 | 6318 | 1.1 | 20.9932 | 7.2 | 0.1042 | 7.6 | 0.0159 | 2.3 | 0.31 | 101.5 | 2.3 | 100.6 | 7.3 | 81.1 | 171.6 | 101.5 | 2.3 |
| EP-09-04B-16 | 601 | 21828 | 2.1 | 17.6447 | 1.9 | 0.5703 | 3.4 | 0.0730 | 2.8 | 0.83 | 454.1 | 12.4 | 458.2 | 12.5 | 478.9 | 41.5 | 454.1 | 12.4 |
| EP-09-04B-17 | 224 | 5633 | 1.0 | 20.0508 | 9.2 | 0.1735 | 9.4 | 0.0252 | 1.8 | 0.19 | 160.7 | 2.8 | 162.5 | 14.1 | 189.1 | 214.3 | 160.7 | 2.8 |
| EP-09-04B-18 | 142 | 3111 | 0.9 | 28.3155 | 23.5 | 0.1174 | 23.5 | 0.0241 | 1.5 | 0.07 | 153.6 | 2.3 | 112.8 | 25.1 | -683.7 | 657.3 | 153.6 | 2.3 |
| EP-09-04B-19 | 649 | 8500 | 0.8 | 18.5401 | 8.8 | 0.2185 | 9.0 | 0.0294 | 1.9 | 0.21 | 186.6 | 3.6 | 200.6 | 16.4 | 368.4 | 199.1 | 186.6 | 3.6 |
| EP-09-04B-20 | 387 | 3353 | 0.9 | 20.7792 | 7.3 | 0.1505 | 7.7 | 0.0227 | 2.7 | 0.34 | 144.5 | 3.8 | 142.3 | 10.3 | 105.4 | 171.8 | 144.5 | 3.8 |
| EP-09-04B-21 | 76 | 1768 | 1.3 | 25.3567 | 22.8 | 0.1357 | 23.0 | 0.0250 | 3.0 | 0.13 | 158.9 | 4.8 | 129.2 | 27.9 | -387.7 | 599.7 | 158.9 | 4.8 |
| EP-09-04B-22 | 108 | 2425 | 1.0 | 18.8960 | 17.1 | 0.1784 | 17.2 | 0.0244 | 2.3 | 0.13 | 155.7 | 3.5 | 166.6 | 26.5 | 325.4 | 390.1 | 155.7 | 3.5 |

**Table A4.1 –** Detrital zircon U-Pb analyses

| Analysis | U (ppm) | $^{206}Pb/^{204}Pb$ | U/Th | Isotopic Ratio | | | | | | Error | Apparent Age (Ma) | | | | | | Best Age (Ma) | |
|---|---|---|---|---|---|---|---|---|---|---|---|---|---|---|---|---|---|---|
| | | | | $^{206}Pb/^{207}Pb$ | ± (%) | $^{207}Pb/^{235}U$ | ± (%) | $^{206}Pb/^{238}U$ | ± (%) | | $^{206}Pb/^{238}U$ | ± (Ma) | $^{207}Pb/^{235}U$ | ± (Ma) | $^{206}Pb/^{207}Pb$ | ± (Ma) | Age | ± |
| EP-09-04B-23 | 272 | 59307 | 2.2 | 9.5801 | 0.4 | 4.1628 | 2.0 | 0.2892 | 1.9 | 0.98 | 1637.7 | 28.1 | 1666.7 | 16.3 | 1703.4 | 8.0 | 1703.4 | 8.0 |
| EP-09-04B-24 | 278 | 7264 | 1.0 | 20.8024 | 9.8 | 0.1632 | 9.9 | 0.0246 | 1.4 | 0.14 | 156.8 | 2.1 | 153.5 | 14.1 | 102.8 | 231.6 | 156.8 | 2.1 |
| EP-09-04B-25 | 70 | 906 | 1.2 | 37.0761 | 59.4 | 0.0907 | 59.4 | 0.0244 | 1.5 | 0.03 | 155.3 | 2.4 | 88.1 | 50.2 | -1498.7 | 410.7 | 155.3 | 2.4 |
| EP-09-04B-26 | 564 | 12613 | 1.1 | 20.8880 | 5.4 | 0.1576 | 5.5 | 0.0239 | 0.6 | 0.10 | 152.1 | 0.9 | 148.6 | 7.6 | 93.0 | 128.8 | 152.1 | 0.9 |
| EP-09-04B-27 | 209 | 7163 | 1.0 | 22.7330 | 15.3 | 0.1827 | 16.0 | 0.0301 | 4.8 | 0.30 | 191.4 | 9.0 | 170.4 | 25.2 | -111.3 | 378.8 | 191.4 | 9.0 |
| EP-09-04B-28 | 171 | 3820 | 1.3 | 25.5396 | 27.2 | 0.1596 | 28.0 | 0.0296 | 6.4 | 0.23 | 187.8 | 11.9 | 150.4 | 39.1 | -406.4 | 721.5 | 187.8 | 11.9 |
| EP-09-04B-29 | 61 | 1305 | 0.7 | 22.0884 | 36.5 | 0.1419 | 36.6 | 0.0227 | 2.2 | 0.06 | 144.9 | 3.2 | 134.7 | 46.2 | -40.9 | 914.6 | 144.9 | 3.2 |
| EP-09-04B-30 | 524 | 12001 | 0.9 | 20.8404 | 7.3 | 0.1667 | 8.1 | 0.0252 | 3.5 | 0.43 | 160.5 | 5.5 | 156.6 | 11.8 | 98.5 | 173.5 | 160.5 | 5.5 |
| EP-09-04B-31 | 467 | 13441 | 1.3 | 20.4518 | 3.7 | 0.2068 | 4.0 | 0.0307 | 1.5 | 0.38 | 194.7 | 3.0 | 190.8 | 7.0 | 142.8 | 86.8 | 194.7 | 3.0 |
| EP-09-04B-32 | 571 | 11940 | 1.2 | 20.3571 | 3.1 | 0.1746 | 3.9 | 0.0258 | 2.4 | 0.61 | 164.1 | 3.9 | 163.4 | 5.9 | 153.7 | 72.8 | 164.1 | 3.9 |
| EP-09-04B-33 | 146 | 3704 | 0.8 | 21.0490 | 20.4 | 0.1732 | 20.4 | 0.0264 | 1.5 | 0.07 | 168.2 | 2.4 | 162.2 | 30.6 | 74.9 | 488.9 | 168.2 | 2.4 |
| EP-09-04B-34 | 271 | 6346 | 0.8 | 20.6042 | 4.3 | 0.1760 | 4.4 | 0.0263 | 0.8 | 0.19 | 167.4 | 1.4 | 164.6 | 6.7 | 125.4 | 101.4 | 167.4 | 1.4 |
| EP-09-04B-35 | 126 | 3471 | 0.7 | 22.8784 | 16.0 | 0.1477 | 16.0 | 0.0245 | 0.6 | 0.04 | 156.1 | 0.9 | 139.9 | 20.9 | -127.0 | 397.1 | 156.1 | 0.9 |
| EP-09-04B-36 | 830 | 20714 | 1.0 | 20.1255 | 2.3 | 0.1780 | 3.1 | 0.0260 | 2.1 | 0.68 | 165.3 | 3.4 | 166.3 | 4.7 | 180.4 | 52.6 | 165.3 | 3.4 |
| EP-09-04B-37 | 309 | 6963 | 0.6 | 20.6749 | 7.3 | 0.1602 | 7.4 | 0.0240 | 1.6 | 0.21 | 153.0 | 2.4 | 150.9 | 10.4 | 117.3 | 171.8 | 153.0 | 2.4 |
| EP-09-04B-38 | 180 | 4427 | 4.0 | 20.0303 | 16.3 | 0.1574 | 16.4 | 0.0229 | 1.8 | 0.11 | 145.7 | 2.6 | 148.4 | 22.7 | 191.5 | 381.6 | 145.7 | 2.6 |
| EP-09-04B-39 | 1275 | 24090 | 0.6 | 20.6314 | 2.1 | 0.1813 | 2.5 | 0.0271 | 1.5 | 0.58 | 172.5 | 2.5 | 169.2 | 3.9 | 122.3 | 48.8 | 172.5 | 2.5 |
| EP-09-04B-40 | 428 | 13720 | 1.2 | 19.7380 | 5.9 | 0.1768 | 6.2 | 0.0253 | 2.0 | 0.33 | 161.2 | 3.2 | 165.3 | 9.5 | 225.6 | 135.8 | 161.2 | 3.2 |
| EP-09-04B-41 | 336 | 91932 | 1.7 | 8.9057 | 0.4 | 5.0248 | 1.6 | 0.3246 | 1.5 | 0.96 | 1811.9 | 23.5 | 1823.5 | 13.1 | 1836.8 | 7.9 | 1836.8 | 7.9 |
| EP-09-04B-43 | 495 | 7783 | 0.8 | 20.0400 | 5.8 | 0.1795 | 6.0 | 0.0261 | 1.3 | 0.22 | 166.1 | 2.1 | 167.7 | 9.2 | 190.4 | 135.4 | 166.1 | 2.1 |
| EP-09-04B-44 | 612 | 10550 | 1.0 | 20.4249 | 4.0 | 0.1801 | 4.2 | 0.0267 | 1.2 | 0.29 | 169.7 | 2.0 | 168.1 | 6.5 | 145.9 | 94.5 | 169.7 | 2.0 |
| EP-09-04B-45 | 628 | 21949 | 0.8 | 20.7543 | 3.2 | 0.1828 | 3.3 | 0.0275 | 0.7 | 0.22 | 175.0 | 1.2 | 170.5 | 5.1 | 108.2 | 75.6 | 175.0 | 1.2 |
| EP-09-04B-46 | 181 | 4879 | 0.8 | 21.5846 | 13.7 | 0.1627 | 13.8 | 0.0255 | 1.4 | 0.10 | 162.1 | 2.3 | 153.1 | 19.6 | 14.8 | 330.8 | 162.1 | 2.3 |
| EP-09-04B-47 | 344 | 8428 | 0.8 | 20.8144 | 5.2 | 0.1953 | 5.8 | 0.0295 | 2.6 | 0.45 | 187.3 | 4.9 | 181.2 | 9.7 | 101.4 | 123.1 | 187.3 | 4.9 |
| EP-09-04B-48 | 879 | 15498 | 0.4 | 21.0702 | 2.8 | 0.1646 | 3.3 | 0.0251 | 1.8 | 0.54 | 160.1 | 2.8 | 154.7 | 4.7 | 72.4 | 66.0 | 160.1 | 2.8 |
| EP-09-04B-49 | 299 | 8026 | 0.9 | 19.8650 | 7.4 | 0.1662 | 7.4 | 0.0239 | 1.0 | 0.14 | 152.5 | 1.6 | 156.1 | 10.7 | 210.7 | 170.7 | 152.5 | 1.6 |
| EP-09-04B-50 | 228 | 6396 | 1.1 | 21.0663 | 10.3 | 0.1956 | 10.4 | 0.0299 | 1.6 | 0.16 | 189.8 | 3.0 | 181.4 | 17.3 | 72.9 | 245.5 | 189.8 | 3.0 |
| EP-09-04B-51 | 187 | 4734 | 0.7 | 22.3457 | 14.1 | 0.1759 | 15.3 | 0.0285 | 5.9 | 0.39 | 181.2 | 10.5 | 164.5 | 23.2 | -69.1 | 345.2 | 181.2 | 10.5 |
| EP-09-04B-52 | 85 | 1908 | 0.9 | 31.1485 | 39.6 | 0.1028 | 39.8 | 0.0232 | 4.0 | 0.10 | 148.0 | 5.9 | 99.3 | 37.7 | -955.3 | 1200.6 | 148.0 | 5.9 |
| EP-09-04B-53 | 66 | 876 | 0.8 | 21.3654 | 24.4 | 0.1578 | 24.5 | 0.0245 | 1.8 | 0.07 | 155.7 | 2.7 | 148.8 | 33.9 | 39.3 | 591.9 | 155.7 | 2.7 |
| EP-09-04B-54 | 697 | 17344 | 1.1 | 20.7949 | 4.8 | 0.1781 | 5.1 | 0.0269 | 1.8 | 0.35 | 170.8 | 3.0 | 166.4 | 7.8 | 103.6 | 112.7 | 170.8 | 3.0 |
| EP-09-04B-55 | 82 | 2024 | 0.7 | 27.2660 | 27.8 | 0.1228 | 27.8 | 0.0243 | 1.5 | 0.05 | 154.7 | 2.3 | 117.6 | 30.9 | -580.3 | 763.7 | 154.7 | 2.3 |
| EP-09-04B-56 | 131 | 4572 | 0.7 | 22.9701 | 14.7 | 0.1739 | 14.8 | 0.0290 | 1.8 | 0.12 | 184.2 | 3.4 | 162.8 | 22.3 | -136.9 | 365.6 | 184.2 | 3.4 |
| EP-09-04B-57 | 137 | 4339 | 0.9 | 22.6952 | 15.9 | 0.1680 | 16.1 | 0.0277 | 1.9 | 0.12 | 175.9 | 3.4 | 157.7 | 23.5 | -107.2 | 394.3 | 175.9 | 3.4 |
| EP-09-04B-58 | 417 | 9328 | 0.6 | 20.4586 | 3.5 | 0.1762 | 3.6 | 0.0261 | 1.1 | 0.30 | 166.4 | 1.8 | 164.8 | 5.5 | 142.1 | 81.6 | 166.4 | 1.8 |
| EP-09-04B-59 | 360 | 10559 | 1.3 | 20.3136 | 6.2 | 0.1719 | 6.3 | 0.0253 | 1.0 | 0.16 | 161.2 | 1.6 | 161.1 | 9.3 | 158.7 | 144.9 | 161.2 | 1.6 |
| EP-09-04B-60 | 220 | 65033 | 2.2 | 9.1438 | 0.6 | 4.9369 | 3.1 | 0.3274 | 3.0 | 0.98 | 1825.8 | 47.8 | 1808.6 | 25.9 | 1788.8 | 10.5 | 1788.8 | 10.5 |
| EP-09-04B-61 | 111 | 21494 | 1.9 | 11.1547 | 1.7 | 3.0283 | 2.0 | 0.2450 | 1.1 | 0.54 | 1412.6 | 13.5 | 1414.8 | 15.1 | 1418.0 | 31.9 | 1418.0 | 31.9 |
| EP-09-04B-62 | 362 | 4875 | 1.2 | 18.7281 | 10.3 | 0.2066 | 10.4 | 0.0281 | 1.6 | 0.16 | 178.4 | 2.8 | 190.7 | 18.1 | 345.6 | 233.7 | 178.4 | 2.8 |
| EP-09-04B-63 | 344 | 8877 | 0.9 | 21.3838 | 2.7 | 0.1919 | 2.9 | 0.0298 | 1.0 | 0.34 | 189.1 | 1.8 | 178.3 | 4.7 | 37.2 | 64.9 | 189.1 | 1.8 |
| EP-09-04B-64 | 198 | 6052 | 0.8 | 20.0373 | 10.1 | 0.2064 | 10.4 | 0.0300 | 2.3 | 0.22 | 190.6 | 4.4 | 190.6 | 18.1 | 190.7 | 236.1 | 190.6 | 4.4 |
| EP-09-04B-65 | 374 | 8942 | 0.6 | 20.3194 | 10.3 | 0.1566 | 10.4 | 0.0231 | 1.4 | 0.13 | 147.1 | 2.0 | 147.7 | 14.3 | 158.0 | 241.7 | 147.1 | 2.0 |

**Table A4.1 –** Detrital zircon U-Pb analyses

| Analysis | U (ppm) | $^{206}Pb/^{204}Pb$ | U/Th | Isotopic Ratio $^{206}Pb/^{207}Pb$ | ± (%) | $^{207}Pb/^{235}U$ | ± (%) | $^{206}Pb/^{238}U$ | ± (%) | Error | Apparent Age (Ma) $^{206}Pb/^{238}U$ | ± (Ma) | $^{207}Pb/^{235}U$ | ± (Ma) | $^{206}Pb/^{207}Pb$ | ± (Ma) | Best Age (Ma) Age | ± |
|---|---|---|---|---|---|---|---|---|---|---|---|---|---|---|---|---|---|---|
| EP-09-04B-66 | 232 | 2181 | 0.8 | 16.0079 | 15.9 | 0.2283 | 16.6 | 0.0265 | 4.7 | 0.28 | 168.6 | 7.8 | 208.8 | 31.3 | 690.2 | 340.8 | 168.6 | 7.8 |
| EP-09-04B-67 | 173 | 4795 | 1.2 | 21.6898 | 10.4 | 0.1599 | 10.6 | 0.0252 | 1.9 | 0.18 | 160.1 | 3.0 | 150.6 | 14.8 | 3.1 | 252.1 | 160.1 | 3.0 |
| EP-09-04B-68 | 627 | 13419 | 0.8 | 20.2536 | 4.3 | 0.1758 | 4.3 | 0.0258 | 0.5 | 0.12 | 164.4 | 0.8 | 164.5 | 6.5 | 165.6 | 100.0 | 164.4 | 0.8 |
| EP-09-04B-69 | 39 | 1460 | 0.8 | 29.8010 | 62.5 | 0.1135 | 62.8 | 0.0245 | 6.6 | 0.10 | 156.3 | 10.2 | 109.2 | 65.1 | -827.3 | 1955.6 | 156.3 | 10.2 |
| EP-09-04B-70 | 572 | 17086 | 0.9 | 20.8766 | 5.1 | 0.1789 | 5.2 | 0.0271 | 1.0 | 0.19 | 172.2 | 1.6 | 167.1 | 8.1 | 94.4 | 121.8 | 172.2 | 1.6 |
| EP-09-04B-71 | 930 | 21228 | 1.0 | 20.6399 | 2.3 | 0.1708 | 2.4 | 0.0256 | 0.8 | 0.34 | 162.7 | 1.3 | 160.1 | 3.6 | 121.3 | 53.0 | 162.7 | 1.3 |
| EP-09-04B-72 | 56 | 1483 | 1.1 | 20.3920 | 40.1 | 0.1511 | 40.3 | 0.0223 | 3.5 | 0.09 | 142.5 | 5.0 | 142.9 | 53.7 | 149.7 | 975.8 | 142.5 | 5.0 |
| EP-09-04B-73 | 451 | 11114 | 2.6 | 20.5289 | 4.0 | 0.1953 | 5.4 | 0.0291 | 3.6 | 0.67 | 184.8 | 6.6 | 181.1 | 9.0 | 134.0 | 94.0 | 184.8 | 6.6 |
| EP-09-04B-74 | 712 | 19441 | 1.2 | 20.5485 | 4.5 | 0.1704 | 4.7 | 0.0254 | 1.3 | 0.29 | 161.6 | 2.1 | 159.7 | 6.9 | 131.7 | 105.9 | 161.6 | 2.1 |
| EP-09-04B-75 | 252 | 8029 | 0.7 | 19.0933 | 5.0 | 0.2191 | 5.5 | 0.0303 | 2.4 | 0.43 | 192.7 | 4.6 | 201.2 | 10.1 | 301.8 | 113.9 | 192.7 | 4.6 |
| EP-09-04B-76 | 453 | 7973 | 0.7 | 19.7429 | 4.5 | 0.1715 | 4.8 | 0.0246 | 1.7 | 0.35 | 156.4 | 2.6 | 160.7 | 7.1 | 225.0 | 103.5 | 156.4 | 2.6 |
| EP-09-04B-77 | 392 | 8887 | 1.0 | 20.8321 | 6.3 | 0.1777 | 6.5 | 0.0268 | 1.7 | 0.26 | 170.8 | 2.8 | 166.1 | 10.0 | 99.4 | 149.4 | 170.8 | 2.8 |
| EP-09-04B-78 | 544 | 15048 | 0.9 | 20.1428 | 4.1 | 0.2124 | 4.4 | 0.0310 | 1.5 | 0.34 | 197.0 | 2.9 | 195.6 | 7.8 | 178.4 | 95.7 | 197.0 | 2.9 |
| EP-09-04B-79 | 173 | 3408 | 1.1 | 19.2275 | 12.2 | 0.1887 | 12.3 | 0.0263 | 1.6 | 0.13 | 167.4 | 2.7 | 175.5 | 19.9 | 285.8 | 280.4 | 167.4 | 2.7 |
| EP-09-04B-80 | 17 | 526 | 0.5 | 7.9039 | 178.0 | 0.3976 | 178.2 | 0.0228 | 9.1 | 0.05 | 145.3 | 13.0 | 339.9 | 567.2 | 2050.1 | 13.9 | 2050.1 | 13.9 |
| EP-09-04B-81 | 462 | 10627 | 0.5 | 19.6326 | 4.4 | 0.1749 | 4.5 | 0.0249 | 1.0 | 0.23 | 158.6 | 1.6 | 163.7 | 6.9 | 237.9 | 102.0 | 158.6 | 1.6 |
| EP-09-04B-82 | 18 | 404 | 0.6 | 13.9779 | 395.3 | 0.2107 | 395.3 | 0.0214 | 2.5 | 0.01 | 136.3 | 3.3 | 194.2 | 857.2 | 972.9 | 0.0 | 136.3 | 3.3 |
| EP-09-04B-83 | 138 | 2867 | 0.9 | 21.2255 | 27.0 | 0.1499 | 27.1 | 0.0231 | 1.3 | 0.05 | 147.1 | 1.9 | 141.8 | 35.8 | 55.0 | 655.2 | 147.1 | 1.9 |
| EP-09-04B-84 | 76 | 2650 | 0.9 | 21.8346 | 22.0 | 0.1729 | 22.0 | 0.0274 | 1.6 | 0.07 | 174.2 | 2.8 | 162.0 | 33.0 | -12.9 | 535.9 | 174.2 | 2.8 |
| EP-09-04B-85 | 581 | 120657 | 6.8 | 9.2852 | 0.4 | 4.3480 | 0.9 | 0.2928 | 0.8 | 0.89 | 1655.5 | 12.2 | 1702.5 | 7.7 | 1760.8 | 7.7 | 1760.8 | 7.7 |
| EP-09-04B-87 | 75 | 1577 | 1.3 | 22.0736 | 29.4 | 0.1542 | 29.5 | 0.0247 | 2.2 | 0.08 | 157.3 | 3.5 | 145.7 | 40.1 | -39.3 | 728.1 | 157.3 | 3.5 |
| EP-09-04B-89 | 1012 | 28158 | 1.5 | 20.1005 | 3.3 | 0.1939 | 3.7 | 0.0283 | 1.7 | 0.47 | 179.7 | 3.1 | 179.9 | 6.1 | 183.3 | 76.4 | 179.7 | 3.1 |
| EP-09-04B-90 | 260 | 4641 | 1.3 | 21.4723 | 10.8 | 0.1457 | 11.0 | 0.0227 | 1.9 | 0.17 | 144.6 | 2.7 | 138.1 | 14.2 | 27.3 | 259.6 | 144.6 | 2.7 |
| EP-09-04B-91 | 140 | 3994 | 1.0 | 19.8341 | 15.1 | 0.1776 | 15.2 | 0.0255 | 2.0 | 0.13 | 162.6 | 3.2 | 166.0 | 23.3 | 214.3 | 351.7 | 162.6 | 3.2 |
| EP-09-04B-92 | 358 | 88273 | 1.3 | 9.6494 | 0.3 | 4.2564 | 3.4 | 0.2979 | 3.4 | 1.00 | 1680.8 | 49.7 | 1685.0 | 27.7 | 1690.2 | 5.8 | 1690.2 | 5.8 |
| EP-09-04B-93 | 219 | 3552 | 1.1 | 23.0129 | 11.1 | 0.1459 | 11.4 | 0.0243 | 2.5 | 0.22 | 155.0 | 3.8 | 138.2 | 14.7 | -141.5 | 275.8 | 155.0 | 3.8 |
| EP-09-04B-94 | 48 | 1091 | 1.2 | 110.1042 | 88.4 | 0.0281 | 88.6 | 0.0225 | 5.0 | 0.06 | 143.3 | 7.1 | 28.2 | 24.6 | 0.0 | 579.4 | 143.3 | 7.1 |
| EP-09-04B-95 | 285 | 6544 | 0.7 | 23.3285 | 9.6 | 0.1493 | 9.8 | 0.0253 | 2.0 | 0.21 | 160.8 | 3.2 | 141.3 | 12.9 | -175.4 | 239.7 | 160.8 | 3.2 |
| EP-09-04B-96 | 195 | 3040 | 1.2 | 24.4848 | 21.0 | 0.0999 | 22.1 | 0.0177 | 6.8 | 0.31 | 113.3 | 7.7 | 96.6 | 20.4 | -297.5 | 542.5 | 113.3 | 7.7 |
| EP-09-04B-97 | 243 | 5127 | 1.1 | 23.3005 | 6.5 | 0.1564 | 6.7 | 0.0264 | 1.5 | 0.22 | 168.1 | 2.5 | 147.5 | 9.2 | -172.4 | 162.1 | 168.1 | 2.5 |
| EP-09-04B-98 | 232 | 5685 | 0.8 | 22.9439 | 10.1 | 0.1533 | 10.1 | 0.0255 | 0.4 | 0.04 | 162.4 | 0.6 | 144.8 | 13.6 | -134.1 | 249.9 | 162.4 | 0.6 |
| EP-09-04B-99 | 132 | 3519 | 0.9 | 24.3781 | 19.3 | 0.1703 | 19.3 | 0.0301 | 0.9 | 0.05 | 191.2 | 1.8 | 159.7 | 28.5 | -286.3 | 495.0 | 191.2 | 1.8 |
| EP-09-04B-100 | 345 | 12934 | 1.3 | 19.8810 | 3.8 | 0.2436 | 4.2 | 0.0351 | 1.7 | 0.41 | 222.6 | 3.8 | 221.4 | 8.4 | 208.8 | 88.6 | 222.6 | 3.8 |

**Table A4.1 notes** - Detrital zircon isotopic and age data. All samples were analyzed at the University of Arizona LaserChron Center following the analytical procedures for laser ablation-multicollector-inductively coupled plasma-mass spectrometry (LA-ICP-MS) outlined in Gehrels et al. (2008). All data were reduced using the NUAgeCalc analysis tool (*http://sites.google.com/a/laserchron.org/laserchron/home*). Only samples that met concordance and reproducibility requirements and had standard errors < 10% were included. 'Best Age' determined using a 1000 Ma cutoff, with Apparent $^{206}Pb/^{238}U$ Age taken for samples < 1000 Ma and Apparent $^{206}Pb/^{207}Pb$ Age accepted for samples > 1000 Ma.

# Figure A4.1

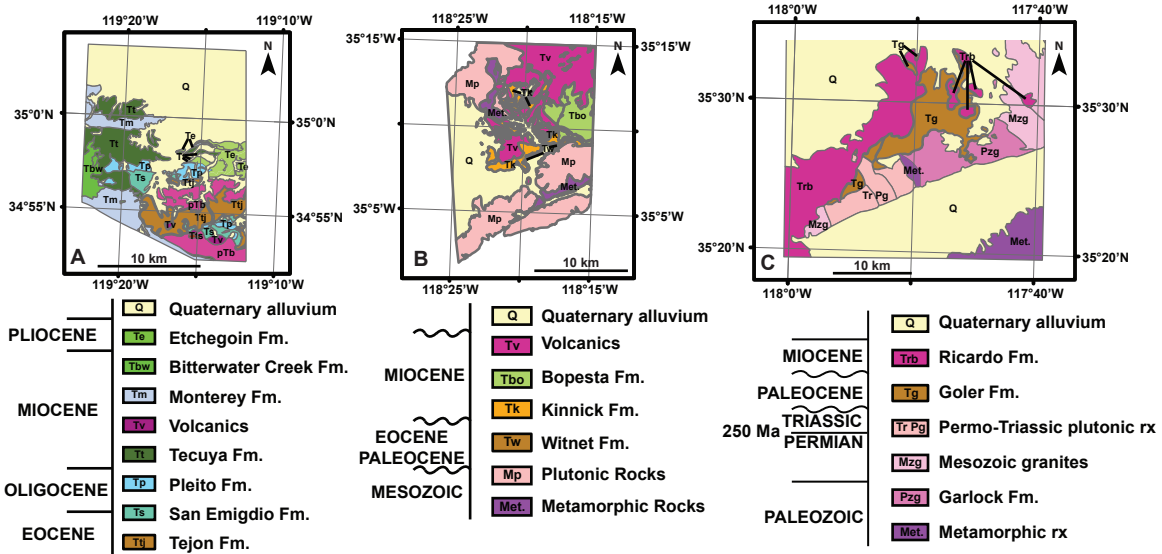


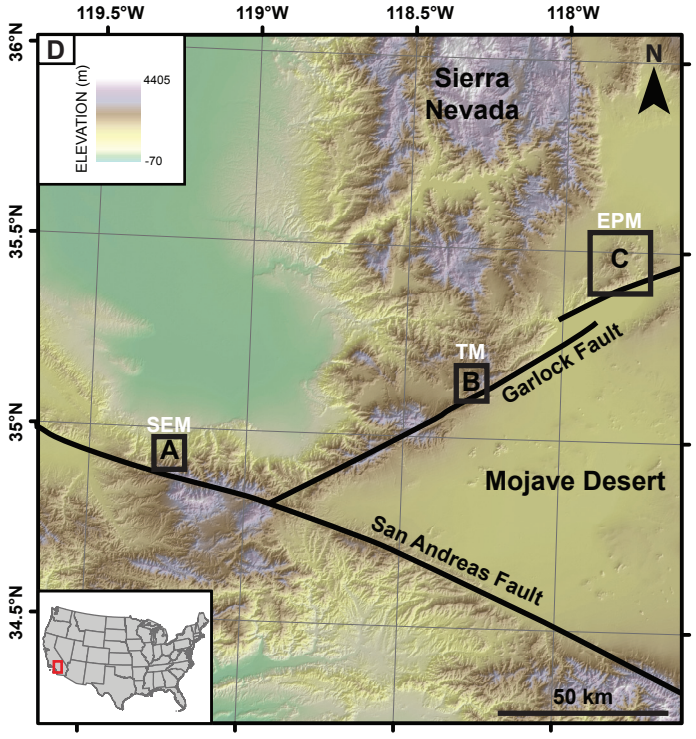


Figure A4.1 - Simplified geologic maps of (A) San Emigdio Mountains (Nilsen, 1987), (B) Tehachapi Mountains (Dibblee and Louke, 1970), and (C) El Paso Mountains (Cox, 1982) with corresponding location and extent on southern Sierra Nevada color DEM (D).

# Figure A4.2

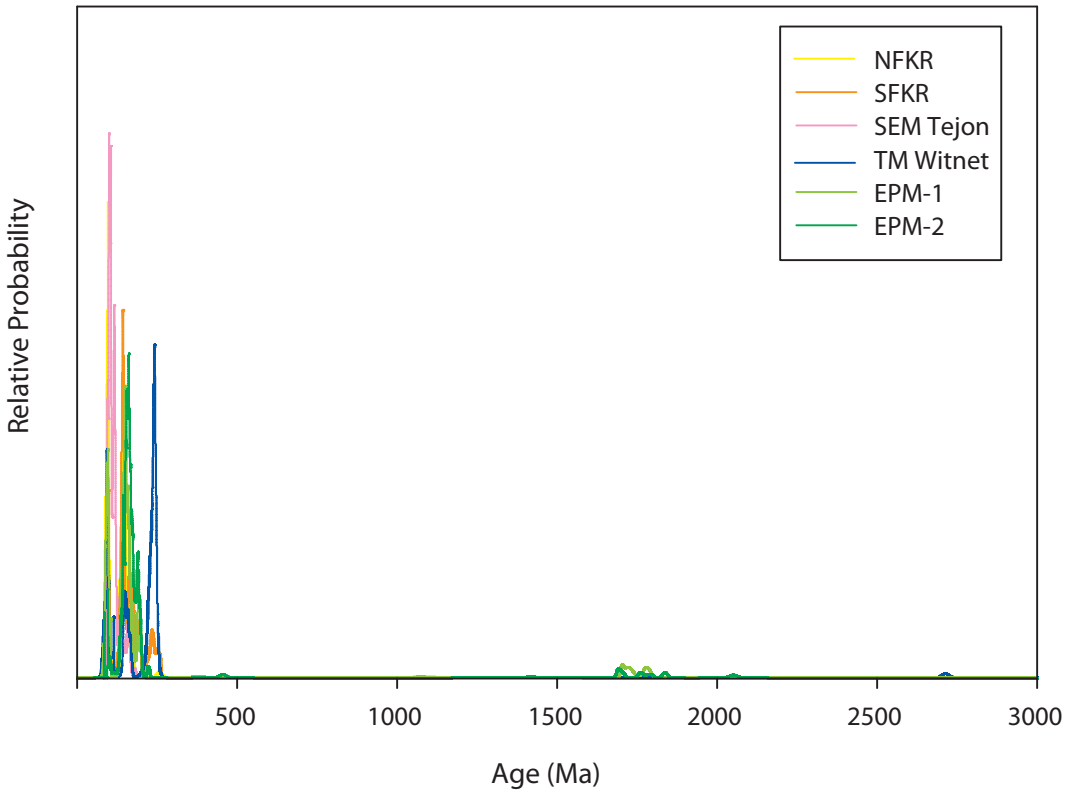


Figure A4.2 - Full U-Pb age spectra for all detrital samples. Note the minimal contribution of ages older than 250 Ma. The small population of ~ 1700 Ma zircons observed in Goler Fm. samples (EPM-1 and EPM-2) are likely derived from Paleozoic miogeoclinal siliciclastic rocks currently exposed in the White-Inyo Mountains and Slate Range regions, as Proterozoic zircon populations are abundant in these Paleozoic sequences (Gehrels et al., 1995).

**Table A 4.2 – Goler Fm. isotopic data**

| ID | $\delta^{13}C_{PDB}$ (‰) | ± | $\delta^{18}O_{PDB}$ (‰) | ± |
|---|---|---|---|---|
| EPM-4 | -3.15 | 0.03 | -12.32 | 0.11 |
| EPM-4 | -3.22 | 0.02 | -12.13 | 0.03 |
| EPM-4 | -3.38 | 0.01 | -12.35 | 0.04 |
| EPM-4 | -3.02 | 0.01 | -12.43 | 0.02 |
| **Average** | **-3.19** | **0.15** | **-12.31** | **0.13** |

**Table A4.2 Notes** - $\delta^{18}O$ and $\delta^{13}C$ data for Goler Fm. lacustrine carbonate. Carbonate was drilled following standard micromilling procedures (Dettman and Lohmann, 1995) and analyzed at the University of Michigan Stable Isotope Lab. ~ 10 mg of carbonate powder for each sample was placed under vacuum at 200° C for one hour to remove volatile contaminants and water. Samples were then placed in individual borosilicate reaction vessels and reacted at 77° ± 1°C with 4 drops of anhydrous phosphoric acid for 8 minutes in a Finnigan MAT Kiel IV preparation device coupled directly to the inlet of a Finnigan MAT 253 triple collector isotope ratio mass spectrometer. Measured precision is < 0.1 ‰ for both $\delta^{18}O$ and $\delta^{13}C$.

# Figure A4.3

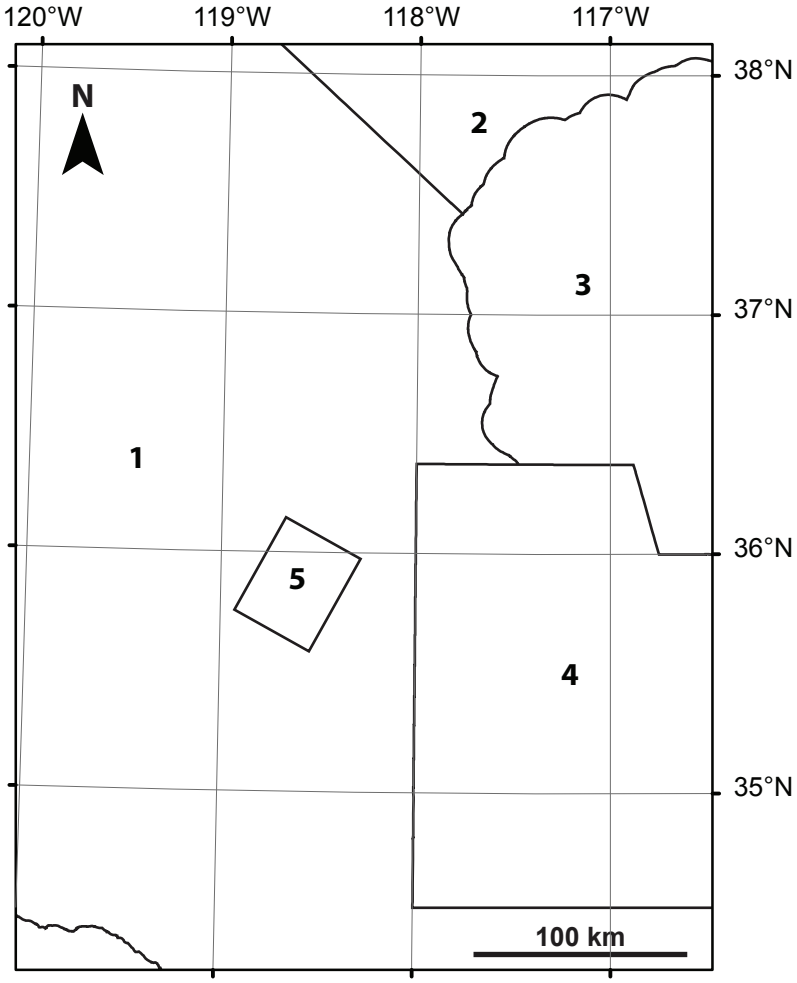


Figure A4.3 - Sources of geologic mapping of plutonic, volcanic and siliciclastic rocks shown in Figure 4.2B. (1) Ludington et al. (2005); (2) Crafford and Harris (2007); (3) Workman et al. (2002); (4) Walker et al. (2002) and (5) Saleeby et al. (2008).

**Table A4.3 –** Sandstone and carbonate sample locations

| | Latitude (°N) | Longitude (°W) | Elevation (m) | Description |
|---|---|---|---|---|
| *Detrital sand* | | | | |
| NFKR | 35.86435 | 118.44802 | 961 | Medium grained, well sorted lithic sand |
| SFKR | 35.69105 | 118.23517 | 827 | Medium grained, well sorted lithic sand |
| *Detrital sandstone* | | | | |
| SEM | 34.94347 | 119.25154 | 873 | Medium grained, well sorted lithic sandstone |
| TM | 35.15366 | 118.28666 | 1357 | Coarse grained, arkose sandstone |
| EPM-1 | 35.51522 | 117.79312 | 1120 | Medium grained, moderately sorted lithic sandstone |
| EPM-2 | 35.50144 | 117.79162 | 1103 | Coarse grained, moderately sorted lithic sandstone |
| *Carbonate* | | | | |
| EPM-4 | 35.46403 | 117.85388 | 1270 | Light gray micritic carbonate |

**Table A4.3 Notes -** Geographic coordinates and lithologic descriptions for all geologic samples analyzed as part of this study. Sample abbreviations same as in Figs. 4.1 and 4.2. See Fig. 4.1 for map locations.

**Table A5.1** – All isotopologue and stable isotopic data

| Sample | $\delta^{13}C$ (‰) | $\delta^{18}O$ (‰) | $\delta_{45}$ (‰) | $\delta_{46}$ (‰) | $\delta_{47}$ (‰) | $\delta_{48}$ (‰) | $\delta_{49}$ (‰) | $\Delta_{48}$ (‰) | $\Delta_{49}$ (‰) | $\Delta_{47}$ (‰) | St. Dev. | S.E. | $\Delta_{47}$ normalized | St. Dev. |
|---|---|---|---|---|---|---|---|---|---|---|---|---|---|---|
| ***Paleocene Goler Formation*** | | | | | | | | | | | | | | |
| EP0803-1 | -2.9 | 27.8 | 0.5096 | -6.9369 | -6.8449 | -17.073 | 361.9 | -3.292 | 379.9 | -0.5454 | 0.040 | 0.015 | 0.5226 | 0.039 |
| EP0803-2 | -3.6 | 26.3 | -0.2223 | -8.3370 | -9.0404 | -21.851 | 259.7 | -5.335 | 280.9 | -0.6157 | 0.017 | 0.006 | 0.5198 | 0.017 |
| EP0803-3 | -3.0 | 27.3 | 0.3784 | -7.3890 | -7.4200 | -18.760 | 327.2 | -4.097 | 346.1 | -0.5414 | 0.047 | 0.016 | 0.5442 | 0.050 |
| ***Late Cretaceous-Eocene Sheep Pass Formation*** | | | | | | | | | | | | | | |
| 10SP06-1 | 4.2 | 28.3 | 7.1043 | -6.4632 | 0.6896 | -16.074 | 96.7 | -3.231 | 102.4 | -0.2308 | 0.033 | 0.012 | 0.6052 | 0.032 |
| 10SP06-2 | 3.9 | 27.9 | 6.8182 | -6.8552 | -0.0376 | -17.832 | 124.8 | -4.227 | 131.9 | -0.2765 | 0.020 | 0.007 | 0.5819 | 0.019 |
| 10SP06-4 | 4.1 | 28.1 | 7.0781 | -6.5811 | 0.5261 | -16.852 | 159.6 | -3.783 | 165.9 | -0.2505 | 0.031 | 0.011 | 0.5905 | 0.031 |
| 10SP06-S1 | 8.4 | 32.9 | 11.2210 | -2.0242 | 9.5884 | -4.589 | 290.7 | -0.547 | 280.5 | 0.0306 | 0.036 | 0.013 | 0.5927 | 0.035 |
| 10SP06-S3 | 8.8 | 33.0 | 11.5935 | -1.8873 | 10.1599 | -0.811 | 910.6 | 2.971 | 894.3 | 0.0820 | 0.028 | 0.011 | 0.6265 | 0.027 |
| 10SP06-S4 | 8.4 | 32.5 | 11.1875 | -2.3653 | 9.2066 | -2.685 | 474.6 | 2.050 | 464.0 | 0.0230 | 0.019 | 0.007 | 0.5968 | 0.018 |
| 10SP02-1 | 0.6 | 35.0 | 4.0204 | 0.0061 | 3.9504 | 0.315 | 128.6 | 0.303 | 123.8 | -0.2011 | 0.024 | 0.009 | 0.5345 | 0.023 |
| 10SP02-3 | 0.5 | 35.1 | 3.9022 | 0.1487 | 3.9904 | 0.662 | -4.0 | 0.364 | -8.4 | -0.1801 | 0.033 | 0.012 | 0.5543 | 0.032 |
| 10SP02-2 | 0.5 | 34.4 | 3.8970 | -0.5276 | 3.3479 | 0.214 | 248.5 | 1.270 | 244.6 | -0.1494 | 0.021 | 0.007 | 0.6048 | 0.020 |
| 10SP02-4 | 0.9 | 35.4 | 4.3106 | 0.4195 | 4.7460 | 5.056 | 754.9 | 4.214 | 745.5 | -0.1136 | 0.015 | 0.005 | 0.5975 | 0.015 |
| 10SP03-1 | -0.1 | 32.1 | 3.2763 | -2.7957 | 0.3541 | -7.328 | 1.5 | -1.754 | 3.5 | -0.2648 | 0.038 | 0.014 | 0.5815 | 0.037 |
| 10SP03-3 | -0.7 | 31.8 | 2.7183 | -3.0311 | -0.4561 | -7.015 | -6.2 | -0.967 | -3.1 | -0.2690 | 0.021 | 0.008 | 0.6023 | 0.021 |
| 10SP03-4 | -0.4 | 31.3 | 2.9319 | -3.4830 | -0.6848 | -7.596 | 327.2 | -0.647 | 332.2 | -0.2722 | 0.014 | 0.005 | 0.6061 | 0.014 |
| ***Carrara marble interlab standard*** | | | | | | | | | | | | | | |
| Carrara-1 | 2.2 | 37.7 | 5.5694 | 2.6858 | 8.1091 | 7.448 | 70.9 | 2.058 | 59.0 | -0.2899 | 0.033 | 0.012 | 0.3178 | 0.032 |
| Carrara-2 | 2.1 | 37.6 | 5.4982 | 2.5398 | 7.8548 | 6.901 | 109.2 | 1.806 | 97.3 | -0.3259 | 0.025 | 0.009 | 0.2896 | 0.023 |
| Carrara-3 | 2.1 | 37.8 | 5.5198 | 2.7171 | 8.1759 | 8.090 | 231.8 | 2.634 | 218.1 | -0.2033 | 0.026 | 0.009 | 0.4023 | 0.025 |

**Table A5.1 Notes** – This table lists all isotopologue data measured on the dual inlet Thermo-Finnigan MAT 253 mass spectrometer at the University of Michigan Stable Isotope Lab. Normalized $\Delta_{47}$ values underwent subsequent correction for acid fractionation factors at 75°C (see caption for Table 5.1 and text for discussion) prior to temperature determination. $\delta^{13}C$ and $\delta^{18}O$ values are measured relative to $CO_2$ reference gas of known isotopic composition but have not been converted to PDB reference.

**References Cited**

Cox, B.F., 1982, Stratigraphy, Sedimentology, and Structure of the Goler Formation (Paleocene), El Paso Mountains, California: Implications for Paleogene Tectonism on the Garlock Fault Zone [Ph.D. Thesis]: Riverside, University of California, 248 p.

Crafford, A.E.J., and Harris, A.G., 2007, Geologic map of Nevada; with a section on a digital conodont database of Nevada, U. S. Geological Survey Data Series, DS-0249, 46 p.

Dettman, D. L., and Lohmann, K. C., 1995, Microsampling carbonates for stable isotope and minor element analysis - physical separation of samples on a 20 micrometer scale: Journal of Sedimentary Research Section A-Sedimentary Petrology and Processes, v. 65, no. 3, p. 566-569.

Dibblee, T.W., Jr., and Louke, G.P., 1970, Geologic map of the Tehachapi quadrangle, Kern County, California: U.S. Geological Survey Miscellaneous Geological Investigations, Map I-607, scale 1:62,500.

Gehrels, G. E., and Dickinson, W. R., 1995, Detrital zircon provenance of Cambrian to Triassic miogeoclinal and eugeoclinal strata in Nevada: American Journal of Science, v. 295, no. 1, p. 18-48.

Gehrels, G. E., Valencia, V. A., and Ruiz, J., 2008, Enhanced precision, accuracy, efficiency, and spatial resolution of U-Pb ages by laser ablation-multicollector-inductively coupled plasma-mass spectrometry: Geochemistry Geophysics Geosystems, v. 9, p. -.

Ludington, S., Moring, B.C., Miller, R.J., Flynn, K., Hopkins, M.J., Stone, P., Bedford, D.R., and Haxel, G.A., 2005, Preliminary integrated geologic map databases for the United States western states; California, Nevada, Arizona, and Washington, version 1.0.

Nilsen, T.H., 1987, Stratigraphy and sedimentology of the Eocene Tejon Formation, western Tehachapi and San Emigdio Mountains, California: U.S. Geological Survey Professional Paper 1268, 110 p.

Saleeby J., Ducea M. N., Busby C., Nadin E., and Wetmore P. H., 2008, Chronology of pluton emplacement and regional deformation in the southern Sierra Nevada batholith California: Geological Society of America Special Paper, v. 438, p. 397-428.

Walker J.D., Black R.A., Berry, A.K., Davis P.J., Andrew A.J., and Mitsdarfer J.M., 2002, Geologic maps of the northern Mojave Desert and southwestern Basin and

Range province California: Explanation of maps on CD-ROM: Geological Society of America Memoir, v. 195, p. 297-299.

Workman, J.B., Menges, C.M., Page, W.R., Taylor, E., Ekren, E.B., Rowley, P.D., Dixon, G.L., Thompson, R.A., and Wright, L.A., 2002, Geologic map of the Death Valley ground-water model area, Nevada and California, p. 26.